UNIVERSITY OF SOUTHAMPTON

FACULTY OF NATURAL AND ENVIRONMENTAL SCIENCE

Ocean and Earth Sciences

THE LONG-TERM EVOLUTION OF MONTSERRAT VOLCANISM

by

Stuart James Hatter

Thesis for the degree of Doctor of Philosophy

March 2018

UNIVERSITY OF SOUTHAMPTON

ABSTRACT

FACULTY OF NATURAL AND ENVIRONMENTAL SCIENCE
Ocean and Earth Sciences

Thesis for the degree of Philosophy

THE LONG-TERM EVOLUTION OF VOLCANISM ON MONTSERRAT

Stuart James Hatter

This thesis investigates the long-term geochemical trends of volcanism on Montserrat and Guadeloupe, islands in the northern Lesser Antilles arc, through both their terrestrial and marine (from International Ocean Discovery Program core U1396C) records, to examine the processes driving geochemical evolution in island arcs.

Detailed mapping of the Silver Hills, the least studied volcanic centre on Montserrat, reveals activity was dominated by andesite dome growth and collapse. New $^{40}Ar/^{39}Ar$ ages from terrestrial samples, combined with new palaeomagnetic and biostratigraphic ages of tephra layers from marine sediment core U1396C, reveal the previously unrecognised overlap in volcanic activity between the Silver and Centre Hills, and Centre and Soufrière Hills.

Pb-Nd-Sr isotope and major and trace element data for the Silver Hills show that lavas fall into two compositional groups; 'normal' lavas and 'low Al_2O_3-high Fe_2O_3' lavas. The latter group formed from parental magmas which experienced up to 25% greater plagioclase fractionation compared to the parent magmas of the normal lavas, likely as a result of lower magmatic H_2O content. There is no systematic geochemical variation between lava domes of the Silver Hills, but there is an observed systematic shift in $^{143}Nd/^{144}Nd$ to progressively less radiogenic values with time, which is inferred to result from mantle heterogeneity.

Tephra layers from core U1396C have been analysed for Pb-Nd-Sr isotope and major and trace element data, which provide a record of the geochemical evolution of volcanism on Montserrat and Guadeloupe over the past ~4.5 Ma; 2.3 and 1.7 Ma longer than their respective terrestrial records. The main geochemical change for the Montserrat source region occurred ~4.5–3.9 Ma, resulting from an increase in slab sediment contribution to the mantle wedge via an aqueous fluid. Tephra layers from Guadeloupe display greater temporal geochemical variation, driven by crustal assimilation of mid-ocean ridge basalt.

Componentry, grain size and grain morphology analyses of the thickest tephra layer in core U1396C derived from Guadeloupe, $T_{2.36}$, reveal it was formed by deposition from fallout from an eruption column, followed by a co-ignimbrite ash cloud from the same eruption. Eruption reconstructions suggest that this deposit likely formed from a VEI 6 eruption.

Table of Contents

Table of Tables

Table of Figures

Academic Thesis: Declaration Of Authorship

I, Stuart James Hatter declare that this thesis entitled 'The long-term evolution of Montserrat volcanism' and the work presented in it are my own and has been generated by me as the result of my own original research.

I confirm that:

1. This work was done wholly or mainly while in candidature for a research degree at this University;
2. Where any part of this thesis has previously been submitted for a degree or any other qualification at this University or any other institution, this has been clearly stated;
3. Where I have consulted the published work of others, this is always clearly attributed;
4. Where I have quoted from the work of others, the source is always given. With the exception of such quotations, this thesis is entirely my own work;
5. I have acknowledged all main sources of help;
6. Where the thesis is based on work done by myself jointly with others, I have made clear exactly what was done by others and what I have contributed myself;
7. Parts of this work have been published as:

Palmer, M. R., S. J. Hatter, T. M. Gernon, R. N. Taylor, M. Cassidy, P. Johnson, A. Le Friant, and O. Ishizuka, 2016. Discovery of a large 2.4 Ma Plinian eruption of Basse-Terre, Guadeloupe, from the marine sediment record. *Geology*, *44*(2), 123–126, doi:10.1130/G37193.1.

S. J. Hatter, M. R. Palmer, T. M. Gernon, R. N. Taylor, P. D. Cole, D. N. Barfod, and M. Coussens, 2018. The evolution of the Silver Hills volcanic centre, and revised $^{40}Ar/^{39}Ar$ geochronology of Montserrat, Lesser Antilles, with implications for island arc volcanism. *Geochemistry, Geophysics, Geosystems,* 19, doi:10.1002/2017GC007053

Signed: .....

Date: .....

Acknowledgements

I would like to thank my supervisors, Martin Palmer, Tom Gernon and Rex Taylor, for having the confidence to entrust me with this PhD project, and giving me this great opportunity. Their expert guidance, support, and feedback have been invaluable in helping me to develop the skills needed to complete this thesis, and I am grateful for them always having an open door. I would also like to thank Martin Jutzeler for our many discussions on determining the mode of deposition of tephra layers, and for his assistance with using the Malvern. Thanks go to Mike Cassidy for his assistance with the grain morphology method, and for general discussions on Montserrat volcanism. Thanks also to Maya Coussens for her help and support throughout this project, and for our many discussions on all things Montserrat. I would also like to thank Melanie Siegburg and Ruth Farley for discussions on lab methods and general volcanology.

I would like to thank Paul Cole for his assistance during the start of fieldwork, and for showing me the sites of Montserrat. Thanks also to Adam Stinton for help with fieldwork, and for looking after my safety.

Thanks to Agnes Michalik for her endless patience and support in the clean geochemistry and instrument labs, it has been invaluable. Thanks also to Andy Milton for his invaluable expertise in running the Neptune, and to Matt Cooper for assistance in the clean lab, and in particular with TIMS. Thanks also to Bob & John and Dan for making the thin sections, and to Tom Knott with his assistance with preparing and running samples for XRF. I would also like to thank Dan Barfod for his guidance and expertise with $^{40}Ar/^{39}Ar$ dating, and also Jim Imlach who assisted with sample preparation. I am also grateful to Jack Palmer and Josh Brown for their assistance with picking samples for $^{40}Ar/^{39}Ar$ dating.

Thanks to my family, Mum, Dad, Lee and Joanna, for your support and encouragement. Special thanks go to the Padwell crew, Josh, Matt, Amy, Nico, James and Sara, for making these past 4 years much more fun, I couldn't have asked for better housemates. Extra thanks go to James Fielding for providing me with a place to live at the breakup of Padwell, for organising many trips to escape Southampton, and for providing support during the later stages of this PhD. Thanks also to Jesse and Helen for introducing me to bouldering, and encouraging me to go regularly to help escape from work and relax. Finally, I would like to thank the 'lunch bunch', Ed, Harriet, Gabrielle, Sev, James, Tim and Matt, for providing entertaining midday breaks.

Chapter 1: Introduction

1.1 Project rationale

Studying the long-term behaviour of volcanism at individual volcanic centres, and throughout the history of a given arc island, may reveal insight into the processes controlling eruption styles and geochemical evolution of magmas, and how they change with time. However, understanding the long-term evolution of arc volcanism from the on-land record alone is difficult; older deposits become progressively buried by successive activity, obscured by vegetation, or eroded out. A complimentary approach to this problem is provided by study of marine sediment cores, which may contain a more complete record of volcanic activity. For example, it has been calculated that ~75% of material erupted from Soufriere Hills from 1995–2005 ended up in the Caribbean Sea (Le Friant et al., 2009). In this context, this thesis investigates the long-term geochemical evolution of volcanism on Montserrat and Guadeloupe through the study of tephra layers from marine sediment core U1396C, to examine which processes play a key role in controlling geochemical evolution in island arcs. In addition, the terrestrial record of the oldest volcanic centre on Montserrat, the Silver Hills, is studied to examine how eruption style and geochemistry of volcanic deposits varies over the course of an individual volcanic centre.

1.2 Lesser Antilles arc

1.2.1 Geological setting and arc structure

The Caribbean plate formed ~100–75 Ma over the Galapagos hotspot, from where it drifted and became inserted between the North and South American plates during the Late Campanian to Late Eocene (Pindell and Barrett, 1990). The Lesser Antilles is a ~750 km long intra-oceanic island arc at the eastern boundary of the Caribbean plate, formed from subduction of the Atlantic crust beneath the Caribbean plate. Subduction was initiated ~40 Ma (Briden et al., 1979), forming the Old arc (Grenada to Anguilla; Figure 1.1). This subduction phase stopped at the beginning of the Late Oligocene as a buoyant ridge of anomalous mid-Cretaceous crust reached the subduction zone in the northern part of the arc. After 9–10 Myr activity resumed, forming the Recent arc (Grenada to Saba; Figure 1.1). South of Martinique, activity resumed along the same place as the Old arc, but north of Martinique there was a progressive westward shift, forming the Inner arc (Dominica to Saba) (Bouysse and Westercamp, 1990).

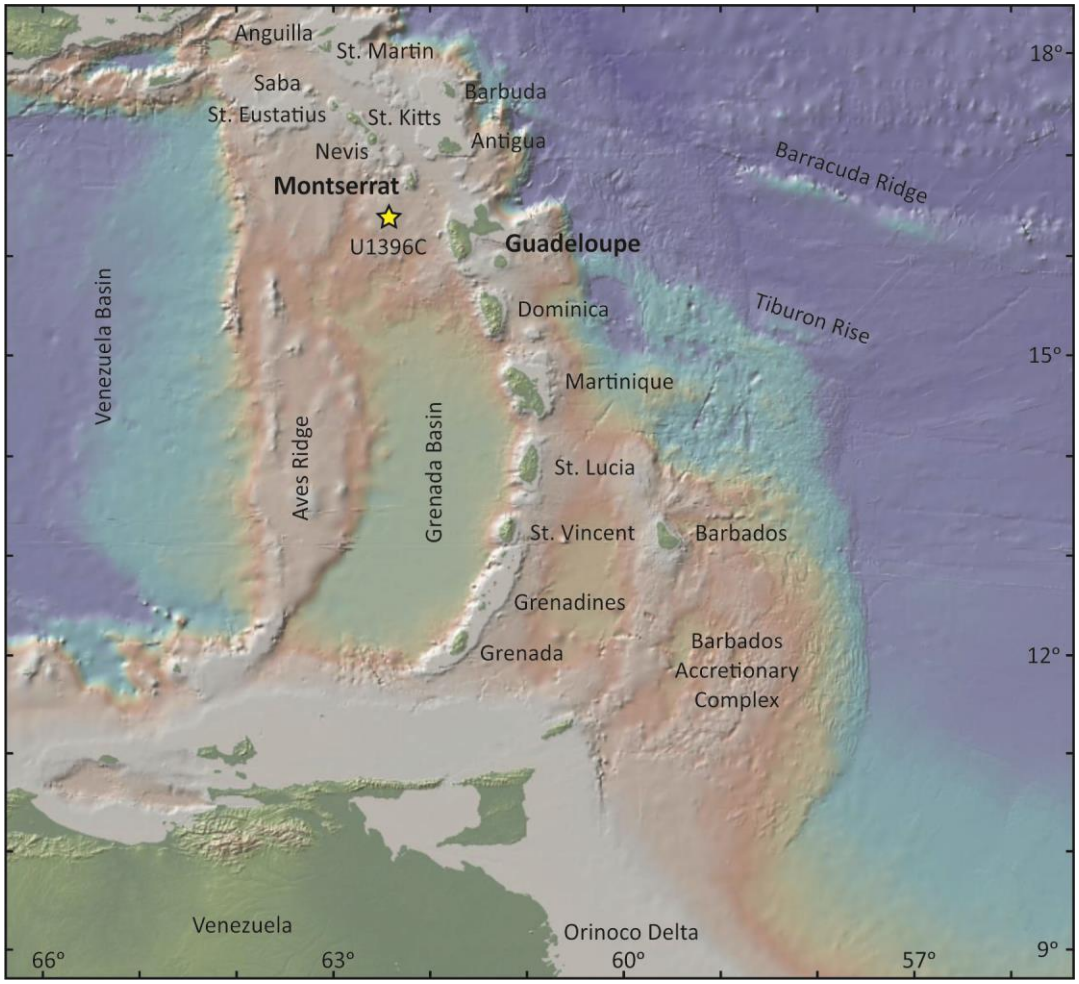

Figure 1.1. Map of Lesser Antilles showing the location of Montserrat, Guadeloupe and core site U1396C.

The age of the basaltic basement of the subducting Atlantic slab approaching the trench varies along the length of the arc, from ~105 Ma in the south (near St. Vincent), to ~83 Ma in the north (near Saba) (Carpentier et al., 2008). The Benioff zone beneath the arc is split into two segments; from Martinique northwards it strikes NNW, with a dip of 50–60° to a maximum depth of 210 km, while from St. Lucia southwards it trends NNE, with a lower dip of 45–50° to a maximum depth of 170 km (Wadge and Shepherd, 1984). The current convergence rate of the Lesser Antilles is ~2 cm/yr (Minster and Jordan, 1978; Pindell and Barrett, 1990).

The forearc region dominantly consists of the Barbados Accretionary Complex, which increases in thickness along the arc from north to south. At its thickest it is 20 km, where it emerges above sea level to form the island of Barbados (Macdonald et al., 2000). This variation in size reflects the north-south change in the thickness of sediment cover on the subducting Atlantic crust, which ranges from 200–300 m north of the Barracuda Rise (Tucholke et al., 1982) to 7 km in the south at 11°N, opposite the Orinoco delta (Westbrook et al., 1984). In the north, sediment is dominantly pelagic, but in the south, sediments contain a large proportion of terrigenous material, sourced from the Archaean Guiana Highlands of the

South American craton via the Orinoco River, and to a lesser extent the Amazon River (Westbrook et al., 1984; White and Dupré, 1986).

The crust beneath the Lesser Antilles varies in thickness along the arc: 27 km around Barbuda (Whitmarsh et al., 1983), ~30 km in the region of Montserrat to Guadeloupe (Boynton et al., 1979; Sevilla et al., 2010), ~30 km and ~34 km beneath Martinique and St. Vincent, respectively, (Boynton et al., 1979), and ~24 km at the southern end of the arc, around Grenada (Christeson et al., 2008). The Lesser Antilles arc is believed to be built upon oceanic crust, similar to that of the Venezuela Basin crust (Boynton et al., 1979; Christeson et al., 2008; Diebold et al., 1999; Sevilla et al., 2010; Speed et al., 1993; Speed and Walker, 1991). Some authors have also speculated that this oceanic crust is overlain by the accretionary prism of the former Aves arc (Davidson and Harmon, 1989; Macdonald et al., 2000). The evidence of crustal assimilation of material with a 'continental' signature indicates that sedimentary material is present within at least some parts of the arc crust (e.g. Bezard et al., 2014; Davidson and Wilson, 2011; Davidson and Harmon, 1989; Thirlwall et al., 1996).

1.2.2 Geochemistry of the Lesser Antilles Arc

The Lesser Antilles arc has a well-documented north-south geochemical variation, with Pb and Sr isotopes becoming more radiogenic and $^{143}Nd/^{144}Nd$ less radiogenic from north to south, accompanied by an increase in K, Sr, Ba and LREE's, and a general increase in ($^{230}Th/^{238}U$) (Brown et al., 1977; Davidson, 1987; Hawkesworth and Powell, 1980; Turner et al., 1996; White and Dupré, 1986). The cause of this geochemical gradient is widely attributed to be from an increasing addition of a sedimentary component towards the south of the arc, sourced from either crust assimilation (Bezard et al., 2014, 2015a, 2015b; Defant et al., 2001; Toothill et al., 2007), the subducting sediment (Carpentier et al., 2008; Cassidy et al., 2012; DuFrane et al., 2009; Labanieh et al., 2010; Turner et al., 1996; White and Dupré, 1986), or a combination of the two (Davidson and Wilson, 2011; Davidson, 1987; Smith et al., 1997; Thirlwall et al., 1996).

Geochemical variations in He and O isotopes provide evidence for along-arc variations in crustal assimilation (Van Soest et al., 2002). In the north of the arc (Saba to Martinique) $^{3}He/^{4}He$ values are mid-ocean ridge basalt- (MORB) like for olivine phenocrysts, but are more radiogenic in pyroxenes, indicating that assimilation occurred at a late stage in the evolution of the magma. In addition, $\delta^{18}O$ values are slightly decreased relative to anticipated mantle values, suggesting assimilation from hydrothermally altered magmatic wall rock from high levels in the crust. For the south of the arc (Martinique to Grenada) both olivine and pyroxene display more radiogenic $^{3}He/^{4}He$ compared to MORB, suggesting that for this part of the arc, assimilation took place earlier in the evolution of the magma at greater depth.

Furthermore, some samples from the southern arc show elevated oxygen isotopes compared with mantle peridotite, which are interpreted to represent assimilation of terrigenous sediment within the crust (Van Soest et al., 2002). However, the northern islands of Saba and St. Eustatius contain evidence for assimilation deeper within the crust of a small amount of biogenic sediment, inferred from positive correlations between $^{208}Pb/^{204}Pb$ (St. Eustatius only), Ba/La and La/Sm with SiO_2 (Defant et al., 2001; Toothill et al., 2007). On St. Lucia, positive correlations between mineral $\delta^{18}O$ and whole-rock Pb, Nd and Sr isotopes indicate that 20–40% crustal assimilation of sedimentary material is responsible for the variation of isotope values observed. Furthermore, it is argued that assimilation is responsible for the isotopic variation along the whole arc, because the range of isotopic values observed on St. Lucia encompasses that majority of values across the Lesser Antilles (Bezard et al., 2014).

While most middle-deep crustal assimilation has an inferred sedimentary assimilant (e.g. Bezard et al., 2014; Davidson, 1987; Defant et al., 2001; Thirlwall et al., 1996; Toothill et al., 2007), there is evidence for a none-sedimentary assimilant on St. Lucia and Martinique. For St. Lucia, covariance of $^{187}Os/^{188}Os$ with MgO provides evidence for assimilation, with the assimilant inferred to have MORB-like $^{87}Sr/^{86}Sr$, and is interpreted to correspond to plagioclase-rich early-arc cumulates in the middle-lower crust (Bezard et al., 2015a). On Martinique, assimilation of variable amounts of both sediment and altered oceanic crust (AOC) has been proposed as a cause of the observed range in $\delta^{11}B$ values (Smith et al., 1997).

There are lavas on Grenada with Pb isotope values which were initially thought to be more radiogenic than the subducting sediment, and so had to result from crustal assimilation (Thirlwall et al., 1996). However, black shales identified within sediment core 144, from Deep Sea Drilling Program (DSDP) Leg 14, were measured to have Pb isotope values much more radiogenic than any lavas on Grenada (Carpentier et al., 2008), and so the radiogenic lavas could have formed from the addition of slab sediment consisting of 18% black shale and 82% marl. This model is supported by Mo isotopes, because lavas of the southern Lesser Antilles have high $^{98}Mo/^{95}Mo$ values, which is inferred to come from the Site 144 black shales, which have high $^{98}Mo/^{95}Mo$. Furthermore, the lack of correlation between $^{98}Mo/^{95}Mo$ and SiO_2 for the radiogenic lavas suggest that the black shales were added from the subducting sediment, not from the crust (Freymuth et al., 2016).

Estimates for the amount of sediment addition from the subducting slab vary: the mixing calculations of White and Dupré, (1986) suggest that most isotopic compositions of the Lesser Antilles volcanic rocks could be explained by a ≤3% slab sediment addition to the mantle wedge, but the mass balance equations of Turner et al., (1996) estimate that sediment addition ranges from ~2% in the north, to ~15% in the south. More recent mixing models calculate that across the Lesser Antilles arc some compositions require bulk sediment

addition of 0.2–2%, while others require sediment partial melt addition of 0.4–2% (assuming 20% partial melting of the sediment). Sediment melt dominates in the south of the arc, with bulk sediment addition becoming increasingly important further north, and accounting for the majority of the geochemical trends in rocks from Saba, St. Eustatius, St. Kitts and Redonda. The amount of sediment addition required also varies within individual islands. For example, Pb-Sr-Nd-Hf isotope mixing models indicate that the range of compositions observed on Martinique can be explained by the addition of 0.2–5% slab sediment. Interestingly, assimilation models of the same study fail to produce the observed isotopic trends (Labanieh et al., 2010).

1.3 Montserrat

Montserrat is an active volcanic island in the north of the recent Lesser Antilles arc. The earliest study of Montserrat identified seven discrete volcanic centres, based on detailed field mapping and the island's geomorphology (Macgregor, 1938). Based on the results of K-Ar dating this was later revised to six volcanic centres, with a different relative order of activity; the oldest age obtained was ~4.3 Ma (Rea, 1974). More recent $^{40}Ar/^{39}Ar$ dating, however, has revealed these early K-Ar dates of Rea, (1974) to be inaccurate, and identify only four volcanic centres on Montserrat: Silver Hills (*c.* 2580-1160 ka), Centre Hills (*c*. 1020-480 ka), Soufrière Hills (*c.* 280 ka to present) and South Soufrière Hills (*c*. 130 ka; Figure 1.2) (Coussens et al., 2017; Harford et al., 2002). These ages reveal a systematic north to south migration of volcanic activity with time (Figure 1.2). The north of the island is comprised of the Silver Hills, a deeply eroded volcanic centre comprised of two-pyroxene andesite (Rea, 1974) with volcaniclastic sequences, debris avalanche deposits and areas of extensive hydrothermal alteration (Harford et al., 2002; Rea, 1974). The Centre Hills is comprised of two-pyroxene andesite and hornblende-hypersthene andesite (Rea, 1974) with abundant pumiceous deposits. Coussens et al., (2017) identified 11 thick (>1 m) pumiceous units derived from sustained explosive eruptions, which occur throughout the life of the Centre Hills, providing evidence for the largest known eruptions on Montserrat (up to magnitude 5). These deposits are interbedded with block-and-ash flow, lahar, fluvial and debris avalanche deposits, along with >10 other, less well-exposed pumiceous deposits (Coussens et al., 2017; Harford et al., 2002).

Deposits of the Soufrière Hills volcanic centre are dominated by andesitic lava domes and block-and-ash flow deposits, with pumice fall, pumice-and-ash flow, lahar and debris avalanche deposits also present (Harford et al., 2002; Rea, 1974; Roobol and Smith, 1998; Smith et al., 2007). The largest known eruptions of the Soufrière Hills occurred ~174 ka, evidenced by multiple pumice-rich pyroclastic density current deposits 1–3 m thick and a

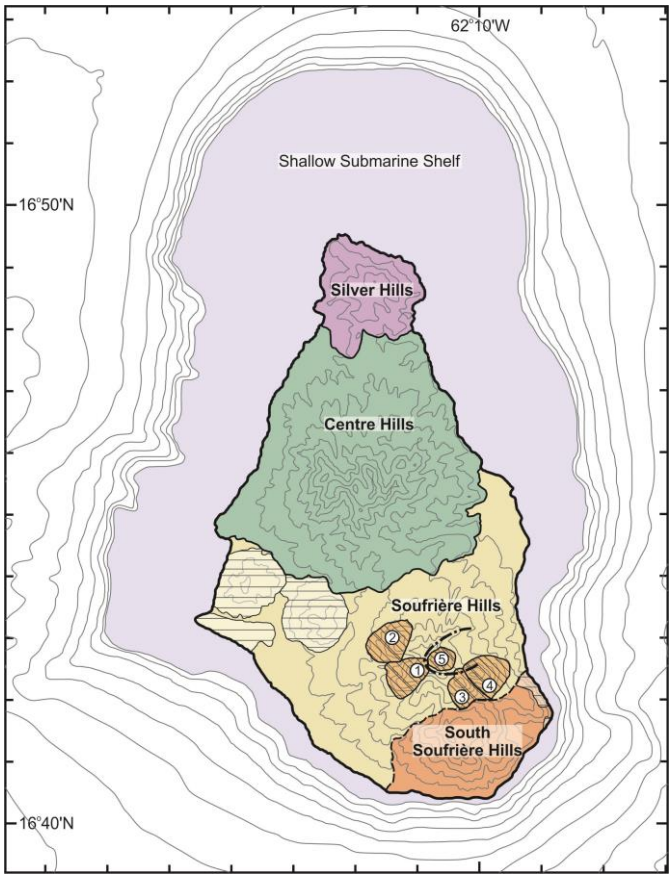

Figure 1.2. Map of Montserrat pre-1995–2010 eruption, with bathymetry (100 m intervals), showing the location of the volcanic centres. Pale areas with horizontal stripes are uplifted regions. Orange areas with diagonal stripes within the Soufrière Hills show the locations of the lava domes: 1, Chances Peak; 2, Gages Mountain; 3, Galway's Mountain; 4, Perches Mountain; 5, Castle Peak. Dot-dashed line shows edge of English's Crater.

pumice fall deposit 1 m thick ~3 km from the probable source (Harford et al., 2002; Smith et al., 2007). The petrology of the erupted andesites changed during the lifetime of the Soufrière Hills, from two-pyroxene andesites during ~280–150 ka, to hypersthene-hornblende andesites from ~110 ka to present. This change in petrology was not accompanied by any change in whole rock geochemistry. The exact cause of this change in petrology is unknown, but is thought to be linked to the development of the short-lived South Soufrière Hills, which was active ~130 ka (Harford et al., 2002). The South Soufrière Hills produced the only known mafic eruptions on Montserrat, with deposits dominated by basaltic to basaltic andesite lava flows with flow collapse breccias and scoria-fall deposits, and some andesitic fallout (Cassidy et al., 2014; Harford et al., 2002; Rea, 1974).

The Soufrière Hills is currently comprised of a central lava dome complex surrounded by andesitic volcaniclastic deposits. The dome complex is comprised of four older domes (Chances Peak, Gages Mountain, Galway's Mountain and Perches Mountain) (Harford et al., 2002), plus the modern dome within English's Crater from the recent eruption (1995–2010; Figure 1.2), which has undergone successive growth and collapse during the recent eruption.

Indeed, the current eruptive phase has been dominated by a mixture of Vulcanian explosions, dome growth and dome collapse events (Kokelaar, 2002; Wadge et al., 2014). The lavas of the recent eruption contain mafic enclaves, which make up 1–12% of the rock, resulting from magma mixing (Barclay et al., 2010; Komorowski et al., 2010; Murphy et al., 1998, 2000; Plail et al., 2014). Three types of enclaves have been identified: type A are mafic (basalt to basaltic andesite), glassy, have chilled margins, and have a low inherited phenocryst content; type B are more evolved (basaltic andesite to andesite), more crystalline with diffuse margins, and have a higher inhered phenocryst content; type C are composite, with a type A interior and type B exterior (Plail et al., 2014). The mafic enclaves result from the intrusion of mafic magma into a more evolved, andesitic magma, with type A enclaves representing the mafic magma, and type B enclaves forming hybrid compositions from mixing of the mafic magma with the host andesite magma (Plail et al., 2014). The intrusion of fresh hot mafic magma introduces heat and volatiles into the magma chamber, which can remobilise the andesitic magma and trigger an eruption. This process is considered to be the main eruption trigger for the Soufrière Hills during the 1995–2010 eruption (Devine et al., 1998; Murphy et al., 1998, 2000).

Various petrological (Barclay et al., 1998; Devine et al., 1998) and geophysical (Elsworth et al., 2008, 2014, Foroozan et al., 2010, 2011; Hautmann et al., 2014; Mattioli et al., 1998; Paulatto et al., 2012) models provide evidence for an upper crustal magma chamber beneath Soufrière Hills at a depth of ~5–7.5 km. There is also evidence for a second, deep chamber located within the lower crust, but there is uncertainty as to its precise depth. Estimates range from ~12 km (Elsworth et al., 2008; Hautmann et al., 2014), to around 17–19 km depth (Elsworth et al., 2014; Foroozan et al., 2010, 2011).

There is limited geochemical data for the Silver Hills, but it is very similar in composition to the Centre Hills. The only observed difference between the two centres is in $^{143}Nd/^{144}Nd$, for which the two centres have a different range of values. However, this is based on a limited data set, with only four and five data points for the Silver Hills and Centre Hills, respectively (Cassidy et al., 2012). There is a more pronounced difference between the Silver and Centre Hills, and the Soufrière Hills, with the later having less radiogenic Pb isotope values, and higher Ba/La and LREE enrichment. This is interpreted to result from a reduced sediment contribution to the mantle source relative to AOC fluid for Soufrière Hills melts (Cassidy et al., 2012), with mixing models calculating that 1–3% sediment melt contribution is required to produce the range of Soufrière Hills compositions (Cassidy et al., 2012; Zellmer et al., 2003). The South Soufrière Hills is the most chemically distinct volcanic centre on Montserrat, with the lowest L/MREE ratios, and highest fluid-mobile element/REE ratios, ($^{238}U/^{232}Th$), and ($^{230}Th/^{232}Th$). Furthermore, its Pb isotope compositions are not only more radiogenic than the Soufrière Hills, but also form a linear array tangential to the main

Lesser Antilles arc array (Cassidy et al., 2012; Zellmer et al., 2003). These geochemical features are interpreted as resulting from reduced slab sediment and increased slab fluid component contribution to the mantle source region, with only ~0.5% sediment addition required to produce the South Soufrière Hills compositions. The unique Pb isotope array also indicates a contribution from a MORB-like mantle wedge influenced by a Galapagos plume-like source (Cassidy et al., 2012). The short-lived and geochemically distinctive South Soufrière Hills is hypothesised to have formed as a result of the regional transtensional stress regime, which allowed for the extraction of magma sourced from a shallower point on the subducting slab, with faulting providing a conduit for magma ascent (Cassidy et al., 2012, 2015).

1.4 Guadeloupe

The Guadeloupe archipelago (Figure 1.3) formed from activity during both the Recent and Old arcs. The eastern islands of Grande-Terre, La Désirade, Petite-Terre and Marie-Galante form part of the Old arc, while the western islands of Basse-Terre and Les Saintes (Terre-de-Haut and Terre-de-Bas) form part of the Recent arc. The islands of the Old arc are comprised of Plio-Pleistocene limestones, underlain by Miocene volcanics (Carlut et al., 2000; Maury et al., 1990).

Volcanism on Basse-Terre, Guadeloupe has been focused at six volcanic centres: Basal Complex (2.79–2.69 Ma), Septentrional Chain (1.80–1.15 Ma), Axial Chain (1.02–0.41 Ma), Bouillante Province (1.20–0.60 Ma), Monts Caraïbes Massif (0.56–0.47 Ma), and the Grande Découverte Volcanic Complex (GDVC; 0.21 Ma to present), which is home to the islands current active volcano La Soufrière (Figure 1.3) (Carlut et al., 2000; Ricci et al., 2015a, 2015b, Samper et al., 2007, 2009).

The Basal Complex was dominated by effusive activity, being comprised of lava flows and domes. The Septentrional Chain was dominated by effusive fissural activity, with exposures ranging from thick basaltic lava flows to the dacitic domes of Les Mamelles (Maury et al., 1990; Samper et al., 2007). The Axial Chain was also dominated by effusive activity, ranging from submarine fissural volcanism producing hyaloclastite, to andesitic lava flows and domes. This was accompanied by explosive eruptions, producing multiple 10 m thick pyroclastic density current deposits, many of which are interbedded with ash and pumice fall deposits (Maury et al., 1990; Samper et al., 2007; Vatin-Perignon et al., 1984). The Bouillante Province was constructed by submarine and subaerial eruptions, including many monogenetic volcanoes, and contains a large compositional range of lavas, from olivine basalts, through andesites and dacites, to quartz-rhyolite lavas, locally interbedded with pyroclastic sequences (Blanc, 1983; Komorowski et al., 2005). The Monts Caraïbes Massif

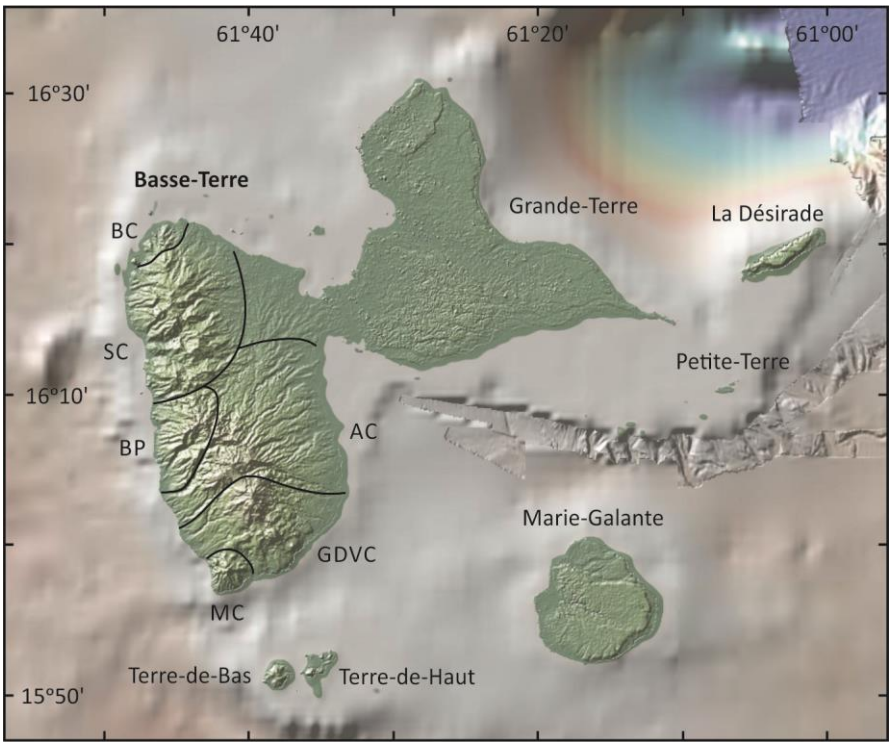

Figure 1.3. Map of the Guadeloupe archipelago, showing the location of the different volcanic centres on Basse-Terre: BC, Basal Complex; SC, Septentrional Chain; BP, Bouillante Province; AC, Axial Chain; MC, Monts Caraïbes Massif; GDVC, Grande Découverte Volcanic Complex.

began with Surtseyan-style submarine activity, followed by hydromagmatic activity, then by a mixture of subaerial lava flows and phreatomagmatic products (Westercamp and Tazieff, 1980). In the later stages of this centre activity transitioned to explosive subaerial eruptions, including dacitic Plinian eruptions. Deposits are intercalated lava flows and pyroclastic sequences (Komorowski et al., 2005).

The GDVC is dominated by effusive activity producing andesitic to dacitic lava flows and domes, with associated pyroclastic products. It has also produced explosive eruptions, including multiple Plinian events (Komorowski et al., 2005; Vatin-Perignon et al., 1984). Within the GDVC, The Trois-Rivières-Madeleine Complex exhibited more mafic eruptions, producing basaltic andesite lava and scoria cones (Komorowski et al., 2005). Within the GDVC is the currently active La Soufrière volcano, which has been active from ~11.5–0 ka. It is characterised by lava dome growth eruptions and their associated block-and-ash flow, pumice- and scoria-and-ash flow, and pumice and scoria fallout deposits (Komorowski et al., 2005). The most recent magmatic eruption of La Soufrière occurred in 1530 AD, producing sub-Plinian scoria fallout, column-collapse pyroclastic density currents, near-vent scoria fountains, and an andesitic lava dome (Boudon et al., 2008). Since 1530 AD, there have been six phreatic eruptions at La Soufrière: 1690, 1797–98, 1812, 1836–37, 1956 and 1976–77 (Komorowski et al., 2005).

Les Saintes islands are formed of two main volcanic islands; Terre-de-Haut (~2.98–2.00 Ma) and Terre-de-Bas (~0.92–0.88 Ma; Figure 1.3), which were built up in four successive stages (Zami et al., 2014). The first stage (~2.98 Ma) of Les Saintes volcanism, which produced Terre-de-Haut, was both effusive and explosive, with a mix of dacitic lava flows and explosive breccias. The second stage (~2.40 Ma) started with phreato-magmatic volcanism and produced pyroclastic density current deposits. The third stage (~2.08–2.00 Ma) was dominated by extrusion of andesitic domes with associated phreato-magmatic eruptions. The fourth stage (~0.916–0.882 Ma) created Terre-de-Bas, predominantly from andesite lava flows (Jacques et al., 1984; Zami et al., 2014).

1.5 International Ocean Discovery Program Expedition 340

1.5.1 Expedition overview

In February to March 2012 International Ocean Discovery Program (IODP) Expedition 340, the "Lesser Antilles Volcanism and Landslides" project, recovered marine sediment cores from nine sites along the Lesser Antilles; four off-shore Montserrat (U1393–7), and five off-shore Martinique (U1397–1401). The broad aim of this project is to develop a better understanding of the constructive and destructive processes related to island-arc volcanism. The project has three main scientific objectives (1–3), and two additional objectives (4–5): (1) identify the mechanisms controlling processes and timing of potentially tsunamigenic, large volcanic debris avalanches emplacement, (2) characterise the eruptive history to assess major volcanic hazards and volcano evolution, (3) characterise the magmatic cycles and long-term magmatic evolution of the arc, (4) characterise non-debris avalanche-related sedimentation processes in the deep ocean around the arc, and (5) determine the processes and element fluxes associated with submarine alteration of volcanic material (Le Friant et al., 2011). The work in this thesis contributes towards objectives (2) and (3), by assessing the eruptive and geochemical evolution of volcanism on Montserrat and Guadeloupe through study of marine tephra layers from core U1396C.

1.5.2 Site U1396

Site U1396 is located ~35 km southwest of Montserrat, and ~75 km northwest of Guadeloupe (16°30.49'N, 62°27.10'W; Figure 1.1). This location was chosen because it is on a topographic high, which reduces any perturbations (e.g. related to turbidites), and because drilling to the target depth of 132 metres below sea floor (mbsf) was predicted to recover sediments which extend back to ~4 Ma. This prediction was based on a calculated sedimentation rate of ~2.3 cm/kyr, derived from analysis of the 5.75 m long sediment core

CAR-MON 2 from the 2002 *Caraval* cruise, which was recovered from a nearby location (Le Friant et al., 2008). Because of the predicted age of sediment, the main object of site U1396 is to characterise the long-term eruptive history of Montserrat (Expedition 340 scientists, 2012).

Three cores were recovered from site U1396. Core U1396A extracted 134.9 m of sediment, with recovery of 140.51 m (104%). However, the core liner shattered during core 2H, leading to poor recovery. To counter this, a second hole (U1396B) was cored 20 m east of site U1396A, where a 9.5 m core was recovered (with recovery of 10.0 m; 105%), which covered the depth affected by the shattered core liner in hole U1396A. The third core, U1396C, recovered 139.4 m of sediment, with a recovery of 149.2 m (105%) (Expedition 340 scientists, 2013). Recovery of >100% is an artefact resulting from depressurisation of the cores on recovery. U1396C was chosen for this study as it contains the most complete record, and is well preserved, with only 3% disturbance (Jutzeler et al., 2016). Furthermore, age-depth models based on biostratigraphy, magnetostratigraphy, astrochronology, and stable isotope chemostratigraphy have been constructed for core U1396C, which provide a chronostratigraphic framework for precisely determining the age of deposition of each tephra layer, with an absolute uncertainty of ~50 kyr (Fraass et al., 2016; Hatfield, 2015).

1.5.3 Previous work on site U1396 tephra layers

The upper 7 m metres of core U1396C, covering ~250 ka, has been studied by Wall-Palmer et al., (2014), who identify volcaniclastic deposits from five different events, which can be correlated to other sediment cores south and southwest of Montserrat. Most of the units were interpreted as density-current deposits (volcaniclastic and bioclastic), with only one fallout deposit identified.

Componentry, grain size, and visual analyses were performed by Coussens et al., (2016) to determine the mode of deposition of tephra layers from the top ~20 m of core U1396C, covering the past ~1 Myr. Of the 24 tephra layers identified, 13 were interpreted as primary fallout deposits, 9 volcaniclastic turbidites, 1 bioclastic turbidite, and 1 mixed bioclastic-volcaniclastic turbidite. Volcaniclastic turbidites are inferred to be derived from pyroclastic density currents entering the sea, while mixed and bioclastic turbidites are likely from either flank collapse or carbonate shelf collapse (Coussens et al., 2016).

Palmer et al., (2016) studied an 18 cm thick tephra layer derived from a 2.36 Ma eruption on Basse-Terre, Guadeloupe (as revealed from Pb isotopes). Componentry, grain size and grain morphology analyses indicate that the lower 12 cm were deposited from primary tephra fallout, while the upper 6 cm were likely deposited from a co-ignimbrite ash

cloud. Eruption reconstruction calculations indicate that this previously unrecognised eruption was deposited from a ~VEI 6 Plinian eruption, which is believed to be the largest documented eruption in the Lesser Antilles.

The largest tephra layer in core U1396C is 1.2 m thick, has an age of ~4 Ma, and Pb isotopes indicate it was derived from an eruption on Montserrat. Detailed grain size, componentry and visual analyses indicate that this tephra layer formed from multiple closely spaced (<2 d) pyroclastic density currents which flowed over the ocean surface, before settling through the water column to deposit on the sea floor (Jutzeler et al., 2017).

1.6 Thesis overview

The volcanological and geochemical evolution of Montserrat is well constrained for the past ~1 Ma, but relatively little is known about older activity. This thesis aims to investigate the >1 Ma evolution of volcanism on Montserrat, by constructing a long-term record of eruption styles and of the geochemical evolution of volcanic deposits. It also aims to examine the geochemical evolution of volcanism on Guadeloupe, to provide insight into the temporal behaviour of processes controlling island arc chemistry. Chapter 2 describes the deposits of the Silver Hills volcanic centre to identify the eruption styles, and provides new age constraints on the timing of volcanic activity on Montserrat. Chapter 3 presents geochemical data for the Silver Hills, which investigates how geochemistry changes over the lifetime of an individual volcanic centre, and between individual domes. Chapter 4 studies the geochemistry of tephra layers from core U1396C to examine what processes control the long-term geochemical evolution of arc island volcanic deposits. Chapter 5 identifies a thick tephra layer sourced from an eruption on Guadeloupe, and reconstructs the eruption parameters.

Chapters 2–5 are presented in paper style format, so the relevant methods are described within each chapter, instead of in a separate methods chapter. A brief outline of each chapter is given below, with the key questions addressed in each one.

Chapter 2: The evolution of the Silver Hills volcanic centre, and revised $^{40}Ar/^{39}Ar$ geochronology of Montserrat, Lesser Antilles, with implications for island arc volcanism

This chapter provides the first detailed mapping of the Silver Hills volcanic centre, and describes the lithofacies and stratigraphy of the deposits. New $^{40}Ar/^{39}Ar$ ages for the Silver, Centre and Soufriere Hills are also presented, which are combined with ages of tephra layers

from core U1396C to produce a revised geochronology of volcanic activity on Montserrat. This new data addresses the following questions:

Q2.1: Did the style of volcanic activity change over the lifetime of the Silver Hills, and how does it compare to the Centre Hills and Soufrière Hills?

Q2.2: Did the petrology of the volcanic deposits of the Silver Hills change over the course of Silver Hills activity?

Q2.3: Has volcanic activity on Montserrat always been focused at one volcanic centre at any given time, or has there been overlap in activity between two volcanic centres?

This chapter has been published in *Geochemistry, Geophysics, Geosystems*.

Chapter 3: Geochemical evolution of the Silver Hills volcanic centre

This chapter presents new Pb-Nd-Sr isotope, trace element, and major element data for the Silver Hills volcanic centre, which are combined with the new $^{40}Ar/^{39}Ar$ dates presented in Chapter 3, to study the temporal evolution of the geochemistry of the Silver Hills. This chapter addresses the following key questions:

Q3.1: Does the chemistry of the Silver Hills volcanic centre systematically change during its lifetime?

Q3.2: Can the lavas of the Silver Hills be produced from fractionation of magmas with similar chemical compositions as the mafic enclaves hosted within the lavas?

This chapter forms the basis of a manuscript in preparation.

Chapter 4: Geochemical evolution of volcanism on Montserrat and Guadeloupe (Lesser Antilles arc), revealed from marine sediment core U1396C

This chapter presents new Pb-Nd-Sr isotope, trace element, and major element data for tephra layers from marine sediment core U1396C, spanning ~4.5 Ma. This core provides the longest accessible record of volcanic activity for both Montserrat and Guadeloupe, to provide insight into their geochemical evolution. This core is used to investigate the following key questions:

Q4.1: How does the geochemistry of arc islands evolve through time, and what is the dominant process driving any change (i.e. variations in mantle source components versus crustal assimilation)?

Q4.2: What is the cause of the difference in isotope geochemistry between Montserrat and Guadeloupe?

This chapter forms the basis of a manuscript in preparation.

Chapter 5: Discovery of a large 2.4 Ma Plinian eruption of Basse-Terre, Guadeloupe, from the marine sediment record

This chapter identifies a thick (18 cm) tephra layer aged 2.36 Ma, and aims to identify its mode of deposition, and reconstruct the eruption size. The following key questions are investigated:

Q5.1: What is the mode of deposition of tephra layer $T_{2.36}$?

Q5.2: What sized eruption produced tephra layer $T_{2.36}$?

This chapter is an expanded version of a paper which is published in *Geology*. It has been expanded to include work which was carried out as part of this project, but did not make it into the final publication due to the short-format nature of the journal.

1.7 References

Barclay, J., Herd, R.A., Edwards, B.R., Christopher, T., Kiddle, E.J., Plail, M., Donovan, A., 2010. Caught in the act: Implications for the increasing abundance of mafic enclaves during the recent eruptive episodes of the Soufrière Hills Volcano, Montserrat. Geophys. Res. Lett. 37, 1–5. doi:10.1029/2010GL042509

Barclay, J., Rutherford, M.J., Carroll, M.R., Murphy, M.D., Devine, J.D., Gardner, J., Sparks, R.S.J., 1998. Experimental phase equilibria constraints on pre-eruptive storage conditions of the Soufrière Hills magma. Geophys. Res. Lett. 25, 3437. doi:10.1029/98GL00856

Bezard, R., Davidson, J.P., Turner, S., Macpherson, C.G., Lindsay, J.M., Boyce, A.J., 2014. Assimilation of sediments embedded in the oceanic arc crust: Myth or reality? Earth Planet. Sci. Lett. 395, 51–60. doi:10.1016/j.epsl.2014.03.038

Bezard, R., Schaefer, B.F., Turner, S., Davidson, J.P., Selby, D., 2015a. Lower crustal assimilation in oceanic arcs: Insights from an osmium isotopic study of the Lesser Antilles. Geochim. Cosmochim. Acta 150, 330–344. doi:10.1016/j.gca.2014.11.009

Bezard, R., Turner, S., Davidson, J.P., Macpherson, C.G., Lindsay, J.M., 2015b. Seeing through the Effects of Crustal Assimilation to Assess the Source Composition beneath the

Southern Lesser Antilles Arc. J. Petrol. 56, 815–844. doi:10.1093/petrology/egv018

Blanc, F., 1983. Corrélation chronologiques et géochimiques des formations volcaniques du sud de la Basse-Terre de Guadeloupe (Petites Antilles). Université Grenoble.

Boudon, G., Komorowski, J.C., Villemant, B., Semet, M.P., 2008. A new scenario for the last magmatic eruption of La Soufrière of Guadeloupe (Lesser Antilles) in 1530 A.D. Evidence from stratigraphy radiocarbon dating and magmatic evolution of erupted products. J. Volcanol. Geotherm. Res. 178, 474–490. doi:10.1016/j.jvolgeores.2008.03.006

Bouysse, P., Westercamp, D., 1990. Subduction of the Atlantic aseismic ridges and late cenozoic evolution of the Lesser Antilles island-arc. Tectonophysics 175, 349–380.

Boynton, C.H., Westbrook, G.K., Bott, M.H.P., Long, R.E., 1979. Seismic Refraction Investigation of Crustal Structure Beneath the Lesser-Antilles Island Arc. Geophys. J. R. Astron. Soc. 58, 371–393. doi:10.1111/j.1365-246X.1979.tb01031.x

Briden, J.C., Rex, D.C., Faller, A.M., Tomblin, J.F., 1979. K-Ar geochronology and palaeomagnetism of volcanic rocks in the Lesser Antilles island arc. Philos. Trans. R. Soc. London A Math. Phys. Eng. Sci. 291, 485–528. doi:10.1098/rsta.1948.0007

Brown, G., Holland, J., Sigurdsson, H., Tomblin, J., Arculus, R., 1977. Geochemistry of the lesser Antilles island arc. Geochim. Cosmochim. Acta 41, 785–801.

Carlut, J., Quidelleur, X., Courtillot, V., Boudon, G., 2000. Paleomagnetic directions and K/Ar dating of 0 to 1 Ma lava flows from La Guadeloupe Island Implications for time-averaged field models. J. Geophys. Res. 105, 835–849. doi:10.1029/1999JB900238

Carpentier, M., Chauvel, C., Mattielli, N., 2008. Pb-Nd isotopic constraints on sedimentary input into the Lesser Antilles arc system. Earth Planet. Sci. Lett. 272, 199–211. doi:10.1016/j.epsl.2008.04.036

Cassidy, M., Edmonds, M., Watt, S.F.L., Palmer, M.R., Gernon, T.M., 2015. Origin of basalts by hybridization in andesite-dominated arcs. J. Petrol. 56, 325–346. doi:10.1093/petrology/egv002

Cassidy, M., Taylor, R.N., Palmer, M.R., Cooper, R.J., Stenlake, C., Trofimovs, J., 2012. Tracking the magmatic evolution of island arc volcanism: Insights from a high-precision Pb isotope record of Montserrat, Lesser Antilles. Geochemistry, Geophys. Geosystems 13, 1–19. doi:10.1029/2012GC004064

Cassidy, M., Trofimovs, J., Watt, S.F.L., Palmer, M.R., Taylor, R.N., Gernon, T.M., Talling, P.J., Le Friant, A., 2014. Multi-stage collapse events in the South Soufrière Hills, Montserrat as

recorded in marine sediment cores. Geol. Soc. London, Mem. 39, 383–397. doi:10.1144/M39.20

Christeson, G.L., Mann, P., Escalona, A., Aitken, T.J., 2008. Crustal structure of the Caribbean - Northeastern South America arc-continent collision zone. J. Geophys. Res. Solid Earth 113, 1–19. doi:10.1029/2007JB005373

Coussens, M., Cassidy, M., Watt, S.F.L., Jutzeler, M., Talling, P.J., Barfod, D., Gernon, T.M., Taylor, R., Hatter, S.J., Palmer, M.R., 2017. Long-term changes in explosive and effusive behaviour at andesitic arc volcanoes: Chronostratigraphy of the Centre Hills Volcano, Montserrat. J. Volcanol. Geotherm. Res. doi:10.1016/j.jvolgeores.2017.01.003

Coussens, M., Wall-Palmer, D., Talling, P.J., Watt, S.F.L., Hatter, S.J., Cassidy, M., Clare, M.A., Jutzeler, M., Hatfield, R., McCanta, M., Kataoka, K.S., Endo, D., Palmer, M.R., Stinton, A., Fujinawa, A., Boudon, G., Le Friant, A., Ishizuka, O., Gernon, T.M., Adachi, T., Aljahdali, M., Breitkreuz, C., Frass, A.J., Hornbach, M.J., Lebas, E., Lafuerza, S., Maeno, F., Manga, M., Martinez-Colon, M., McManus, J., Morgan, S., Saito, T., Slagle, A.L., Subramanyam, K.S.V., Tamura, Y., Trofimovs, J., Villemant, B., Wang, F., Expedition 340 scientists, 2016. Synthesis: stratigraphy and age control for IODP Sites U1394, U1395, and U1396 offshore Montserrat in the Lesser Antilles. Proc. Integr. Ocean Drill. Progr. 340, 19. doi:10.2204/iodp.proc.340.204.2016

Davidson, J., Wilson, M., 2011. Differentiation and source processes at Mt Pelée and the Quill; Active volcanoes in the Lesser Antilles arc. J. Petrol. 52, 1493–1531. doi:10.1093/petrology/egq095

Davidson, J.P., 1987. Crustal contamination versus subduction zone enrichment: Examples from the Lesser Antilles and implications for mantle source compositions of island arc volcanic rocks. Geochim. Cosmochim. Actamica 51, 2185–2198.

Davidson, J.P., Harmon, R.S., 1989. Oxygen isotope constraints on the petrogenesis of volcanic arc magmas from Martinique, Lesser Antilles. Earth Planet. Sci. Lett. 95, 255–270.

Defant, M.J., Sherman, S., Maury, R.C., Bellon, H., De Boer, J., Davidson, J., Kepezhinskas, P., 2001. The geology, petrology, and petrogenesis of Saba Island, Lesser Antilles. J. Volcanol. Geotherm. Res. 107, 87–111. doi:10.1016/S0377-0273(00)00268-7

Devine, J.D., Murphy, M.D., Rutherford, M.J., Barclay, J., Sparks, R.S.J., Carroll, M.R., Young, S.R., Gardner, J.E., 1998. Petrologic evidence for pre-eruptive pressure-temperature conditions, and recent reheating, of andesitic magma erupting at the Soufrière Hills Volcano, Montserrat, W.I. Geophys. Res. Lett. 25, 3669–3672. doi:10.1029/98GL01330

Diebold, J., Driscoll, N., Abrams, L., Buhl, P., Donnelly, T., Laine, E., Leroy, S., Toy, A., 1999. New insights on the formation of the caribbean basalt province revealed by multichannel seismic images of volcanic structures in the Venezuelan basin, in: Mann, P. (Ed.), Caribbean Basins. Sedimentary Basins of the World. Elsevier Science B. V., Amsterdam, pp. 561–589. doi:10.1016/S1874-5997(99)80053-7

DuFrane, S.A., Turner, S., Dosseto, A., van Soest, M., 2009. Reappraisal of fluid and sediment contributions to Lesser Antilles magmas. Chem. Geol. 265, 272–278. doi:10.1016/j.chemgeo.2009.03.030

Elsworth, D., Foroozan, R., Taron, J., Mattioli, G.S., Voight, B., 2014. Geodetic imaging of magma migration at Soufriere Hills Volcano 1995 to 2008, in: Wadge, G., Robertson, R.E.A., Voight, B. (Eds.), The Eruption of Soufrière Hills Volcano, Montserrat from 2000 to 2010. Geological Society, London, Memoirs, pp. 219–227. doi:10.1144/M39.12

Elsworth, D., Mattioli, G., Taron, J., Voight, B., Herd, R., 2008. Implications of magma transfer between multiple reservoirs on eruption cycling. Science, 322, 246–248. doi:10.1126/science.1161297

Expedition 340 scientists, 2013. Site U1396, in: Le Friant, A., Ishizuka, O., Stroncik, N.A., Expedition 340 scientists, (Eds.), Proceedings of the Integrated Ocean Drilling Program, 340. Integrated Ocean Drilling Program Managment Internation, Inc, Tokyo. doi:10.2204/iodp.proc.340.106.2013

Expedition 340 scientists, 2012. Lesser Antilles volcanism and landslides: implications for hazard assessment and long-term magmatic evolution of the arc. IODP Prelim. Rep. 340. doi:10.2204/iodp.pr.340.2012

Foroozan, R., Elsworth, D., Voight, B., Mattioli, G.S., 2011. Magmatic-metering controls the stopping and restarting of eruptions. Geophys. Res. Lett. 38, 1–5. doi:10.1029/2010GL046591

Foroozan, R., Elsworth, D., Voight, B., Mattioli, G.S., 2010. Dual reservoir structure at Soufrière Hills Volcano inferred from continuous GPS observations and heterogeneous elastic modeling. Geophys. Res. Lett. 37, 1–5. doi:10.1029/2010GL042511

Fraass, A.J., Wall-Palmer, D., Leckie, R.M., Hatfield, R.G., Burns, S.J., Le Friant, A., Ishizuka, O., Aljahdali, M., Jutzeler, M., Martinez-Colon, M., Palmer, M.R., Talling, P.J., 2016. A revised Plio-Pleistocene age model and paleoceanography of the northeastern Caribbean Sea: IODP Site U1396 off Montserrat, Lesser Antilles. Stratigraphy, 13, 183–203.

Freymuth, H., Elliott, T., van Soest, M., Skora, S., 2016. Tracing subducted black shales in the

Lesser Antilles arc using molybdenum isotope ratios. Geology 44, 987–990. doi:10.1130/G38344.1

Harford, C.L., Pringle, M.S., Sparks, R.S.J., Young, S.R., 2002. The volcanic evolution of Montserrat using 40Ar/39Ar geochronology. Geol. Soc. London, Mem. 21, 93–113. doi:10.1144/GSL.MEM.2002.021.01.05

Hatfield, R.G., 2015. Data report: stratigraphic correlation of Site U1396 and creation of a composite depth scale and splice 340, 1–17. doi:10.2204/iodp.proc.340.202.2015

Hautmann, S., Witham, F., Christopher, T., Cole, P., Linde, A.T., Sacks, I.S., Sparks, R.S.J., 2014. Strain field analysis on Montserrat (W.I.) as tool for assessing permeable flow paths in the magmatic system of Soufrière Hills Volcano. Geochemistry, Geophys. Geosystems 1–15. doi:10.1002/2013GC005087.

Hawkesworth, C.J., Powell, M., 1980. Magma genesis in the Lesser Antilles Island Arc. Earth Planet. Sci. Lett. 51, 297–308.

Jacques, D., Maury, R.C., Bellon, H., 1984. Géologie et géochronologie 40K-40Ar des îles des Saintes (Guadeloupe). Comptes-rendus des séances l'Académie des Sci. Série 2, Mécanique-physique, Chim. Sci. l'univers, Sci. la terre 299, 721–726.

Jutzeler, M., Manga, M., White, J.D.L., Talling, P.J., Proussevitch, A.A., Watt, S.F.L., Cassidy, M., Taylor, R.N., Le Friant, A., Ishizuka, O., 2017. Submarine deposits from pumiceous pyroclastic density currents traveling over water: An outstanding example from offshore Montserrat (IODP 340). Bull. Geol. Soc. Am. 129, 392–414. doi:10.1130/B31448.1

Jutzeler, M., Talling, P.J., White, J.D.L., Expedition 340 Scientists, 2016. Data report: Coring disturbances in IODP 340, a detailed list of intervals with fall-in and flow-in, in: Le Friant, A., Ishizuka, O., Stroncik, N.A., Expedition 340 Scientists (Eds.), Proc. IODP, 340. Integrated Ocean Drilling Program Management International, Inc., Tokyo, Japan.

Kokelaar, B.P., 2002. Setting, chronology and consequences of the eruption of Soufrière Hills Volcano, Montserrat (1995-1999). Erupt. Soufrière Hills Volcano, Montserrat, from 1995 to 1999 21, 1–43. doi:10.1144/GSL.MEM.2002.021.01.02

Komorowski, J.C., Boudon, G., Smet, M., Beauducel, F., Antenor-Habazac, C., Bazin, S., Hammouya, G., 2005. Guadeloupe, in: Unit, S.R. (Ed.), Volcanic Hazard Atlas of the Lesser Antilles. University of the West Indies, St Augustine, Trinidad, W.I., pp. 67–104.

Komorowski, J.C., Legendre, Y., Christopher, T., Bernstein, M., Stewart, R., Joseph, E., Fournier, N., Chardot, L., Finizola, A., Wadge, G., Syers, R., Williams, C., Bass, V., 2010. Insights into

processes and deposits of hazardous vulcanian explosions at Soufrière Hills Volcano during 2008 and 2009 (Montserrat, West Indies). Geophys. Res. Lett. 37, 1–6. doi:10.1029/2010GL042558

Labanieh, S., Chauvel, C., Germa, A., Quidelleur, X., Lewin, E., 2010. Isotopic hyperbolas constrain sources and processes under the Lesser Antilles arc. Earth Planet. Sci. Lett. 298, 35–46. doi:10.1016/j.epsl.2010.07.018

Le Friant, A., Deplus, C., Boudon, G., Sparks, R.S.J., Trofimovs, J., Talling, P., 2009. Submarine deposition of volcaniclastic material from the 1995 – 2005 eruptions of Soufrière Hills volcano , Montserrat. J. Geol. Soc. London 166, 171–182. doi:10.1144/0016-76492008-047.Submarine

Le Friant, A., Ishizuka, O., Stroncik, N., 2011. Lesser Antilles volcanism and landslides: drilling volcanic landslides deposits and volcanoclastic sediments in the Lesser Antilles arc : implications for hazard assessment and long-term magmatic evolution of the arc. Integr. Ocean Drill. Program. Sci. Prospect. Exped. 340 86. doi:10.2204/iodp.sp.340.2011

Le Friant, A., Lock, E.J., Hart, M.B., Boudon, G., Sparks, R.S.J., Leng, M., Smart, C.W., Komorowski, J.-C., Deplus, C., Fisher, J.K., 2008. Late Pleistocene tephrochronology of marine sediments adjacent to Montserrat, Lesser Antilles volcanic arc. J. Geol. Soc. London. 165, 279–289. doi:10.1144/0016-76492007-019

Macdonald, R., Hawkesworth, C.J., Heath, E., 2000. The Lesser Antilles volcanic chain: A study in arc magmatism. Earth Sci. Rev. 49, 1–76. doi:10.1016/S0012-8252(99)00069-0

Macgregor, A.G., 1938. The Royal Society Expedition to Montserrat, B.W.I. The Volcanic History and Petrology of Montserrat, with Observations on Mt Pelée, in Martinique. Philos. Trans. R. Soc. Lond. B. Biol. Sci. 229, 1–90.

Mattioli, G.S., Dixon, T.H., Farina, F., Howell, E.S., Jansma, P.E., Smith, A.L., 1998. GPS Measurement Of Surface Deformation Around Soufriere Hills Volcano, Montserrat From October 1995 to July 1996. Geophys. Res. Lett. 25, 3417–3420.

Maury, R.C., Westbrook, G.K., Baker, P.E., Bouysse, P., Westercamp, D., 1990. Geology of the Lesser Antilles, in: Dengo, G., Case, J.E. (Eds.), The Geology of North America, Vol. H, The Caribbean Region. Geological Society of America, Boulder, Colorado, pp. 141–166.

Minster, J.B., Jordan, T.H., 1978. Present-day plate motions. J. Geophys. Res. 83, 5331. doi:10.1029/JB083iB11p05331

Murphy, M.D., Sparks, R.S.J., Barclay, J., Carroll, M.R., Brewer, T.S., 2000. Remobilization of

Andesite Magma by Intrusion of Mafic Magma at the Soufrière Hills Volcano, Montserrat, West Indies. J. Petrol. 41, 21–42. doi:10.1093/petrology/41.1.21

Murphy, M.D., Sparks, R.S.J., Barclay, J., Carroll, M.R., Lejeune, A.M., Brewer, T.S., Macdonald, R., Black, S., Young, S., 1998. The role of magma mixing in trigerring the current eruption of the Soufrière Hills volcano, Montserrat, West Indies. Geophys. Res. Lett. 25, 3433–3436. doi:10.1029/98GL00713

Palmer, M.R., Hatter, S.J., Gernon, T.M., Taylor, R.N., Cassidy, M., Johnson, P., Le Friant, A., Ishizuka, O., 2016. Discovery of a large 2.4 Ma Plinian eruption of Basse-Terre, Guadeloupe, from the marine sediment record. Geol. 44, 123–126. doi:10.1130/G37193.1

Paulatto, M., Annen, C., Henstock, T.J., Kiddle, E., Minshull, T.A., Sparks, R.S.J., Voight, B., 2012. Magma chamber properties from integrated seismic tomography and thermal modeling at Montserrat. Geochemistry, Geophys. Geosystems 13, 1–18. doi:10.1029/2011GC003892

Pindell, J., Barrett, S., 1990. Geological evolution of the Caribbean region: A plate tectonic perspective, in: The Geology of North America, Vol. H. Geological Society of America, Boulder, Colorado, pp. 405–432.

Plail, M., Barclay, J., Humphreys, M.C.S., Edmonds, M., Herd, R.A., Christopher, T.E., 2014. Characterization of mafic enclaves in the erupted products of Soufrière Hills Volcano, Montserrat, 2009 to 2010. Geol. Soc. London, Mem. 39, 343–360. doi:10.1144/M39.18

Rea, W.J., 1974. The volcanic geology and petrology of Montserrat, West Indies. J. Geol. Soc. London. 130, 341–366. doi:10.1144/gsjgs.130.4.0341

Ricci, J., Lahitte, P., Quidelleur, X., 2015a. Construction and destruction rates of volcanoes within tropical environment: Examples from the Basse-Terre Island (Guadeloupe, Lesser Antilles). Geomorphology 228, 597–607. doi:10.1016/j.geomorph.2014.10.002

Ricci, J., Quidelleur, X., Lahitte, P., 2015b. Volcanic evolution of central Basse-Terre Island revisited on the basis of new geochronology and geomorphology data. Bull. Volcanol. 77, 84. doi:10.1007/s00445-015-0970-7

Roobol, M.J., Smith, A.L., 1998. Pyroclastic stratigraphy of the Soufrière Hills volcano, Montserrat - Implications for the present eruption. Geophys. Res. Lett. 25, 3393–3396. doi:10.1029/98GL00643

Samper, A., Quidelleur, X., Komorowski, J.-C., Lahitte, P., Boudon, G., 2009. Effusive history of

the Grande Découverte Volcanic Complex, southern Basse-Terre (Guadeloupe, French West Indies) from new K–Ar Cassignol–Gillot ages. J. Volcanol. Geotherm. Res. 187, 117–130. doi:10.1016/j.jvolgeores.2009.08.016

Samper, A., Quidelleur, X., Lahitte, P., Mollex, D., 2007. Timing of effusive volcanism and collapse events within an oceanic arc island: Basse-Terre, Guadeloupe archipelago (Lesser Antilles Arc). Earth Planet. Sci. Lett. 258, 175–191. doi:10.1016/j.epsl.2007.03.030

Sevilla, W.I., Ammon, C.J., Voight, B., De Angelis, S., 2010. Crustal structure beneath the Montserrat region of the Lesser Antilles island arc. Geochemistry, Geophys. Geosystems 11, 13. doi:10.1029/2010GC003048

Smith, A.L., Roobol, M.J., Schellekens, J.H., Mattioli, G.S., 2007. Prehistoric stratigraphy of the Soufrière Hills - South Soufrière Hills volcanic complex, Montserrat, West Indies. Geology 115, 115–127. doi:10.1086/509271

Smith, H.J., Leeman, W.P., Davidson, J., Spivack, A.J., 1997. The B isotopic composition of arc lavas from Martinique, Lesser Antilles. Earth Planet. Sci. Lett. 146, 303–314. doi:10.1016/S0012-821X(96)00209-9

Speed, R.C., Smith-Horowitz, P.L., Perch-Nielsen, K. v. S., Saunders, J.B., Sanfilippo, A.B., 1993. Southern Lesser Antilles Arc Platform: Pre-Late Miocene Stratigraphy, Structure, and Tectonic Evolution, in: Speed, R.C., Smith-Horowitz, P.L., Perch-Nielsen J, K.V.S., Saunders, B., Sanfilippo, A.B. (Eds.), Southern Lesser Antilles Arc Platform: Pre-Late Miocene Stratigraphy, Structure, and Tectonic Evolution. Geological Society of America.

Speed, R.C., Walker, J.A., 1991. Oceanic crust of the Grenada Basin in the Southern Lesser Antilles arc platform 96, 3835–3851.

Thirlwall, M.F., Graham, A.M., Arculus, R.J., Harmon, R.S., Macpherson, C.G., 1996. Resolution of the effects of crustal assimilation, sediment subduction, and fluid transport in island arc magmas: Pb-Sr-Nd-O isotope geochemistry of Grenada, Lesser Antilles. Geochim. Cosmochim. Acta 60, 4785–4810. doi:10.1016/S0016-7037(96)00272-4

Toothill, J., Williams, C. a., MacDonald, R., Turner, S.P., Rogers, N.W., Hawkesworth, C.J., Jerram, D. a., Ottley, C.J., Tindle, a. G., 2007. A complex petrogenesis for an arc magmatic suite, St Kitts, Lesser Antilles. J. Petrol. 48, 3–42. doi:10.1093/petrology/egl052

Tucholke, B.E., Houtz, R.E., Ludwig, W.J., 1982. Maps of sediment thickness and depth to basement in the western North Atlantic Ocean basin.

Turner, S., Hawkesworth, C., Van Calsteren, P., Heath, E., Macdonald, R., Black, S., 1996. U-series isotopes and destructive plate margin magma genesis in the Lesser Antilles. Earth Planet. Sci. Lett. 142, 191–207. doi:10.1016/0012-821X(96)00078-7

Van Soest, M.C., Hilton, D.R., Macpherson, C.G., Mattey, D.P., 2002. Resolving Sediment Subduction and Crustal Contamination in the Lesser Antilles Island Arc: a Combined He-O-Sr Isotope Approach. J. Petrol. 43, 143–170. doi:10.1093/petrology/43.1.143

Vatin-Perignon, N., Semet, M.P., Blanc, F., Joron, J.L., 1984. Petrochemistry of quaternary pumiceous pyroclastic products in southern Guadeloupe (F.W.I.). Bull. Volcanol. 47, 749–767. doi:10.1007/BF01952342

Wadge, G., Shepherd, J.B., 1984. Segmentation of the Lesser Antilles subduction zone. Earth Planet. Sci. Lett. 71, 297–304. doi:10.1016/0012-821X(84)90094-3

Wadge, G., Voight, B., Sparks, R.S.J., Cole, P.D., Loughlin, S.C., Robertson, R.E.A., 2014. An overview of the eruption of Soufrière Hills Volcano, Montserrat from 2000 to 2010. Geol. Soc. London, Mem. 39, 1–40. doi:10.1144/M39.1

Wall-Palmer, D., Coussens, M., Talling, P.J., Jutzeler, M., Cassidy, M., Marchant, I., Palmer, M.R., Watt, S.F.L., Smart, C.W., Fisher, J.K., Hart, M.B., Fraass, A., Trofimovs, J., Le Friant, A., Ishizuka, O., Adachi, T., Aljahdali, M., Boudon, G., Breitkreuz, C., Endo, D., Fujinawa, A., Hatfield, R., Hornbach, M.J., Kataoka, K., Lafuerza, S., Maeno, F., Manga, M., Martinez-Colon, M., McCanta, M., Morgan, S., Saito, T., Slagle, A.L., Stinton, A.J., Subramanyam, K.S. V., Tamura, Y., Villemant, B., Wang, F., 2014. Late Pleistocene stratigraphy of IODP Site U1396 and compiled chronology offshore of south and south west Montserrat, Lesser Antilles. Geochemistry, Geophys. Geosystems 15, 3000–3020. doi:10.1002/2014GC005402

Westbrook, G.K., Mascle, A., Biju-Duval, B., 1984. Geophysics and the structure of the Lesser Antilles forearc, in: Biju-Duval, B., Moore, J.C. (Eds.), Initial Reports of the Deep Sea Drilling Program 78A. U.S. Government Printing Office, Washington, pp. 23–28.

Westercamp, D., Tazieff, H., 1980. Martinique, Guadeloupe, Saint-Martin, La Desirade, in: Guides Géologiques Régionaux. Paris, pp. 350–390.

White, W.M., Dupré, B., 1986. Sediment subduction and magma genesis in the Lesser Antilles: Isotopic and trace element constraints. J. Geophys. Res. 91, 5927. doi:10.1029/JB091iB06p05927

Whitmarsh, R.B., Keen, C.E., Steinmetz, L., Tomblin, J., Whitmarsh, R.B., Donegan, M., Lilwall, R.C., Loncarevic, B.D., Nichols, B., Shepherd, J., 1983. A lithospheric seismic refraction

profile in the western North Atlantic Ocean. Geophys. J. Int. 75, 23–69. doi:10.1111/j.1365-246X.1983.tb01912.x

Zami, F., Quidelleur, X., Ricci, J., Lebrun, J.-F., Samper, A., 2014. Initial sub-aerial volcanic activity along the central Lesser Antilles inner arc: New K-Ar ages from Les Saintes volcanoes. J. Volcanol. Geotherm. Res. 287, 12–21. doi:10.1016/j.jvolgeores.2014.09.011

Zellmer, G.F., Hawkesworth, C.J., Sparks, R.S.J., Thomas, L.E., Harford, C.L., Brewer, T.S., Loughlin, S.C., 2003. Geochemical Evolution of the Soufrière Hills Volcano, Montserrat, Lesser Antilles Volcanic Arc. J. Petrol. 44, 1349–1374. doi:10.1093/petrology/44.8.1349

Chapter 2: The evolution of the Silver Hills volcanic centre, and revised $^{40}Ar/^{39}Ar$ geochronology of Montserrat, Lesser Antilles, with implications for island arc volcanism

This chapter has been published in *Geochemistry, Geophysics, Geosystems*:

S. J. Hatter, M. R. Palmer, T. M. Gernon, R. N. Taylor, P. D. Cole, D. N. Barfod, and M. Coussens, 2018. The evolution of the Silver Hills volcanic centre, and revised $^{40}Ar/^{39}Ar$ geochronology of Montserrat, Lesser Antilles, with implications for island arc volcanism. *Geochemistry, Geophysics, Geosystems,* 19, doi:10.1002/2017GC007053

The paper was written by S. J. Hatter, with feedback provided by all co-authors. M. R. Palmer and P. D. Cole helped with fieldwork, and laboratory work was carried out by S. J. Hatter. D. N. Barfod performed the $^{40}Ar/^{39}Ar$ dating at the NERC Argon Isotope Facility, from a successfully funded application by Hatter and Gernon to NERC for 15 $^{40}Ar/^{39}Ar$ dates.

Abstract

Studying the older volcanic centres on Montserrat, Centre Hills and Silver Hills, may reveal how volcanic activity can change over long time periods (≥1 Myr), and whether the recent activity at the Soufrière Hills is typical of volcanism throughout Montserrat's history. Here, we present the first detailed mapping of the Silver Hills, the oldest and arguably least studied volcanic centre on Montserrat. Volcanism at the Silver Hills was dominated by episodic andesite lava dome growth and collapse, produced Vulcanian style eruptions, and experienced occasional sector collapse events, similar to the style of volcanic activity that has been documented for the Centre Hills and Soufrière Hills. We also present an updated geochronology of volcanism on Montserrat, by revising existing ages and obtaining new $^{40}Ar/^{39}Ar$ dates and palaeomagnetic ages from marine tephra layers. We show that the centres of the Silver, Centre, and Soufrière Hills were active during at least ~2.17–1.03 Ma, ~1.14–0.38 Ma, and ~0.45 Ma–present, respectively. Combined with timings of volcanism on Basse-Terre, Guadeloupe these ages suggest that ~0.5–1 Ma is a common lifespan for volcanic centres in the Lesser Antilles. These new dates identify a previously unrecognized overlap in activity between the different volcanic centres, which appears to be a common phenomenon in island arcs. We also identify an older stage of Soufrière Hills activity ~450–290 ka characterized by the eruption of hornblende-orthopyroxene-phyric lavas, demonstrating that

the petrology of the Soufrière Hills eruptive products has changed at least twice throughout the volcano's development.

2.1 Introduction

Lava dome growth and collapse is a common process at arc volcanoes, e.g. as observed at Merapi volcano, Indonesia (Andreastuti et al., 2000), Mt St Helens, USA (Hoblitt et al., 1980) and Unzen volcano, Japan (Hoshizumi et al., 1999), but volcanic activity can be highly variable over the lifetime of an individual volcanic edifice (e.g. Hildreth & Lanphere, 1994; Komorowski et al., 2005; Myers et al., 1985; Pioli et al., 2015). This is exemplified in the Lesser Antilles arc, where volcanism is dominated by dome-forming eruptions, but varies in composition and style both between discrete volcanic edifices on individual islands, and during the lifetime of an individual volcano. For example, eruptive activity at volcanic centres on Guadeloupe and Martinique has varied from effusive basaltic lava flows forming shield volcanoes, to andesitic dome eruptions to Plinian eruptions (Germa et al., 2011a, 2011b; Komorowski et al., 2005; Maury et al., 1990; Samper et al., 2007). Understanding what causes these changes in eruption styles is crucial to aiding predictions concerning the long-term behaviour of a volcano.

Volcanism on Montserrat has been of particular interest since the onset of renewed volcanism at the Soufrière Hills Volcano in 1995. As a consequence, it has become one of the most studied volcanoes on Earth. Since 1995 the eruption has had substantial social and economic impacts on the island, including destroying its capital, Plymouth (Kokelaar, 2002), and so gaining insight into the evolution of volcanic activity at Soufrière Hills through time is of considerable interest. Both marine and terrestrial records show that the style of past Soufrière Hills activity has changed little throughout its known ca. 282 kyr history (e.g. Le Friant et al., 2008; Smith et al., 2007), but it may not necessarily continue to behave in this way. For example, Caricchi et al. (2014) suggest that larger eruptions tend to occur towards the end of a volcano's lifetime, raising the possibility that future Soufrière Hills eruptions may be of higher magnitude. Within this context, it is important to note that Soufrière Hills is the latest in a series of volcanic centres on Montserrat. Thus, study of the extinct volcanoes on Montserrat provides an opportunity to investigate volcanic activity over longer time periods, on the order of ~1 Myr, in order to document possible changes. Here, we provide the first detailed account of the physical volcanology of Montserrat's oldest volcanic centre, the Silver Hills, in an attempt to better understand how its activity has evolved through time. We also present supporting data and observations from a marine sediment core that contains eruption products from Montserrat, and provide new $^{40}Ar/^{39}Ar$ dates for the Silver, Centre

and Soufrière Hills to better constrain the timing of volcanic activity, providing an updated chronology of volcanism on the island.

2.2 Geological Setting

Montserrat is an active volcanic island in the Lesser Antilles Arc (Figure 2.1a), formed from the westward subduction of Atlantic crust beneath the Caribbean plate at a rate of *ca.* 2 cm/yr (Minster & Jordan, 1978). Detailed geological mapping of Montserrat was first carried out by Macgregor (1938), who identified seven discrete volcanoes, based on the island's geomorphology. This was revised by Rea (1974), who used K-Ar dates to identify six volcanoes, with different relative ages to those proposed by Macgregor (1938). The K-Ar dates of Rea (1974) indicate that activity on Montserrat began at ~4.3 Ma at Roche's Bluff. However, more recent $^{40}Ar/^{39}Ar$ dating by Harford et al. (2002) suggests that Montserrat is comprised of only three volcanic centres: Silver Hills (*ca*. 2580–1160 ka), Centre Hills (*ca*. 1021–550 ka) and South Soufrière Hills-Soufrière Hills (*ca*. 282 ka to present; Figure 2.1b). Of these centres, the Silver Hills is the least studied. It is a deeply eroded volcanic centre consisting of two-pyroxene andesite (Rea, 1974) with volcaniclastic sequences, debris avalanche deposits and areas of extensive hydrothermal alteration (Harford et al., 2002). The Centre Hills consists of two-pyroxene andesite and hornblende-hypersthene andesite (Rea, 1974) with block-and-ash flow, pumice-and-ash flow, pumice-fall, lahar, fluvial and debris avalanche deposits (Harford et al., 2002). The deposits of the Centre Hills also provide evidence for the largest known eruptions on Montserrat, up to magnitude 5 (Coussens et al., 2017).

The earliest identified period of activity at the Soufrière Hills volcanic centre began ~280 ka with the eruption of two-pyroxene andesites up until ~130 ka. At ~130 ka a period of mafic volcanism formed the South Soufrière Hills (Harford et al., 2002), with deposits dominated by basaltic to basaltic andesite lava flows with mass-wasting and scoria-fall deposits, and some andesitic fallout (Cassidy et al., 2014; Harford et al., 2002; Rea, 1974). Andesites erupted from Soufrière Hills following ~130 ka exhibit a different mineralogy, changing from two-pyroxene andesites to hypersthene-hornblende andesites, but with no concurrent change in whole-rock geochemistry (Harford et al., 2002). The largest known eruptions of Soufrière Hills occurred ~174 ka (Coussens et al., 2017; Harford et al., 2002; Smith et al., 2007). This period of activity produced multiple pumice-rich pyroclastic density current deposits 1–3 m thick and a pumice fall deposit 1 m thick ~3 km from the probable source, providing the only evidence of possible Plinian eruptions from the Soufrière Hills volcano.

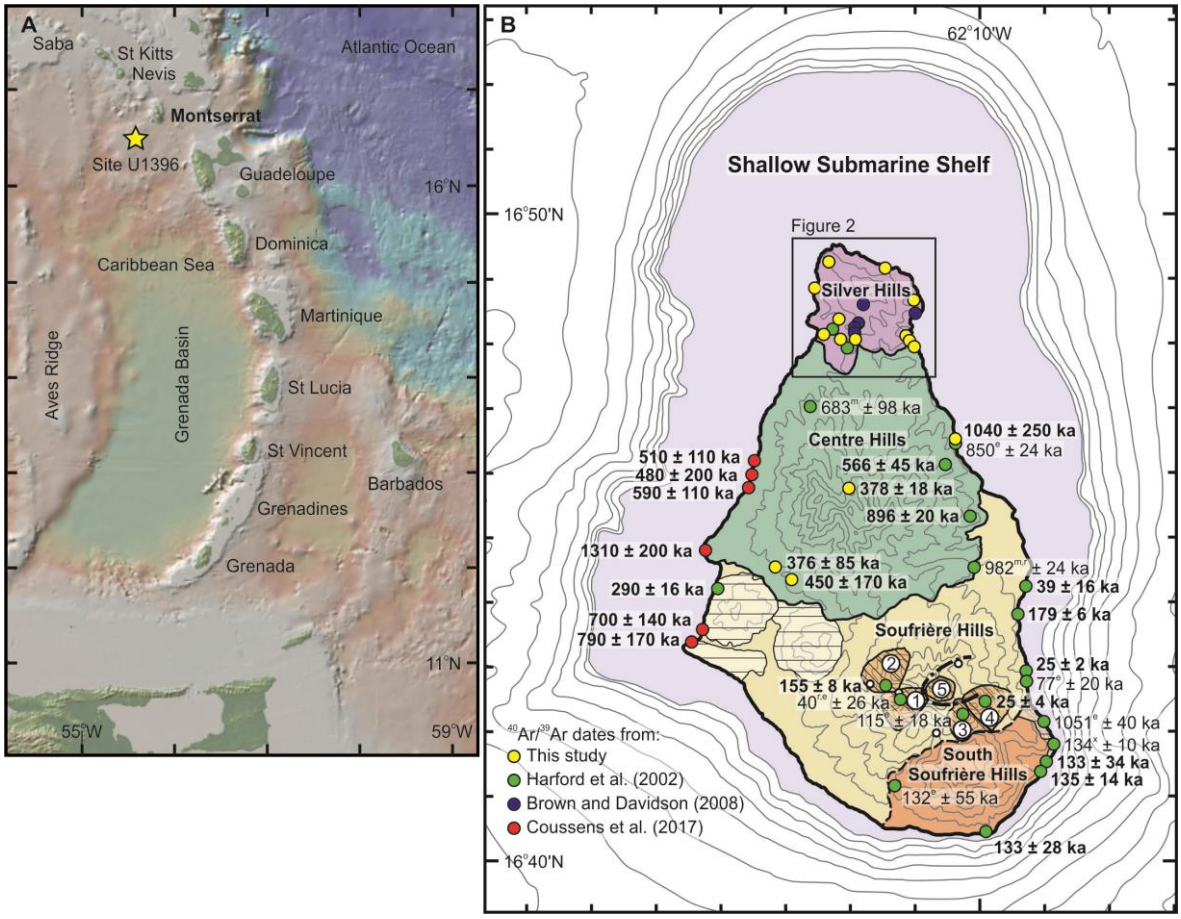

Figure 2.1. (a) Map of the Lesser Antilles, showing the location of IODP Expedition 340 core site U1396. (b) Map of Montserrat, with pre-1995–2010 eruption topography and bathymetry (100 m intervals), showing the location of the volcanic centres and $^{40}Ar/^{39}Ar$ dates. Pale areas with horizontal stripes are uplifted regions. Orange areas with diagonal stripes within the Soufrière Hills show the locations of the lava domes: 1, Chances Peak; 2, Gages Mountain; 3, Galway's Mountain; 4, Perches Mountain; 5, Castle Peak. Dot-dashed line shows edge of English's Crater. White dots mark the locations of Soufrières, which are (from left to right): Gages Lower, Gages Upper, Galway's and Tar River. Accepted ages in bold. Ages viewed with caution: ^{m} maximum age; ^{r} Ar recoil; ^{x} excess Ar; ^{e} MSWD exceeds critical value; see text for details.

Currently, the Soufrière Hills comprises a central dome complex surrounded by volcaniclastic deposits, which are andesitic in composition. The dome complex comprises four old domes: Chances Peak (<200 ka), Gages Mountain (151 ± 8 ka), Galway's Mountain (112 ± 18 ka) and Perches Mountain (24 ± 4 ka) (Harford et al., 2002), and a dome within English's Crater created by the recent eruption (1995–2010; Figure 2.1b). The modern dome covers a fifth older dome, Castle Peak (formed *ca*. 1650 AD) (Young et al., 1996), and has undergone multiple successive growth and collapse phases during the recent eruption. Indeed, the current eruptive phase has been dominated by a combination of Vulcanian explosions, dome growth and dome collapse events (Kokelaar, 2002; Wadge et al., 2014),

which is probably characteristic of Soufrière Hills activity over the past ~280 kyr (Rea, 1974; Roobol & Smith, 1998; Smith et al., 2007).

Large landslide deposits discovered offshore of Montserrat reveal that Soufrière Hills has undergone multiple flank collapse events (Coussens et al., 2016; Deplus et al., 2001; Le Friant et al., 2004; Lebas et al., 2011). Additionally, a debris avalanche occurred during the recent eruption on 26th December 1997, resulting from dome growth over a hydrothermally weakened sector of the wall of English's crater (Sparks et al., 2002; Voight et al., 2002).

No evidence of submarine volcanism or the emergence of the island has been identified on Montserrat, with only subaerial activity documented. However, constraints on the timing of the emergence of Montserrat come from marine sediment core U1396C, ~35 km SW of Montserrat (Figure 2.1a). A 1.2 m thick *ca.* 4 Ma tephra layer has been identified within the core, and detailed sedimentological analyses indicate that it was derived from a subaerial pyroclastic density current eruption which travelled over the sea surface to deposit at site U1396. Thus, the emergence of Montserrat can be constrained to >4 Ma (Jutzeler et al. 2017), ~1.4 Myr before activity of the known volcanic centres began.

2.3 Methods

2.3.1 Field Work

Field mapping was undertaken in the Silver Hills, Montserrat in May 2014 and 2015 at a scale of 1:25000, with samples collected for $^{40}Ar/^{39}Ar$ dating and geochemical analysis. The Silver Hills is highly eroded with a current subaerial area of ~6.5 km^2. The patchy nature of exposures coupled with the generally limited spatial extent of individual units means that radiometric dates are vital to constrain a stratigraphy for the Silver Hills deposits.

2.3.2 $^{40}Ar/^{39}Ar$ Dating

Twelve lava and three pumice samples were prepared at the Scottish Universities Environmental Research Centre (SUERC) Argon Isotope Facility (AIF), where they were crushed in a jaw-crusher, sieved in to a 250–500 μm size fraction, leached in 20% HNO_3, and passed through a Frantz magnetic barrier laboratory separator (model LB-1) to separate plagioclase phenocrysts from the groundmass. Plagioclase separates were then leached in 5% HF to remove any glass attached to the crystals. 200 mg and 1 g of clean plagioclase phenocryst separates and groundmass (lavas only), respectively, were then hand-picked for $^{40}Ar/^{39}Ar$ dating.

The samples were irradiated for one hour in the Oregon State University reactor, Cd-shielded facility, and analyzed on a GVi instruments ARGUS V multi-collector mass spectrometer using a variable sensitivity faraday collector array in static collection (non-peak hopping) mode (Mark et al., 2009; Sparks et al., 2008) at SUERC AIF. Alder Creek sanidine (1.2056 ± 0.0019 Ma, 1σ) (Renne et al., 2011) was used to monitor ^{39}Ar production and establish neutron flux values (J) for the samples. The reader is directed to Coussens et al. (2017) for more details of the method. The average total system blank for laser extractions, measured between each sample run, was 1.5 ± 0.7 × 10^{-15} mol ^{40}Ar, 1.2 ± 1.3 × 10^{-17} mol ^{39}Ar and 8.5 ± 3.6 × 10^{-18} mol ^{36}Ar for lava samples, and 1.7 ± 0.1×10^{-15} mol ^{40}Ar, 1.6 ± 0.5 × 1.1^{-17} mol ^{39}Ar and 1.6 ± 0.7 × 10^{-17} mol ^{36}Ar for pumice samples. All blank, interference and mass discrimination calculations were performed with the *MassSpec* software package (versions 8.058 and 8.16 for andesite and pumice samples respectively, authored by Al Deino, Berkeley Geochronology Centre).

Plateau ages, or composite plateau ages for replicated samples, are chosen as the best estimates of the emplacement ages. Accepted plateau ages must be derived from a minimum of three contiguous steps (minimum ^{39}Ar content of each step is ≥0.1% of total ^{39}Ar release) which overlap in age within 2σ uncertainty, and contains a minimum of 50% of ^{39}Ar released for the combined steps. The scatter between ages of the steps must be low with a MSWD (mean square weighted deviation) less than the 95% probability cut-off (Wendt & Carl, 1991). Further, the inverse isochron formed by the plateau steps must yield an age indistinguishable from the plateau age at 2σ uncertainty, and the $^{40}Ar/^{36}Ar$ of the trapped component composition derived from the inverse isochron must be indistinguishable from the composition of air (298.56 ± 0.61, 2σ) at the 2σ uncertainty level.

For fall deposits or ignimbrites, the single crystal approach is used to determine an eruptive age because this allows for discrimination of juvenile crystals and crystals derived from other sources, e.g., xenocrysts or antecrysts, but pumice samples yielded low-K plagioclase that could not be analyzed as single crystals. Instead, a multi-grain, two-step heating approach was adopted to increase signal sizes allowing for more precise measurements. The presence of older xenocrysts in these multi-grain aliquots could bias age results, an effect dependent on the age of the xenocryst and its relative potassium content. To account for this possibility, the experiment was repeated (n≥15) and the youngest, Gaussian distributed population of ages was calculated from the set of analyses.

Each individual gas analysis represents an aliquot of 50-100 single grains, loaded into a 4 mm well in a copper planchette. An initial step at ~0.5 watts of power was used to drive off atmospheric gas and liberate argon from any alteration phases that might be present. A

second fusion step at 15 watts of power yielded age information associated with the plagioclase crystals.

2.3.3 Whole Rock Geochemistry

Nb and Y were analyzed on a Thermo Fisher Scientific X-Series 2 ICP-MS at the University of Southampton following the method of Coussens et al. (2017), in which 0.05 g of powdered sample is analyzed for terrestrial samples, and 0.01 g for U1396C samples. Precision is better than 3% (see Appendix A for more detail).

Pb and Nd isotopes were measured from 50 and 200 mg (for pumice and lava samples respectively) of hand-picked rock chips 0.5–1 mm in size. Samples were leached and digested following the method of Cassidy et al. (2012), and Pb was isolated from the matrix using AGX-1x8 200-400 mesh anion exchange resin, following the method of Kamber and Gladu (2009). For Nd, the dissolved samples were first passed through cation columns containing AG50-X8 200-400 mesh resin, then through LN Spec columns (Eichrom Industries, Illinois, USA). Pb and Nd isotopes were measured on a MC-ICP-MS (Neptune) at the University of Southampton. Pb isotopes were corrected for instrumental mass fractionation using the SBL74 double spike (Taylor et al., 2015). SRM NBS981 gave $^{206}Pb/^{204}Pb = 16.9400 \pm 0.0023$, $^{207}Pb/^{204}Pb = 15.4965 \pm 0.0026$ and $^{208}Pb/^{204}Pb = 36.7124 \pm 0.0076$ on n = 108 measurements during the course of this study. Measured values for standard JNdi are $^{143}Nd/^{144}Nd = 0.512116 \pm 0.000012$ (n = 36).

2.3.4 Core Sample Acquisition

Samples were analyzed from marine sediment core U1396C, from International Ocean Discovery Program (IODP) Expedition 340. This site is located ~35 km southwest of Montserrat (Figure 2.1a). The core is 145.92 m long and provides a record extending back ~4.5 Ma (Expedition 340 scientists, 2013). This study investigates the tephra layers deposited in the past ~2.35 Ma (the interval represented by the terrestrial record on Montserrat), which have been sampled for geochemical analysis. These samples have been previously analyzed for Pb isotopes by Palmer et al. (2016).

2.4 Timing of Montserrat Volcanism

2.4.1 Existing $^{40}Ar/^{39}Ar$ Dates

The $^{40}Ar/^{39}Ar$ ages of Montserrat from previous studies are compiled in Table 2.1. All of these studies used the same strict criteria outlined above (section 2.3.2) to determine plateau

Table 2.1. Compiled literature $^{40}Ar/^{39}Ar$ dates on Montserrat. Ages from Harford et al. (2002) and Brown and Davidson (2008) presented here are recalculated ages (see text for details).

Sample	Rock type	Location/ unit	Grid reference mE mN	Material	Plateau age (ka)	±2σ	MSWD	N	% ^{39}Ar
MVO144[1]	Lava	Silver Hill	378025 1857050	Plagioclase	2614[m]	121	0.69	7/11	65.3
SH07-F[2]	Lava	Yellow Hole	380408 1857634	Groundmass	**1520[i]**	**51**	0.58	7/7	100.0
SH07-C[2]	Lava	Drummonds	379033 1857296	Groundmass	**1430[i]**	**19**	1.09	7/7	100.0
SH07-D[2]	BAF	Drummonds	378873 1857117	Groundmass	**1412[i]**	**20**	0.66	7/8	>95.0
SH07-B[2]	BAF	Silver Hill	379081 1857776	Groundmass	**1397[i]**	**20**	0.46	7/7	100.0
SH07-E[2]	Lava	Drummonds	378859 1857000	Groundmass	**1395[i]**	**17**	0.82	7/7	100.0
11.1.4C[3]	PAF	South Lime Kiln Bay	374681 1851092	Plagioclase	**1310**	**200**	0.95	6/7	
MVO755[1]	Lava	Silver Hill	378650 1856400	Groundmass	1192[r]	95	20.79[e]	5/16	64.6
MVO135[1]	s-BAF	Roche's Bluff	383975 1846150	Whole-rock	1051	40	4.37[e]	7/14	62.1
MOV148[1]	Lava	Harris	382150 1850450	Whole-rock	982[m,r]	24	4.99[e]	10/12	93.0
MVO131[1]	Lava	Trant's	382050 1851975	Whole-rock	**896**	**20**	1.40	12/12	100.0
MVO831[1]	BAF	Lower Centre Hills	381763 1853525	Groundmass	850	24	2.01[e]	9/14	73.7
BP[3]	PF	Bransby Pumice	374092 1848396	Plagioclase	**790**	**170**	0.87	6/7	
4.2.3G[3]	PAF	Old Road Bay	374638 1848989	Plagioclase	**700**	**140**	0.88	5/6	
MVO147[1]	PAF	Upper Centre Hills	377600 1855050	Plagioclase	683[m]	98	0.93	5/12	76.4
3.1.2A[3]	PAF	Woodlands Bay	375879 1852755	Plagioclase	**590**	**110**	1.14	7/7	100.0
MVO809[1]	BAF	Upper Centre Hills	381475 1853750	Groundmass	**566**	**45**	1.01	14/14	100.0
3.4.2H[3]	PAF	Bunkum Bay	376014 1853421	Plagioclase	**510**	**110**	0.41	5/7	
3.1.8C[3]	PAF	Attic	375951 1853042	Plagioclase	**480**	**200**	0.99	3/8	
MVO785[1]	BAF	Garibaldi Hill	374990 1850025	Groundmass	**290**	**16**	0.15	6/15	66.7
MVO819[1]	—	SH-1[4]	383238 1849275	Groundmass	182	10	2.48[e]	5/10	91.5
				Groundmass	178	6	1.03	5/9	66.7
				Composite	**179**	**6**	0.53		
MVO152[1]	Lava	Gages Dome	379275 1847175	Whole-rock	230	14	0.23	5/14	53.6
				Groundmass	163	12	3.23	2/10	53.7
				Groundmass	153	6	1.06	5/9	64.2
				Composite	**155**	**8**	1.84		
MVO139[1]	Lava	Landing Bay	383950 1845000	Whole-rock	142	18	1.28	5/11	61.1
				Groundmass	128	18	2.89[e]	14/17	87.1
				Composite	**135**	**14**	1.13		
MVO136[1]	Lava	Roche's Bluff	384250 1845650	Whole-rock	134[i,x]	10	0.79	10/11	97.4
MVO830[1]	Breccia	Roche's Bluff	383975 1845050	Groundmass	**133**	**34**	0.64	8/16	76.0
MVO791[1]	Lava	Shoe Rock	381600 1843150	Groundmass	**133**	**28**	0.35	6/10	70.7
MVO1099[1]	—	SSH-F[4]	379750 1844325	Groundmass	157	18	1.00	6/9	55.5
				Groundmass	102	20	0.45	3/9	63.0
				Composite	132	55	16.67[e]		
18654[1]	Lava	Galway's Dome	—	Groundmass	124	8	1.96	5/10	58.2
				Groundmass	106	10	0.52	4/10	59.4
				Composite	115	18	8.45[e]		

MVO777[1]	—	SH-II[4]	383675	1847250	Groundmass	86	10	1.23	3/8	63.2
					Groundmass	66	12	0.33	3/9	60.4
					Composite	77	20	6.53[e]		
MVO149[1]	Lava	Chances Dome	379900	1846825	Whole-rock	40[r]	26	15.9[e]	4/11	54.2
MVO127[1]	—	SH-III[4]	383550	1849975	Groundmass	**39**	**16**	0.13	3/10	72.5
MVO154[1]	Lava	Perches Dome	382100	1846750	Whole-rock	33	8	1.61	5/11	65.3
					Groundmass	25	4	0.54	5/9	65.9
					Groundmass	24	6	0.20	4/10	68.3
					Composite	**25**	**4**	0.18		
MVO775[1]	—	SH-III[4]	383425	1847675	Groundmass	**25**	**2**	0.93	4/9	64.0
MVO104[1]	BAF	1996 Dome	—		Groundmass	**22**	**44**	0.25	4/10	63.8
					Plagioclase	439	192	3.26[e]	7/10	71.1

[1] Harford et al. (2002); [2] Brown and Davidson (2008); [3] Coussens et al. (2017); [4] unit name from Smith et al. (2007). BAF, block-and-ash flow deposit; PAF, pumice-and-ash flow deposit; S-BAF, submarine-BAF; PF, pumice fall deposit. Ages considered reliable are in bold. Ages viewed with caution: [m] maximum age; [r] Ar recoil; [x] excess Ar; [e] MSWD exceeds critical value. [i] isochron age. N, number of plateau steps used to determine age/total number of steps; $\%^{39}Ar$, percentage of total ^{39}Ar in N.

ages. The ages of Harford et al. (2002) and Brown and Davidson (2008) have been recalculated with modern decay constants and standard ages using the Renne et al. (2010, 2011) optimization model, resulting in slightly increased ages. All ages referenced from these authors are the recalculated ages (see Appendix Table 2.1 for original and recalculated ages). Here, we review the dates from these previous studies to identify which ages are reliable, and which should be viewed with caution.

Harford et al. (2002) obtained ages for all of the Montserrat volcanic centres (Figure 2.1b; Table 2.1). Some of their ages, however, should be viewed with caution, as either their plateau profiles contain evidence of xenocrystic components or Ar recoil, they have a saddle-shaped plateau typical of lavas with excess argon, or have a MSWD which exceeds the critical 95% confidence level. Of the dates considered reliable, two are from the Centre Hills, six are from the Soufrière Hills, and three are from the South Soufrière Hills, with none from the Silver Hills (Table 2.1).

Five $^{40}Ar/^{39}Ar$ ages were acquired for the Silver Hills by Brown and Davidson (2008), in the range of ~1.52–1.40 Ma, but only cover a small area of the Silver Hills centre, four of which are part of the same stratigraphic sequence (Figure 2.2; Table 2.1). These ages were measured from groundmass (i.e. no xenocrystic material). Coussens et al. (2017) obtained five $^{40}Ar/^{39}Ar$ ages from Centre Hills deposits (~0.79–0.48 Ma; Figure 2.1b; Table 2.1) and one from a fault block within the Centre Hills (~1.31 Ma), which they interpret as originating from the Silver Hills volcanic centre. These ages were obtained from plagioclase phenocrysts, so the presence of xenocrysts cannot be ruled out.

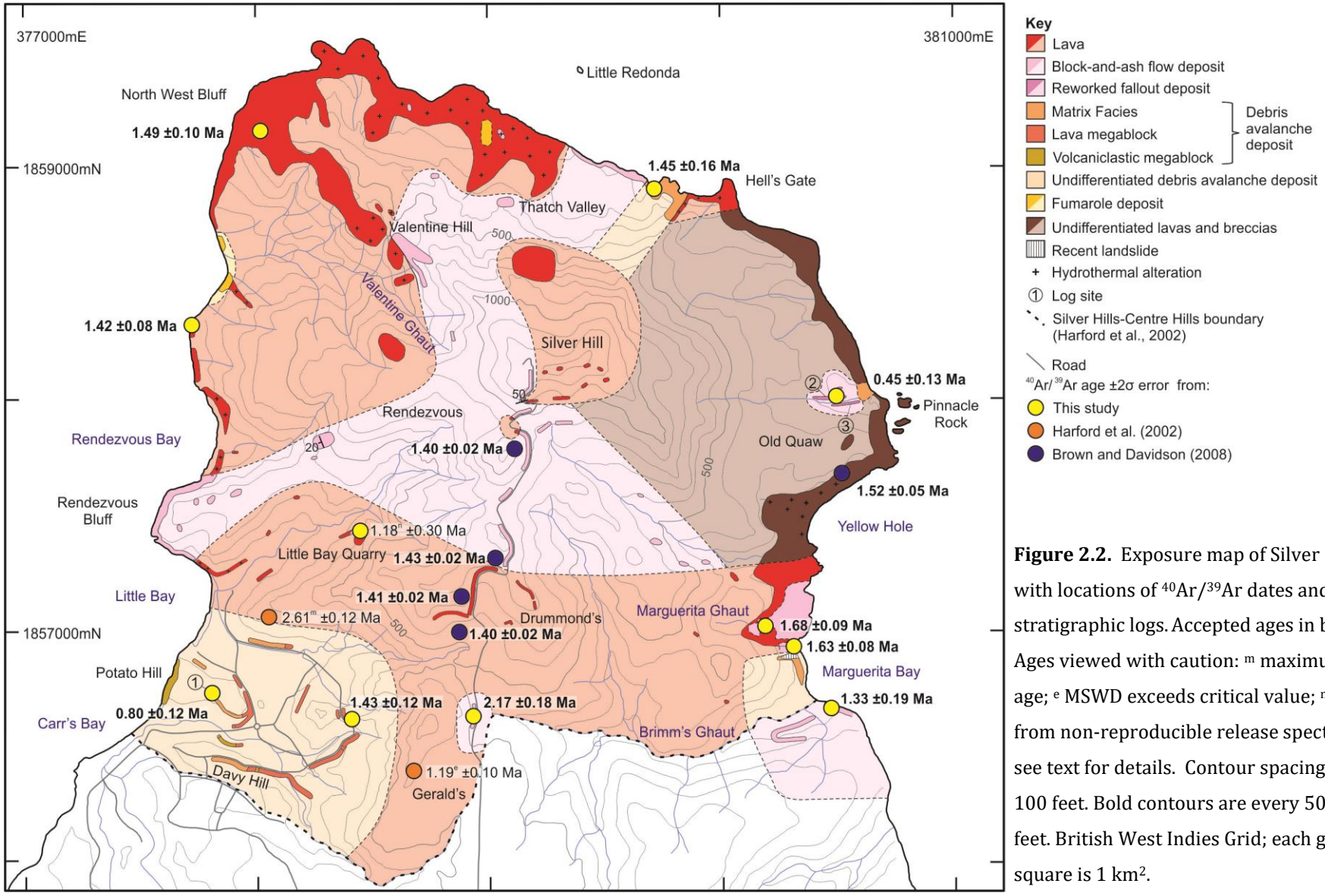

Figure 2.2. Exposure map of Silver Hills with locations of $^{40}Ar/^{39}Ar$ dates and stratigraphic logs. Accepted ages in bold. Ages viewed with caution: ^{m} maximum age; ^{e} MSWD exceeds critical value; ^{n} age from non-reproducible release spectra; see text for details. Contour spacing is 100 feet. Bold contours are every 500 feet. British West Indies Grid; each grid square is 1 km^2.

The questionable quality of the Silver Hills ages reported by Harford et al. (2002), and the limited spatial and stratigraphic extent of the Silver Hills ages reported in Brown and Davidson (2008) mean that the timing of volcanic activity is poorly known for the Silver Hills. This highlights the need for new $^{40}Ar/^{39}Ar$ dates, to better constrain the timing of Silver Hills activity, and aid the development of a detailed stratigraphy of the Silver Hills deposits.

2.4.2 New $^{40}Ar/^{39}Ar$ Dates

Here we present fifteen new $^{40}Ar/^{39}Ar$ ages for Montserrat (Figures 2.3–2.4; Table 2.2; Appendix Tables 2.2–2.3): geographically eleven are from the Silver Hills (~2.17–0.45 Ma; Figure 2.2) and four are from the Centre Hills (~1.04–0.38 Ma; Figure 2.1b). All samples produced plateau ages that match our strict criteria. The first run of sample 17/76-AL did not yield a plateau, however, and therefore did not meet the criteria for a reliable age, whereas the second run yielded a release profile that meets our criteria and yielded an age of 1.18 ± 0.30 Ma. Nevertheless, this age is viewed with caution as overall the sample shows significant heterogeneity and non-reproducible release spectra (Figure 2.3).

Harford et al. (2002) note evidence for xenocrysts in their ages obtained from plagioclase phenocrysts, leading them to interpret these ages as maximum ages, rather than true eruption ages. The influence of xenocrysts in our sample ages can be assessed by examining the data from samples 05/03-AL and 15/70-AC, for which both groundmass and plagioclase ages were measured. For both samples the plagioclase age is systematically older than the groundmass age, suggesting that the plagioclase may contain a minor xenocrystic component, but there is overlap in the 2σ errors of the two phases, which suggests that the plagioclase ages encompass the true eruption age within their 2σ errors. The plagioclase ages obtained by Coussens et al. (2017) also likely represent the eruption ages, because they were obtained on similar material, and have similar scale 2σ errors.

In the following sections, only the dates that are considered to be reliable are used in developing a detailed stratigraphy of the Silver Hills deposits, and when discussing the timing of volcanic activity.

2.5 Lithofacies of the Silver Hills Deposits

Here we adopt the non-genetic terminology of volcanic rocks proposed by White and Houghton (2006); lithofacies terms and abbreviations used are given in Table 2.3. For debris avalanche deposits we use the terms “megablock facies” (Voight et al., 2002) and “matrix facies” (Crandell et al., 1984; Voight et al., 2002). All deposits described from the Silver Hills were extrusive; no central conduit deposits (e.g. vent breccias) or dykes were observed.

Table 2.2. New $^{40}Ar/^{39}Ar$ dates for the Silver Hills, Centre Hills and Soufrière Hills.

Sample	Rock type	Location/unit	Grid reference mE mN	Material	Isochron age (ka)	±2σ	$^{40}Ar/^{36}Ar_{(i)}$	±2σ	MS WD	Plateau age (ka)	±2σ	MS WD	N	% ^{39}Ar	^{39}Ar (mol)	Ca/K
22/84-AC	BAF	South Silver Hill	378940 1856619	Plagioclase	2160	200	300.6	8.4	1.20	2220	220	1.08	8/12	84.8	5.3E-17	105
				Plagioclase	2300	630	290.0	23.0	1.50	2110	210	1.38	7/12	96.2	4.1E-17	99
				Composite	2140	260	299.5	8.0	1.30	**2170**	**180**	1.19	15/24		9.5E-17	103
14/25-AL	Lava	Marguerita Ghaut	380235 1857105	Plagioclase	1680	230	298.6	8.3	1.20	**1682**	**94**	0.99	6/10	90.5	8.4E-17	76
15/70-AC	BAF	North Marguerita Bay	380310 1856978	Groundmass	1580	140	298.2	0.4	0.71	1630	140	0.71	6/12	77.6	6.6E-16	5
				Plagioclase	1710	260	302.0	24.0	1.20	1770	210	1.11	11/12	99.6	6.1E-17	135
				Composite	1640	80	298.2	0.67	1.20	**1634**	**83**	1.06	17/24		7.2E-16	123
22/47-AL	Lava	North West Bluff	378130 1859071	Plagioclase	1550	130	293.0	13.0	0.97	**1493**	**98**	0.95	11/12	99.4	8.3E-17	79
20/42-AC	MF	Thatch Valley	379710 1858870	Plagioclase	1340	140	302.2	3.8	1.20	**1450**	**160**	1.13	11/12	99.8	5.6E-17	107
11/09-AL	LMB	Culture Hill	378378 1856630	Plagioclase	1510	180	296.5	30	0.49	**1430**	**120**	0.54	10/13	94.2	1.0E-16	64
17/77-AL	Lava	North Rendezvous Bay	377754 1858327	Plagioclase	1260	330	305.0	12.0	1.00	**1424**	**80**	1.17	8/11	99.1	1.1E-16	54
12/13-AC	BAF	South Marguerita Bay	380452 1856780	Plagioclase	1250	350	306.0	16.0	1.10	1390	220	1.04	8/10	98.9	3.7E-17	127
				Plagioclase	1520	780	285.0	25.0	1.10	1160	360	1.04	7/12	88.3	2.0E-17	130
				Composite	1360	280	297.0	13.0	1.10	**1330**	**190**	1.05	15/22		5.7E-17	128
17/76-AL	Lava	Little Bay Quarry	378449 1857434	Plagioclase	Excess ^{40}Ar					No resolvable plateau						
				Plagioclase	1250	440	296.0	13.0	0.54	1180[n]	300	0.50	9/13	62.6	3.0E-17	93
21/81-AC	BAF	East Centre Hills	381671 1853642	Plagioclase	1020	390	301.0	13.0	0.67	**1040**	**250**	0.62	12/12	100.0	5.3E-17	123
05/03-AL	Lava	Dry Waterfall	378605 1852689	Groundmass	370	20	308.0	14.0	1.80	377	18	1.67	11/13	89.8	1.0E-15	6
				Plagioclase	530	90	290.8	8.9	0.37	406	69	0.59	8/12	95.8	1.2E-16	54
				Composite	376	18	299.5	3.8	1.30	**378**	**18**	1.20	19/25		1.1E-15	53
28/57-AC	BAF	Spring Ghaut	376605	Plagioclase	400	140	298.3	3.7	1.20	392	98	1.04	8/11	95.0	7.3E-17	79

			1850521												
				Plagioclase	240	340	300.4	4.8	0.53	330	170	0.54	7/10	96.9	5.2E-17	74
				Composite	360	110	298.9	2.1	0.84	**376**	**85**	0.78	15/21		1.2E-16	77
Pumice samples										**Probability density Function Age (ka)**						
23/86-PF	PF	Potato Hill	377806 1856742	Plagioclase						**800**	**120**	1.03	15/19			107
20/79-PC	PAF	South Centre Hills	376612 1850198	Plagioclase						**450**	**170**	0.79	9/15			84
16/72-PR	r-PF	Old Quaw Ghaut	380443 1857979	Plagioclase						**450**	**130**	1.23	14/18			66

Abbreviations same as Table 2. MF, debris avalanche deposit matrix facies; LMB, lava megablock within debris avalanche deposit; r-PF, reworked-PF. Preferred ages for this study in bold. [n] age from non-reproducible release spectra. See supplementary Table 2 for decay rates, isotopic constants and nucleogenic production ratios.

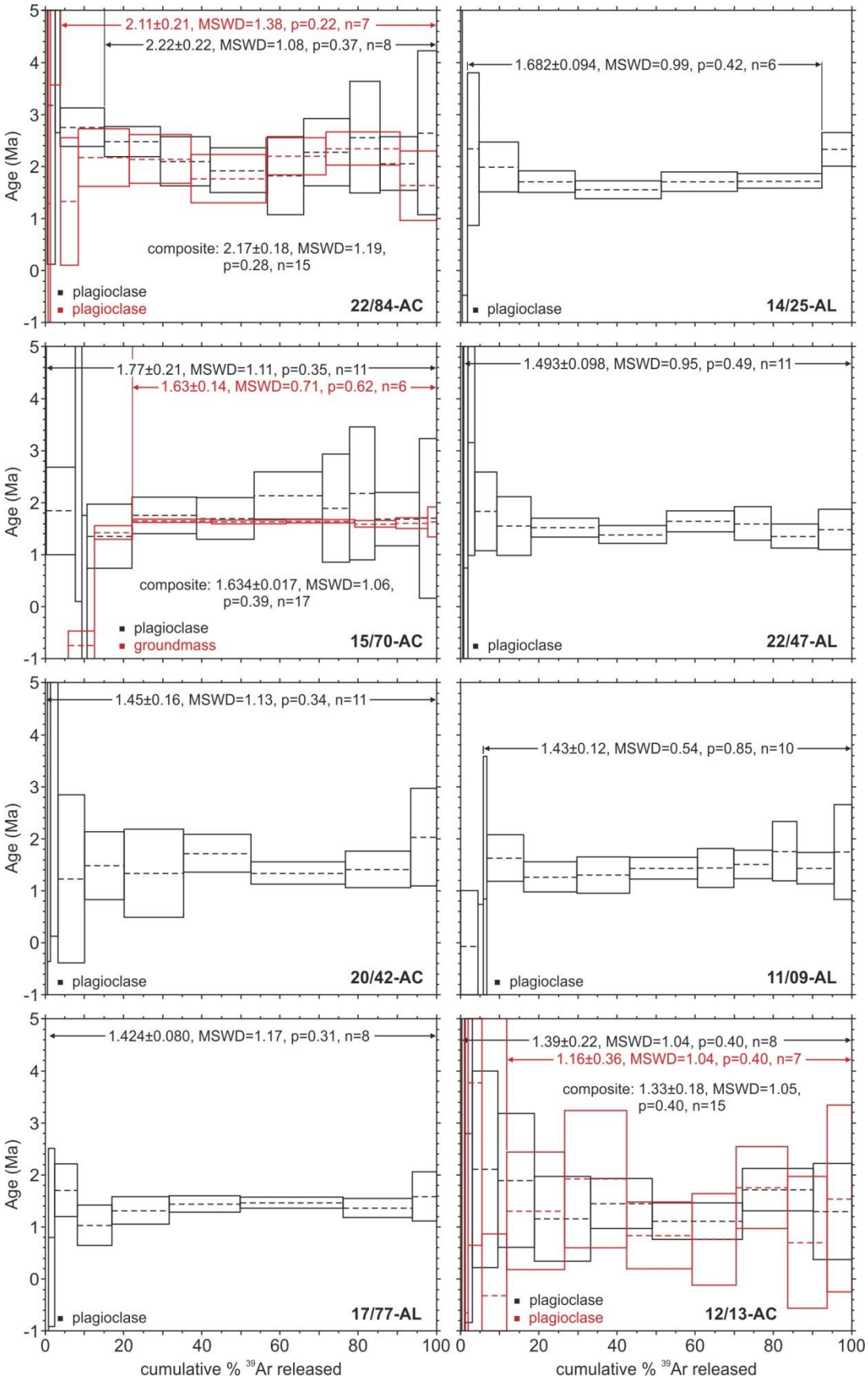

Figure 2.3. Plateau age diagrams for the twelve lava samples. Ages in Ma ± 2σ. Red and black plateaus depict separate analyses from the same sample, with the material analysed (plagioclase or groundmass) noted in the bottom left of each plot.

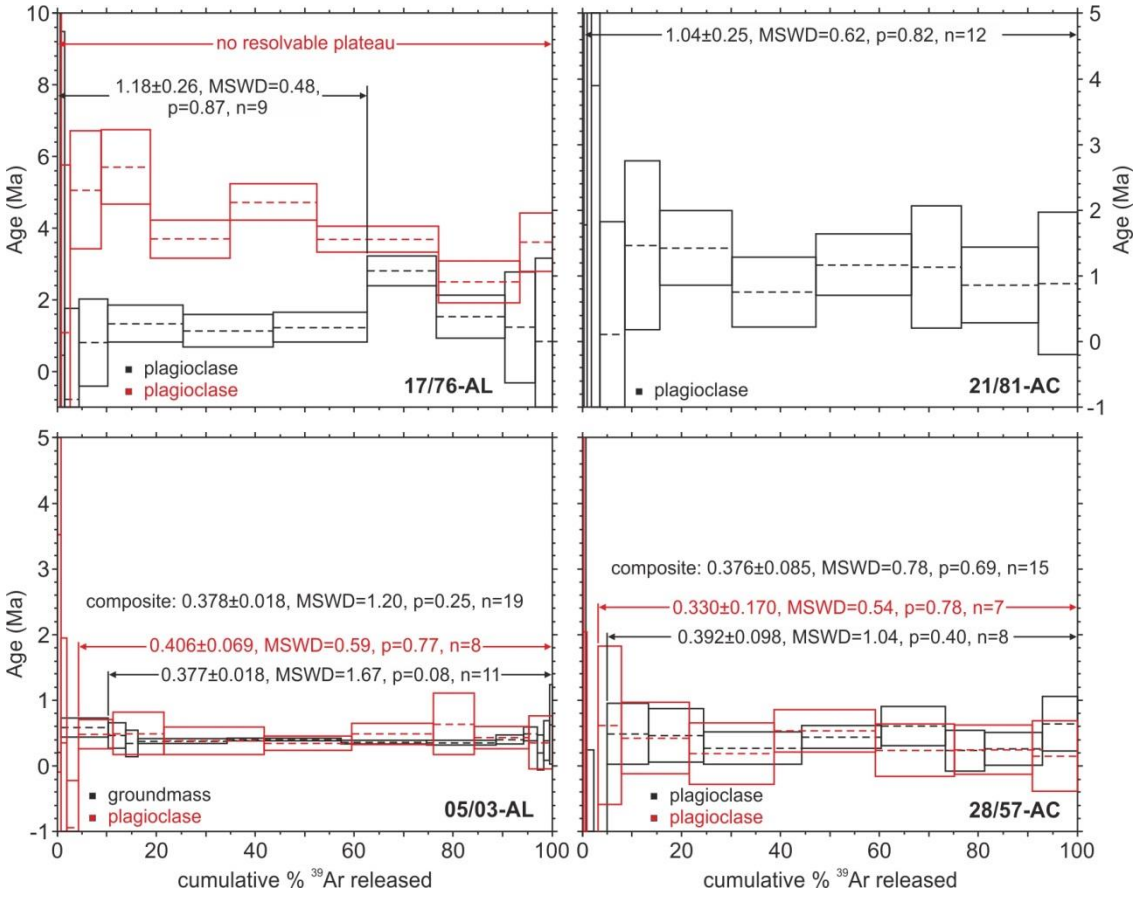

Figure 2.3 continued.

2.5.1 Lava and Intensely Hydrothermally Altered Lava

The lava exposures are dominantly composed of plagioclase-pyroxene-phyric andesite (~30–60 vol. % phenocrysts), with minor dacite and basaltic andesite with the same phenocryst populations. Lava thickness ranges from meters to hundreds of meters, with some exposures showing alignment of elongate crystals. The lava commonly locally transitions to breccia.

In some regions the lava flows are extensively hydrothermally altered to an extent that no primary magmatic minerals are identifiable, and they exhibit a crumbly texture. The present day exposures may be white or orange and yellow in colour, with the latter being associated with abundant centimetre-scale gypsum crystals. These altered exposures are surrounded by a halo of less hydrothermally altered rocks, with the degree of hydrothermal alteration decreasing outward.

2.5.1.1 Interpretation

The lavas form lava flows and domes, and the transitioning to breccia is interpreted as resulting from local autobrecciation of the lava along its margins. The zones of intensely hydrothermally altered lava are interpreted as the sites of fumarolic activity on the Silver Hills. The presence of gypsum crystals and pervasive variable discoloration make them

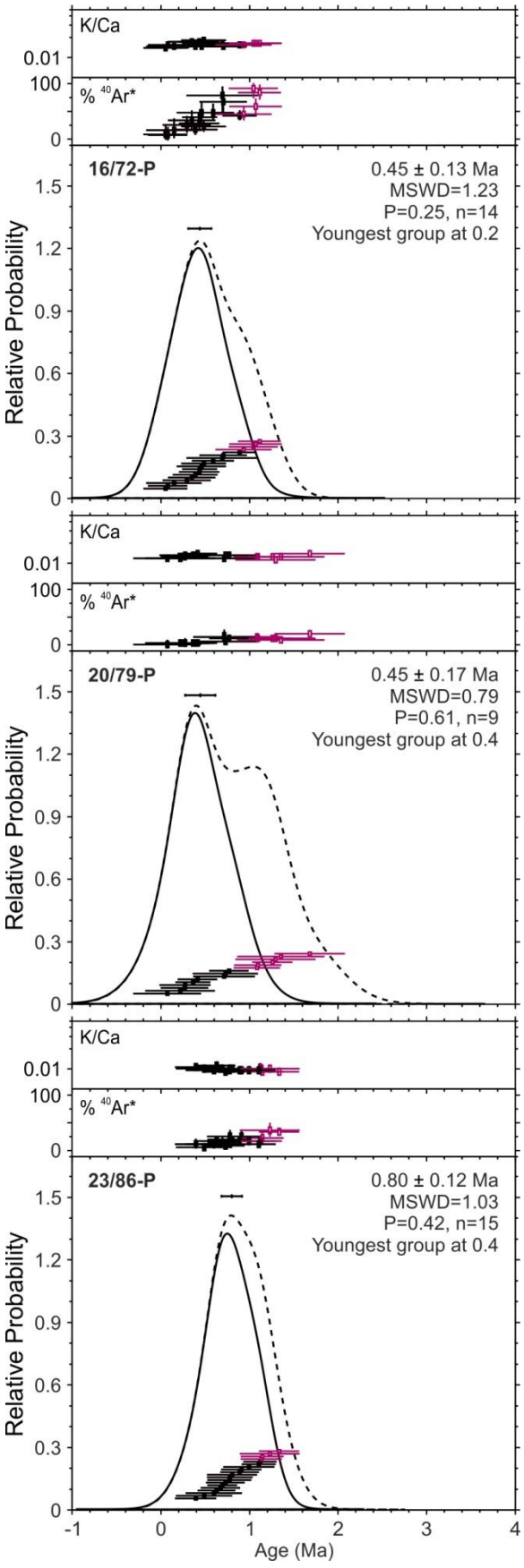

Figure 2.4. Age-probability spectra for the three pumice samples. Dotted lines show spectra including all data, solid lines show spectra after data rejection. Data at 1σ, results at 2σ, ages in Ma ± 2σ. Includes error in J. Filtering: nMAD = 1.5.

comparable to the recent deposits of Galway's Soufrière (Voight et al., 2002), which also shows the intensity of hydrothermal alteration decreasing with distance from the fumaroles.

2.5.2 Massive to Diffusely Stratified, Lapilli-Tuff to Tuff-Breccia (m-dsLT-TBr)

The m-dsLT-TBr are poorly sorted, variably clast- and matrix-supported and consist of centimetre- to meter-scale sub-rounded to angular andesite clasts, up to 20% of which are hydrothermally altered. Some units of this facies display normal and inverse grading at their upper and lower boundaries, respectively.

2.5.2.1 Interpretation

This facies is interpreted as block-and-ash flow deposits due to its massive structure, poor sorting, clast size range and grading. These characteristics are comparable to the block-and-ash flow deposits produced by dome collapses at Soufrière Hills Volcano during the 1995–2010 eruption (Cole et al., 2002; Stinton et al., 2014).

2.5.3 Massive Tuff-Breccia and Breccia, with Megablocks (mTBr-Br$_{MB}$)

This facies is similar in appearance to the m-dsLT-TBr facies, but with three key differences: absence of grading, presence of jigsaw-fit fractures in some clasts, and the occurrence of megablocks. The megablocks are tens to hundreds of meters in scale, and can be split into two categories: lava

Table 2.3. Lithofacies abbreviations used. Adapted from Branney and Kokelaar (2002). m-dsLT_{lensBr}, for example, means massive to diffuse-stratified lapilli-tuff with lenses of breccia.

Symbol	Lithofacies
T	Tuff
LT	Lapilli-tuff
TBr	Tuff-breccia
Br	Breccia
m	Massive
p	Pumice-rich
ds	Diffuse-stratified
//s	Parallel-stratified
(n)	Normal-graded
(i)	Inverse-graded
lensBr	Lens(es) of breccia
MB	Megablock

megablocks and volcaniclastic megablocks. Lava megablocks vary from poorly- to highly-fractured and show variable hydrothermal alteration. Some of the megablocks are faulted. Volcaniclastic megablocks are blocks of other volcaniclastic facies (e.g. mLT) hosted within surrounding mTBr, and are either composed of a single unit or a layered sequence. Some megablocks are sheared, and others contain parts which appear to intrude into the surrounding breccia. Interdigitation of units within layered volcaniclastic megablocks is common. Most boundaries between megablocks and breccia are sharp, but some display signs of mixing.

2.5.3.1 Interpretation

The presence of megablocks within the mTBr suggests that they are parts of debris avalanche deposits; the megablocks are large coherent fragments of the original volcanic edifice that have been transported by debris avalanches with little internal deformation. Layered volcaniclastic megablocks may preserve their original structure and stratigraphy. The matrix facies consists of a poorly-sorted massive breccia formed from the mingling of disaggregated megablocks and entrained material. Jigsaw-fit fracturing of clasts is a common feature of debris avalanche deposits (e.g. Crandell et al., 1984; Ui, 1983; Ui & Glicken, 1986), as are the fluidal textures at the edges of megablocks and deformation of units within individual volcaniclastic megablocks (e.g. interdigitation of units) (e.g. Takarada et al., 1999; Ui & Glicken, 1986; van Wyk de Vries & Davies, 2015). Faulting is another well-documented feature of some megablocks (e.g. Glicken, 1996; Ui et al., 1986; Ui & Glicken, 1986; van Wyk de Vries & Davies, 2015).

2.5.4 Massive Lapilli-Tuff, with regular Lapilli-Tuff and Tuff-Breccia Lenses ($mLT_{lensLT\text{-}TBr}$)

The mLT are poorly-sorted, matrix-supported and consist of centimetre-scale rounded to sub-rounded andesite clasts, ~10% of which are hydrothermally altered. The LT-TBr lenses are poorly sorted, clast supported and consist of centimetre- to decimetre-scale rounded andesite clasts, up to 5% of which are hydrothermally altered. They typically have meter- and decimetre-scale length and thickness, respectively, with decimetre-scale spacing.

2.5.4.1 Interpretation

This facies is interpreted as lahar deposits, on the basis that they contain multiple coarse lenses of rounded to sub-rounded andesite clasts in variably massive and parallel to cross-stratified coarse ash to coarse lapilli. They are similar to modern lahar deposits present in the Belham Valley, on the west flank of Soufrière Hills (Barclay et al., 2007).

2.5.5 Pumiceous, Massive to Diffusely Stratified, Lapilli-Tuff to Tuff-Breccia (pm-dsLT-TBr)

This facies can be split into two subfacies: well-sorted and poorly-sorted. Occurrences of the well-sorted subfacies are clast-supported with centimetre-scale sub-angular to angular clasts of andesitic pumice and andesite. Clast proportions are typically ~90% pumice and ~10% andesite, with the pumice clasts being consistently coarser than the andesite clasts. Exposures of the poorly-sorted subfacies are variably clast- and matrix-supported and consist of centimetre- to decimetre-scale rounded to angular clasts. The clast proportions are typically in the range of 65–99% pumice, 1–33% andesite and 0–5% HA andesite. Locally, exposures of this subfacies have erosional bases.

2.5.5.1 Interpretation

The well-sorted subfacies are interpreted as primary fallout deposits, due to the high degree of sorting and predominance of angular pumice with subordinate smaller lithics. The poorly-sorted subfacies are interpreted as pumice-and-ash flow deposits, due to their poor sorting, rounded clasts and erosional bases, similar to pumice-and-ash flow deposits produced from recent Vulcanian eruptions of Soufrière Hills (Cole et al., 2002, 2014).

2.6 Stratigraphy of the Silver Hills

2.6.1 Little Bay to South Drummonds, >2 Ma

The oldest dated unit is an isolated exposure of dacitic mLT-TBr at south Drummonds. This unit contains meter-scale blocks, has a minimum thickness of 3 m, and is dated at 2.170 ± 0.180 Ma (Figure 2.2).

2.6.2 Marguerita Ghaut and North Marguerita Bay, ~1.7–1.6 Ma

Marguerita Ghaut contains mTBr and coherent andesite and basaltic andesite lava exposures, with sharp boundaries between them. The mTBr has an age of 1.682 ± 0.094 Ma (Figure 2.2).

The eastern mouth of the ghaut contains a ~35 m thick sequence of mTBr, and an andesite block from the base of this sequence has an age of 1.634 ± 0.083 Ma (Figure. 2.2).

North Marguerita Bay contains a debris avalanche deposit consisting of a volcaniclastic megablock, which is comprised of seven units (units MB1–7; Figure 2.5a) surrounded by matrix facies. Units MB1–3 are the only units in the Silver Hills to contain poorly vesicular andesite clasts. The boundary between units MB2 and MB3 varies from sharp to diffuse, as does the boundary between units MB3 and MB4 which also has an erosional surface. Unit MB5 is interdigitated with MB6 (Figure 2.5a and c), likely resulting from minor deformation within the megablock.

This megablock is overlain by unit MB8, a mTBrMB with a minimum thickness of 15 m. It cuts down through units MB3–7 (Figure 2.5a–b), and contains a ~0.8 x 3.5 m megablock of hydrothermally altered mLT, with a sharp boundary. Unit MB8 has a lateral boundary with unit MB9; a mTBrMB with a minimum thickness of 7 m. The lateral boundary has a mingled shape with a sharp contact, and there is an isolated megablock of MB8 'floating' within MB9 (Figure 2.5d). The mingled boundary between units MB8 and MB9 is the result of incomplete mixing of debris that is typical of debris avalanche deposits (Siebert, 1984). Unit MB9 is either part of a volcaniclastic megablock, or is matrix facies of a different composition.

2.6.3 Yellow Hole to Old Quaw, ~1.5 Ma

The Yellow Hole exposures consist of extensively hydrothermally altered andesite lava overlain by non-altered lava dated at 1.520 ± 0.051 Ma (Brown & Davidson, 2008). At the mouth of Old Quaw ghaut is a debris avalanche deposit (Figure 2), with a megablock of hydrothermally altered lava next to non-altered mBr (matrix facies), and the boundary between them varies from sharp to transitional. There is an isolated block of the breccia within the hydrothermally altered lava, most likely resulting from internal deformation during transport (Siebert, 1984).

2.6.4 North West Bluff, ~1.5–4 Ma

North West Bluff is a ~200 m high peak made of andesite lava with areas of local (<1 m^2 in size) hydrothermal alteration, and an age of 1.493 ± 0.098 Ma. Exposure of this lava continues as a ridge heading southeast from North West Bluff to Valentine Hill (Figure 2.2), which consists of hydrothermally altered lava overlain by non-altered lava. In northwest Thatch Valley, the lavas have undergone extensive hydrothermal alteration, and locally becomes the 'intensely hydrothermally altered lava' facies.

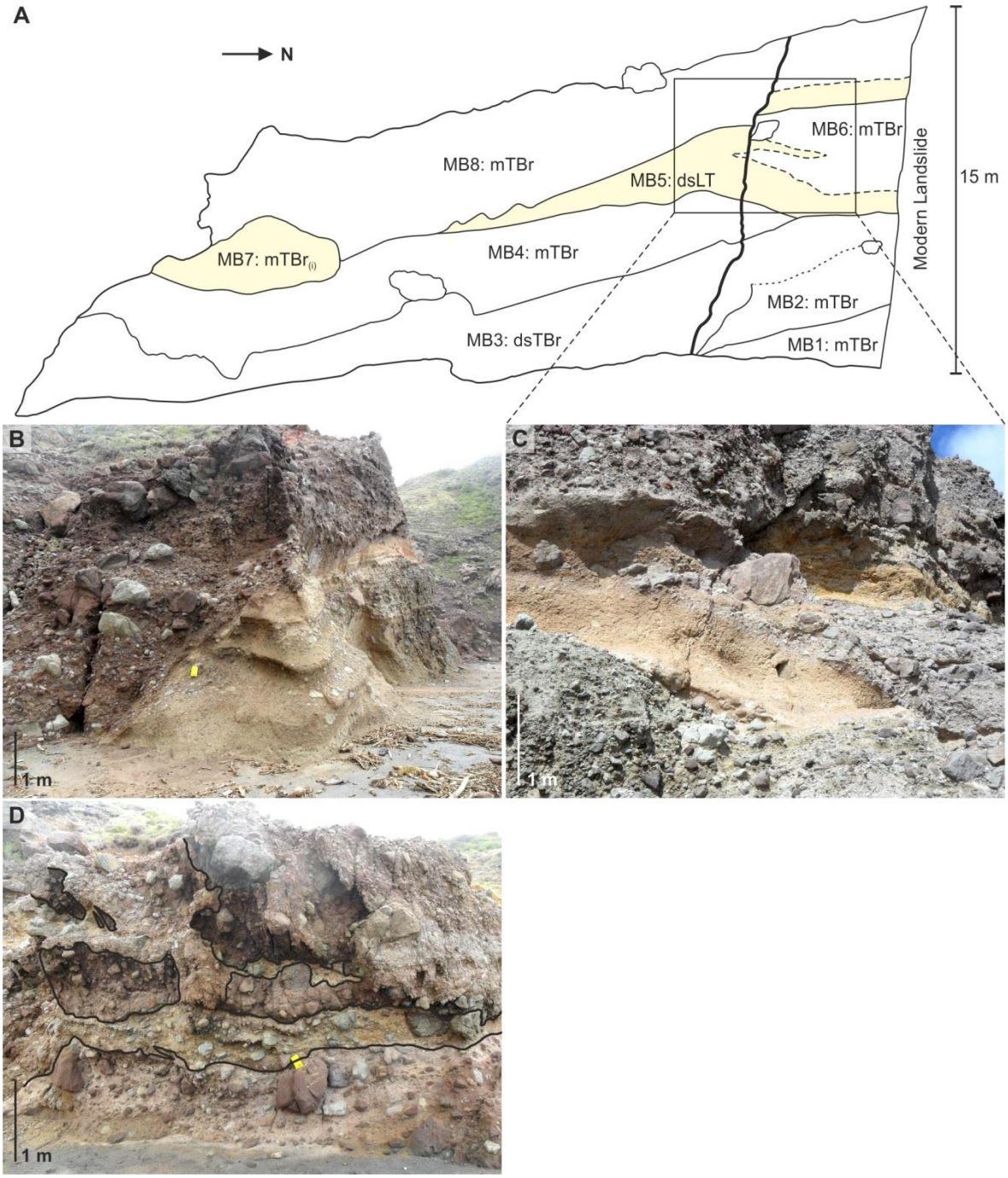

Figure 2.5. (a) Sketch of exposure along north Marguerita Bay, showing the relationship between units. Heavy black line = joint. Yellow colouring denotes the golden brown coloured units. (b) Southern corner of the exposure shown in (a), showing unit MB8 (left) cutting down through units MB3–4 (right). (c) Interdigitation of units MB5 (golden brown) and MB6 (grey). (d) Mingled boundary between units MB8 (grey) and MB9 (golden brown), with isolated blocks of MB8 floating in MB9. See supplementary material for unit descriptions.

North-central Thatch Valley contains a ~45 m thick (minimum) mTBr which has an age of 1.450 ± 0.160 Ma (Figure 2.2). Some clasts contain jigsaw-fit fractures, which supports an origin as a debris avalanche deposit, but the limited size of the exposure, coupled with the buried boundaries with surrounding units makes this difficult to confirm.

The andesite and dacite lava around and north of Rendezvous Bay is of a similar age, 1.424 ± 0.080 Ma (Figure 2.2). There is exposure of 'intensely hydrothermally altered lava' midway between Rendezvous Bay and North West Bluff.

2.6.5 Silver Hill, ~1.4 Ma

Andesite lavas and mLT-Br's tens of meters thick are exposed alongside the road between Drummonds and Silver Hill, and have been dated at 1.430 ± 0.019 to 1.395 ± 0.017 Ma (Brown & Davidson, 2008) (Figure 2.2). Rendezvous Bluff consists of a ~50 m high sequence of m-dsTBr overlying the lavas of Rendezvous Bay. Near Rendezvous they have a flow direction away from Silver Hill (Figure 2.2), and so are likely contemporaneous with the block-and-ash flow deposits between Silver Hill and Drummonds.

Further block-and-ash flow deposits from this period can be found overlying the basal hydrothermally altered lava of Valentine Hill (Figure 2.2). A ridge of this lava extends southeast from Valentine Hill, and on the southwestern side of this ridge the lava is overlain by ~20 m of m-dsTBr's (units V1–4) infilling a palaeovalley (Figure 2.6).

The lavas of Thatch Valley are locally overlain by mTBr, which locally has a hydrothermally altered matrix. These breccias are likely contemporaneous with the other mTBr units.

2.6.6 South Marguerita Bay, ~1.3 Ma

South Marguerita Bay contains a sequence of dacitic mLT-TBr tens of meters thick. The upper unit of this sequence is dated at 1.330 ± 0.190 Ma (Figure 2.2). Coussens et al. (2017) obtained an age of 1.310 ± 0.200 for their 'South Lime Kiln Bay pumice' unit, which is a poorly-sorted pmLT located in a fault block within the Centre Hills (Figure 2.1b). Due to its age, and location in a fault block, they interpret this deposit as originating from the Silver Hills.

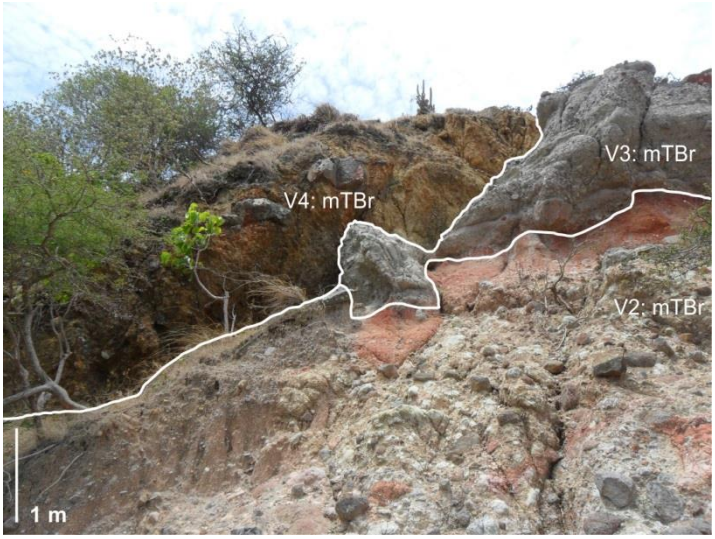

Figure 2.6. Block-and-ash flow deposits (units V2–4) by Valentine Hill.

2.6.7 Little Bay, ~1.0–0.8 Ma

The largest debris avalanche deposit of the Silver Hills is located in the Little Bay region, spanning Potato Hill, Davy Hill and Little Bay (Figure 2.2). The largest megablock within the Little Bay debris avalanche deposit is exposed east of Potato Hill. This megablock is intensely fractured andesite lava (Figure 2.7a) which is locally brecciated (Figure 2.7b). The megablock contains slightly sinuous near-vertical strike-slip and oblique-slip faults. The local brecciation within these megablock lavas may be attributed to autobrecciation, or alternatively the formation of small pockets of matrix facies where the megablock is beginning to disaggregate. Faulting is a well-documented feature in debris avalanche megablocks (e.g. Glicken, 1996; Ui et al., 1986; Ui and Glicken, 1986; van Wyk de Vries & Davies, 2015). The faults in this lava megablock are not observed in nearby exposures beyond the megablock, suggesting that they formed during transport of the debris avalanche, as opposed to being later features.

Within the megablock, the lava transitions westward into mTBrMB containing hydrothermally altered zones up to 6 m wide, which locally appear to 'inject' into the surrounding breccia. These fluidal textures are common in debris avalanche deposits between two differing matrix compositions (van Wyk de Vries & Davies, 2015).

At east Davy Hill the lava megablock is variably clastic with alternating hydrothermally altered and non-altered near-vertical bands and lenses (~0.3–1.5 m thick), with the lava becoming dominantly hydrothermally altered further west. Within the hydrothermally altered lava there is a ~15 m wide channel filled with five pyroclastic units, some of which are pumiceous (units DH1–5; Figure 2.8a). The boundaries between the different flow units are mostly sharp, with many showing erosive bases. Locally, however, these boundaries become diffuse and poorly-defined, particularly the boundary between unit DH1 and units

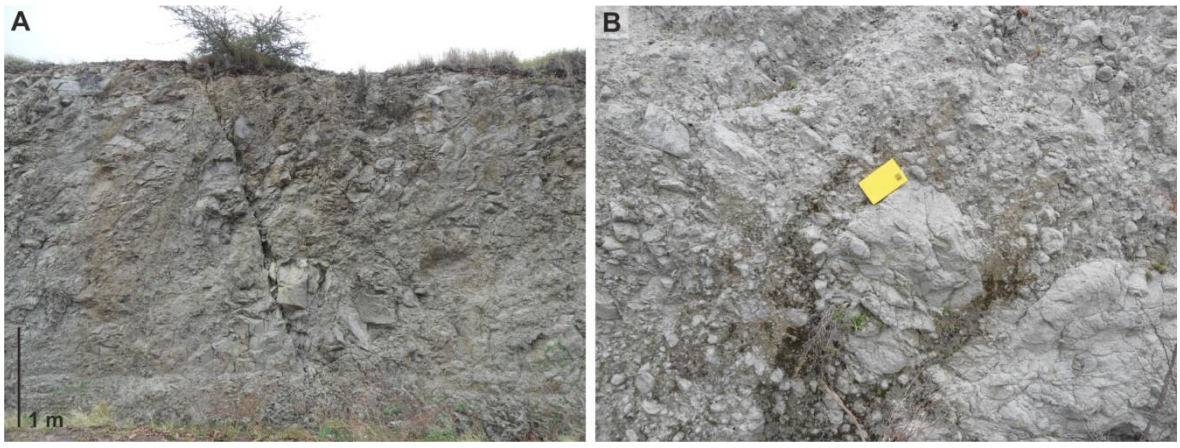

Figure 2.7. (a) Highly fractured andesite lava, east of Potato Hill, which is locally brecciated (b). Notebook for scale is 19 x 12 cm.

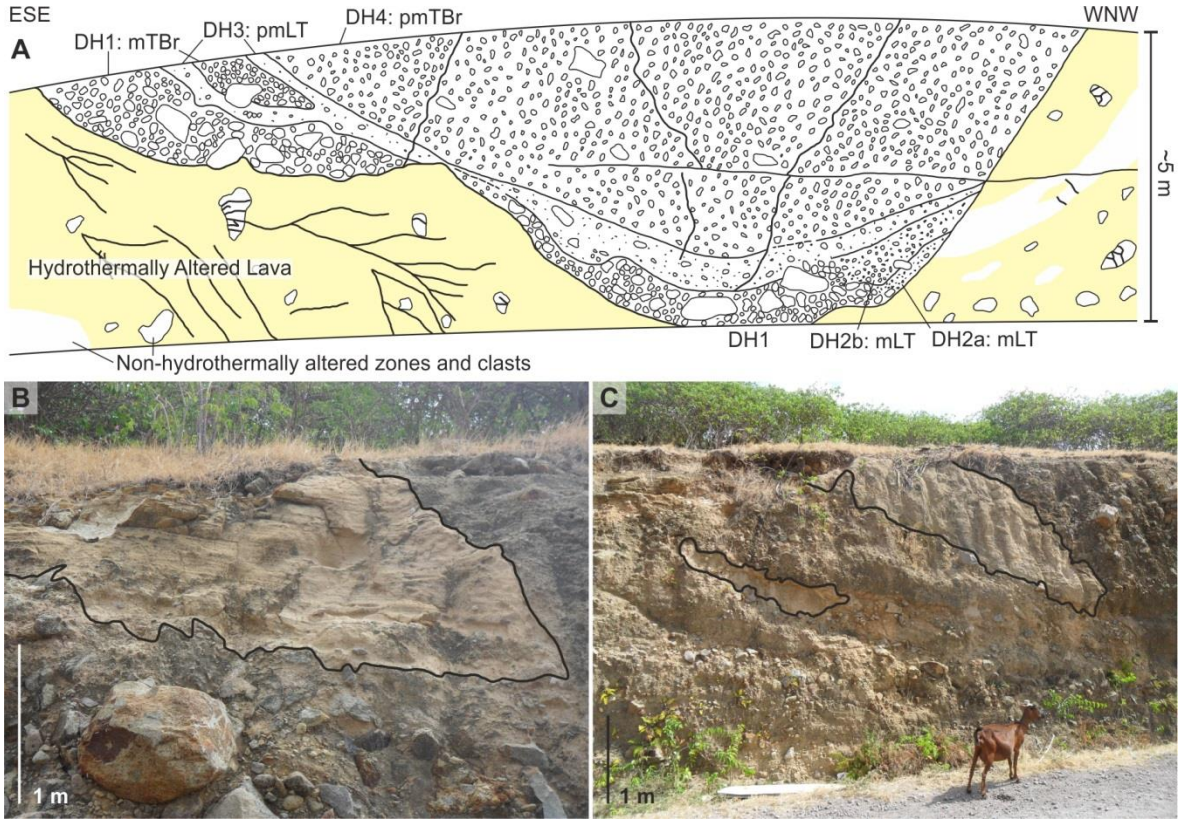

Figure 2.8. (a) Field sketch of a road cutting at GR 378001 1856419 (road to Davy Hill) showing a pyroclastic sequence (units DH1–4) filling a channel in hydrothermally altered lava. Facing SSW. (b) Single-unit volcaniclastic megablock of stratified tuff, and (c) sheared single-unit volcaniclastic megablocks of tuff, within unit DH5 (highlighted by black lines).

DH2a–b. Units DH1 and DH3 appear to be interdigitated, resulting from deformation within a volcaniclastic megablock.

The western boundary of this lava megablock on Davy Hill is marked by a curved steep west-dipping boundary. East of this boundary the lava is overlain by units DH1 and DH4, and unit DH1 contains a ~2 x 0.2 m lens of parallel and cross-stratified ash. West of the boundary is unit DH5 (matrix facies; mTBrMB), which contains irregular shaped meter-scale lenses of stratified tuff (Figure 2.8b) and sheared tuff lenses (Figure 2.8c), which are interpreted as single-unit volcaniclastic megablocks.

The exposure around the eastern base of Potato Hill comprises variably brecciated and highly fracture hydrothermally altered andesite lava, which is locally the 'intensely hydrothermally altered lava' facies. The hydrothermally altered lava has a sharp, near-vertical curved and wavy boundary with the intensely fractured and non-altered lava. This lava is overlain by a non-altered TBr (unit PH1), which becomes increasingly hydrothermally altered up-sequence. The alteration halo around the intensely hydrothermally altered lava is 'cut short' by the near-vertical boundary with the non-altered lava, suggesting that they may represent two different megablocks within the Little Bay Debris avalanche deposit. Similarly

sharp boundaries are observed between touching megablocks in debris avalanche deposits from the Shiveluch Volcano, Kamchatka (Belousov et al., 1999).

The west coast sea cliffs of Potato Hill contain a >20 m thick sequence of non-pumiceous to pumiceous m-sT-TBr. Some units contain small centimetre- to decimetre-scale injections into overlying units, and some are truncated by near-vertical minor faults with centimetre-scale displacement. These are common features in megablocks of layered volcaniclastic sequences (e.g. Takarada et al., 1999; Ui and Glicken, 1986), and so these units may form a volcaniclastic megablock within the Little Bay debris avalanche deposit.

2.6.8 Potato Hill, ~0.8 Ma

Overlying unit PH1 at Potato Hill is a pumiceous pyroclastic sequence (units PH2–4; Figure 2.2 and 2.9a). Unit PH3 (primary fallout deposit) has been dated at 0.800 ± 0.120 Ma (Figure 2.2), and has a Centre Hills origin (see section 2.8.1). This constrains the timing of the Little Bay debris avalanche to >0.8 Ma.

2.6.9 Old Quaw Ghaut, ~0.45 Ma

The Old Quaw debris avalanche deposit is overlain by a horizontally bedded volcaniclastic sequence containing four units, three of which are separated by palaeosols (units OQ1–4; Figure 2.9b), and were likely deposited in a palaeovalley. The base of this sequence, a $mLT_{lensLT\text{-}TBr}$ (unit OQ1), is overlain by pumiceous deposits which display noticeable variation between two exposures ~60 m apart (log sites 2–3; Figures 2.2 and 2.9b). Units OQ2a and 3a laterally transition between the well- and poorly-sorted subfacies' of pmLT-TBr with small (centimetre-scale) erosional channels. At log site 2 they grade into coarser and finer grained poorly-sorted pmLT-TBr's, respectively, with higher proportions of lithic clasts and matrix. This grading of unit OQ2a is also displayed at log site 3, but here unit OQ3a is missing. Unit OQ2a has been dated at 0.450 ± 0.130 Ma. The transition between the well- and poorly-sorted subfacies within the same unit suggests that units OQ2–3 are reworked fallout deposits. This interpretation is supported by the $^{40}Ar/^{39}Ar$ age and Pb isotope data, because the pumice clasts from unit OQ2a have a Soufrière Hills signature (see section 2.8.1). It is considered unfeasible for a pyroclastic density current to reach the eastern Silver Hills from the Soufrière Hills, hence these pumice clasts are likely to be derived from fallout from an eruption column. This unit is the oldest known deposit from a Soufrière Hills eruption.

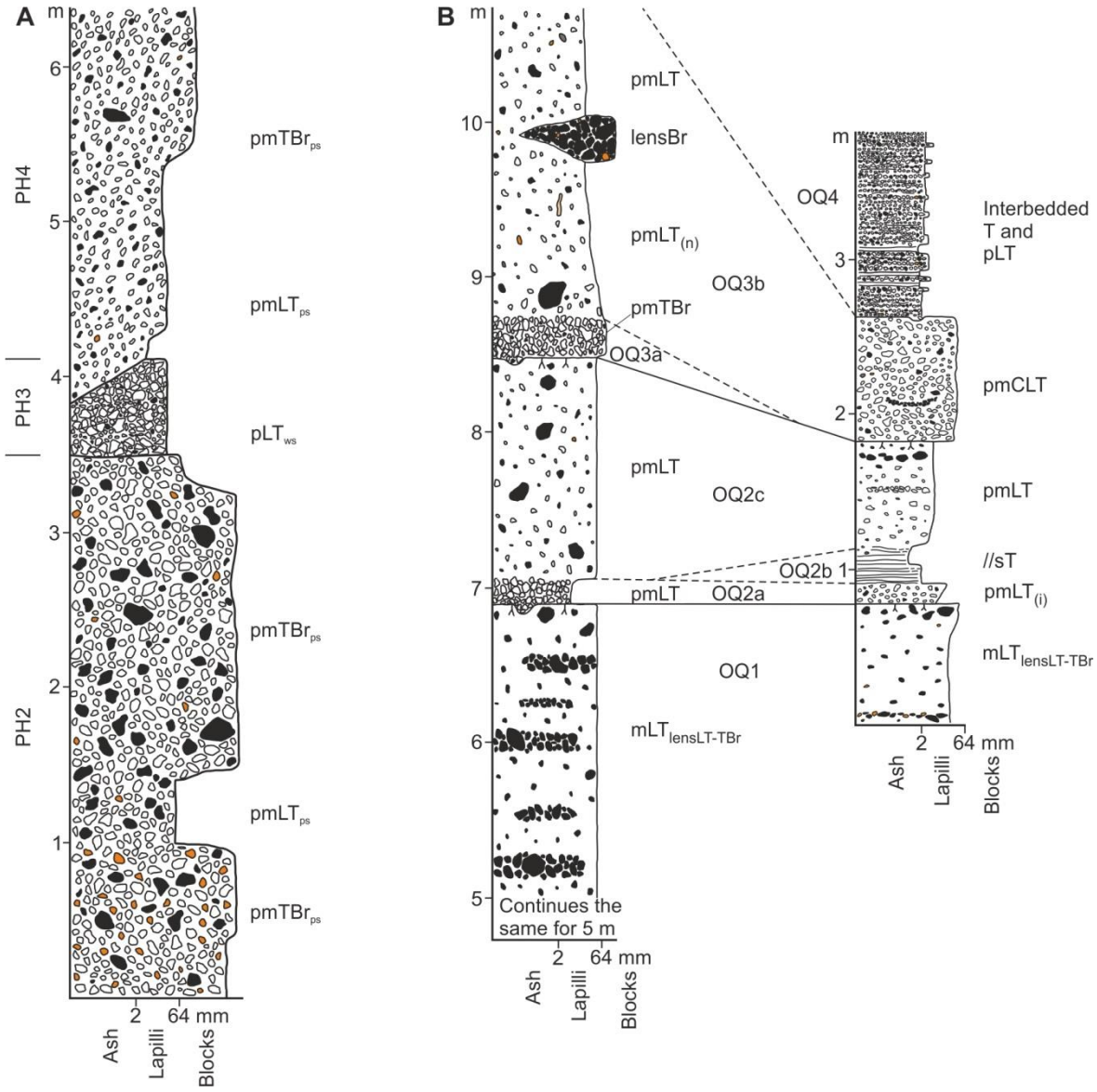

Figure 2.9. (a) Stratigraphic log from log site 1 at the top of Potato Hill. Units PH2 and 4 are the poorly-sorted sub-facies, unit PH3 is well-sorted sub-facies. (b) Stratigraphic logs from log sites 2 (left) and 3 (right) in Old Quaw Ghaut. Note the significant variation between the two sites, just ~60 m apart. Black clasts represent andesite, orange clasts hydrothermally altered andesite, white clasts pumice.

2.7 Expanded Stratigraphy of the Centre Hills

2.7.1 East Coast, ~1 Ma

Sample 21/81-AC comes from a basaltic andesite mTBr on the east coast of Centre Hills (Figure 2.1b), which lies at the base of the stratigraphy of Coussens et al. (2017). The age of 1.040 ± 0.250 Ma is within error of the oldest dates for this centre (Coussens et al., 2017; Harford et al., 2002).

2.7.2 Southwest Centre Hills, ~0.45 Ma

Pumice from a pumiceous mTBr in the southwest Centre Hills has an $^{40}Ar/^{39}Ar$ age of 450 ± 170 ka (Figure 2.1b), and a Soufrière Hills Pb isotope signature (see section 2.8.1). This provides further evidence for Soufrière Hills volcanism at ~450 ka.

2.7.3 Dry Waterfall and Spring Ghaut, ~0.38 Ma

Andesite lava from Dry Waterfall (central Centre Hills) has been dated at 378 ± 18 ka (Figure 2.1b), and has a Centre Hills Pb isotope value (section 2.8.1), providing the youngest known age for Centre Hills volcanism. A dacitic mTBr from Spring Ghaut (southwest Centre Hills) has been dated at 376 ± 85 ka (Figure 2.1b), and has a Soufrière Hills Pb isotope signature. This demonstrates an overlap in activity between Centre Hills and Soufrière Hills volcanism.

2.8 Provenance

Many intra-oceanic arcs display along-arc geochemical heterogeneity, caused by variations in source component contributions (e.g. Izu-Bonin-Mariana arc: Elliott et al. (1997); Ishizuka et al. (2007); Tonga-Kermadec-Lau arc: Ewart et al. (1998); Lesser Antilles arc: Macdonald et al. (2000)). Such variation has also been observed on individual islands, allowing the eruption deposits of distinct volcanic centres to be distinguished using isotope and trace element ratios. For example, Pagan island in the Mariana arc contains two volcanic centres ~8 km apart, Mount Pagan and South Pagan, whose eruption deposits can be distinguished using trace element ratios (e.g. Ba/Th, Ba/La, Nb/Zr) (Marske et al., 2011). The island of Hachijojima in the Izu-Bonin arc comprises two volcanic centres ~7 km apart, Higashiyama and Nishiyama, the deposits of which can be distinguished using Pb isotopes, and Zr/Y and La/Sm ratios (Ishizuka et al., 2008). In the Lesser Antilles, there is a clear north-south gradient in the Sr, Nd and Pb isotope ratios, and trace element patterns of volcanic rocks along the entire arc that has persisted for ~5 Myr (Labanieh et al., 2010; Lindsay et al., 2005). This geographical pattern is also observed on individual islands, such as Martinique, where $^{143}Nd/^{144}Nd$ can be used to separate deposits from Pitons du Carbet and Mont Conil-Mont Pelée, which overlapped in activity 545–322 ka (Germa et al., 2011b; Labanieh et al., 2012). For Montserrat, Pb isotopes have been shown to clearly distinguish Soufrière Hills deposits from those of the Centre and Silver Hills, and $^{143}Nd/^{144}Nd$ can be used to differentiate between Silver Hills and Centre Hills deposits (Cassidy et al., 2012).

For some samples in this study there is ambiguity over which volcanic centre they are from, such as 16/72-PR, which is geographically within the Silver Hills, but has a

Centre/Soufrière Hills age. Here, we use trace element and isotope geochemistry to help constrain their provenance (data is presented in Appendix Table 2.4).

2.8.1 Terrestrial Deposits

Most of the samples analyzed in this paper fit within the Silver Hills-Centre Hills Pb isotope field, with three samples falling in the Soufrière Hills field: 28/57-AC, 16/72-PR and 20/79-PC (Figure 2.10).

Silver Hills and Centre Hills samples can be distinguished on a plot of $^{143}Nd/^{144}Nd$ vs Nb/Y (Figure 2.11). Four samples with uncertain origin (i.e. from either Silver Hills or Centre Hills volcanism) are highlighted on Figure 8a: pumice from Davy Hill, Potato Hill and Lime Kiln Bay, and a lava clast from South Marguerita Bay. Pumice from a fault block in South Lime Kiln Bay (sample 11.1.4C), which is geographically part of the Centre Hills, has been dated at ~1.31 Ma, leading to the interpretation that this deposit originated from Silver Hills volcanism (Coussens et al., 2017). This interpretation is supported by $^{143}Nd/^{144}Nd$ vs Nb/Y, in which this same sample plots within the Silver Hills field (Figure 2.11a).

The Silver Hills-Centre Hills boundary defined by Harford et al. (2002) follows Brimm's Ghaut, which runs through Marguerita Bay (Figure 2.2). Sample 12/13-AC from south Marguerita Bay (south of the boundary) has been dated at ~1.33 Ma, suggesting a Silver Hills origin. This is supported by $^{143}Nd/^{144}Nd$ vs Nb/Y (Figure 2.11a), suggesting that the boundary between the Silver Hills and Centre Hills is further south than previously thought.

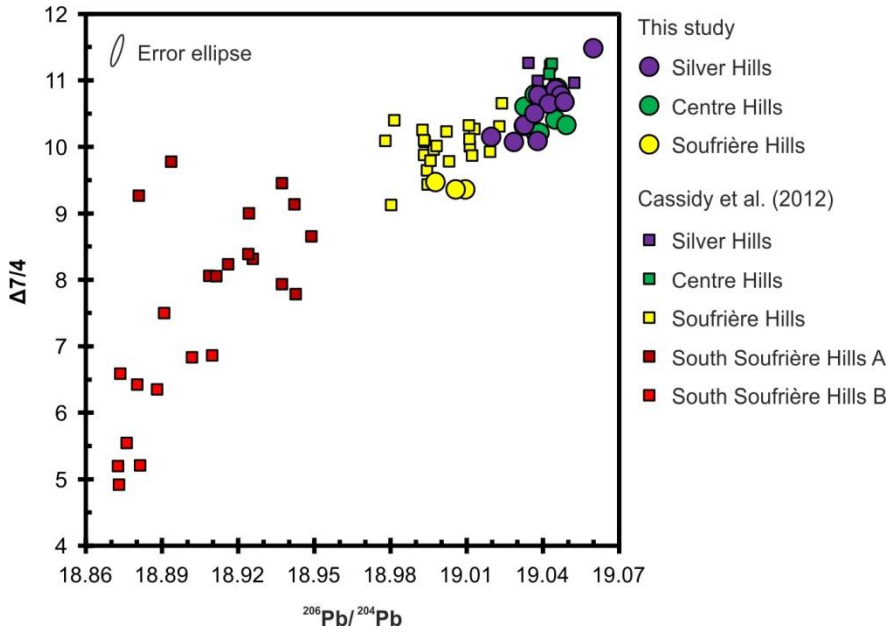

Figure 2.10. Pb isotopes showing separation between the South Soufrière Hills, Soufrière Hills and Centre and Silver Hills. Δ7/4 is $^{207}Pb/^{204}Pb$ calculated to the Northern Hemisphere Reference Line (Hart, 1984).

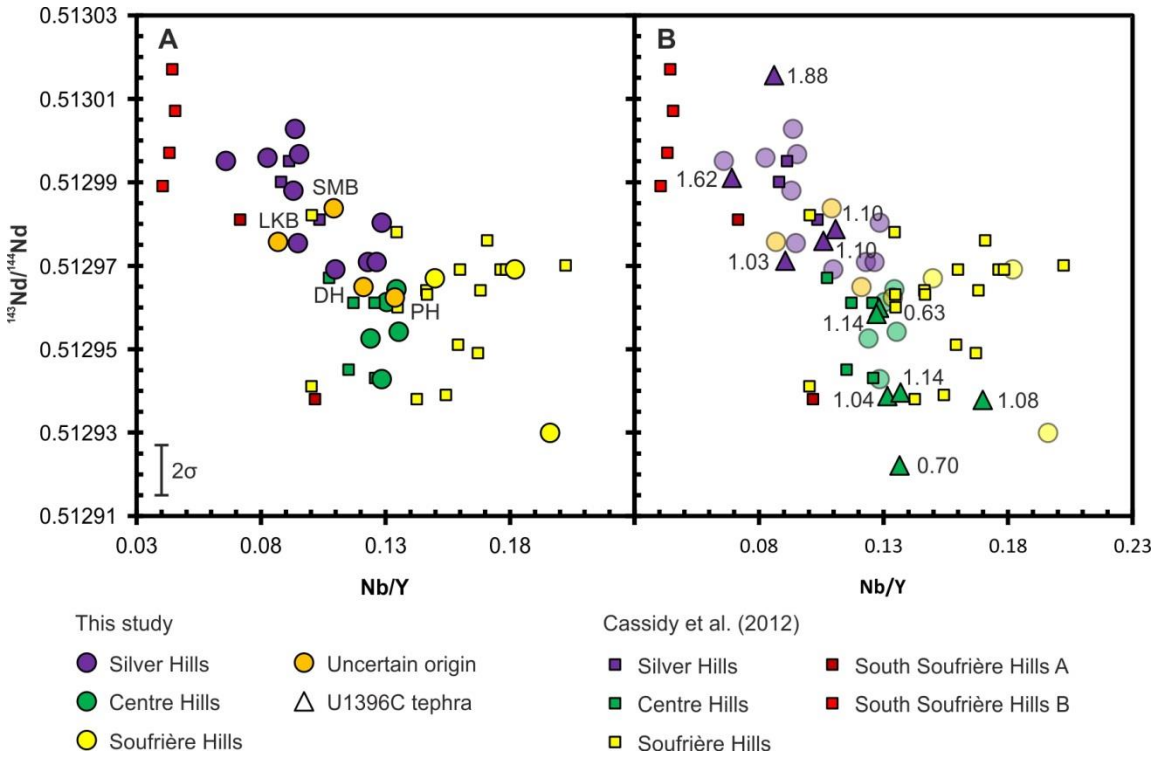

Figure 2.11. Nb/Y vs 143Nd/144Nd separating between Silver and Centre Hills. (a) Terrestrial samples, and identifying the provenance of samples with uncertain origin: SMB, South Marguerita Bay; LKB, Lime Kiln Bay; DH, Davy Hill; PH, Potato Hill. (b) Marine tephra samples from core U1396C. Numbers note age of tephra layers in Ma. Faded terrestrial samples are shown for comparison. Error on Nb/Y smaller than symbols.

Sample 23/86-PF (unit PH3 on Potato Hill) is geographically within the Silver Hills, but has an age of ~0.8 Ma, suggesting this deposit is derived from the Centre Hills (Figure 2.2). This interpretation is supported by a Centre Hills geochemical signature (Figure 2.11a). The pumice sample from Davy Hill (24/88-PC) is also geographically within the Silver Hills, but falls in the Centre Hills field in Figure 2.11a, suggesting a Centre Hills origin. Because this sample is part of the Little Bay debris avalanche deposit, this suggests that the debris avalanche occurred during the early stages of Centre Hills volcanism.

2.8.2 Marine Tephra Deposits

Marine sediment core U1396C contains fifteen tephra layers with thicknesses >1 cm within the ~2.35–0.37 Ma time span covered by our new $^{40}Ar/^{39}Ar$ ages. The age assignments of the tephra layers are derived from palaeomagnetic, biostratigraphic and foraminifera $\delta^{18}O$ correlations (Fraass et al., 2016; Hatfield, 2015). Pb isotope analyses show that thirteen of these layers are from Montserrat and the other two are from Guadeloupe (Palmer et al., 2016). Of the Montserrat layers, eight contain enough pumice or fresh non-vesicular lava grains for geochemical analysis (Table 2.4). Of particular interest are the five tephra layers in the 1–1.3 Ma period (the gap in the terrestrial age record between the Silver and Centre Hills)

Table 2.4. Tephra layers in core U1396C spanning the time interval 2.35–0.37 Ma.

Tephra layer	Age (Ma)	Provenance	Pumice?*
2H1W-66/81	0.63	Centre Hills	Yes
2H2W-39.5/52	0.70	Centre Hills	Yes
2H2W-148.5/2H3W-14	0.77	Centre Hills	No
2H4W-94.5/98	0.86	Centre Hills	No
2H7W-62.5/67	1.02	Centre Hills	TF
3H1W-10/12	1.03	Silver Hills	Yes
3H1W-24/27.5	1.03	Guadeloupe	Yes
3H1W-50.5/53	1.04	Centre Hills	NVL
3H2W-23.5/26	1.08	Centre Hills	Yes
3H2W-58/67	1.10	Silver Hills	Yes
3H2W-142.5/149	1.14	Centre Hills	Yes
3H6-32/37	1.41	Guadeloupe	Yes
3H7W-33/40	1.49	Silver Hills	TF
4H2W-29/32	1.62	Silver Hills	Yes
4H6W-42/44	1.88	Silver Hills	Yes

*Contains enough pumice for geochemical analysis. TF, too fine-grained to separate pumice from the other components; NVL, fresh non-vesicular lava grains analysed.

with sufficient pumice. Figure 8b shows that the layers with ages of 1.10 Ma and 1.03 Ma fall within the Silver Hills field, and 1.14, 1.08 and 1.04 Ma fall within the Centre Hills field (Figure 2.11b). The absolute uncertainty in the age of any individual tephra layer is ~50 kyr, but the stratigraphic order of the layers is certain. Hence, we can be confident that there was overlap in activity between the Silver and Centre Hills for at least ~130 ka.

2.9 Petrology

The lavas of the Silver Hills volcanic centre are porphyritic (~30–60 vol. % phenocrysts) with a phenocryst assemblage of ~65–75% plagioclase up to 4 mm, ~15–20% orthopyroxene up to 6 mm and ~5–15% clinopyroxene up to 5 mm. Quartz and amphibole are locally present in minor amounts. Zoning is observed in some clinopyroxene and orthopyroxene phenocrysts, and all plagioclase phenocrysts, with many of the latter displaying sieve textures. The groundmass is generally microcrystalline and composed of plagioclase, orthopyroxene, clinopyroxene and Fe-Ti oxides (Figure 2.12), with some samples showing alignment of elongate crystals.

Enclaves are abundant within Silver Hills lavas, and comprise up to 20 vol. %. They have coarser groundmasses (composed of plagioclase, orthopyroxene, clinopyroxene and Fe-

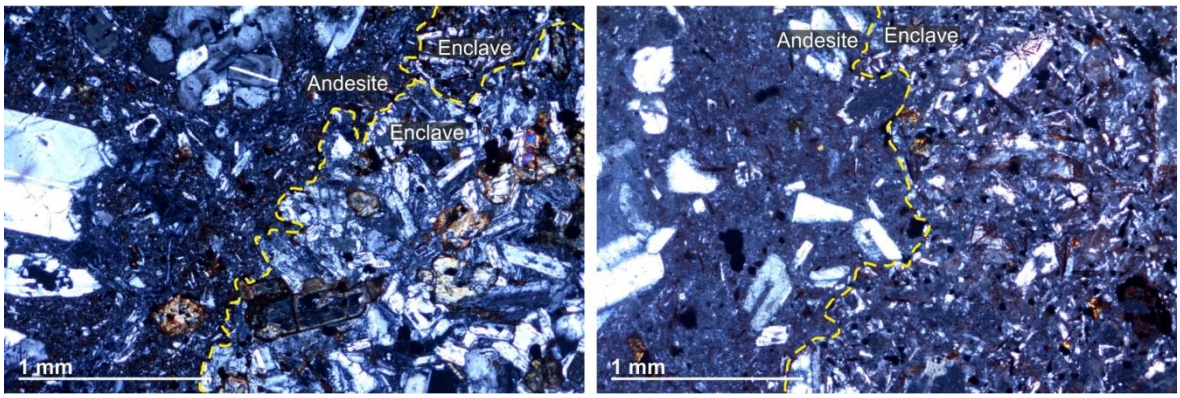

Figure 2.12. Thin section images of andesite lava and enclave textures, and boundaries between them.

Ti oxides) than the host andesite, with a higher proportion of pyroxenes (Figure 2.12). Many of the enclaves have a diktytaxitic groundmass, with interlocking, randomly-orientated elongate crystals, similar to enclaves erupted during the 1995–2010 eruption of the Soufrière Hills (Plail et al., 2014).

The Centre Hills samples have a similar phenocryst assemblage as the Silver Hills lavas, closely matching the samples described by Coussens et al. (2017). The Soufrière Hills samples are porphyritic (~30 vol. % phenocrysts) with a phenocryst assemblage of ~65–75% plagioclase, 15–20% orthopyroxene and 10–15% amphibole, with minor clinopyroxene and quartz, similar to the Soufrière Hills lavas erupted in the past ~130 kyr (Harford et al., 2002).

2.10 Discussion

2.10.1 Evolution of the Silver Hills Volcanic Centre

Subaerial volcanic activity began in the Silver Hills prior to 2 Ma, with the oldest rocks present as lava domes around the Little Bay area and dome collapse deposits built up the south Drummonds region (Figure 2.13). At ~1.7–1.6 Ma, activity migrated to the eastern part of Silver Hills, forming the lava domes and associated deposits of Marguerita Bay. Part of this edifice collapsed to form the Marguerita Bay debris avalanche deposit. Activity continued in this region up until ~1.5 Ma, forming the lavas of Yellow Hole, with collapse of this edifice forming the Old Quaw debris avalanche. Next, activity shifted to the northwestern part of the Silver Hills, forming the lava domes of North West Bluff, Thatch Valley and Rendezvous Bay at ~1.5–1.4 Ma, with concomitant hydrothermal activity producing the observed fumarole deposits in this region. At ~1.4 Ma activity shifted again to form lava domes at Silver Hill and Drummonds, which collapsed to form block-and-ash flow deposits throughout the north, west and centre of the Silver Hills. Collapse of these edifices with part of the young Centre Hills edifice created the Little Bay debris avalanche deposit at around ~1–0.8 Ma. The block-

and-ash flow deposits of south Marguerita Bay suggest that lava dome growth was still active in the Drummonds area ~1.35–1.30 Ma (Figure 2.13). The youngest deposits found in the Silver Hills region are reworked pumice fall deposits in Old Quaw, which Pb isotopes indicate to be derived from eruptions of the early stages of Soufrière Hills volcanism ~0.45 Ma.

2.10.2 Comparisons with Soufrière Hills and Centre Hills

The Silver Hills is the smallest volcanic centre on Montserrat in terms of subaerial exposure, but bathymetric data may provide an insight into its original size. Montserrat is surrounded by a shallow submarine shelf, which extends up to 5 km wide around the Silver Hills (Figure 2.1b), and is interpreted as representing the original expanse of the Silver Hills (Le Friant et al., 2004). Assuming that the Silver Hills originally had a similar size to the Soufrière Hills, the estimated minimum original volume of the Silver Hills above 100 m below sea level (the depth of the submarine shelf) is 17 km^3; the subaerial part of the Soufrière Hills is ~12 km^3 (Le Friant et al., 2004).

The Soufrière Hills is cut by several N 110 ± 10°E striking normal faults (e.g. Belham Valley Fault, Richmond Hill Fault, Kinsale-St. Patricks Fault), parallel to offshore faults, which are all part of the Montserrat-Havers fault system. The five Soufrière Hills domes are aligned along this ~N110°E trend (Figure 1b), suggesting there is a tectonic control on the location of eruptive vents in the Soufrière Hills (Feuillet et al., 2010). A notable morphological feature of the Silver Hills is the ~N110°E orientation of the northern coastline, which could suggest that the location of eruptive vents of the Silver Hills was also controlled by regional WNW oriented fault systems. However, no tectonic faults were identified during fieldwork to support this hypothesis.

Our work on the deposits of the Silver Hills volcano has shown its past volcanic activity to be similar to that of the Soufrière Hills, with both characterized by lava dome growth and collapse coupled with Vulcanian eruptions and periodic flank/sector collapses. Soufrière Hills does, however, exhibit evidence of larger, sustained eruptions at ~450 and ~179 ka, whereas there is no record of large eruptions emanating from the Silver Hills. The Centre Hills activity is also characterized by lava dome growth and collapse with Vulcanian eruptions, but also produced multiple Plinian eruptions (possibly up to magnitude 5) throughout its eruptive history (Coussens et al., 2017; Harford et al., 2002). The consistency in the style of volcanic activity throughout the lifespan of the Silver Hills adds support to the hypothesis of Harford et al. (2002) that future activity at Soufrière Hills is likely to continue in the same style as the 1995–2010 eruption.

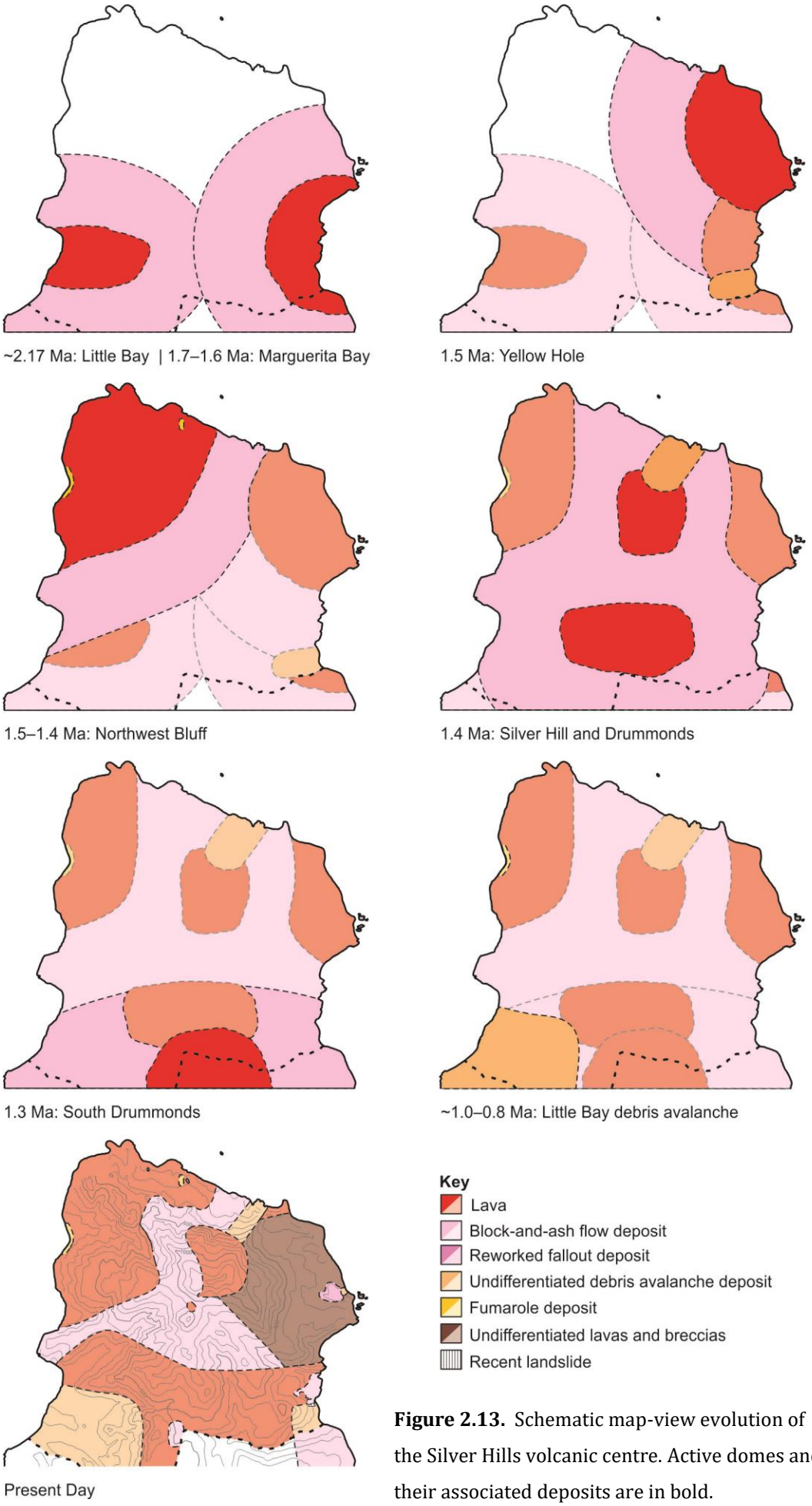

Figure 2.13. Schematic map-view evolution of the Silver Hills volcanic centre. Active domes and their associated deposits are in bold.

It is worth noting, however, that the exposed massifs of the Soufrière Hills and Centre Hills are both currently larger in size than Silver Hills, and that the Plinian deposits of both the former are situated along coastal exposures that are now missing from Silver Hills. Additionally, the current size of the sub-aerial portion of Silver Hills is approximately the same size as the central dome complex of the Soufrière Hills which, like the central part of Centre Hills, is dominated by massive andesite dome-lava and their collapse deposits (Harford et al., 2002). Thus it is feasible that any large sustained explosive eruptions that Silver Hills may have produced are not preserved on land, akin to the Basal Complex, the oldest volcanic centre on Basse-Terre, Guadeloupe. This is another deeply eroded volcano whose sub-aerial record is dominated by effusive eruption products, with no evidence of large explosive activity. However, the study of a marine sediment core has revealed that this seemingly effusive centre produced a large Plinian eruption (Volcanic Explosivity Index ~6) towards the end of its life, at ~2.4 Ma, which is believed to be the largest known eruption in the Lesser Antilles (Palmer et al., 2016). While the Silver Hills may not have produced eruptions of this magnitude, this example serves to highlight a potential preservation bias within the Silver Hills' terrestrial record.

2.10.3 Comparisons with Other Arc Volcanic Centres

Many arc volcanoes dominated by andesitic and dacitic lava dome formation nevertheless also experience periodic Plinian eruptions, similar to that inferred for the Centre Hills (Coussens et al., 2017). For example, the 1902 Plinian eruption of Santa Maria, a dominantly andesitic (Rose, 1972) stratovolcano in Guatemala, was one of the 10 largest eruptions ever observed (Bennett et al., 1992), yet volcanic activity at Santa Maria has been dominated by eruptions of lava flows and domes, with their associated collapse pyroclastic deposits (Rose, 1972, 1973, 1987). Indeed, the active Santiaguito dome complex has built up inside the crater produced from the 1902 eruption. In Chile, Volcán Quizapu produced two of the largest historic eruptions of South America, which were of a similar composition, yet one was effusive (a ~5 km^3 mingled andesite-dacite lava flow in 1846–1847), and one was explosive (a ~4.5 km^3 dacitic Plinian eruption in 1932) (Hildreth & Drake, 1992). The transition between effusive and explosive eruptions at Volcán Quizapu has been linked to the extent of mafic magma recharge and mixing prior to eruption. The 1932 Plinian eruption had a relatively minor recharge component, while the recharge magma comprised <10–45 vol% of the lava erupted throughout 1846–1847 (Ruprecht & Bachmann, 2010). The resident magma temperatures for both eruptions is estimated to be ~870°C (Ridolfi et al., 2010), but the greater volume of recharge magma of the 1846–1847 eruption led to an eruption temperature up to 130°C hotter than the 1932 eruption. It is thought that this higher magmatic temperature enhanced syneruptive magma degassing and led to effusive eruptive

behaviour, by accelerating volatile diffusion, lowering melt viscosity, and inhibiting brittle fragmentation (Ruprecht & Bachmann, 2010).

Magma recharge and mixing is also considered to be responsible for the long-term (~500–0 ka) low explosivity of Mount Hood, Oregon, another andesite-dacite arc volcano with no evidence for large explosive eruptions (Koleszar et al., 2012; Scott et al., 1997). Viscosity models show that mafic recharge beneath Mount Hood may result in a 5–10-fold decrease in viscosity of the silicic resident magma, facilitating greater volatile diffusion, and delaying or precluding fragmentation during magma ascent. The continued low explosivity of activity at Mount Hood over 500 kyr is thought to be due to somewhat constant mixing proportions and timescales, whereas variability in mixing proportions and timescales leads to variation in eruption styles between effusive and explosive (Koleszar et al., 2012), such as observed at Volcán Quizapu (Ruprecht & Bachmann, 2010). Further, Koleszar et al. (2012) invoke this model to explain the long-term low explosivity (i.e. absence of Plinian eruptions) in other andesitic-dacitic arc volcanoes where magma mixing is a common process, such as Unzen volcano, Japan (Hoshizumi et al., 1999; Venezky & Rutherford, 1999), and Mount Dutton, Alaska (Miller et al., 1999).

On Montserrat, this model may also explain the low explosivity behaviour of the Silver Hills and Soufrière Hills, because the lavas of these centres contain abundant mafic enclaves, indicating magma mixing has consistently played a major role in controlling eruption styles at these volcanic centres (e.g. Murphy et al., 1998; this study). Furthermore, for the Centre Hills deposits, enclaves are only present within lavas, and not in the pumiceous (explosive) deposits (Coussens et al., 2017). This suggests that the absence of, or at least reduced extent of, magma recharge and mixing may have played a significant role in producing large explosive eruptions at the Centre Hills. However, this model relies on the recharge magma raising the temperature of the resident magma to prevent explosive eruptions, but geothermometry studies estimate that magma storage temperatures beneath the Centre Hills (~810–1080°C; Coussens et al., 2017) were similar to those of the 1995–2010 Soufrière Hills eruption (~785–1100°C; Barclay et al., 1998; Christopher et al., 2014; Devine et al., 1998, 2003, Murphy et al., 1998, 2000). This suggests that increased temperature alone cannot be responsible for the explosive eruptions of the Centre Hills. Coussens et al. (2017) showed that the composition of Centre Hills deposits remained constant, thus ruling out compositional control on eruption styles. They suggest instead that explosive eruptions may have been the result of local changes in magma storage conditions (variable magma temperature or viscosity) and pre-eruptive dynamics.

In the Lesser Antilles, Silver Hills volcanism is typical of that documented along the northern arc, in that andesitic dome growth and collapse—with small explosive eruptions—

has dominated volcanic activity at Saba, St. Eustatius, St. Kitts, and Nevis, with no evidence for larger, sustained eruptions (Baker, 1984, 1985; Baker et al., 1980; Davidson & Wilson, 2011; Defant et al., 2001). Petrological evidence (e.g. reverse-zoned phenocrysts) indicate that magma recharge and mixing is a common process at Saba and St. Kitts (Baker et al., 1980; Toothill et al., 2007), which following the model of Koleszar et al. (2012), suggests that the characteristics of magma recharge and mixing have been constant for the northern islands, thus inhibiting the potential for large explosive eruptions and maintaining low explosivity behaviour. The central and southern islands display similar activity to the northern islands, but with Plinian eruptions identified at La Soufriere, Guadeloupe (Komorowski et al., 2005), Morne Diablotins and Morne Trois Pitons-Microtrin, Dominica (Boudon et al., 2017), Mont Pelée, Martinique (Roobol & Smith, 1976; Westercamp & Traineau, 1983), Qualibou, St Lucia (Wohletz et al., 1986), and Soufrière, St Vincent (Rowley, 1978; Wright et al., 1984), more akin to the Centre Hills volcanism (Coussens et al., 2017). In Dominica, mafic enclaves are present in lavas from multiple volcanic centres, but are notably absent from pumiceous deposits (Howe et al., 2015), further supporting a link between magma recharge and mixing and eruption explosivity. Further detailed studies comparing evidence for magma mixing (e.g. enclave abundances, reverse-zoned phenocrysts) between eruption styles are required to further investigate the link between magma mixing and eruption explosivity in the Lesser Antilles.

2.10.4 Revised Geochronology of Volcanism on Montserrat

Here, we present a revised geochronology of volcanic activity of Montserrat's three main volcanic centres (Figure 2.14), based on a review of existing ages, new $^{40}Ar/^{39}Ar$ dates, and palaeomagnetic ages from marine tephra layers.

Previously, Silver Hills volcanism was dated to range from ~2.6–1.2 Ma (Brown & Davidson, 2008; Harford et al., 2002), but as discussed some of these dates are unreliable. Silver Hill volcanism can now be more reliably constrained to at least ~2.17–1.03 Ma. Coussens et al. (2017) divided Centre Hills volcanism into two periods of activity, spanning >0.95 to ~0.60 Ma and ~0.60 to ~0.40 Ma. The new Centre Hills dates presented in this study expand the timing of Centre Hills volcanism by ~0.2 Myr, to ~1.14–0.38 Ma.

Three stages of Soufrière Hills volcanism have been previously recognized: >300–175 ka, 175–130 ka and 112 ka to recent (Coussens et al., 2017; Harford et al., 2002). Our new ages identify a fourth, earlier stage, ~450–300 ka, characterized by the eruption of hornblende-orthopyroxene andesites, similar to lavas erupted since ~112 ka, and in contrast to the two-pyroxene andesites erupted ~290–130 ka (Harford et al., 2002; Rea, 1974). This means that the petrology of the Soufrière Hills eruptive products has changed at least twice

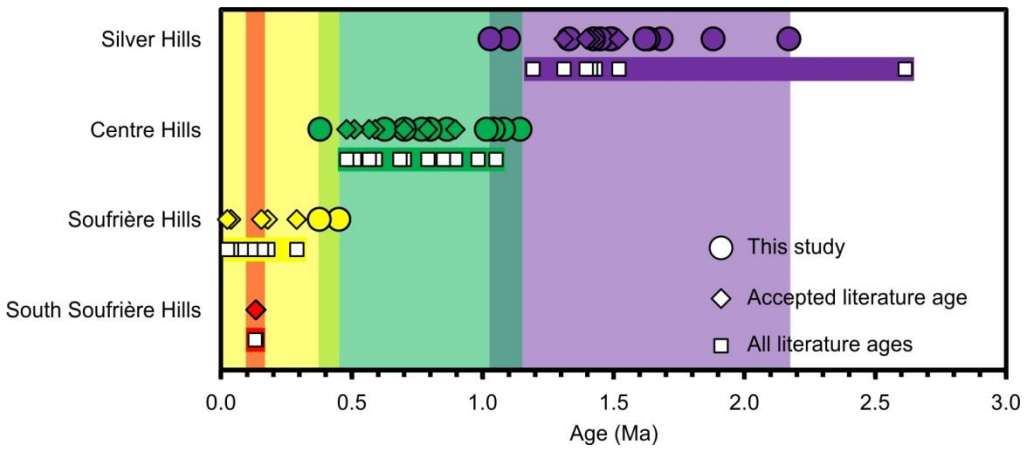

Figure 2.14. Timing of volcanic activity on Montserrat. Coloured bands define our revised timings of volcanism for the different volcanic centres. All literature ages are shown for comparison. Literature ages from Harford et al. (2002); Brown and Davidson, (2008); Coussens et al. (2017).

throughout the volcano's development. Garibaldi Hill, which contains a two-pyroxene andesite block-and-ash flow deposit dated at 290 ka (Harford et al., 2002), contains both two-pyroxene and hornblende-hypersthene andesites, but the stratigraphic relationship between the two andesite types is not documented (Rea, 1974). A detailed stratigraphy of Garibaldi Hill may provide further details as to when the change from hornblende-hypersthene to two-pyroxene andesite took place, and if it was an instant or a gradual change.

Our new ages show that Silver, Centre and Soufriere Hills were active for at least 1.14 Myr, 0.76 Myr, and 0.45 Myr, respectively. The most comparable island to Montserrat in the Lesser Antilles arc is the neighbouring island of Basse-Terre, Guadeloupe. It also formed following tectonic adjustments during the Mid-Miocene and similarly shows a north-south migration in the locus of volcanism over a similar time interval. There is also high quality age data available for the volcanic centres on Basse-Terre; with 2.79–2.68 Ma, 1.81–1.15 Ma, 1.02–0.44 Ma, 0.56–0.47 Ma and 0.21 Ma – present recorded for the Basal Complex, Septentrional Chain, Axial Chain, Monts Caraïbes Massif and Grande Découverte Volcanic Complex, respectively (Carlut et al., 2000; Ricci et al., 2015a, 2015b, Samper et al., 2007, 2009). With the exception of the oldest Basal Complex (which is heavily eroded and has limited subaerial exposure) and Monts Caraïbes Massif (which has limited subaerial exposure and only two dates), these intervals of activity (0.66 Myr, 0.58 Myr, and 0.21 Myr) for the different centres on Basse-Terre are similar to those observed on Montserrat. These observations suggest that ~0.5–1.0 Ma is a common lifespan for volcanic centres in the region. The question arises, therefore, as to whether this apparent timescale of volcanic centre duration is purely stochastic or whether it has more fundamental significance. For example, the duration of a volcanic centre may be related to the life cycle of volcanic edifices. Modelling of edifice loading indicates that progressive growth of a volcanic structure results in the confining pressure increasing to the extent that the centre is forced to migrate laterally

(Pinel et al., 2010). Alternatively, the duration of a volcanic centre may be related to deeper processes. For example, it has been suggested that partial melting in the mantle wedge yields rising diapirs of partially molten material that rise through the mantle with frequencies of order 10^5–10^6 years (Hall & Kincaid, 2001; Stern, 2002). Further detailed geochronology of volcanic centres on other islands of the Lesser Antilles is required to assess these hypotheses in more detail.

Our new ages also provide evidence for a ~130 kyr overlap in activity between the Silver and Centre Hills, and ~70 kyr overlap between the Centre and Soufrière Hills. There was also overlap between the Soufrière and South Soufrière Hills (Cassidy et al., 2012, 2014). Overlap in volcanic activity between two or more centres on an individual island has also been documented on Martinique, where Trois Ilets and Pitons du Carbet were both active from 998 to 345 ka. Here, further coeval activity occurred at Mont Conil-Mont Pelée during 545–345 ka (Germa et al., 2010, 2011b). On Dominica, there has been coeval activity between at least up to four volcanic centres over much of the lifetime of the island (Smith et al., 2013, and references therein). The volcanic centres of Basse-Terre, Guadeloupe have been extensively dated, and overlap in activity has only been identified between two centres: the Axial Chain and Monts Caraïbes during 555–472 ka (Carlut et al., 2000; Ricci et al., 2015a, 2015b, Samper et al., 2007, 2009).

The overlap in volcanic activity between centres on these four islands suggests that it is a common phenomenon in the Lesser Antilles and, indeed, in other arc systems. For example, in the Izu-Bonin-Mariana arc, most islands contain a single volcanic centre, but islands with multiple centres have experienced coeval activity at two neighbouring volcanic centres. These are: Hachijojima, where Higashiyama and Nishiyama (7 km apart) have been concurrently active for at least 10 ka (Ishizuka et al., 2008); Pagan island, where Mount Pagan and South Pagan (~8 km apart) have experienced coeval activity for at least 64 ka (Marske et al., 2011); and Izu-Oshima, which has been simultaneously active with the neighbouring Izu-Tobu volcanic field for at least 40–50 ka, which at their closest are only ~4 km apart (Ishizuka et al., 2015 and references therein). The distance separating sites of coeval activity in the Izu-Bonin-Mariana and Lesser Antilles arcs (typically <10 km) relative to the depth to the melt generation zone above the subducting slab (of the order ~100 km; Stern, 2002) suggests that a rising diapir or plume of partial melt may bifurcate to form separate magma chambers at intermediate depths (~15 km; Odbert et al., 2014) beneath the individual volcanic centres.

2.11 Conclusions

We describe the rocks of the Silver Hills volcanic centre, which are dominated by andesite lavas and breccias, formed from effusive lava dome eruptions and dome collapses. Pumiceous flow deposits are also present, providing evidence of explosive activity from Vulcanian style eruptions. There is evidence of widespread hydrothermal alteration, with three fumarole deposits identified, resulting from hydrothermal activity concurrent with Silver Hills volcanism. Four debris avalanche deposits were also identified, indicating that the volcano experienced periodic sector collapses. These observations suggest that the Silver Hills was characterized by the same type of volcanic activity as has been observed at the Centre Hills and Soufrière Hills. The notable absence of evidence of sustained explosive eruptions at Silver Hills, which occurred in the early stages of Soufrière Hills' development and throughout Centre Hills' activity, may be the result of consistent mafic magma recharge and mixing, which could raise magma temperatures and inhibit the potential for large explosive eruptions.

New $^{40}Ar/^{39}Ar$ dates, combined with ages from marine tephra layers and a review of existing ages, have yielded a revised geochronology of volcanic activity of Montserrat's three main centres, which were active during at least ~2.17–1.03 Ma, ~1.14–0.38 Ma, and ~0.45 Ma–present for the Silver, Centre, and Soufrière Hills centres, respectively. Two key findings come from these new dates: the previously unknown overlaps in volcanic activity between both the Silver and Centre Hills and Centre and Soufrière Hills, and the discovery of a new, older stage of Soufrière Hills activity ~450–290 ka with the eruption of hornblende-orthopyroxene lavas. Combined with ages of volcanic centres on Basse-Terre, Guadeloupe, our ages suggest that ~0.5–1 Ma is a common lifespan for volcanic centres in the Lesser Antilles. Furthermore, overlap in activity between closely spaced (<10 km) volcanic centres appears to be a common phenomenon in island arcs, as it has been observed on multiple islands in the Lesser Antilles and Izu-Bonin-Mariana arcs.

2.12 References

Andreastuti, S.D., Alloway, B. V., Smith, I.E.M., 2000. A detailed tephrostratigraphic framework at Merapi Volcano, Central Java, Indonesia: implications for eruption predictions and hazard assessment. J. Volcanol. Geotherm. Res. 100, 51–67. doi:10.1016/S0377-0273(00)00133-5

Baker, P.E., 1985. Volcanic hazards on St Kitts and Montserrat, West Indies. J. Geol. Soc. London 142, 279–295. doi:10.1130/MEM164-p169

Baker, P.E., 1984. Geochemical evolution of St Kitts and Montserrat, Lesser Antilles. J. Geol. Soc. London. 141, 401–411. doi:10.1144/gsjgs.141.3.0401

Baker, P.E., Buckley, F., Padfield, T., 1980. Petrology of the volcanic rocks of Saba, West Indies. Bull. Volcanol. 43, 337–346. doi:10.1007/BF02598037

Barclay, J., Alexander, J., Sušnik, J., 2007. Rainfall-induced lahars in the Belham Valley, Montserrat, West Indies. J. Geol. Soc. London. 164, 815–827. doi:10.1144/0016-76492006-078

Barclay, J., Rutherford, M.J., Carroll, M.R., Murphy, M.D., Devine, J.D., Gardner, J., Sparks, R.S.J., 1998. Experimental phase equilibria constraints on pre-eruptive storage conditions of the Soufrière Hills magma. Geophys. Res. Lett. 25, 3437. doi:10.1029/98GL00856

Bennett, E.H.S., Rose, W.I., Conway, F.M., 1992. Santa María, Guatemala: A decade volcano. Eos, Trans. Am. Geophys. Union 73, 521–522. doi:10.1029/91EO00387

Boudon, G., Balcone-Boissard, H., Solaro, C., Martel, C., 2017. Revised chronostratigraphy of recurrent ignimbritic eruptions in Dominica (Lesser Antilles arc): Implications on the behavior of the magma plumbing system. J. Volcanol. Geotherm. Res. 343, 135–154. doi:10.1016/j.jvolgeores.2017.06.022

Branney, M.J., Kokelaar, B.P., 2002. Pyroclastic density currents and the sedimentation of ignimbrites, Geol Soc London, Mem 27. Geol Soc London, Mem 27. doi:10.1007/s13398-014-0173-7.2

Brown, K., Davidson, C., 2008. 40Ar/39Ar geochronology of the Silver Hills andesite, Montserrat, West Indies. B. A. Sr. Integr. Exerc. Carlton College, Northfield, Minnesota.

Caricchi, L., Annen, C., Blundy, J., Simpson, G., Pinel, V., 2014. Frequency and magnitude of volcanic eruptions controlled by magma injection and buoyancy. Nat. Geosci. 7, 126–130. doi:10.1038/ngeo2041

Carlut, J., Quidelleur, X., Courtillot, V., Boudon, G., 2000. Paleomagnetic directions and K/Ar dating of 0 to 1 Ma lava flows from La Guadeloupe Island Implications for time-averaged field models. J. Geophys. Res. 105, 835–849. doi:10.1029/1999JB900238

Cassidy, M., Taylor, R.N., Palmer, M.R., Cooper, R.J., Stenlake, C., Trofimovs, J., 2012. Tracking the magmatic evolution of island arc volcanism: Insights from a high-precision Pb isotope record of Montserrat, Lesser Antilles. Geochemistry, Geophys. Geosystems 13, 1–19. doi:10.1029/2012GC004064

Cassidy, M., Trofimovs, J., Watt, S.F.L., Palmer, M.R., Taylor, R.N., Gernon, T.M., Talling, P.J., Le

Friant, A., 2014. Multi-stage collapse events in the South Soufrière Hills, Montserrat as recorded in marine sediment cores. Geol. Soc. London, Mem. 39, 383–397. doi:10.1144/M39.20

Christopher, T.E., Humphreys, M.C.S., Barclay, J., Genareau, K., De Angelis, S.M.H., Plail, M., Donovan, A., 2014. Petrological and geochemical variation during the Soufrière Hills eruption, 1995 to 2010. Geol. Soc. London, Mem. 39, 317–342. doi:10.1144/M39.17

Cole, P.D., Calder, E.S., Sparks, R.S.J., Clarke, A.B., Druitt, T.H., Young, S.R., Herd, R.A., Harford, C.L., Norton, G.E., 2002. Deposits from dome-collapse and fountain-collapse pyroclastic flows at Soufrière Hills Volcano, Montserrat. Geol. Soc. London, Mem. 21, 231–262. doi:10.1144/GSL.MEM.2002.021.01.11

Cole, P.D., Smith, P.J., Stinton, A.J., Odbert, H.M., Bernstein, M.L., Komorowski, J.C., Stewart, R., 2014. Vulcanian explosions at Soufrière Hills Volcano, Montserrat between 2008 and 2010. Geol. Soc. London, Mem. 39, 93–111. doi:10.1144/M39.5

Coussens, M., Cassidy, M., Watt, S.F.L., Jutzeler, M., Talling, P.J., Barfod, D., Gernon, T.M., Taylor, R., Hatter, S.J., Palmer, M.R., 2017. Long-term changes in explosive and effusive behaviour at andesitic arc volcanoes: Chronostratigraphy of the Centre Hills Volcano, Montserrat. J. Volcanol. Geotherm. Res. doi:10.1016/j.jvolgeores.2017.01.003

Coussens, M., Wall-Palmer, D., Talling, P.J., Watt, S.F.L., Cassidy, M., Jutzeler, M., Clare, M.A., Hunt, J.E., Manga, M., Gernon, T.M., Palmer, M.R., Hatter, S.J., Boudon, G., Endo, D., Fujinawa, A., Hatfield, R., Hornbach, M.J., Ishizuka, O., Kataoka, K., Le Friant, A., Maeno, F., McCanta, M., Stinton, A.J., 2016. The relationship between eruptive activity, flank collapse, and sea level at volcanic islands: A long-term (>1 Ma) record offshore Montserrat, Lesser Antilles. Geochemistry, Geophys. Geosystems 17, 2591–2611. doi:doi:10.1002/2015GC006053.

Crandell, D.R., Miller, C.D., Glicken, H.X., Christiansen, R.L., Newhall, C.G., 1984. Catastrophic debris avalanche from ancestral Mount Shasta volcano, California. Geology 12, 143–146. doi:10.1130/0091-7613(1984)12<143:CDAFAM>2.0.CO;2

Davidson, J., Wilson, M., 2011. Differentiation and source processes at Mt Pelée and the Quill; Active volcanoes in the Lesser Antilles arc. J. Petrol. 52, 1493–1531. doi:10.1093/petrology/egq095

Defant, M.J., Sherman, S., Maury, R.C., Bellon, H., De Boer, J., Davidson, J., Kepezhinskas, P., 2001. The geology, petrology, and petrogenesis of Saba Island, Lesser Antilles. J. Volcanol. Geotherm. Res. 107, 87–111. doi:10.1016/S0377-0273(00)00268-7

Deplus, C., Friant, A. Le, Boudon, G., Komorowski, J.C., Villemant, B., Harford, C., Segoufin, J., Cheminee, J.L., 2001. Submarine evidence for large-scale debris avalances in the Lesser Antilles arc. Earth Planet. Sci. Lett. 192, 145–157. doi:10.1016/S0012-821X(01)00444-7

Devine, J.D., Murphy, M.D., Rutherford, M.J., Barclay, J., Sparks, R.S.J., Carroll, M.R., Young, S.R., Gardner, J.E., 1998. Petrologic evidence for pre-eruptive pressure-temperature conditions, and recent reheating, of andesitic magma erupting at the Soufrière Hills Volcano, Montserrat, W.I. Geophys. Res. Lett. 25, 3669–3672. doi:10.1029/98GL01330

Devine, J.D., Rutherford, M.J., Norton, G.E., Young, S.R., 2003. Magma Storage Region Processes Inferred from Geochemistry of Fe–Ti Oxides in Andesitic Magma, Soufrière Hills Volcano, Montserrat, W.I. J. Petrol. 44, 1375–1400. doi:10.1093/petrology/44.8.1375

Elliott, T., Plank, T., Zindler, A., White, W., Bourdon, B., 1997. Element transport from slab to volcanic front at the Mariana arc. J. Geophys. Res. 102, 14991–15019. doi:10.1029/97JB00788

Ewart, A., Collerson, K.D., Regelous, M., Wendt, J.I., Niu, Y., 1998. Geochemical Evolution within the Tonga- Kermadec-Lau Arc-Back-arc Systems : the Role of Varying Mantle Wedge Composition in Space and Time. J. Petrol. 39, 331–368. doi:10.1093/petroj/39.3.331

Expedition 340 scientists, 2013. Site U1396, in: Le Friant, A., Ishizuka, O., Stroncik, N.A., Expedition 340 scientists, (Eds.), Proceedings of the Integrated Ocean Drilling Program, 340. Integrated Ocean Drilling Program Managment Internation, Inc, Tokyo. doi:10.2204/iodp.proc.340.106.2013

Feuillet, N., Leclerc, F., Tapponnier, P., Beauducel, F., Boudon, G., Le Friant, A., Deplus, C., Lebrun, J.-F., Nercessian, A., Saurel, J.-M., Clément, V., 2010. Active faulting induced by slip partitioning in Montserrat and link with volcanic activity: New insights from the 2009 GWADASEIS marine cruise data. Geophys. Res. Lett. 37, 1–6. doi:10.1029/2010GL042556

Fraass, A.J., Wall-Palmer, D., Leckie, R.M., Hatfield, R.G., Burns, S.J., Le Friant, A., Ishizuka, O., Aljahdali, M., Jutzeler, M., Martinez-Colon, M., Palmer, M.R., Talling, P.J., 2016. A revised Plio-Pleistocene age model and paleoceanography of the northeastern Caribbean Sea: IODP Site U1396 off Montserrat, Lesser Antilles. Stratigraphy 13, 183–203.

Germa, A., Quidelleur, X., Labanieh, S., Chauvel, C., Lahitte, P., 2011a. The volcanic evolution of Martinique Island: Insights from K-Ar dating into the Lesser Antilles arc migration since the Oligocene. J. Volcanol. Geotherm. Res. 208, 122–135. doi:10.1016/j.jvolgeores.2011.09.007

Germa, A., Quidelleur, X., Labanieh, S., Lahitte, P., Chauvel, C., 2010. The eruptive history of Morne Jacob volcano (Martinique Island, French West Indies): Geochronology, geomorphology and geochemistry of the earliest volcanism in the recent Lesser Antilles arc. J. Volcanol. Geotherm. Res. 198, 297–310. doi:10.1016/j.jvolgeores.2010.09.013

Germa, A., Quidelleur, X., Lahitte, P., Labanieh, S., Chauvel, C., 2011b. The K-Ar Cassignol-Gillot technique applied to western Martinique lavas: A record of Lesser Antilles arc activity from 2 Ma to Mount Pelée volcanism. Quat. Geochronol. 6, 341–355. doi:10.1016/j.quageo.2011.02.001

Glicken, H., 1996. Rockslide-debris avalanche of may 18, 1980, Mount St. Helens volcano, Washington. Open-file Rep. 96-677 1–5.

Hall, P.S., Kincaid, C., 2001. Diapiric Flow at Subduction Zones: A Recipe for Rapid Transport. Science (80-.). 292, 2472–2475. doi:10.1126/science.1060488

Harford, C.L., Pringle, M.S., Sparks, R.S.J., Young, S.R., 2002. The volcanic evolution of Montserrat using 40Ar/39Ar geochronology. Geol. Soc. London, Mem. 21, 93–113. doi:10.1144/GSL.MEM.2002.021.01.05

Hart, S.R., 1984. A large-scale isotope anomaly in the Southern Hemisphere mantle. Nature 309, 753–757. doi:10.1038/309753a0

Hatfield, R.G., 2015. Data report: stratigraphic correlation of Site U1396 and creation of a composite depth scale and splice 340, 1–17. doi:10.2204/iodp.proc.340.202.2015

Hildreth, W., Drake, R.E., 1992. Volcán Quizapu, Chilean Andes. Bull. Volcanol. 54, 93–125. doi:10.1007/BF00278002

Hildreth, W., Lanphere, M.A., 1994. Potassium-argon geochronology of a basalt-andesite-dacite arc system: The Mount Adams volcanic field, Cascade Range of southern Washington. Geol. Soc. Am. Bull. 106, 1413–1429. doi:10.1130/0016-7606(1994)106<1413:PAGOAB>2.3.CO;2

Hoblitt, R.P., Crandell, D.R., Mullineaux, D.R., 1980. Mount St . Helens eruptive behavior during the past 1 , 500 yr. Geology 8, 555–559. doi:10.1130/0091-7613(1980)8<555

Hoshizumi, H., Uto, K., Watanabe, K., 1999. Geology and eruptive history of Unzen volcano, Shimabara Peninsula, Kyushu, SW Japan. J. Volcanol. Geotherm. Res. 89, 81–94. doi:10.1016/S0377-0273(98)00125-5

Howe, T.M., Lindsay, J.M., Shane, P., 2015. Evolution of young andesitic-dacitic magmatic systems beneath Dominica, Lesser Antilles. J. Volcanol. Geotherm. Res. 297, 69–88.

doi:10.1016/j.jvolgeores.2015.02.009

Ishizuka, O., Geshi, N., Itoh, J., Kawanabe, Y., TuZino, T., 2008. The magmatic plumbing of the submarine Hachijo NW volcanic chain, Hachijojima, Japan: Long-distance magma transport? J. Geophys. Res. Solid Earth 113. doi:10.1029/2007JB005325

Ishizuka, O., Taylor, R.N., Geshi, N., Oikawa, T., Kawanabe, Y., Ogitsu, I., 2015. Progressive mixed-magma recharging of Izu-Oshima volcano, Japan: A guide to magma chamber volume. Earth Planet. Sci. Lett. 430, 19–29. doi:10.1016/j.epsl.2015.08.004

Ishizuka, O., Taylor, R.N., Yuasa, M., Milton, J.A., Nesbitt, R.W., Uto, K., Sakamoto, I., 2007. Processes controlling along-arc isotopic variation of the southern Izu-Bonin arc. Geochemistry, Geophys. Geosystems 8. doi:10.1029/2006GC001475

Kamber, B.S., Gladu, A.H., 2009. Comparison of Pb Purification by Anion-Exchange Resin Methods and Assessment of Long-Term Reproducibility of Th/U/Pb Ratio Measurements by Quadrupole ICP-MS. Geostand. Geoanalytical Res. 33, 169–181. doi:10.1111/j.1751-908X.2009.00911.x

Kokelaar, B.P., 2002. Setting, chronology and consequences of the eruption of Soufrière Hills Volcano, Montserrat (1995-1999). Erupt. Soufrière Hills Volcano, Montserrat, from 1995 to 1999 21, 1–43. doi:10.1144/GSL.MEM.2002.021.01.02

Koleszar, A.M., Kent, A.J.R., Wallace, P.J., Scott, W.E., 2012. Controls on long-term low explosivity at andesitic arc volcanoes: Insights from Mount Hood, Oregon. J. Volcanol. Geotherm. Res. 219–220, 1–14. doi:10.1016/j.jvolgeores.2012.01.003

Komorowski, J.C., Boudon, G., Smet, M., Beauducel, F., Antenor-Habazac, C., Bazin, S., Hammouya, G., 2005. Guadeloupe, in: Unit, S.R. (Ed.), Volcanic Hazard Atlas of the Lesser Antilles. University of the West Indies, St Augustine, Trinidad, W.I., pp. 67–104.

Labanieh, S., Chauvel, C., Germa, A., Quidelleur, X., 2012. Martinique: A clear case for sediment melting and slab dehydration as a function of distance to the trench. J. Petrol. 53, 2441–2464. doi:10.1093/petrology/egs055

Labanieh, S., Chauvel, C., Germa, A., Quidelleur, X., Lewin, E., 2010. Isotopic hyperbolas constrain sources and processes under the Lesser Antilles arc. Earth Planet. Sci. Lett. 298, 35–46. doi:10.1016/j.epsl.2010.07.018

Le Friant, A., Harford, C.L., Deplus, C., Boudon, G., Sparks, R.S.J., Herd, R. a., Komorowski, J.C., 2004. Geomorphological evolution of Montserrat (West Indies): importance of flank collapse and erosional processes. J. Geol. Soc. London. 161, 147–160. doi:10.1144/0016-

764903-017

Le Friant, A., Lock, E.J., Hart, M.B., Boudon, G., Sparks, R.S.J., Leng, M., Smart, C.W., Komorowski, J.-C., Deplus, C., Fisher, J.K., 2008. Late Pleistocene tephrochronology of marine sediments adjacent to Montserrat, Lesser Antilles volcanic arc. J. Geol. Soc. London. 165, 279–289. doi:10.1144/0016-76492007-019

Lebas, E., Le Friant, A., Boudon, G., Watt, S.F.L., Talling, P.J., Feuillet, N., Deplus, C., Berndt, C., Vardy, M.E., 2011. Multiple widespread landslides during the long-term evolution of a volcanic island: Insights from high-resolution seismic data, Montserrat, Lesser Antilles. Geochemistry, Geophys. Geosystems 12. doi:10.1029/2010GC003451

Lindsay, J.M., Trumbull, R.B., Siebel, W., 2005. Geochemistry and petrogenesis of late Pleistocene to Recent volcanism in Southern Dominica, Lesser Antilles. J. Volcanol. Geotherm. Res. 148, 253–294. doi:10.1016/j.jvolgeores.2005.04.018

Macdonald, R., Hawkesworth, C.J., Heath, E., 2000. The Lesser Antilles volcanic chain: A study in arc magmatism. Earth Sci. Rev. 49, 1–76. doi:10.1016/S0012-8252(99)00069-0

Macgregor, A.G., 1938. The Royal Society Expedition to Montserrat, B.W.I. The Volcanic History and Petrology of Montserrat, with Observations on Mt Pelée, in Martinique. Philos. Trans. R. Soc. Lond. B. Biol. Sci. 229, 1–90.

Mark, D.F., Barfod, D., Stuart, F.M., Imlach, J., 2009. The ARGUS multicollector noble gas mass spectrometer: Performance for 40 Ar/ 39 Ar geochronology. Geochemistry, Geophys. Geosystems 10, n/a-n/a. doi:10.1029/2009GC002643

Marske, J.P., Pietruszka, A.J., Trusdell, F.A., Garcia, M.O., 2011. Geochemistry of southern Pagan Island lavas, Mariana arc: The role of subduction zone processes. Contrib. to Mineral. Petrol. 162, 231–252. doi:10.1007/s00410-010-0592-1

Maury, R.C., Westbrook, G.K., Baker, P.E., Bouysse, P., Westercamp, D., 1990. Geology of the Lesser Antilles, in: Dengo, G., Case, J.E. (Eds.), The Geology of North America, Vol. H, The Caribbean Region. Geological Society of America, Boulder, Colorado, pp. 141–166.

Miller, T.P., Chertkoff, D.G., Eichelberger, J.C., Coombs, M.L., 1999. Mount Dutton volcano, Alaska: Aleutian arc analog to Unzen volcano, Japan. J. Volcanol. Geotherm. Res. 89, 275–301. doi:10.1016/S0377-0273(99)00004-9

Minster, J.B., Jordan, T.H., 1978. Present-day plate motions. J. Geophys. Res. 83, 5331. doi:10.1029/JB083iB11p05331

Murphy, M.D., Sparks, R.S.J., Barclay, J., Carroll, M.R., Brewer, T.S., 2000. Remobilization of

Andesite Magma by Intrusion of Mafic Magma at the Soufrière Hills Volcano, Montserrat, West Indies. J. Petrol. 41, 21–42. doi:10.1093/petrology/41.1.21

Murphy, M.D., Sparks, R.S.J., Barclay, J., Carroll, M.R., Lejeune, A.M., Brewer, T.S., Macdonald, R., Black, S., Young, S., 1998. The role of magma mixing in trigerring the current eruption of the Soufrière Hills volcano, Montserrat, West Indies. Geophys. Res. Lett. 25, 3433–3436. doi:10.1029/98GL00713

Myers, J.D., Marsh, B.D., Sinha, A.K., 1985. Strontium isotopic and select trace element variations between two Aleutian volcanic centres (Adak and Atka): Implications for the development of arc volcanic plumbing systems. Contrib. to Mineral. Petrol. 91, 221–234.

Odbert, H.M., Ryan, G.A., Mattioli, G.S., Hautmann, S., Gottsmann, J., Fournier, N., Herd, R.A., 2014. Volcano geodesy at the Soufrière Hills Volcano, Montserrat: a review, in: Wadge, G., Robertson, R.E.A., Voight, B. (Eds.), The Eruption of Soufrière Hills Volcano, Montserrat from 2000 to 2010. Geological Society, London, Memoirs, pp. 195–217. doi:10.1144/M39.11

Palmer, M.R., Hatter, S.J., Gernon, T.M., Taylor, R.N., Cassidy, M., Johnson, P., Le Friant, A., Ishizuka, O., 2016. Discovery of a large 2.4 Ma Plinian eruption of Basse-Terre, Guadeloupe, from the marine sediment record. Geol. 44, 123–126. doi:10.1130/G37193.1

Pinel, V., Jaupart, C., Albino, F., 2010. On the relationship between cycles of eruptive activity and growth of a volcanic edifice. J. Volcanol. Geotherm. Res. 194, 150–164. doi:10.1016/j.jvolgeores.2010.05.006

Pioli, L., Scalisi, L., Costantini, L., Di Muro, A., Bonadonna, C., Clavero, J., 2015. Explosive style, magma degassing and evolution in the Chaimilla eruption, Villarrica volcano, Southern Andes. Bull. Volcanol. 77. doi:10.1007/s00445-015-0976-1

Plail, M., Barclay, J., Humphreys, M.C.S., Edmonds, M., Herd, R.A., Christopher, T.E., 2014. Characterization of mafic enclaves in the erupted products of Soufrière Hills Volcano, Montserrat, 2009 to 2010. Geol. Soc. London, Mem. 39, 343–360. doi:10.1144/M39.18

Rea, W.J., 1974. The volcanic geology and petrology of Montserrat, West Indies. J. Geol. Soc. London. 130, 341–366. doi:10.1144/gsjgs.130.4.0341

Renne, P.R., Balco, G., Ludwig, K.R., Mundil, R., Min, K., 2011. Response to the comment by W.H. Schwarz et al. on "Joint determination of 40K decay constants and 40Ar*/40K for the Fish Canyon sanidine standard, and improved accuracy for 40Ar/39Ar geochronology" by P. R. Renne et al. (2010). Geochim. Cosmochim. Acta 75, 5097–5100.

doi:10.1016/j.gca.2011.06.021

Renne, P.R., Mundil, R., Balco, G., Min, K., Ludwig, K.R., 2010. Joint determination of 40K decay constants and 40Ar*/40K for the Fish Canyon sanidine standard, and improved accuracy for 40Ar/39Ar geochronology. Geochim. Cosmochim. Acta 74, 5349–5367. doi:10.1016/j.gca.2010.06.017

Ricci, J., Lahitte, P., Quidelleur, X., 2015a. Construction and destruction rates of volcanoes within tropical environment: Examples from the Basse-Terre Island (Guadeloupe, Lesser Antilles). Geomorphology 228, 597–607. doi:10.1016/j.geomorph.2014.10.002

Ricci, J., Quidelleur, X., Lahitte, P., 2015b. Volcanic evolution of central Basse-Terre Island revisited on the basis of new geochronology and geomorphology data. Bull. Volcanol. 77, 84. doi:10.1007/s00445-015-0970-7

Ridolfi, F., Renzulli, A., Puerini, M., 2010. Stability and chemical equilibrium of amphibole in calc-alkaline magmas: An overview, new thermobarometric formulations and application to subduction-related volcanoes. Contrib. to Mineral. Petrol. doi:10.1007/s00410-009-0465-7

Roobol, M.J., Smith, A.L., 1998. Pyroclastic stratigraphy of the Soufrière Hills volcano, Montserrat - Implications for the present eruption. Geophys. Res. Lett. 25, 3393–3396. doi:10.1029/98GL00643

Roobol, M.J., Smith, A.L., 1976. Mount Pelée, Martinique: A pattern of alternating eruptive styles. Geology 4, 521–524. doi:10.1130/0091-7613(1976)4<521:MPMAPO>2.0.CO;2

Rose, W.I., 1987. Santa María, Guatemala: bimodal soda-rich calc-alkalic stratovolcano. J. Volcanol. Geotherm. Res. 33, 109–129.

Rose, W.I., 1973. Pattern and mechanism of volcanic activity at the Santiaguito Volcanic Dome, Guatemala. Bull. Volcanol. 37, 73–94. doi:10.1007/BF02596881

Rose, W.I., 1972. Santiaguito Volcanic Dome, Guatemala. Geol. Soc. Am. Bull. 83, 1413–1434.

Rowley, K., 1978. Late Pleistocene pyroclastic deposits of Soufrière Volcano, St. Vincent, West Indies. Bull. Geol. Soc. Am. 89, 825–835. doi:10.1130/0016-7606(1978)89<825:LPPDOS>2.0.CO;2

Ruprecht, P., Bachmann, O., 2010. Pre-eruptive reheating during magma mixing at Quizapu volcano and the implications for the explosiveness of silicic arc volcanoes. Geology 38, 919–922. doi:10.1130/G31110.1

Samper, A., Quidelleur, X., Komorowski, J.-C., Lahitte, P., Boudon, G., 2009. Effusive history of the Grande Découverte Volcanic Complex, southern Basse-Terre (Guadeloupe, French West Indies) from new K–Ar Cassignol–Gillot ages. J. Volcanol. Geotherm. Res. 187, 117–130. doi:10.1016/j.jvolgeores.2009.08.016

Samper, A., Quidelleur, X., Lahitte, P., Mollex, D., 2007. Timing of effusive volcanism and collapse events within an oceanic arc island: Basse-Terre, Guadeloupe archipelago (Lesser Antilles Arc). Earth Planet. Sci. Lett. 258, 175–191. doi:10.1016/j.epsl.2007.03.030

Scott, W.E., Pierson, T.C., Schilling, S.P., Costa, J.E., Gardner, C.A., Vallance, J.W., Major, J.J., 1997. Volcano Hazards in the Mount Hood Region, Oregon. US Geol. Surv. Open-File Rep. 1–14.

Siebert, L., 1984. Large volcanic debris avalanches: Characteristics of source areas, deposits, and associated eruptions. J. Volcanol. Geotherm. Res. 22, 163–197. doi:10.1016/0377-0273(84)90002-7

Smith, A.L., Roobol, M.J., Mattioli, G.S., Fryxell, J.E., Daly, G.E., Fernandez, L.A., 2013. The volcanic geology of the mid-arc island of Dominica, Lesser Antilles: The surface expression of a island-arc batholith. Geological Society of America, Boulder, Colorado.

Smith, A.L., Roobol, M.J., Schellekens, J.H., Mattioli, G.S., 2007. Prehistoric stratigraphy of the Soufrière Hills - South Soufrière Hills volcanic complex, Montserrat, West Indies. Geology 115, 115–127. doi:10.1086/509271

Sparks, R.S.J., Barclay, J., Calder, E.S., Herd, R. a., Komorowski, J.-C., Luckett, R., Norton, G.E., Ritchie, L.J., Voight, B., Woods, a. W., 2002. Generation of a debris avalanche and violent pyroclastic density current on 26 December (Boxing Day) 1997 at Soufrière Hills Volcano, Montserrat. Geol. Soc. London, Mem. 21, 409–434. doi:10.1144/GSL.MEM.2002.021.01.18

Sparks, R.S.J., Folkes, C.B., Humphreys, M.C.S., Barfod, D.N., Clavero, J., Sunagua, M.C., McNutt, S.R., Pritchard, M.E., 2008. Uturuncu volcano, Bolivia: Volcanic unrest due to mid-crustal magma intrusion. Am. J. Sci. 308, 727–769. doi:10.2475/06.2008.01

Stern, R.J., 2002. Subduction zones. Rev. Geophys. 40. doi:10.1029/2001RG000108

Stinton, A.J., Cole, P.D., Stewart, R.C., Odbert, H.M., Smith, P., 2014. The 11 February 2010 partial dome collapse at Soufrière Hills Volcano, Montserrat. Geol. Soc. London, Mem. 39, 133–152. doi:10.1144/M39.7

Takarada, S., Ui, T., Yamamoto, Y., 1999. Depositional features and transportation mechanism

of valley-filling Iwasegawa and Kaida debris avalanches, Japan. Bull. Volcanol. 60, 508–522. doi:10.1007/s004450050248

Taylor, R.N., Ishizuka, O., Michalik, A., Milton, J.A., Croudace, I.W., 2015. Evaluating the precision of Pb isotope measurement by mass spectrometry. J. Anal. At. Spectrom. 30, 198–213. doi:10.1039/C4JA00279B

Toothill, J., Williams, C. a., MacDonald, R., Turner, S.P., Rogers, N.W., Hawkesworth, C.J., Jerram, D. a., Ottley, C.J., Tindle, a. G., 2007. A complex petrogenesis for an arc magmatic suite, St Kitts, Lesser Antilles. J. Petrol. 48, 3–42. doi:10.1093/petrology/egl052

Ui, T., 1983. Volcanic dry avalanche deposits — Identification and comparison with nonvolcanic debris stream deposits. J. Volcanol. Geotherm. Res. 18, 135–150. doi:10.1016/j.jvolgeores.2008.06.025

Ui, T., Glicken, H., 1986. Internal structural variations in a debris-avalanche deposit from ancestral Mount Shasta, California, USA. Bull. Volcanol. 48, 189–194. doi:10.1007/BF01087673

Ui, T., Kawachi, S., Neall, V.E., 1986. Fragmentation of debris avalanche material during flowage — Evidence from the Pungarehu Formation, Mount Egmont, New Zealand. J. Volcanol. Geotherm. Res. 27, 255–264. doi:10.1016/0377-0273(86)90016-8

van Wyk de Vries, B., Davies, T., 2015. Landslides, Debris Avalanches and Volcanic Gravitational Deformation, in: Sigurdsson, H., Houghton, B., McNutt, S.R., Rymer, H., Stix, J. (Eds.), Encylopedia of Volcanoes. Elsevier Inc., pp. 665–685.

Venezky, D.Y., Rutherford, M.J., 1999. Petrology and Fe–Ti oxide reequilibration of the 1991 Mount Unzen mixed magma. J. Volcanol. Geotherm. Res. 213–230. doi:10.1016/S0377-0273(98)00133-4

Voight, B., Komorowski, J.-C., Norton, G.E., Belousov, A.B., Belousova, M., Boudon, G., Francis, P.W., Franz, W., Heinrich, P., Sparks, R.S.J., Young, S.R., 2002. The 26 December (Boxing Day) 1997 sector collapse and debris avalanche at Soufrière Hills Volcano, Montserrat. Geol. Soc. London, Mem. 21, 363–407. doi:10.1144/GSL.MEM.2002.021.01.17

Wadge, G., Voight, B., Sparks, R.S.J., Cole, P.D., Loughlin, S.C., Robertson, R.E.A., 2014. An overview of the eruption of Soufrière Hills Volcano, Montserrat from 2000 to 2010. Geol. Soc. London, Mem. 39, 1–40. doi:10.1144/M39.1

Wendt, I., Carl, C., 1991. The statistical distribution of the mean squared weighted deviation. Chem. Geol. Isot. Geosci. Sect. 86, 275–285. doi:10.1016/0168-9622(91)90010-T

Westercamp, D., Traineau, H., 1983. The past 5,000 years of volcanic activity at Mt. Pelée Martinique (F.W.I): Implications for assessment of volcanic hazards. J. Volcanol. Geotherm. Res. 17, 159–185. doi:10.1016/0377-0273(83)90066-5

White, J.D.L., Houghton, B.F., 2006. Primary volcaniclastic rocks. Geology 34, 677–680. doi:10.1130/G22346.1

Wohletz, K., Heiken, G., Ander, M., Goff, F., Vuataz, F.-D., Wadge, G., 1986. The Qualibou caldera, St. Lucia, West Indies. J. Volcanol. Geotherm. Res. 27, 77–115. doi:10.1016/0377-0273(86)90081-8

Wright, J. V., Roobol, M.J., Smith, A.L., Sparks, R.S.J., Brazier, S.A., Rose, W.I., Sigurdsson, H., 1984. Late Quaternary explosive silicic volcanism on St Lucia, West Indies. Geol. Mag. 121, 1–15. doi:10.1017/S0016756800027904

Young, S.R., Hoblitt, R.P., Smith, A.L., Devine, J.D., Wadge, G., Shepherd, J.B., 1996. Dating of explosive volcanic eruptions associated with dome growth at the Soufrière Hills volcano, Monserrat, West Indies, in: Second Caribbean Conference on Natural Hazards and Hazard Management.

Chapter 3: Geochemical evolution of the Silver Hills volcanic centre

This Chapter was written by S. J. Hatter, with feedback from M. R. Palmer, T. M. Gernon and R. N. Taylor. Laboratory work and data analysis were carried out by S. J. Hatter.

Abstract

The geochemical evolution of Montserrat has been well-documented for the past ~1 Ma, but comparatively little is known for the oldest volcanic centre, Silver Hills (~2.2–1.0 Ma). Major and trace element, and Pb-Nd-Sr isotope data are presented for samples from the Silver Hills to investigate how geochemistry changes over the lifetime of an individual volcanic centre, and between individual domes. Lavas of the Silver Hills fall into two groups: (1) 'normal' composition lavas, which have major element compositions which match those of the Centre Hills and Soufrière Hills, and (2) 'low Al_2O_3-high Fe_2O_3' lavas, which contain up to 3 wt. % lower Al_2O_3 and higher Fe_2O_3 then the normal lavas for a given SiO_2, and are interpreted to have formed from parent magmas which experienced up to 25% plagioclase fractionation, likely as a result of lower magmatic H_2O content. The Silver Hills lava domes are geochemically indistinguishable from one another, except for U/Th values for the North Marguerita Bay and Yellow Hole domes. Silver Hills volcanism displays a systematic shift in $^{143}Nd/^{144}Nd$ to progressively less radiogenic values with time, which does not correlate with SiO_2, suggesting it is related to changes in the magma source components. Changes in the proportions of mantle to sediment to AOC fluid, as well as heterogeneity within the slab components, can be ruled out as the cause because they would all likely affect both Pb and Nd isotopes simultaneously. Thus heterogeneity in the mantle wedge remains the only feasible cause for the observed change in $^{143}Nd/^{144}Nd$, comparable to km-scale heterogeneity observed in mid-Atlantic ridge basalts.

3.1 Introduction

Island arc magmas are formed by partial melting of the mantle wedge, which is modified by addition of hydrous fluids and melts from the subducting sediment and altered oceanic crust (AOC). This imparts a distinctive geochemical signature onto island arc magmas (Arculus and Powell, 1986). In the Lesser Antilles, there is an along-arc variation in the thickness and geochemistry of the subducting sediment, with the southern arc having greater input of continental material derived from the Orinoco River of the South American Continent (Carpentier et al., 2008; Plank and Langmuir, 1998; White et al., 1985) (Figure 3.1). The

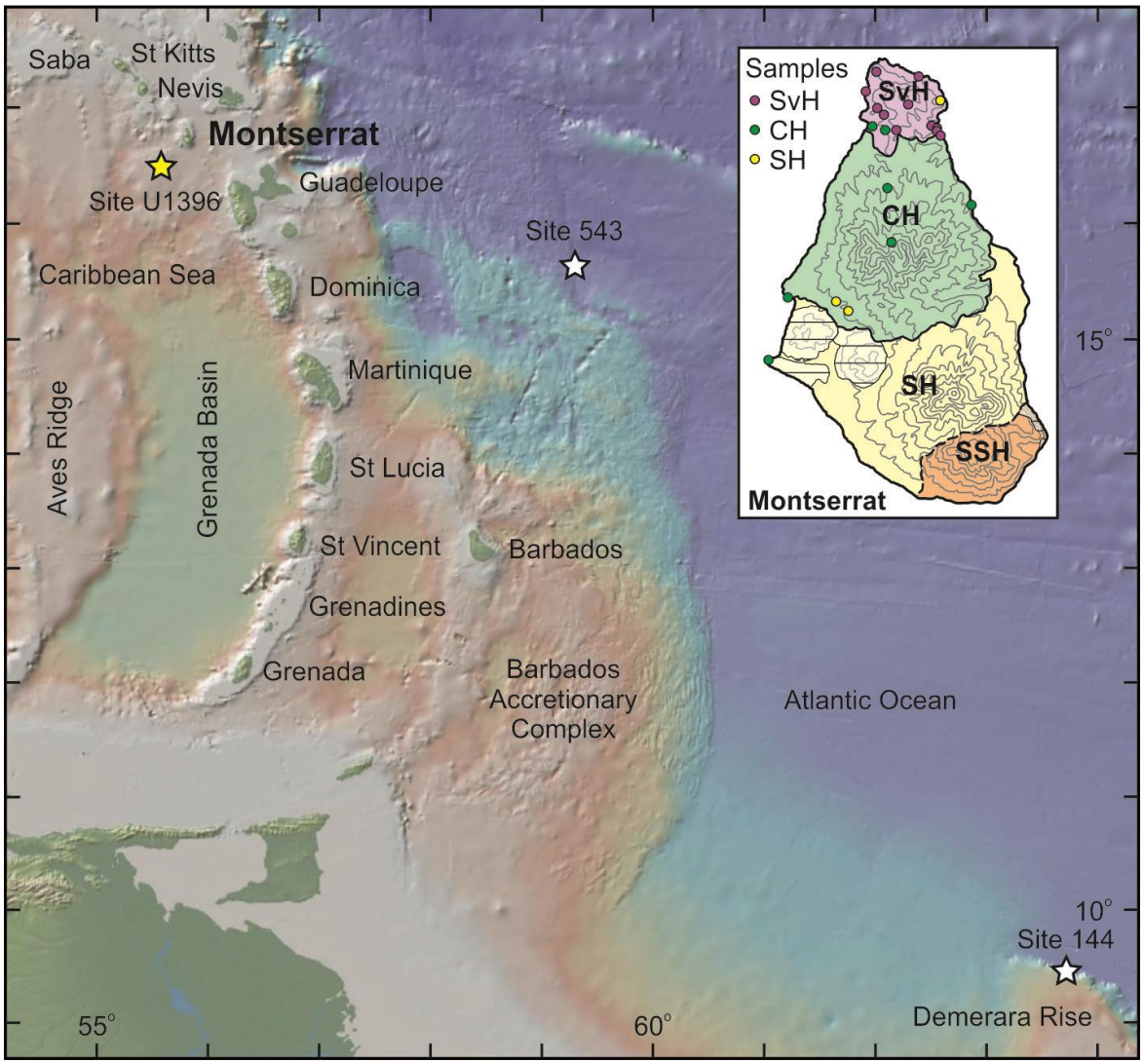

Figure 3.1. Map of the Lesser Antilles showing the location of Montserrat, International Ocean Discovery Program (IODP) site U1396, and Deep Sea Drilling Project (DSDP) sites 144 and 543. Inset map of Montserrat shows the different volcanic centres: SvH, Silver Hills; CH, Centre Hills; SH, Soufrière Hills; SSH, South Soufrière Hills.

sediment thickness overlying the basement ranges from 200–300 m north of the Barracuda Ridge (Figure 3.1) (Tucholke et al., 1982) to 7 km at 11°N, opposite the Orinoco delta (Pichot et al., 2012). At 15°7 N DSDP Site 543 410 m of sediment cover the basaltic basement and the décollement is located at 170 m depth, meaning only the lowermost 240 m of sediment are subducted. Further south, the depth of the décollement is poorly constrained, so the thickness of sediment being subducted is not well known (Carpentier et al., 2008, and references therein). This north-south variation in subducting sediment is generally thought to be responsible for the observed north-south geochemical gradient of lava compositions along the arc, with Pb-Nd-Sr-U-Th isotopes, fluid mobile elements and light rare-earth elements (LREE) displaying the greatest variation (e.g. DuFrane et al., 2009; Hawkesworth and Powell, 1980; Labanieh et al., 2010; Lindsay et al., 2005; Turner et al., 1996). Estimates vary for the percentage of sediment added to the mantle wedge beneath the Lesser Antilles,

with some studies calculating ~<1–2% bulk sediment addition in the north of the arc, and ~10–15% in the south (Carpentier et al., 2008; Turner et al., 1996). However, DuFrane et al. (2009) calculate that the amount of sediment addition in the southern arc may be reduced to <4% if it is introduced as a 20% partial melt, instead of by bulk addition.

As well as varying sediment addition, the along-arc geochemical trend is also variably controlled by crustal assimilation (e.g. Bezard et al., 2014; Davidson and Harmon, 1989; Thirlwall et al., 1996). A study of He, O and Sr isotopes of lavas along the arc show that there is notable variation in the extent of crustal assimilation along the arc, with minimal to no assimilation in the northern islands (Saba to Martinique), and major assimilation in the southern islands (Martinique to Grenada) (Van Soest et al., 2002).

On a smaller scale, studies have shown that individual islands display temporal geochemical variations (e.g. Hawkesworth et al., 1979; Lindsay et al., 2005; Toothill et al., 2007). On Montserrat, studies have looked at the role of source components and crustal assimilation in the formation of lavas, and how they change between the different volcanic centres (Cassidy et al., 2012; Zellmer et al., 2003). Zellmer et al. (2003) also studied the differentiation history of the Soufrière Hills and South Soufrière Hills lavas. This chapter adds to the work of these authors by presenting new major and trace element, and Pb-Nd-Sr isotope data for the Silver Hills and Centre Hills. Combined with newly acquired $^{40}Ar/^{39}Ar$ dates from Hatter et al., (2018), our data provide a greater temporal resolution of geochemical variation during the lifetime of the different volcanic centres on Montserrat, as well as between domes of individual volcanic centres. The differentiation history of these samples is also studied.

3.2 Geological background

Montserrat is a northern island in the Lesser Antilles arc, comprising four volcanic centres: Silver Hills (*ca.* 2.17–1.03 Ma), Centre Hills (*ca.* 1.14–0.38 Ma), Soufrière Hills (*ca.* 0.45 Ma–present) and South Soufriere Hills (*ca.* 130 ka) (Harford et al., 2002; *Hatter et al.,* submitted) (Figure 3.1). The Silver Hills and Centre Hills display very similar geochemical compositions, with Nb/Y vs $^{143}Nd/^{144}Nd$ being the only known geochemical discriminator between these two centres; the Silver Hills has higher $^{143}Nd/^{144}Nd$ and lower Nb/Y than the Centre Hills (Hatter et al., 2018). The Soufrière Hills is also similar in composition to the Centre and Silver Hills, but has less radiogenic Pb isotopes, higher Ba/La, and greater LREE enrichment, which are interpreted to be the result of a greater relative slab fluid and partial sediment melt contribution to the magma source region (Cassidy et al., 2012). The South Soufrière Hills has the most distinct geochemistry on Montserrat, with the least radiogenic Pb isotopes, lowest LREE/medium-REE (MREE) values, and the highest ($^{238}U/^{232}Th$), ($^{230}Th/^{232}Th$), and fluid

mobile element/REE ratios, resulting from an increased slab fluid and reduced slab sediment contribution to the magma source region compared with the Soufrière, Centre and Silver Hills (Cassidy et al., 2012; Zellmer et al., 2003).

Zellmer et al. (2003) observe that lava-hosted mafic enclaves from the recent eruption of Soufrière Hills (1995–2010) exhibit REE abundances greater than their host andesite lavas, which they interpret as meaning that the Soufrière Hills lavas cannot be formed from differentiation of their mafic enclaves. The Soufrière Hills lavas can, however, be formed by modelling differentiation of magma with a composition similar to the more evolved South Soufrière Hills lavas (~54 wt. SiO_2) by ~50% fractionation of a 50:50 mix of amphibole and plagioclase (Zellmer et al., 2003). However, the South Soufriere Hills lavas are isotopically distinct from all other lavas on Montserrat, and are interpreted to be sourced from a different part of the mantle by transtensional tectonics (Cassidy et al., 2012, 2015).

Volcanic activity from the recent Soufrière Hills eruption (1995–2010) was separated into five extrusive phases: November 1995–March 1998 (phase 1), November 1999–July 2003 (phase 2), August 2005–April 2007 (phase 3), July 2008–January 2009 (phase 4), and October 2009–February 2010 (phase 5) (Wadge et al., 2014). Christopher et al. (2014) analysed the major and trace element concentrations of the erupted andesite lavas for each phase, and the only temporal trend they identified was a systematic interphase (phases 1-5) variation in bulk-rock FeO, and to a lesser extent in MgO. This interphase FeO variation is also present in the mafic enclaves, in which it is more pronounced, with up to 2 wt. % difference in FeO content between phase 1 and 3 enclaves at 50 wt. % SiO_2. The difference between mean enclave and host andesite FeO changes through time, from 2.3 wt. % in phase1, to 1.4 wt. % in phase 5. This coupled FeO variation is interpreted to result from assimilation of the andesite by the intruding basalt lava, and the variation as being caused by interphase changes in the composition of the intruding basalt arriving from depth. There is no systematic interphase variation in trace element concentrations (Christopher et al., 2014).

3.3 Methods

3.3.1 Sample acquisition

Eighteen samples (including 6 enclaves) were collected from the Silver Hills, and ten from parts of the Centre Hills that have not previously been studied (Figure 3.1). However, Pb isotope analysis reveals that three of these samples are actually derived from the Soufrière Hills (Hatter et al., 2018).

Samples were also analysed from marine sediment core U1396C, from International Ocean Discovery Program expedition 340 (see Figure 3.1 for location). This core is 145.92 m long covering ~4.5 Ma, containing tephra layers from Montserrat and Guadeloupe (Expedition 340 scientists, 2013; Palmer et al., 2016). Only tephra layers identified by Hatter et al. (2018) to be from the Centre Hills and Silver Hills, and which contained enough pumice for geochemical analysis, were sampled.

3.3.2 Whole rock geochemistry

Trace elements were analysed using XRF and ICP-MS. Co, Cr, Cu, Nb, Ni, Sc, V, Y and Zr were measured at the University of Leicester on a PANalytical Axios Advanced XRF spectrometer on 32 mm diameter pressed powder pellets produced by mixing 7 g of powdered sample with 15-17 drops of a 7% PVA solution (Moviol 8-88). Rare earth elements (REE), Rb, Sr, Cs, Ba, Hf, Pb, Th and U were measured by a Thermo Fisher Scientific X-Series 2 ICP-MS at the University of Southampton following the method of Coussens et al. (2017), in which 0.05 g of powdered sample is analysed for terrestrial samples, and 0.01 g for U1396C samples. Precision is better than 6% for Cs, Pb, Th and U, and better than 2% for the rest (see Appendix A for more detail).

Major elements were analysed by XRF on fused glass beads produced by mixing 0.6 g of sample with metaborate flux (80% Li metaborate, 20% Li tetraborate) at a ratio of 1:5. Precision is generally ≤2%.

For the enclave samples major elements and all trace elements were analysed by ICP-MS, using the same mother solutions as for trace elements. Precision is better than 3% for all, except K which is better than 6%. The SiO_2 values were calculated as 100% minus the sum of total majors measured (Al_2O_3, CaO, Fe_2O_3, MgO, MnO, K_2O & Na_2O), P_2O_5 and loss on ignition (LOI). For P_2O_5 the average value from all XRF samples was used, which is 0.121 wt. % (n=22, range 0.048–0.223 wt. %). Pumice samples gave ~1–2 wt. % higher LOI values than lavas, so for enclave LOI the highest value from just the lava samples was used, which is 1.616 wt. % (n=17, range 0.373–1.616 wt. %, average 0.675 wt. %). The highest value was used for LOI as the enclave samples are visibly more weathered than the lava samples, suggesting that the enclave LOI values could be higher. This uncertainty of the SiO_2 values from the poorly constrained LOI can be reduced by normalising the major element data to volatile-free. Increasing the LOI from 1.6 to 3.9 wt. % (the highest pumice value) decreases the calculated SiO_2 content by 2.3 wt. %, but when normalised to volatile-free, this difference reduces to 1.0–1.1 wt. % for the six enclave samples (Table 3.1). Thus even with the uncertainty in the LOI value, the error in the calculated SiO_2 values is considered to be on the order of ± ~1.5 wt. % volatile-free.

Table 3.1. Difference in volatile-free major element concentrations between 1.6% and 3.9% LOI

Sample	Na_2O	MgO	Al_2O_3	K_2O	CaO	TiO_2	MnO	FeO^T	P_2O_5	SiO_2	Total
1.6% volatiles											
12/15-ACE	2.94	3.77	19.86	0.26	10.56	0.69	0.22	7.99	0.12	53.59	100.00
14/23-ACE	3.09	3.74	18.49	0.41	9.29	0.75	0.19	9.48	0.12	54.43	100.00
19/39-ALE	3.31	1.59	21.18	0.73	7.55	0.78	0.19	9.34	0.12	55.20	100.00
19/41-ALE	2.98	2.24	19.63	0.71	7.82	0.83	0.07	9.33	0.12	56.27	100.00
20/42-ALE	2.66	2.62	19.65	0.65	7.29	0.64	0.12	7.92	0.12	58.32	100.00
01/63-ALE	2.92	3.16	19.74	0.50	8.10	0.79	0.14	9.11	0.12	55.41	100.00
3.9% volatiles											
12/15-ACE	3.01	3.86	20.33	0.27	10.81	0.70	0.23	8.18	0.13	52.49	100.00
14/23-ACE	3.17	3.83	18.93	0.42	9.51	0.77	0.20	9.70	0.13	53.35	100.00
19/39-ALE	3.39	1.62	21.69	0.75	7.73	0.80	0.19	9.56	0.13	54.14	100.00
19/41-ALE	3.05	2.30	20.09	0.72	8.01	0.85	0.07	9.55	0.13	55.23	100.00
20/42-ALE	2.72	2.68	20.11	0.67	7.46	0.66	0.12	8.11	0.13	57.33	100.00
01/63-ALE	2.99	3.24	20.21	0.52	8.29	0.81	0.14	9.32	0.13	54.35	100.00
Difference											
12/15-ACE	0.12	0.15	0.79	0.01	0.42	0.03	0.01	0.32	0.00	-1.10	0.75
14/23-ACE	0.12	0.15	0.74	0.02	0.37	0.03	0.01	0.38	0.00	-1.08	0.74
19/39-ALE	0.13	0.06	0.85	0.03	0.30	0.03	0.01	0.37	0.00	-1.06	0.72
19/41-ALE	0.12	0.09	0.78	0.03	0.31	0.03	0.00	0.37	0.00	-1.04	0.71
20/42-ALE	0.11	0.10	0.78	0.03	0.29	0.03	0.00	0.32	0.00	-0.99	0.67
01/63-ALE	0.12	0.13	0.79	0.02	0.32	0.03	0.01	0.36	0.00	-1.06	0.72

Pb, Nd and Sr isotopes were measured from 50 and 200 mg (for pumice and lava samples respectively) of hand-picked rock chips 0.5–1 mm in size. Samples were leached and digested following the method of Cassidy et al., (2012), and Pb was isolated from the matrix using AGX-1x8 200-400 mesh anion exchange resin, following the method of Kamber and Gladu, (2009). For Nd, the dissolved samples were first passed through cation columns containing AG50-X8 200-400 mesh resin, then through LN Spec columns (Eichrom Industries, Illinois, USA). Sr spec™ resin was used for Sr separation, following the method of Smet et al., (2010). Pb and Nd isotopes were measured on a MC-ICP-MS (Neptune) at the University of Southampton, and Sr isotopes were measured on a ThermoFisher Triton Plus thermal ionisation mass spectrometer. Pb isotopes were corrected for instrumental mass fractionation using the SBL74 double spike (Taylor et al., 2015). SRM NBS981 gave $^{206}Pb/^{204}Pb = 16.9400 \pm 0.0023$, $^{207}Pb/^{204}Pb = 15.4965 \pm 0.0026$ and $^{208}Pb/^{204}Pb = 36.7124 \pm 0.0076$ on $n = 108$ measurements during the course of this study. Measured values for standards JNdi and SRM NBS987 are $^{143}Nd/^{144}Nd = 0.512116 \pm 0.000012$ ($n = 36$) and $^{87}Sr/^{86}Sr = 0.710238 \pm 0.000024$ ($n = 18$), respectively.

3.4 Results

3.4.1 Major and trace element data

The lavas of the Silver Hills volcanic centre range in composition from basaltic andesite to dacite (57–65 wt. %), with the majority being andesite, and fall within the low-K field of Gill, (1981) (Figure 3.2). The Centre Hills samples range from low-K basaltic andesite to andesite (56–62 wt. % SiO_2), and the Soufrière Hills samples range from low- to medium-K andesite to dacite (63–65 wt. % SiO_2; Figure 3.2).

The Centre and Soufrière Hills samples fit the linear major element vs SiO_2 trends previously recorded for these centres, with K_2O and Na_2O increasing and Fe_2O_3, TiO_2, Al_2O_3, MgO and CaO decreasing with increasing SiO_2 (e.g. Christopher et al., 2014; Coussens et al., 2017; Zellmer et al., 2003) (Figure 3.2). The Silver Hills data display considerably more scatter, and can be split into two groups. The first is the 'normal' composition lavas, which have major element compositions matching the linear trends defined by the Centre and Soufrière Hills lavas. The second group have notably lower Al_2O_3 and higher Fe_2O_3 contents than the normal lavas, with a difference of up to 3 wt. % at a given SiO_2 value (Figure 3.2). They also have, to a lesser extent, higher TiO_2 and MgO, and lower CaO, Na_2O and K_2O, suggesting that these 'low Al_2O_3-high Fe_2O_3' lavas have a different petrogenetic history to the normal lavas.

The calculated SiO_2 values for the Silver Hills enclaves show they are more mafic than their host lavas; four enclaves are basaltic andesites (54–56 wt. % SiO_2) hosted in andesite lavas, and one is andesite (58 wt. % SiO_2) hosted in a dacite lava (Figure 3.2). This is supported by La and Zr concentrations, which increase with increasing SiO_2, and have lower concentrations in the enclaves than in the host lavas (Figure 3.3). They are similar in composition to the mafic enclaves from the 1995–2010 eruption of the Soufrière Hills, which range from 49–57 wt. % SiO_2 content (Figure 3.2) (Murphy et al., 2000; Plail et al., 2014; Zellmer et al., 2003).

The enclaves generally fall within the main linear arrays on major element vs. SiO_2 plots, with the exception of Al_2O_3, which tends towards the higher end of concentrations for a given SiO_2 content (Figure 3.2). Notably, they do not show the same low Al_2O_3-high Fe_2O_3 contents as the lavas, suggesting that either the enclaves represent the Silver Hills magma compositions before differentiation to form the low Al_2O_3-high Fe_2O_3 lavas, or that the Silver Hills lavas are not formed from differentiation of the enclave magmas. This question will be addressed later on.

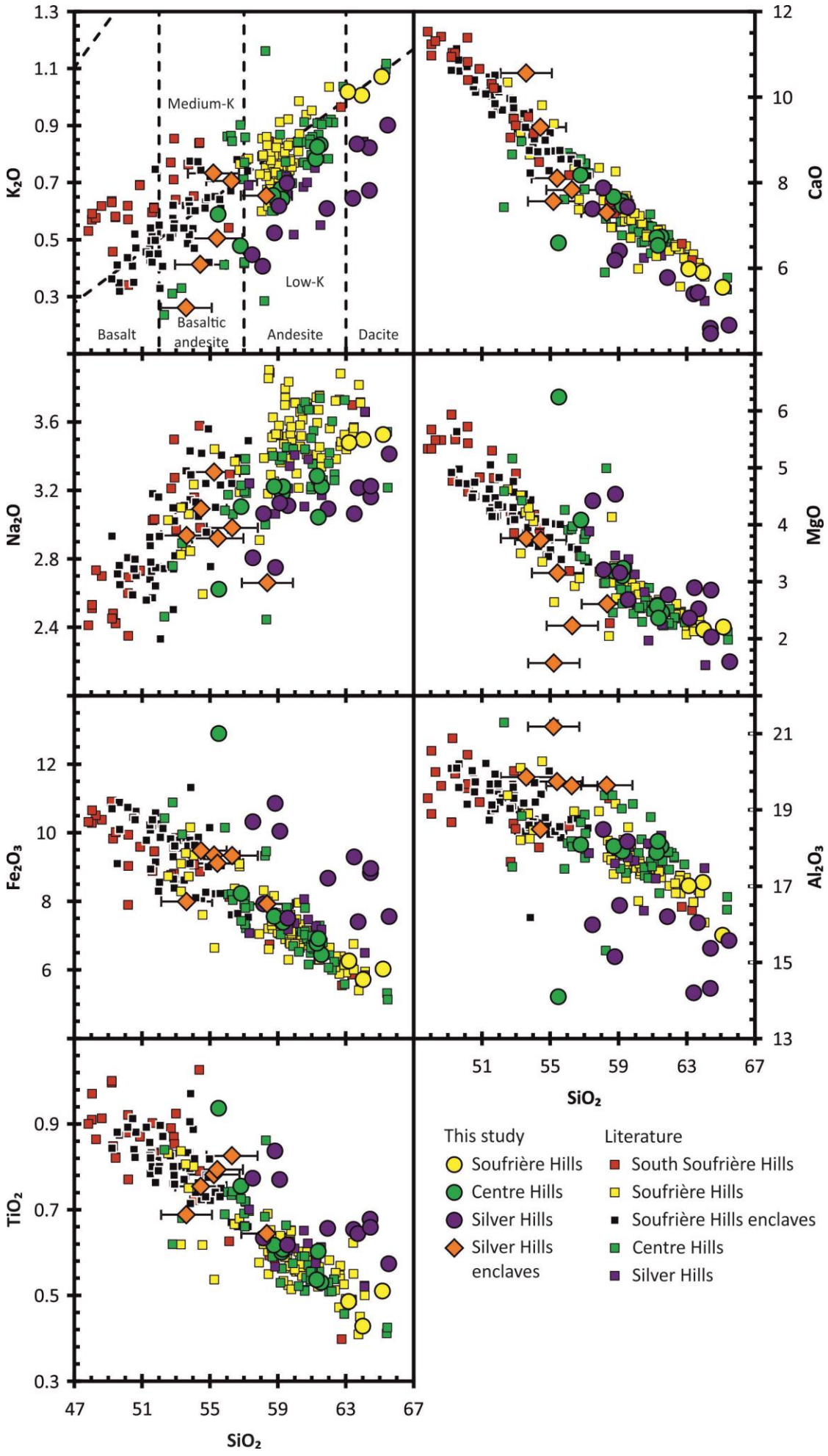
K2O
Medium-K
Low-K
Basalt
Basaltic andesite
Andesite
Dacite
CaO
Na2O
MgO
Fe2O3
Al2O3
TiO2
SiO2
SiO2
This study
Soufrière Hills
Centre Hills
Silver Hills
Silver Hills enclaves
Literature
South Soufrière Hills
Soufrière Hills
Soufrière Hills enclaves
Centre Hills
Silver Hills

Figure 3.2. Harker variation diagrams for the volcanic centres on Montserrat. All data is normalised to volatile free. The error bars for the Silver Hills enclaves show the uncertainty from the calculated SiO_2 values. Soufrière Hills enclaves are all from the 1995–2010 eruption. Low- and medium-K fields as defined by *Gill,* (1981). Literature data for this and subsequent figures are from (Baker, 1984; Cassidy et al., 2012, 2015; Coussens et al., 2017; Davidson, 1987; Devine et al., 1998; Harford et al., 2002; Murphy et al., 1998, 2000; Plail et al., 2014).

All but two of the samples show LREE enrichment with trough-shaped M-HREE (Figure 3.4; trace element data is presented in Appendix Table 3.2), with the Soufrière Hills samples having lower HREE abundances and greater LREE enrichment than the Centre and Silver Hills samples, matching those of Cassidy et al. (2012). Two enclaves have similar M-HREE patterns but with a flatter LREE profile. Most of the Silver Hills samples display a negative Eu anomaly resulting from plagioclase fractionation, whereas most enclaves have no, or only a poorly developed, Eu anomaly. The Centre and Soufrière Hills samples typically do not exhibit a Eu anomaly (Figure 3.4). The pronounced trough-shaped H-MREE and LREE enrichment pattern for all centres suggests that amphibole crystallisation played a prominent role in the formation of these magmas. This is supported by the minor amounts of amphibole observed within some samples from both the Silver Hills and Centre Hills (Hatter et al., 2018). Some samples also display a small negative Ce anomaly (Figure 3.4).

3.4.2 Isotope data

Sr isotope data, presented in Figure 3.5, were obtained for all of the lava and pumice samples, but not the enclaves (isotope data is presented in Appendix Table 3.3). All three centres display a similar range of values, with 0.703599–0.703621 for Soufrière Hills, 0.703587–0.703698 for Centre Hills, and 0.703547–0.703671 for Silver Hills, matching the data from Cassidy et al. (2012).

Pb and Nd isotopes for the lava and pumice samples in this study were obtained by Hatter et al. (2018); this study presents data for the six Silver Hills enclave samples. Pb and Nd isotopes of the Silver Hills enclaves fall within the field defined by the Silver Hills lavas, and for $^{143}Nd/^{144}Nd$ they are mostly in the higher range of values (Figure 3.6). Most individual enclaves are isotopically distinct from their host lavas. The same is true for the one Soufrière Hills mafic enclave that has been analysed for Pb and Nd isotopes (Cassidy et al., 2012). Only the enclaves from Rendezvous Bay are within error of their host lava in all three Pb isotope ratios, but are still distinct in $^{143}Nd/^{144}Nd$. The two Rendezvous Bay enclaves are only isotopically distinct from each other in $^{207}Pb/^{204}Pb$; in all other Pb and Nd isotopes they are within error (Figure 3.6).

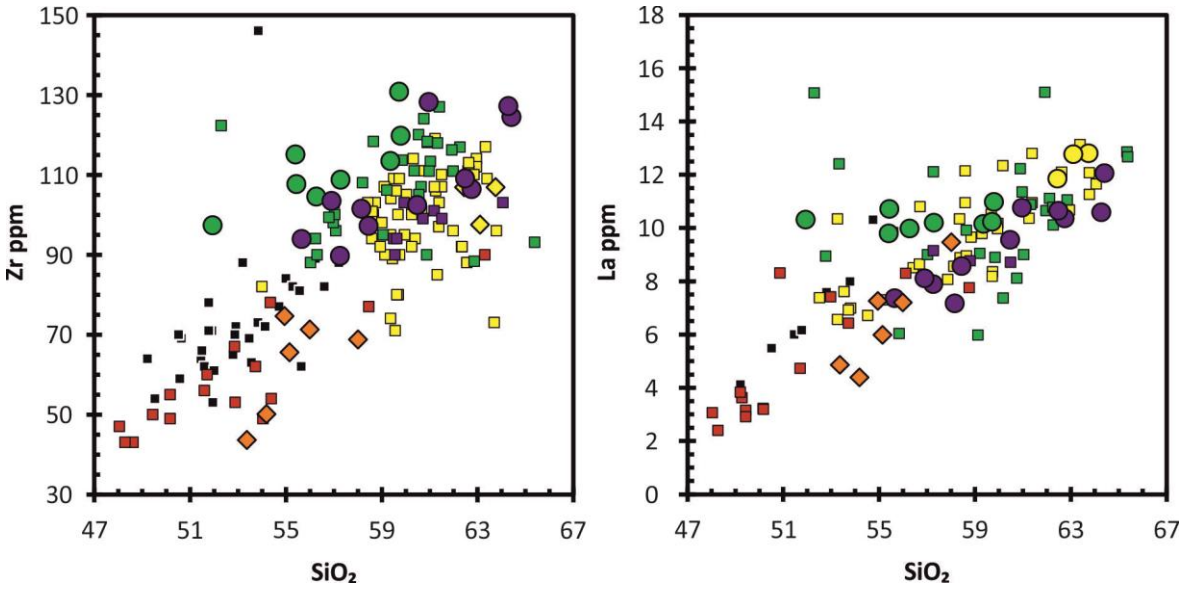

Figure 3.3. SiO_2 vs Zr and La, showing that the Silver Hills enclaves are more mafic than their host lavas. Symbols same as Figure 3.2.

3.5 Geochemical variation between Silver Hills domes

Figure 3.7 shows the variation in select major and trace element ratios between the different domes of the Silver Hills, arranged in approximate stratigraphic order. Lavas from the 1995–2010 eruption of the Soufrière Hills have also been plotted to give an indication of typical chemical variation displayed during a single eruptive period. There appears to be no systematic temporal trend in major elements, with the dacitic and low Al_2O_3-high Fe_2O_3 lavas occurring throughout the lifespan of the Silver Hills (Figure 3.7a). This apparent uniformity is also observed in trace element ratios, which display overlap between all domes (comparable to the current Soufrière Hills variation; Figure 3.7b). The only exception to this is U/Th, for which North Marguerita Bay and Yellow Hole have distinctly lower values. There is also no systematic change in Pb or Sr isotopes, with a consistent range of values through the activity of the Silver Hills (Figure 3.7c).

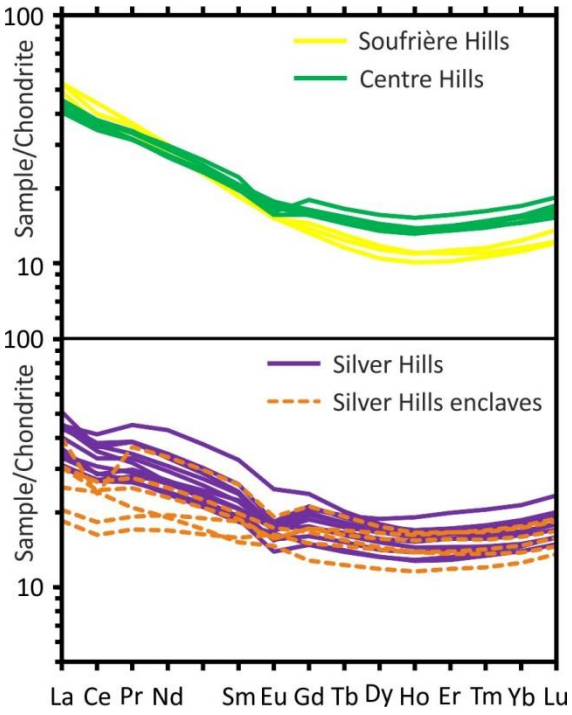

Figure 3.4. REE trends for samples from Soufrière, Centre and Silver Hills, and Silver Hills enclaves, normalised to chondrite (Sun and McDonough, 1989).

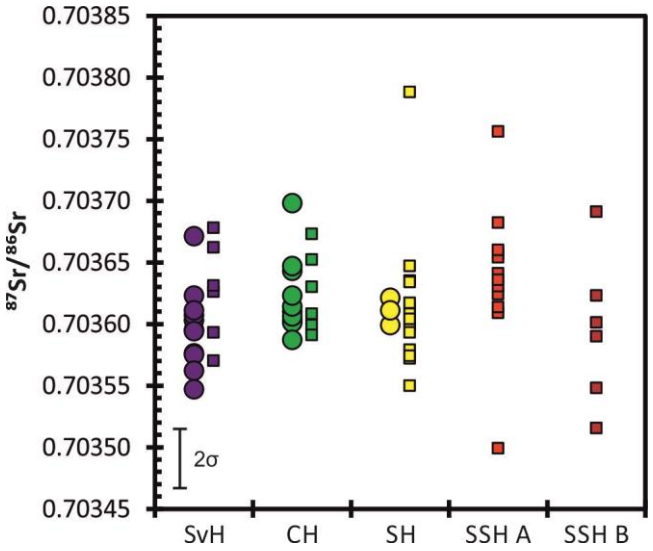

Figure 3.5. $^{87}Sr/^{86}Sr$ for each volcanic centre on Montserrat. Circles, this study; Squares, Cassidy et al., (2012). SvH, Silver Hills; CH, Centre Hills; SH, Soufrière Hills; SSH, South Soufrière Hills.

$^{143}Nd/^{144}Nd$ on-the-other-hand, with the exception of the oldest dome, shows a decrease from older to younger domes (Figure 3.7c). This is clearer when plotted against time (Figure 3.8), where it can be see that, with the exception of the oldest deposit (~2.17 Ma), $^{143}Nd/^{144}Nd$ systematically decreases during the lifetime of the Silver Hills. $^{143}Nd/^{144}Nd$ values drop further for the oldest Centre Hills deposits, which then (with the exception of the sample with the lowest value) generally increase in value during the lifetime of the Centre Hills. $^{143}Nd/^{144}Nd$ then stabilises during the course of Soufrière Hills activity, with the exception of the high values obtained in the South Soufrière Hills.

3.6 Discussion

3.6.1 Crustal assimilation

Evidence for crustal assimilation in Montserrat magmatism is observed in hydrogen isotope compositions of amphiboles from lava erupted during the 1995–2010 eruption of the Soufrière Hills. The lavas contained amphiboles with heterogeneous δD values, which are on average higher than known primary magmatic values. These elevated δD values are interpreted as resulting from assimilation of hydrothermally altered andesite during storage in a shallow andesitic magma chamber (Harford and Sparks, 2001). Further evidence for crustal assimilation comes from oxygen isotopes, as lavas from the recent Soufrière Hills eruption have whole-rock $\delta^{18}O$ values higher than typical non-altered ocean island arc samples, which are interpreted as resulting from assimilation of hydrothermally altered previous intrusions. However, differentiation modelling indicates that assimilation has not significantly affected trace element trends (Zellmer et al., 2003). Further, no correlation

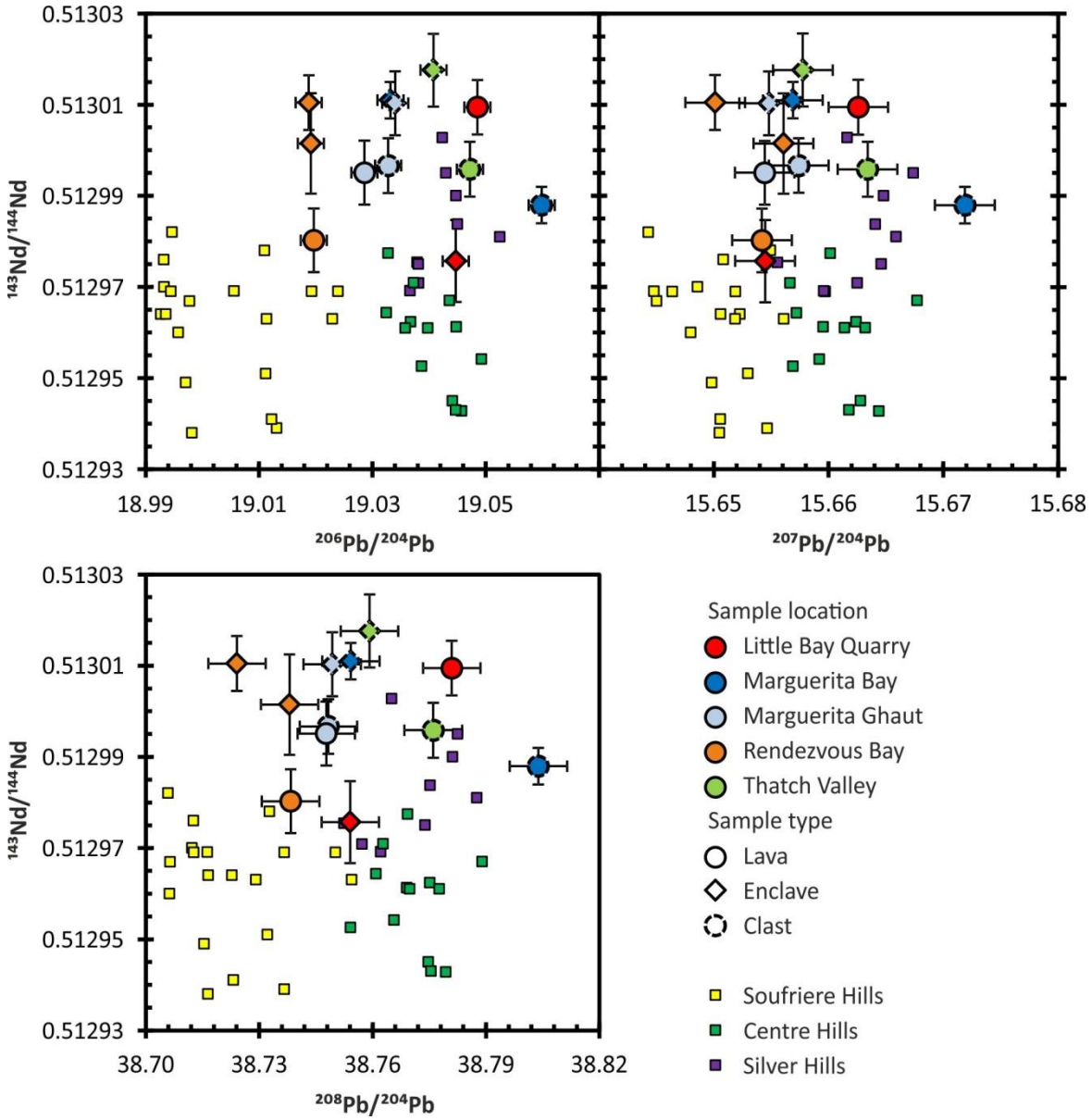

Figure 3.6. Pb vs Nd isotopes of enclaves and their host lavas. Clast samples are from block-and-ash flow deposits, so the enclaves and lava clasts from these deposits are not necessarily from the same eruption. Enclave data from this study; all other data from Cassidy et al. (2012) and Hatter et al. (2018).

between Pb, Nd or Sr isotopes against SiO_2 is observed for any of the volcanic centres on Montserrat, suggesting that these isotopes have been unaffected by crustal assimilation (Cassidy et al., 2012). Our data provide further support for this, showing no correlation between Pb, Nd or Sr isotopes against SiO_2 (Figure 3.9). Thus any crustal assimilation that has occurred does not appear to be in sufficient quantities to affect the Pb, Nd or Sr isotope composition of Montserrat volcanics, indicating that the change in Nd isotopes is not the result of crustal assimilation.

There is evidence to suggest that crustal assimilation has played a role in the evolution of magmas at Mt Pelée, Martinique, and to a lesser extent at The Quill, St. Eustatius, as for

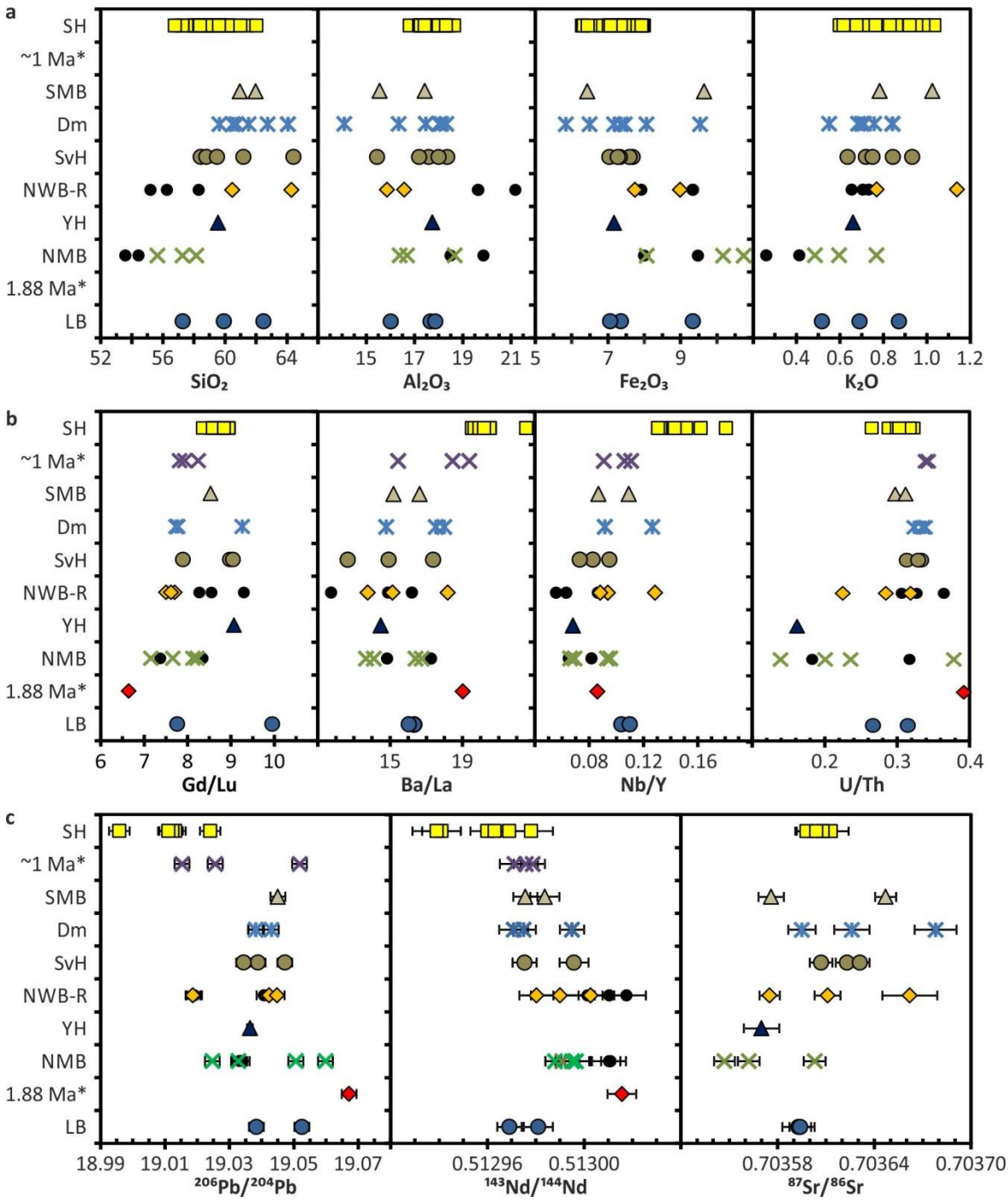

Figure 3.7. Inter-dome variation in a) major elements, b) trace elements and c) isotopes. Domes are arranged in approximate stratigraphic order, younging upwards. SH, Soufrière Hills (1995–2010 eruption); SMB, South Marguerita Bay; Dm, Drummonds; SvH, Silver Hill; NWB-R, Northwest Bluff to Rendezvous Bay; YH, Yellow Hole; NMB, North Marguerita Bay; LB, Little Bay. *Samples are from marine sediment core U1396C, and do not match any known periods of activity from the terrestrial record. Black circles represent enclaves. SH major and trace element data from Devine et al., (1998); Murphy et al., (2000); Zellmer et al., (2003), and isotope data from Cassidy et al., (2012).

these islands there is a positive correlation of SiO_2 with Pb and Sr isotope ratios, but not with $^{143}Nd/^{144}Nd$ (Davidson and Wilson, 2011). On St Kitts, Nd and Sr isotopes do not vary with SiO_2, but Pb isotopes do, suggesting that crustal assimilation has only affected Pb isotope

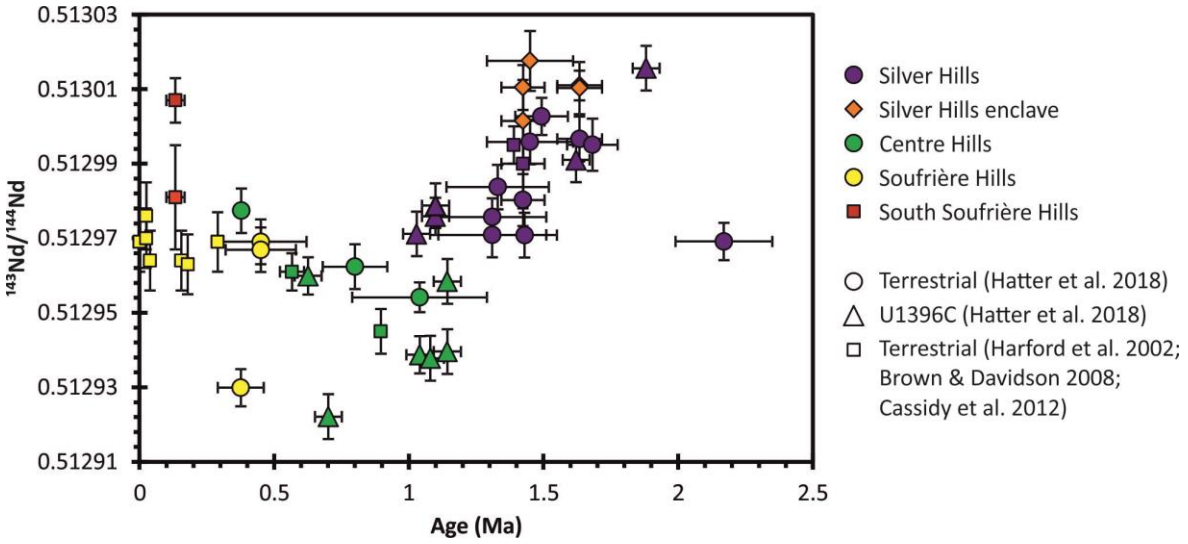

Figure 3.8. Variation in $^{143}Nd/^{144}Nd$ with time for all volcanic centres on Montserrat.

ratios (Toothill et al., 2007). Collectively these examples suggest that Pb and Sr isotopes are more sensitive to crustal assimilation than $^{143}Nd/^{144}Nd$ in the Lesser Antilles, providing further evidence that crustal assimilation is not responsible for the observed change in $^{143}Nd/^{144}Nd$ between Silver and Centre Hills.

3.6.2 Petrogenesis of Silver Hills lavas

3.6.2.1 Role of enclave fractionation

The difference in Pb and Nd isotope ratios between the Silver Hills enclaves and their host lavas shows that these lavas could not have formed via fractionation of the enclave parent magmas. The enclave isotope values are, however, still within the range of the Silver Hills lava, so they could potentially represent the magma compositions (i.e. major and trace elements) which differentiated to form the Silver Hills lavas. However, many trace element concentrations of the enclaves are higher than in the lavas despite having lower SiO_2 values, particularly REEs (Figure 3.4). These elements are incompatible in the fractionating assemblage, meaning their concentrations would increase with increasing fractionation, and so their greater abundance in the enclaves indicates that Silver Hills lavas could not have formed from differentiation of magmas of similar composition to the enclaves.

3.6.2.2 Formation of 'low Al_2O_3-high Fe_2O_3' lavas

As well as having distinct major element concentrations, the low Al_2O_3-high Fe_2O_3 lavas also have more pronounced negative Eu anomalies and lower Sr/Nd ratios than the normal lavas (Figure 3.10), suggesting that plagioclase fractionation (f_{plag}) may be responsible for this difference in lava chemistry. If late stage plagioclase fractionation is responsible, the low Al_2O_3-high Fe_2O_3 lavas might be expected to contain fewer plagioclase phenocrysts than the

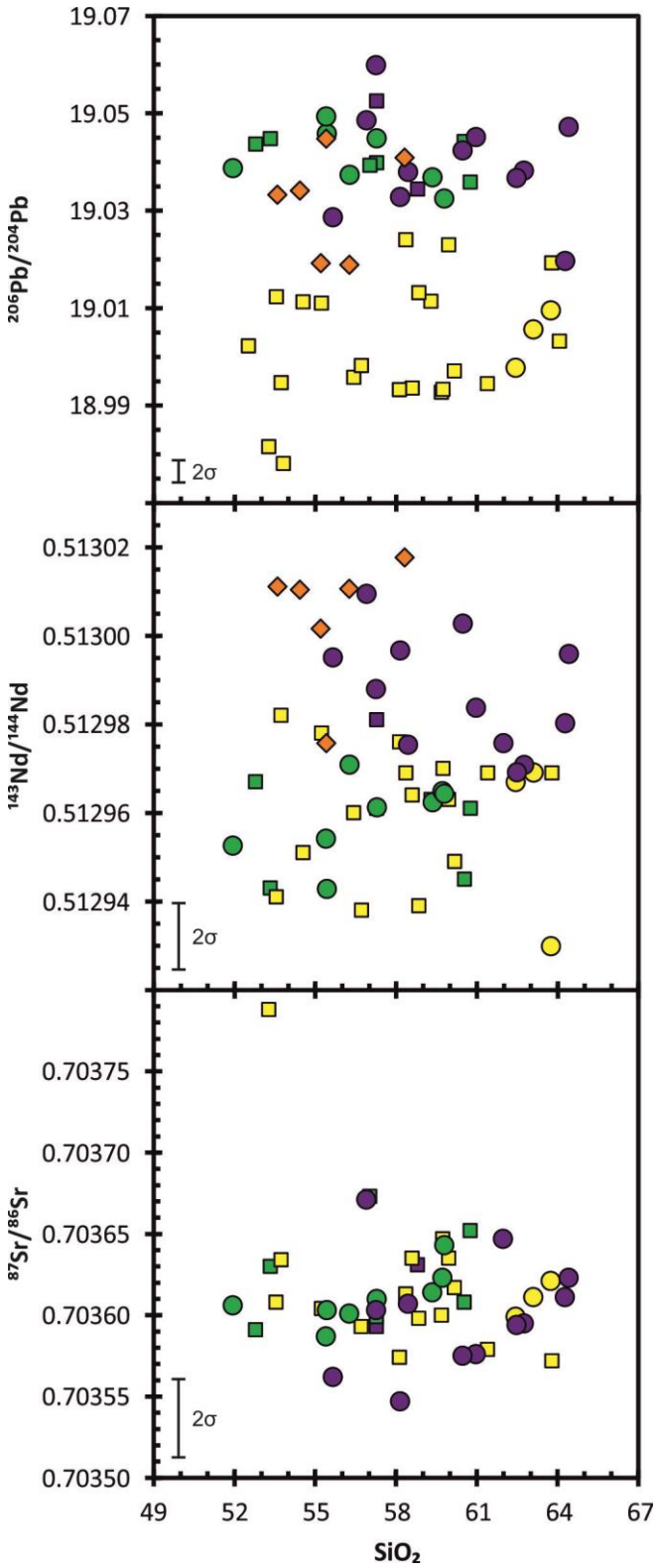

Figure 3.9. SiO_2 vs $^{206}Pb/^{204}Pb$, $^{143}Nd/^{144}Nd$ and $^{87}Sr/^{86}Sr$. Symbols same as Figure 3.2. Literature data (squares) from Cassidy et al., (2012). The SiO_2 data from this study is combined with the isotope data from Hatter et al. (2018)for the same samples.

normal composition lavas. However, the range in plagioclase phenocryst abundance is broadly the same for lavas of both compositions (Hatter et al., 2018).

An alternative explanation is that the change in major element chemistry reflects differences in the H_2O content of the parent melt. Experimental studies show that the presence of H_2O in basaltic magmas suppresses plagioclase crystallisation relative to olivine and clinopyroxene, resulting in higher Al_2O_3 and lower Fe_2O_3 contents in the residual melt compared with anhydrous crystallisation (e.g. Danyushevsky, 2001; Green and Ringwood, 1967; Sisson and Grove, 1993). This hypothesis can be tested using mass balance equations. For the starting composition of the parent melt, the mafic enclave from the recent eruption of Soufrière Hills with the lowest SiO_2 content (49.22 wt. %) was used (Zellmer et al., 2003), because it is less evolved than the Silver Hills enclaves that have been analysed (~53–58 wt. % SiO_2). For plagioclase both the average core and rim compositions of phenocrysts in the Soufrière Hills mafic enclaves were used (Murphy et al., 2000). The results are displayed in Table 3.2, and show that a 3 wt. % increase in Fe_2O_3 requires ~23% f_{plag}, while a 3 wt.% decrease in Al_2O_3 in the residual melt requires ~18–28% f_{plag}, depending on the An number. Plagioclase fractionating from the parent melt is likely to have a high An number, similar to the phenocryst core compositions of Murphy et al., (2000), which will subsequently decrease with increasing fractionation. Thus the change in Al_2O_3 is likely caused by ~20–25% f_{plag}, consistent with the 23% required for Fe_2O_3. Further support for this model comes from trace element modelling. Using partition coefficients from Bindeman et al., (1998), 20–25% f_{plag} would decrease Sr/Nd values in the residual melt by ~8.5–10.5 (Table 3.2), which matches the observed difference in Sr/Nd values between the two suites of lavas (Figure 3.10). Thus we conclude that the low Al_2O_3-high Fe_2O_3 lavas formed from parental melts that experienced

Table 3.2. Change in melt chemistry after x% plagioclase fractionation

	Parent melt*	**Phenocryst Core⁺**	**Δf_x**		**$f_{3\ wt.\%}$**	**Phenocryst Rim⁺**	**Δf_x**		**$f_{3\ wt.\%}$**
			***x*=20**	***x*=30**			***x*=20**	***x*=30**	
n		22				5			
SiO_2	49.22	46.17	0.84	1.43		55.26	-1.45	-2.49	
Al_2O_3	20.08	34.26	-3.49	-5.98	18%	28.04	-1.96	-3.36	28%
Fe_2O_3	10.69	0.50	2.55	4.37	23%	0.41	2.57	4.41	23%
MnO	0.20	0.01	0.05	0.08		0.00	0.05	0.09	
MgO	4.92	0.07	1.21	2.08		0.06	1.21	2.08	
CaO	10.62	18.25	-1.88	-3.22		11.08	-0.10	-0.18	
Na_2O	2.93	1.35	0.40	0.68		5.49	-0.63	-1.09	
K_2O	0.36	0.02	0.09	0.15		0.09	0.07	0.12	
An		0.88				0.57			
		D_x	***x*=20**	***x*=25**					
Sr ppm	282.62	1.572	-33.87	-42.88					
Nd ppm	9.14	0.138	1.94	2.57					
Sr/Nd	30.92		-8.47	-10.45					

n, number of analyses; An, anorthite number; *Composition of Soufrière Hills mafic enclave with lowest SiO_2 wt.% (MVO 1133) (Zellmer, 2003); ⁺ average mafic enclave plagioclase phenocryst compositions (Murphy, 2000); D_x, plagioclase/melt partition coefficients from Bindeman et al., (1998); Δf_x, change in melt composition after *x* percent plagioclase fractionation; $f_{3\ wt.\%}$, percent plagioclase fractionation required to decrease Al_2O_3 and increase Fe_2O_3 by 3 wt. % in the residual melt.

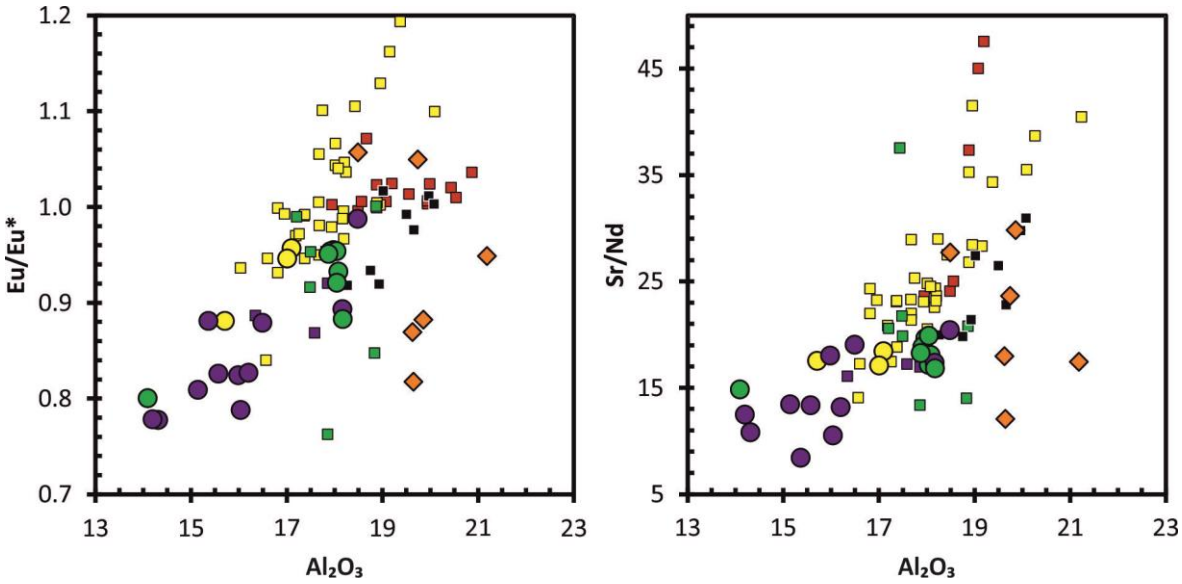

Figure 3.10. Al_2O_3 vs Eu/Eu* and Sr/Nd, suggesting that plagioclase fractionation may be an important process in forming the low Al_2O_3-high Fe_2O_3 lavas (Silver Hills samples with Al_2O_3<17 wt. %). Eu/Eu* is europium anomaly, where Eu* is the calculated Eu concentration if there were no anomaly. Symbols same as Figure 3.2.

up to 25% f_{plag}, likely as a result of lower melt H_2O content, with subsequent separation of residual melt from the plagioclase cumulates. This separation of residual melt from plagioclase cumulates suggests that the plagioclase phenocrysts present in the erupted lavas formed at a later stage of magma evolution, which is why there is no discernible difference in plagioclase phenocryst abundances and textures between the low Al_2O_3-high Fe_2O_3 and normal lavas.

An interesting implication to come from this modelling is that magmas of varying water content were simultaneously present within the Silver Hills system, because both low Al_2O_3-high Fe_2O_3 and normal lavas were erupted from the same domes (Figure 3.7). This is further supported by the enclave compositions, which generally follow the major element vs SiO_2 trends of the normal lavas, but with a bit more scatter (which may to some extent be due to the unknown LOI values), and notably none of them trend towards the low Al_2O_3-high Fe_2O_3 lavas common in the Silver Hills lavas, in which they are hosted. This suggests that either the enclave magmas had low H_2O contents but did not stall within the crust long enough for plagioclase fractionation to occur, or the enclave magmas had a higher H_2O content than their host magmas, similar to the normal composition lavas. The range in enclave compositions suggests that some fractionation of the enclave parent magmas has occurred, but do not trend towards a low Al_2O_3-high Fe_2O_3 composition, suggesting that they did not have low H_2O contents. This could be tested by measuring the H_2O content of melt inclusions from both the enclaves and lavas.

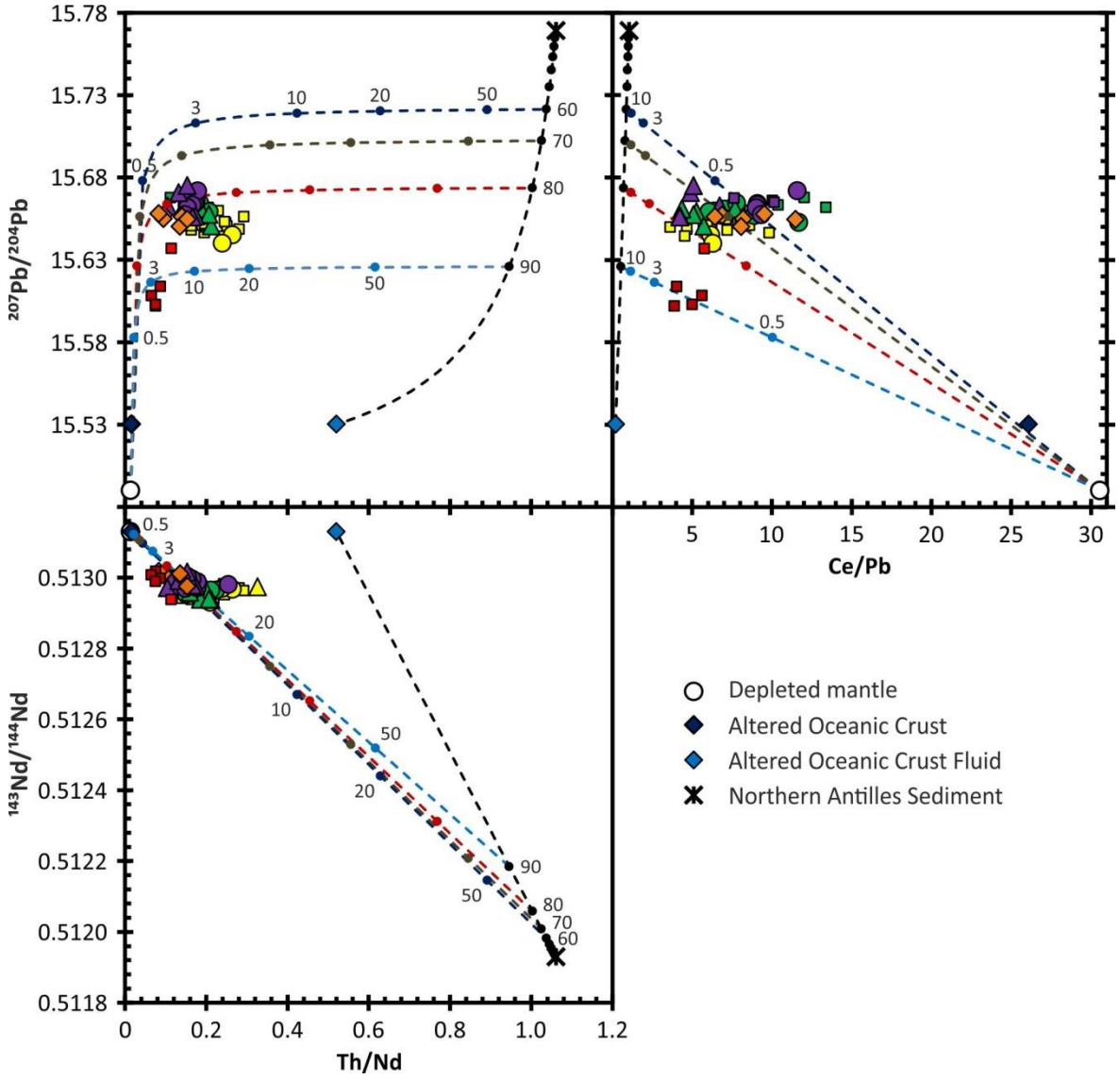

Figure 3.11. Trace element versus isotope mixing models for the different source components producing Montserrat lavas. Modelled mixing lines are between sediment and AOC, and between this mixing line and depleted MORB mantle. Numbers indicate percentage of component added. Depleted MORB mantle from DuFrane et al., (2009); Workman and Hart, (2005). Northern Antilles sediment is a 20% partial melt of the bulk site 543 sediment from Plank and Langmuir, (1998), using the bulk partition coefficients of Johnson and Plank, (1999). A 20% partial sediment melt was used because Cassidy et al., (2012) showed it creates mixing lines which match the Montserrat data, whereas bulk sediment addition does not. AOC from Bach et al., (2003); Hauff et al., (2003); Kelley et al., (2003). AOC fluid from DuFrane et al., (2009).

3.6.3 Examining the role of magma source components in changing $^{143}Nd/^{144}Nd$

Here the cause of the systematic decrease in $^{143}Nd/^{144}Nd$ over the course of activity at Silver Hills is examined, which is followed by a drop in $^{143}Nd/^{144}Nd$ between the end of Silver Hills volcanism, and onset of Centre Hills volcanism, with no concomitant change in Pb or Sr isotopes. As discussed, crustal assimilation can be ruled out as the cause of these observed

trends in isotope values, and while fractionation is an important process in the petrogenetic history of Montserrat's lavas, it does not change isotope ratios. Thus, a change in source component contributions remains the only likely explanation, which will now be examined to determine the most likely cause of the observed shift in $^{143}Nd/^{144}Nd$.

Trace element and isotope values of the different magma source components beneath Montserrat are presented in Figure 3.11. Using the same compositions as DuFrane et al., (2009) and Cassidy et al., (2012), mixing lines model the relative proportions of each component required to form the observed lava compositions. They show that increasing the sediment contribution relative to the AOC fluid would create the observed decrease in $^{143}Nd/^{144}Nd$, but would also produce a concomitant increase in $^{207}Pb/^{204}Pb$. Furthermore, the modelling suggests that this would have a greater effect on $^{207}Pb/^{204}Pb$ than $^{143}Nd/^{144}Nd$ (Figure 3.11). This is likely because Pb is preferentially partitioned into the slab fluid, whilst Nd is not (Brenan et al., 1995), and since the modelling predicts that the AOC fluid component is more abundant than sediment (Figure 3.11), changing the proportion of slab fluid will have a greater effect on Pb isotopes than Nd. Thus, the change in the proportion of sediment to AOC fluid can be ruled out as the cause of the change in $^{143}Nd/^{144}Nd$.

Alternatively, this could be the result of heterogeneity within the subducted sediment. The closest approximation to the composition of sediment that has entered the subduction zone comes from the sediments currently outboard of the Lesser Antilles, which have been studied for lithological and geochemical variation through DSDP sediment cores from sites 543 and 144 (Figure 3.1) (Carpentier et al., 2008, 2009; Plank and Langmuir, 1998; White et al., 1985). Using a depth to the Benioff zone of ~140 km (Wadge and Shepherd, 1984), and assuming a constant rate of subduction of 2 cm/yr, it takes ~8.9 Myr from the slab entering the subduction zone to it reaching the depth of sediment melting (~140 km). Thus the sediment which was added to the mantle wedge beneath the Silver Hills entered the subduction zone ~11.1 Ma (using the oldest Silver Hills age of ~2.2 Ma) (Hatter et al., 2018). The Orinoco and Amazon River deltas were still a major source of terrigenous sediment to the Atlantic crust outboard of the Lesser Antilles ~11.1 Ma (Pichot et al., 2012, and references therein), and late Palaeogene terrigenous turbidites derived from the South American continent have been identified north of the Barracuda Ridge (Pichot et al., 2012). Thus there is no evidence for any major change in sediment sources or depositional process on the subducting Atlantic crust, and so the sediments analysed from DSDP sites 543 and 144 are considered to represent a reasonable approximation to the composition of the sediments which subducted beneath the Silver Hills. Indeed, site 543 and 143 sediment compositions have been used to successfully model the sediment contribution to the source components for multiple islands along the Lesser Antilles arc (e.g. Carpentier et al., 2008; Cassidy et al., 2012; DuFrane et al., 2009). The various sediment compositions from sites 543 and 144

(Carpentier et al., 2008) show a negative correlation in $^{207}Pb/^{204}Pb$ vs $^{143}Nd/^{144}Nd$ (Figure 3.12), so any heterogeneity in the sediment is likely to change both Pb and Nd isotope values. Furthermore, the Silver Hills lavas show no change in trace element compositions for elements which are dominated by the sediment input, such as Th and Nd (e.g. Cassidy et al., 2012; DuFrane et al., 2009; Zellmer et al., 2003), whose concentrations range from 1–17 and 5–54 ppm, respectively, in sediments from sites 543 and 144 (Carpentier et al., 2008). Because there is no change in either Pb isotopes or Th and Nd contents of Silver Hills lavas, sediment heterogeneity is considered unlikely to be responsible for the observed trend in $^{143}Nd/^{144}Nd$.

Reducing the proportion of mantle to sediment + AOC fluid mix (i.e. reduced mantle signature) would reduce $^{143}Nd/^{144}Nd$, but there is disagreement in the models as to what affect this would have on $^{207}Pb/^{204}Pb$. Th/Nd vs $^{207}Pb/^{204}Pb$ predicts that $^{207}Pb/^{204}Pb$ could remain around the same values, whilst Ce/Pb vs $^{207}Pb/^{204}Pb$ predicts $^{207}Pb/^{204}Pb$ will move towards more radiogenic values. However, trace element ratios containing high field strength elements (HFSE) may be more revealing. They are the most immobile elements during slab-fluxing processes (dehydration and melting), so their abundance in arc rocks is dominated by the mantle wedge (McCulloch and Gamble, 1991). Thus reducing the proportion of mantle to sediment + AOC fluid mix would increase fluid mobile/HFSE and Th or Nd/HFSE (sediment tracers) ratios. There is no observed change in such ratios between the Silver Hills and Centre Hills, indicating that the change in $^{143}Nd/^{144}Nd$ was not caused by a reduced mantle component.

Since changes in the relative proportions of the mantle wedge, subducted sediment and AOC fluid, and any heterogeneity in the slab components, can be confidently ruled out, the observed shift in $^{143}Nd/^{144}Nd$ must be controlled by heterogeneity in the mantle wedge. This could also explain why the only trace element ratio that changes between the Silver Hills and Centre Hills is Nb/Y, because HFSE abundances are dominated by mantle wedge contributions. The systematic decrease in $^{143}Nd/^{144}Nd$ during the development of the Silver Hills (i.e. ~2.17–1.03 Ma) could be the result of a progressive increase in the amount of 'new' mantle that is melting to form the Montserrat magmas. The decrease in $^{143}Nd/^{144}Nd$ creates a difference in values of 0.000045 (0.513016–0.512971). For comparison, widespread km-scale mantle isotopic heterogeneity has been observed along the MAR, with the largest observed change in $^{143}Nd/^{144}Nd$ over a distance of <10 km length of the ridge being 0.000274 (from 0.512459 to 0.512733) (Agranier et al., 2005, and references therein). This shows that the scale of mantle isotopic heterogeneity inferred for beneath the Silver Hills is common within the Atlantic mantle.

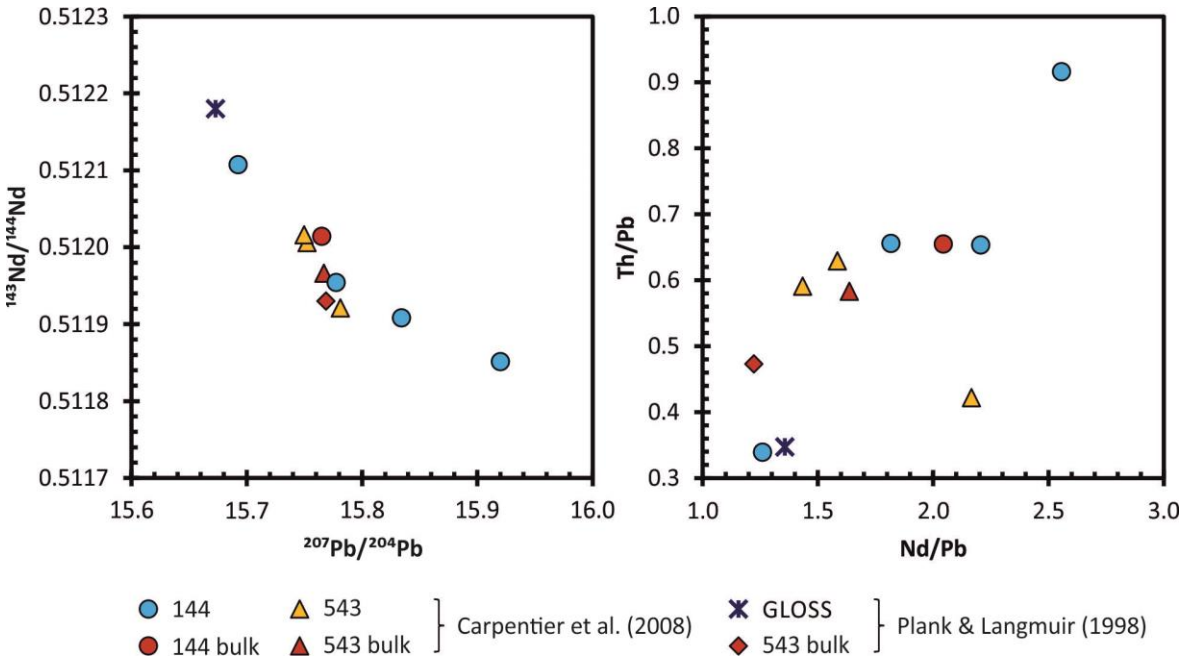

Figure 3.12. Isotopic and trace element variation between different marine sediment units from Deep Sea Drilling Program sites 144 and 543, situated east of the Lesser Antilles on the Atlantic crust (Figure 3.1). GLOSS (GLObal Subducting Sediments) is the calculated average global composition of sediments currently being subducted.

3.7 Conclusions

New major and trace element, and Pb-Nd-Sr isotope data are presented for the Silver Hills and Centre Hills, to assess the geochemical variation and petrogenetic history of these lavas. The lavas of the Centre Hills, and some of the Silver Hills, match the linear major element versus SiO_2 trends observed for the Soufriere Hills and Centre Hills of previous authors. For the majority of Silver Hills lavas however, they displayed a marked deviation from this trend, most notably containing low Al_2O_3 and high Fe_2O_3 for a given value of SiO_2. These low Al_2O_3-high Fe_2O_3 lavas also contain higher negative Eu anomalies and lower Sr/Nd. Mass-balance equations show that these compositions can be formed from up to 25% f_{plag}, which is interpreted as the result of lower magmatic H_2O content.

The various domes of the Silver Hills are mostly geochemically indistinguishable from one another, with the only observed difference being lower U/Th values for the North Marguerita Bay and Yellow Hole domes. Over the course of the Silver Hills activity there is also a shift in $^{143}Nd/^{144}Nd$ to progressively less radiogenic values with time. This is then followed by a drop to even lower values with the onset of Centre Hills volcanism. There is no evidence for crustal assimilation affecting Nd isotopes on Montserrat, so this change in $^{143}Nd/^{144}Nd$ is related to changes in the magma source components. Changes in the proportions of mantle to sediment to AOC fluid, as well as heterogeneity within the slab

components, would all likely simultaneously affect both Pb and Nd isotopes, as well as various trace element ratios which remain unchanged between the two centres, so can all be ruled out as a cause. Thus heterogeneity in the mantle wedge remains the only feasible cause for the observed change in $^{143}Nd/^{144}Nd$, which is accompanied by an increase in Nb/Y.

3.8 References

Agranier, A., Blichert-Toft, J., Graham, D., Debaille, V., Schiano, P., Albarède, F., 2005. The spectra of isotopic heterogeneities along the mid-Atlantic Ridge. Earth Planet. Sci. Lett. 238, 96–109. doi:10.1016/j.epsl.2005.07.011

Arculus, R.J., Powell, R., 1986. Source Component Mixing in Regions of Arc Magma Generation. J. Geophys. Res. 91, 5913–5926.

Bach, W., Bernhard, P.E., Hart, S.R., Blusztajn, J.S., 2003. Geochemistry of hydrothermally altered oceanic crust: DSDP/ODP Hole 504B - Implications for seawater-crust exchange budgets and Sr-and Pb-isotopic evolution of the mantle. Geochemistry, Geophys. Geosystems 4, 40–55. doi:10.1029/2002GC000419

Baker, P.E., 1984. Geochemical evolution of St Kitts and Montserrat, Lesser Antilles. J. Geol. Soc. London. 141, 401–411. doi:10.1144/gsjgs.141.3.0401

Bezard, R., Davidson, J.P., Turner, S., Macpherson, C.G., Lindsay, J.M., Boyce, A.J., 2014. Assimilation of sediments embedded in the oceanic arc crust: Myth or reality? Earth Planet. Sci. Lett. 395, 51–60. doi:10.1016/j.epsl.2014.03.038

Bindeman, I.N., Davis, A.M., Drake, M.J., 1998. Ion microprobe study of plagioclase- basalt partition experiments at natural concentration levels of trace elements. Geochim. Cosmochim. Acta 62, 1175–1193. doi:10.1016/S0016-7037(98)00047-7

Brenan, J.M., Shaw, H.F., Ryerson, F.J., 1995. Experimental evidence for the origin of lead enrichment in convergent-margin magmas. Nature 378, 54–56. doi:10.1038/378592a0

Carpentier, M., Chauvel, C., Mattielli, N., 2008. Pb-Nd isotopic constraints on sedimentary input into the Lesser Antilles arc system. Earth Planet. Sci. Lett. 272, 199–211. doi:10.1016/j.epsl.2008.04.036

Carpentier, M., Chauvel, C., Maury, R.C., Mattielli, N., 2009. The “zircon effect” as recorded by the chemical and Hf isotopic compositions of Lesser Antilles forearc sediments. Earth Planet. Sci. Lett. 287, 86–99. doi:10.1016/j.epsl.2009.07.043

Cassidy, M., Edmonds, M., Watt, S.F.L., Palmer, M.R., Gernon, T.M., 2015. Origin of basalts by

hybridization in andesite-dominated arcs. J. Petrol. 56, 325–346. doi:10.1093/petrology/egv002

Cassidy, M., Taylor, R.N., Palmer, M.R., Cooper, R.J., Stenlake, C., Trofimovs, J., 2012. Tracking the magmatic evolution of island arc volcanism: Insights from a high-precision Pb isotope record of Montserrat, Lesser Antilles. Geochemistry, Geophys. Geosystems 13, 1–19. doi:10.1029/2012GC004064

Christopher, T.E., Humphreys, M.C.S., Barclay, J., Genareau, K., De Angelis, S.M.H., Plail, M., Donovan, A., 2014. Petrological and geochemical variation during the Soufrière Hills eruption, 1995 to 2010. Geol. Soc. London, Mem. 39, 317–342. doi:10.1144/M39.17

Coussens, M., Cassidy, M., Watt, S.F.L., Jutzeler, M., Talling, P.J., Barfod, D., Gernon, T.M., Taylor, R., Hatter, S.J., Palmer, M.R., 2017. Long-term changes in explosive and effusive behaviour at andesitic arc volcanoes: Chronostratigraphy of the Centre Hills Volcano, Montserrat. J. Volcanol. Geotherm. Res. doi:10.1016/j.jvolgeores.2017.01.003

Danyushevsky, L. V, 2001. The effect of small amounts of H2O on crystallisation of mid-ocean ridge and backarc basin magmas. J. Volcanol. Geotherm. Res. 110, 265–280.

Davidson, J., Wilson, M., 2011. Differentiation and source processes at Mt Pelée and the Quill; Active volcanoes in the Lesser Antilles arc. J. Petrol. 52, 1493–1531. doi:10.1093/petrology/egq095

Davidson, J.P., 1987. Crustal contamination versus subduction zone enrichment: Examples from the Lesser Antilles and implications for mantle source compositions of island arc volcanic rocks 51, 2185–2198.

Davidson, J.P., Harmon, R.S., 1989. Oxygen isotope constraints on the petrogenesis of volcanic arc magmas from Martinique, Lesser Antilles. Earth Planet. Sci. Lett. 95, 255–270.

Devine, J.D., Murphy, M.D., Rutherford, M.J., Barclay, J., Sparks, R.S.J., Carroll, M.R., Young, S.R., Gardner, J.E., 1998. Petrologic evidence for pre-eruptive pressure-temperature conditions, and recent reheating, of andesitic magma erupting at the Soufrière Hills Volcano, Montserrat, W.I. Geophys. Res. Lett. 25, 3669–3672. doi:10.1029/98GL01330

DuFrane, S.A., Turner, S., Dosseto, A., van Soest, M., 2009. Reappraisal of fluid and sediment contributions to Lesser Antilles magmas. Chem. Geol. 265, 272–278. doi:10.1016/j.chemgeo.2009.03.030

Expedition 340 scientists, 2013. Site U1396, in: Le Friant, A., Ishizuka, O., Stroncik, N.A., Expedition 340 scientists, (Eds.), Proceedings of the Integrated Ocean Drilling Program,

340. Integrated Ocean Drilling Program Managment Internation, Inc, Tokyo. doi:10.2204/iodp.proc.340.106.2013

Gill, J.B., 1981. Orogenic Andesites and Plate Tectonics. Springer Verlag, Berlin.

Green, T.H., Ringwood, A.E., 1967. Crystallization of basalt and andesite under high pressure hydrous conditions. Earth Planet. Sci. Lett. 3, 481–489. doi:10.1016/0012-821X(67)90083-0

Harford, C.L., Pringle, M.S., Sparks, R.S.J., Young, S.R., 2002. The volcanic evolution of Montserrat using 40Ar/39Ar geochronology. Geol. Soc. London, Mem. 21, 93–113. doi:10.1144/GSL.MEM.2002.021.01.05

Harford, C.L., Sparks, R.S.J., 2001. Recent remobilisation of shallow-level intrusions on Monserrat revealed by hydrogen isotope compositions of amphiboles. Earth Planet. Sci. Lett. 185, 285–297.

Hatter, S.J., Palmer, M.R., Gernon, T.M., Taylor, R.N., Cole, P.D., Barfod, D.N., Coussens, M., 2018. The Evolution of the Silver Hills Volcanic Center, and Revised 40Ar/39Ar Geochronology of Montserrat, Lesser Antilles, With Implications for Island Arc Volcanism. Geochemistry, Geophys. Geosystems 19. doi:10.1002/2017GC007053

Hauff, F., Hoernle, K., Schmidt, A., 2003. Sr-Nd-Pb composition of Mesozoic Pacific oceanic crust (Site 1149 and 801, ODP Leg 185): Implications for alteration of ocean crust and the input into the Izu-Bonin-Mariana subduction system. Geochemistry, Geophys. Geosystems 4. doi:10.1029/2002GC000421

Hawkesworth, C.J., O'Nions, R.K., Arculus, R.J., 1979. Nd and Sr isotope geochemistry of island arc volcanics, Grenada, Lesser Antiles. Earth Planet. Sci. Lett. 45, 237–248.

Hawkesworth, C.J., Powell, M., 1980. Magma genesis in the Lesser Antilles Island Arc. Earth Planet. Sci. Lett. 51, 297–308.

Johnson, M.C., Plank, T., 1999. Dehydration and melting experiments constrain the fate of subducted sediments. Geochemistry Geophys. Geosystems 1, 1. doi:10.1029/1999GC000014

Kamber, B.S., Gladu, A.H., 2009. Comparison of Pb Purification by Anion-Exchange Resin Methods and Assessment of Long-Term Reproducibility of Th/U/Pb Ratio Measurements by Quadrupole ICP-MS. Geostand. Geoanalytical Res. 33, 169–181. doi:10.1111/j.1751-908X.2009.00911.x

Kelley, K.A., Plank, T., Ludden, J., Staudigel, H., 2003. Composition of altered oceanic crust at

ODP Sites 801 and 1149. Geochemistry, Geophys. Geosystems 4. doi:10.1029/2002GC000435

Labanieh, S., Chauvel, C., Germa, A., Quidelleur, X., Lewin, E., 2010. Isotopic hyperbolas constrain sources and processes under the Lesser Antilles arc. Earth Planet. Sci. Lett. 298, 35–46. doi:10.1016/j.epsl.2010.07.018

Lindsay, J.M., Trumbull, R.B., Siebel, W., 2005. Geochemistry and petrogenesis of late Pleistocene to Recent volcanism in Southern Dominica, Lesser Antilles. J. Volcanol. Geotherm. Res. 148, 253–294. doi:10.1016/j.jvolgeores.2005.04.018

McCulloch, M.T., Gamble, J.A., 1991. Geochemical and geodynamical constraints on subduction zone magmatism. Earth Planet. Sci. Lett. 102, 358–374. doi:http://dx.doi.org/10.1016/0012-821X(91)90029-H

Murphy, M.D., Sparks, R.S.J., Barclay, J., Carroll, M.R., Brewer, T.S., 2000. Remobilization of Andesite Magma by Intrusion of Mafic Magma at the Soufrière Hills Volcano, Montserrat, West Indies. J. Petrol. 41, 21–42. doi:10.1093/petrology/41.1.21

Murphy, M.D., Sparks, R.S.J., Barclay, J., Carroll, M.R., Lejeune, A.M., Brewer, T.S., Macdonald, R., Black, S., Young, S., 1998. The role of magma mixing in trigerring the current eruption of the Soufrière Hills volcano, Montserrat, West Indies. Geophys. Res. Lett. 25, 3433–3436. doi:10.1029/98GL00713

Palmer, M.R., Hatter, S.J., Gernon, T.M., Taylor, R.N., Cassidy, M., Johnson, P., Le Friant, A., Ishizuka, O., 2016. Discovery of a large 2.4 Ma Plinian eruption of Basse-Terre, Guadeloupe, from the marine sediment record. Geol. 44, 123–126. doi:10.1130/G37193.1

Pichot, T., Patriat, M., Westbrook, G.K., Nalpas, T., Gutscher, M.A., Roest, W.R., Deville, E., Moulin, M., Aslanian, D., Rabineau, M., 2012. The Cenozoic tectonostratigraphic evolution of the Barracuda Ridge and Tiburon Rise, at the western end of the North America-South America plate boundary zone. Mar. Geol. 303–306, 154–171. doi:10.1016/j.margeo.2012.02.001

Plail, M., Barclay, J., Humphreys, M.C.S., Edmonds, M., Herd, R.A., Christopher, T.E., 2014. Characterization of mafic enclaves in the erupted products of Soufrière Hills Volcano, Montserrat, 2009 to 2010. Geol. Soc. London, Mem. 39, 343–360. doi:10.1144/M39.18

Plank, T., Langmuir, C.H., 1998. The chemical composition of subducting sediment and its consequences for the crust and mantle. Chem. Geol. 145, 325–394. doi:10.1016/S0009-2541(97)00150-2

Sisson, T.W., Grove, T.L., 1993. Experimental investigations of the role of H2O in calc-alkaline differentiation and subduction zone magmatism. Contrib. to Mineral. Petrol. 113, 143–166.

Smet, I., De Muynck, D., Vanhaecke, F., Elburg, M., 2010. From volcanic rock powder to Sr and Pb isotope ratios: a fit-for-purpose procedure for multi-collector ICP–mass spectrometric analysis. J. Anal. At. Spectrom. 25, 1025–1032. doi:10.1039/b926335g

Sun, S. -s., McDonough, W.F., 1989. Chemical and isotopic systematics of oceanic basalts: implications for mantle composition and processes. Geol. Soc. London, Spec. Publ. 42, 313–345. doi:10.1144/GSL.SP.1989.042.01.19

Taylor, R.N., Ishizuka, O., Michalik, A., Milton, J.A., Croudace, I.W., 2015. Evaluating the precision of Pb isotope measurement by mass spectrometry. J. Anal. At. Spectrom. 30, 198–213. doi:10.1039/C4JA00279B

Thirlwall, M.F., Graham, A.M., Arculus, R.J., Harmon, R.S., Macpherson, C.G., 1996. Resolution of the effects of crustal assimilation, sediment subduction, and fluid transport in island arc magmas: Pb-Sr-Nd-O isotope geochemistry of Grenada, Lesser Antilles. Geochim. Cosmochim. Acta 60, 4785–4810. doi:10.1016/S0016-7037(96)00272-4

Toothill, J., Williams, C. a., MacDonald, R., Turner, S.P., Rogers, N.W., Hawkesworth, C.J., Jerram, D. a., Ottley, C.J., Tindle, a. G., 2007. A complex petrogenesis for an arc magmatic suite, St Kitts, Lesser Antilles. J. Petrol. 48, 3–42. doi:10.1093/petrology/egl052

Tucholke, B.E., Houtz, R.E., Ludwig, W.J., 1982. Maps of sediment thickness and depth to basement in the western North Atlantic Ocean basin.

Turner, S., Hawkesworth, C., Van Calsteren, P., Heath, E., Macdonald, R., Black, S., 1996. U-series isotopes and destructive plate margin magma genesis in the Lesser Antilles. Earth Planet. Sci. Lett. 142, 191–207. doi:10.1016/0012-821X(96)00078-7

Van Soest, M.C., Hilton, D.R., Macpherson, C.G., Mattey, D.P., 2002. Resolving Sediment Subduction and Crustal Contamination in the Lesser Antilles Island Arc: a Combined He-O-Sr Isotope Approach. J. Petrol. 43, 143–170. doi:10.1093/petrology/43.1.143

Wadge, G., Shepherd, J.B., 1984. Segmentation of the Lesser Antilles subduction zone. Earth Planet. Sci. Lett. 71, 297–304. doi:10.1016/0012-821X(84)90094-3

Wadge, G., Voight, B., Sparks, R.S.J., Cole, P.D., Loughlin, S.C., Robertson, R.E.A., 2014. An overview of the eruption of Soufrière Hills Volcano, Montserrat from 2000 to 2010. Geol. Soc. London, Mem. 39, 1–40. doi:10.1144/M39.1

White, W.M., Dupré, B., Vidal, P., 1985. Isotope and trace element geochemistry of sediments from the Barbados Ridge- Demerara Plain region , Atlantic Ocean. Geochim. Cosmochim. Acta 49, 1875–1886.

Workman, R.K., Hart, S.R., 2005. Major and trace element composition of the depleted MORB mantle (DMM). Earth Planet. Sci. Lett. 231, 53–72. doi:10.1016/j.epsl.2004.12.005

Zellmer, G.F., Hawkesworth, C.J., Sparks, R.S.J., Thomas, L.E., Harford, C.L., Brewer, T.S., Loughlin, S.C., 2003. Geochemical Evolution of the Soufrière Hills Volcano, Montserrat, Lesser Antilles Volcanic Arc. J. Petrol. 44, 1349–1374. doi:10.1093/petrology/44.8.1349

Chapter 4: Geochemical evolution of volcanism on Montserrat and Guadeloupe (Lesser Antilles Arc), revealed from marine sediment core U1396C

This Chapter was written by S. J. Hatter, with feedback from by M. R. Palmer, T. M. Gernon and R. N. Taylor. Laboratory work and data analysis were carried out by S. J. Hatter.

Abstract

The geochemical variation along the Lesser Antilles arc is well documented, but few studies have produced detailed geochemical evolution histories for individual islands. Here, trace element and Pb-Nd-Sr isotope data are presented for samples from International Ocean Discovery Program marine sediment core U1396C, from offshore Montserrat. The islands of Montserrat and Guadeloupe are the dominant source of tephra to this core, allowing us to reconstruct the geochemical evolution of these two neighbouring islands over the past 4.5 Myr; 2.3 and 1.7 Ma longer than their respective terrestrial records. The most notable change in geochemistry for the Montserrat source occurs 4.5–3.9 Ma, with an increase in Pb isotope and fluid-mobile trace element ratios, most likely caused by an increase in slab sediment contribution to the mantle wedge via an aqueous fluid. The Guadeloupe source displays greater variability in trace element and isotope ratios through time, with correlations between Pb, Nd, Sr isotopes and incompatible trace elements (rare earth elements in particular) indicating that this variation is dominantly controlled by crustal contamination. Furthermore, covariance of Dy/Yb with $^{143}Nd/^{144}Nd$ suggests that assimilation and fractional crystallisation (AFC) is taking place, with amphibole playing a key role in the fractionating assemblage. AFC modelling is most compatible with a depleted mid-ocean ridge basalt assimilant, sourced from the lower crust, with assimilation greatest at ~3.2 Ma. Finally, mixing models comparing the Guadeloupe samples least affected by assimilation with those from Montserrat indicate that melts forming beneath Guadeloupe contain a greater sediment contribution than those forming beneath Montserrat, which is consistent with the along-arc trend of the Lesser Antilles.

4.1 Introduction

The Lesser Antilles arc has a well-documented north-south geochemical variation, best defined by decreasing $^{143}Nd/^{144}Nd$, increasing Sr-Pb isotope ratios, and increasing abundances of fluid-mobile elements and light rare earth elements (LREE) towards the south

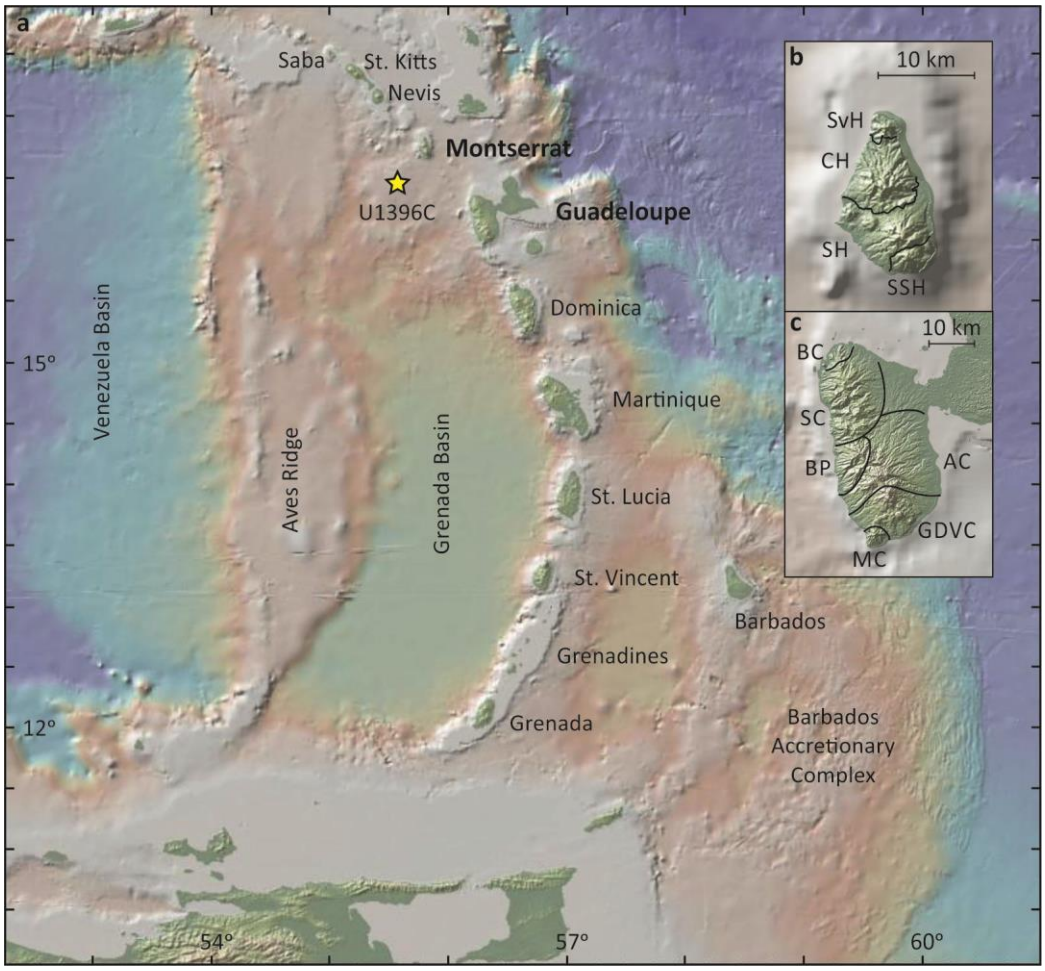

Figure 4.1. (a) Map of Lesser Antilles showing the location of Montserrat, Guadeloupe, and core site U1396C. (b) Map of Monserrat showing the different volcanic centres: SvH, Silver Hills; CH, Centre Hills; SH, Soufrière Hills; SSH, South Soufrière Hills. (c) Map of Basse-Terre, Guadeloupe, showing the location of the different volcanic centres: BC, Basal Complex; SC, Septentrional Chain; BP, Bouillante Province; AC, Axial Chain; MC, Monts Caraïbes Massif; GDVC, Grande Découverte Volcanic Complex.

of the arc (e.g. Brown et al., 1977; DuFrane et al., 2009; Hawkesworth and Powell, 1980; White and Dupré, 1986). This geochemical variation is widely attributed to result from an increasing addition of a sedimentary component in the magmas from north to south, derived from either crustal assimilation (e.g. Bezard et al., 2015a, 2015b; Davidson and Harmon, 1989; Thirlwall et al., 1996; Van Soest et al., 2002) or sediment addition to the mantle wedge from the subducting slab (e.g. Carpentier et al., 2008; DuFrane et al., 2009; Freymuth et al., 2016; Labanieh et al., 2010, 2012; Turner et al., 1996; White and Dupré, 1986). The amount of slab sediment required to produce the geochemical compositions in the north of the arc has been calculated as ~<1–2% bulk sediment addition, while in the south it has been calculated as ~10–15% bulk sediment addition (Carpentier et al., 2008; DuFrane et al., 2009; Turner et al., 1996), or <4% if added as a 20% partial melt (DuFrane et al., 2009).

The extent of crustal assimilation also varies along the Lesser Antilles, playing a greater role in the south of the arc. Volcanic rocks in the north of the arc (Saba to Martinique) have

mid-ocean ridge basalt (MORB)-like $^{3}He/^{4}He$ values in olivine phenocrysts, but low values in pyroxenes. These low $^{3}He/^{4}He$ pyroxene values are interpreted as resulting from late-stage assimilation in high-level crustal magma chambers. The $\delta^{18}O$ of these samples is also slightly decreased relative to mantle values, suggesting that the assimilant was hydrothermally altered magmatic wall rocks (Van Soest et al., 2002). For the south of the arc (Martinique to Grenada) both olivine and pyroxene display more radiogenic He isotopes compared to MORB, suggesting that for this part of the arc assimilation took place earlier in the evolution of the magma at greater depth. Furthermore, some samples from the southern arc show elevated oxygen isotopes compared with mantle peridotite, which are interpreted to represent assimilation of terrigenous sediment within the crust (Van Soest et al., 2002).

Whilst there has been a lot of work on the spatial geochemical variation within and between different islands in the Lesser Antilles, only on Martinique have these studies provided a tightly constrained temporal context to the data (Labanieh et al., 2010, 2012). Here, isotope and trace element data are presented for two islands in the northern Lesser Antilles, Montserrat and Guadeloupe, from tephra layers in marine sediment core U1396C. Because samples have come from a marine sediment core, each sample is accurately dated from palaeomagnetism and biostratigraphy, allowing us to determine the geochemical evolution of these two islands over the past 4.5 Ma; 2.3 and 1.7 Ma longer than the terrestrial records of volcanism on Montserrat and Guadeloupe, respectively (Hatter et al., 2018; Samper et al., 2007).

4.2 Geological Setting

4.2.1 Lesser Antilles

Subduction of the Atlantic crust beneath the Caribbean plate initiated at ~40 Ma (Briden et al., 1979), forming the Old arc of the Lesser Antilles (Grenada to Anguilla). This subduction phase stopped at the beginning of the Late Oligocene as a buoyant ridge of anomalous mid-Cretaceous crust reached the subduction zone in the northern part of the arc. After 9–10 Myr, activity resumed, forming the Recent arc (Grenada to Saba; Figure 4.1a), with a current convergence rate of ~2 cm/yr (Minster and Jordan, 1978). South of Martinique, activity resumed along the same place as the Old arc, but north of Martinique there was a progressive westward shift, forming the Inner arc (Dominica to Saba) (Bouysse and Westercamp, 1990).

The Benioff zone beneath the Lesser Antilles arc is split into two segments; from Martinique northwards it strikes NNW, with a dip of 50–60° to a maximum depth of 210 km, while from St. Lucia southwards it trends NNE, with a lower dip of 45–50° to a maximum

depth of 170 km. The Benioff zone has a mean depth of ~140 km and ~130–140 km beneath Montserrat and Guadeloupe, respectively (Wadge and Shepherd, 1984).

The crust beneath the Lesser Antilles varies in thickness along the arc: 27 km around Barbuda (Whitmarsh et al., 1983), ~30 km in the region of Montserrat to Guadeloupe (Boynton et al., 1979; Sevilla et al., 2010), ~30 km and ~34 km beneath Martinique and St. Vincent, respectively, (Boynton et al., 1979), and ~24 km at the southern end of the arc, around Grenada (Christeson et al., 2008). The Lesser Antilles arc is believed to be built upon oceanic crust, similar to that of the Venezuela Basin crust (Boynton et al., 1979; Christeson et al., 2008; Diebold et al., 1999; Sevilla et al., 2010; Speed et al., 1993; Speed and Walker, 1991). Some authors have also speculated that this oceanic crust is overlain by the accretionary prism of the former Aves arc (Davidson and Harmon, 1989; Macdonald et al., 2000). The evidence for assimilation of material with a 'continental' signature indicates that sedimentary material is present within at least some parts of the arc crust (e.g. Bezard et al., 2014; Davidson and Wilson, 2011; Davidson and Harmon, 1989; Thirlwall et al., 1996).

4.2.2 Montserrat

Volcanism on Montserrat has been focused at four different volcanic centres of overlapping activity: Silver Hills (2.17–1.03 Ma), Centre Hills (1.14–0.38 Ma), Soufrière Hills (0.45 Ma to present) and South Soufrière Hills (0.13 Ma; Figure 4.1b) (Brown and Davidson, 2008; Coussens et al., 2017; Harford et al., 2002; Hatter et al., 2018). Volcanism on Montserrat has been the subject of many detailed studies, so the geochemistry of these four volcanic centres is well constrained (Cassidy et al., 2012, 2015; Christopher et al., 2014; Coussens et al., 2017; Hatter et al., 2018; Zellmer et al., 2003; Chapter 3). The Silver Hills and Centre Hills are geochemically very similar, with Nb/Y vs $^{143}Nd/^{144}Nd$ being the clearest geochemical discriminator between these two centres (Hatter et al., 2018). The Silver Hills has higher $^{143}Nd/^{144}Nd$ and generally lower Nb/Y than the Centre Hills, which may be the result of mantle heterogeneity (Chapter 3). A further change in chemistry occurs between the Centre Hills and Soufrière Hills, with lavas from the latter having less radiogenic Pb isotope ratios, higher Ba/La, and greater LREE enrichment. These features suggest that the melts forming beneath the Soufrière Hills contained a greater relative slab fluid and partial melt contribution to the mantle wedge (Cassidy et al., 2012). The short-lived South Soufrière Hills displayed the most pronounced change in chemistry, with the least radiogenic Pb isotope ratios of Montserrat, lowest LREE/middle-REE (MREE) and highest fluid-mobile element/REE values. These features are interpreted to result from a higher slab fluid and lower slab sediment contribution to the mantle wedge, compared with the Soufrière, Centre and Silver Hills (Cassidy et al., 2012; Zellmer et al., 2003).

4.2.3 Guadeloupe

Volcanism on the Guadeloupe archipelago during the Recent arc has mainly focused on the western island of Basse-Terre, which has been subject to extensive dating studies. The timing of volcanic activity of the island's six volcanic centres is well constrained: Basal Complex (2.79–2.69 Ma), Septentrional Chain (1.80–1.15 Ma), Axial Chain (1.02–0.41 Ma), Bouillante Province (1.20–0.60 Ma), Monts Caraïbes Massif (0.56–0.47 Ma), and the Grande Découverte Volcanic Complex (GDVC; 0.21 Ma–present), which is home to the islands current active volcano La Soufrière (Figure 4.1b) (Carlut et al., 2000; Ricci et al., 2015a, 2015b, Samper et al., 2007, 2009).

Despite this extensive dating, there has been no published in-depth temporal geochemical study of the volcanic centres on Guadeloupe, with most geochemical work focusing on the GDVC (Boudon et al., 2008; Feuillard et al., 1983; Samper et al., 2009; Touboul et al., 2007). Moreover, the only studies to investigate petrogenetic processes beneath Guadeloupe (e.g. slab contribution, crustal assimilation) have been part of arc-wide studies, so only include a small sample size from Guadeloupe, which are also mostly from the GDVC (Chabaux et al., 1999; DuFrane et al., 2009; Van Soest et al., 2002; White and Dupré, 1986). Thus, comparatively little has been published about the geochemical evolution of Guadeloupe volcanism.

4.3 Methods

4.3.1 Sample acquisition

Samples were taken of tephra layers from marine sediment core U1396C, from International Ocean Discovery Program expedition 340. The core site is located ~35 km SW of Montserrat and ~75 km west of Guadeloupe, and the core is 145.92 m long with a recovery of 105%. Recovery of >100% is an artefact resulting from depressurisation of the cores on recovery. Core U1396C is well preserved, with only 3% disturbance (Jutzeler et al., 2016), containing >150 visible tephra layers going back to ~4.5 Ma (Expedition 340 scientists, 2013; Fraass et al., 2016). The ages of the tephra layers are derived from palaeomagnetic, biostratigraphic and foraminifera $\delta^{18}O$ correlations, with an absolute uncertainty of ~50 kyr (Fraass et al., 2016; Hatfield, 2015).

4.3.2 Componentry analysis

Sub-samples of the tephra layers were submerged in Milli-Q water, placed in a sonic bath for ~10 minutes, passed through a 100 μm sieve and dried in a ~40–50°C oven. Both fractions

were then placed into separate glass vials. For componentry analysis, ~300–400 grains of the >100 μm fraction were counted and placed into the following categories based on the classifications of Cassidy et al. (2014), Le Friant et al. (2008) and Wall-Palmer et al. (2014): (1) vesicular juvenile, which are unaltered pumice grains; (2) non-vesicular juvenile, which are light to dark grey crystalline lava fragments commonly containing phenocrysts; (3) scoria, which are glassy black and dark brown vesicular to poorly-vesicular grains; (4) glass shards and crystal fragments; (5) altered grains, which are lava or pumice grains which display orange-red discolouration, thought to be the result of hydrothermal alteration; and (6) bioclasts, which are predominantly foraminifera tests.

4.3.3 Geochemistry

Geochemical analyses were performed on hand-picked grains from the >100 μm size fraction. For most samples vesicular juvenile grains were analysed, but for some tephra layers, scoria grains were the most abundant component, so these were analysed instead. Some tephra layers contained sufficient vesicular juvenile and scoria grains for geochemical analyses of both components. Trace elements were measured by a Thermo Fisher Scientific X-Series 2 ICP-MS at the University of Southampton following the method of Coussens et al., (2017), in which 0.01 g of powdered sample was analysed. Precision was calculated from repeat analyses of international reference materials, and is better than 6% for Cs, Pb, Th and U, and better than 2% for the rest (see Appendix A for more detail).

For most tephra layers there was not sufficient material for XRF analysis, so major elements were also analysed by ICP-MS, using the same mother solutions as for trace elements. Precision is better than 6% for K, and is better than 3% for the rest. The SiO_2 values were calculated as 100% minus the sum of total majors measured (Al_2O_3, CaO, Fe_2O_3, MgO, MnO, K_2O & Na_2O), P_2O_5 and loss on ignition (LOI). Major element XRF analysis of pumice grains from a ~4 Ma 1.2 m thick tephra layer from core U1396C analysis gave P_2O_5 and LOI values of 0.069 and 6.88 wt. %, respectively (Jutzeler et al., 2017), so these values are used to calculate SiO_2. As discussed in Chapter 3, normalising major element data to volatile-free helps reduce the error in the calculated SiO_2 values caused by estimating LOI values, so all data is presented normalised to volatile-free.

Pb, Nd and Sr isotopes were measured from 50 mg of hand-picked pumice grains, and samples were leached and digested following the method of Cassidy et al., (2012). Throughout the course of this study, three different methods were used to isolate Pb from the sample matrix. Method 1 follows that of Cassidy et al. (2012) which uses AG1x8 200-400 mesh anion exchange resin, with 6 M HCl and 1M HBr to elute the sample matrix, and 6M HCl to collect the Pb fraction. Method 2 uses Sr spec™ resin following the procedure of Smet et al.

(2010), using 7M HNO_3 to remove the sample matrix, Milli-Q water to collect the Sr fraction, and 8M HCl to collect the Pb fraction. Method 3 also uses AGX-1x8 200-400 mesh anion exchange resin, but follows the method of Kamber and Gladu (2009), using 2M HCl to elute the matrix, and 10.8M HCl to collect the Pb fraction. Method 2 has the benefit of separating Sr as well as Pb from the same sample run, but it was discovered that during the process some of the resin from the column passes into the sample solution. When run through the mass spectrometer, this resin accumulates on machine parts, which then have to be cleaned between runs. For this reason, this method was only applied for one batch of samples, which is why Sr isotope data has only been collected on a limit number of samples. For Nd, the waste fraction from Pb columns was collected, and prepared for Nd columns. Samples were first passed through cation columns containing AG50-X8 200-400 mesh resin, then through LN Spec columns (Eichrom Industries, Illinois, USA). Pb and Nd isotopes were measured on a MC-ICP-MS (Neptune) at the University of Southampton, and Sr isotopes were measured on a ThermoFisher Triton Plus thermal ionisation mass spectrometer. Pb isotopes were corrected for instrumental mass fractionation using the SBL74 double spike (Taylor et al., 2015). SRM NBS981 gave $^{206}Pb/^{204}Pb = 16.9400 \pm 0.0023$, $^{207}Pb/^{204}Pb = 15.4965 \pm 0.0026$ and $^{208}Pb/^{204}Pb = 36.7124 \pm 0.0076$ on $n = 108$ measurements during the course of this study. Measured values for standards JNdi and SRM NBS987 are $^{143}Nd/^{144}Nd = 0.512116 \pm 0.000012$ ($n = 36$) and $^{87}Sr/^{86}Sr = 0.710238 \pm 0.000024$ ($n = 18$), respectively.

4.4 Results

4.4.1 Core componentry

Componentry analysis was performed for 87 tephra layers (data is presented in Appendix Table 4.1). For thick (>5 cm) tephra layers multiple counts were made from different levels within the layer. There is variability in the component proportions of tephra layers throughout the core, but for most samples the dominant component group is either glass shards and crystal fragments or vesicular juveniles. In all samples, the crystal populations are colourless plagioclase, black oxides (likely Fe-Ti oxides) and light to dark green pyroxenes. Some samples contain dark green amphibole, but these are similar in appearance to the pyroxenes, so dark green pyroxenes and amphiboles can only be confidently distinguished when cleavage is visible. Vesicular juvenile grains vary in colour between layers, covering a spectrum from white and grey, through light brown to brown-grey. For some samples this range of colour was present within a single tephra layer.

For many of the samples the vesicular juvenile and non-vesicular juvenile components were typically coarser than the glass and crystal components, meaning that the glass and

crystal components are over-represented in the componentry analysis compared to the vesicular juvenile and non-vesicular juvenile components, leading to a positive bias in glass and crystal values. For example, samples 3H2-25 and 4H6-42 contain abundant pumice clasts which are significantly coarser (≤12 mm and ≤4 mm respectively) than the other components, which are ≤1.5 mm and ≤0.7 mm respectively. As a result, the percent proportions for these samples are not representative of the volume percent, and thus under-represents the pumice content in componentry analyses. Samples affected by this issue are labelled in Appendix Table 4.1.

The component proportions have been normalised to bioclast-free ($\%_{bf}$) and plotted against time (Figure 4.2), and show that there is no systematic trend to the variation in the proportion of components in tephra layers throughout core U1396C. The only notable difference between Montserrat and Guadeloupe tephra layers (see section 4.4.3 for determining provenance) is the abundance of mafic clasts, which are greater in Guadeloupe (maximum 73.6$\%_{bf}$) samples than Montserrat (maximum 12.5$\%_{bf}$; Figure 4.2). Tephra layers with a high proportion of scoria grains (>20$\%_{bf}$) for Guadeloupe are only present during ~4.45–3.72 Ma and 2.81–2.35 Ma (Figure 4.2).

4.4.2 Mode of deposition

Marine tephra layers can be deposited by one of three processes: primary fallout from an eruption column, volcaniclastic turbidites derived from a pyroclastic density current entering the sea, or bioclastic turbidites derived from a shelf collapse. The most useful tools for confidently determining the mode of deposition of marine tephra layers are visual observations (e.g. sedimentary structures, nature of upper and lower contacts), grain-size distribution, sorting, grain morphology, and componentry analysis (e.g. Cassidy et al., 2014; Gudmundsdóttir et al., 2011; Jutzeler et al., 2017). However, some of the methods used to obtain such data can be destructive and/or time-consuming, and are beyond the scope of this study. For the purposes of this study, however, it is not necessary to determine the exact mode of deposition of every tephra layer, but instead to distinguish between primary eruption deposits (both fallout deposits and volcaniclastic turbidites) and reworked deposits (bioclastic turbidites). The most useful tool for this distinction is the bioclast content of the tephra layer, because this gives an indication of how much entrained material is present within a layer. Bioclastic flow deposits offshore Montserrat typically contain ~55–99% bioclasts (Trofimovs et al., 2010, 2013), whereas pyroclastic density current-derived turbidites from the recent eruption of the Soufrière Hills (1995–2010) contain <6% bioclasts (Trofimovs et al., 2008, 2012, 2013) for deposits up to 55 km from source. Trofimovs et al., (2013) also identified a ~6 ka mixed bioclastic-volcaniclastic deposit with the bioclast

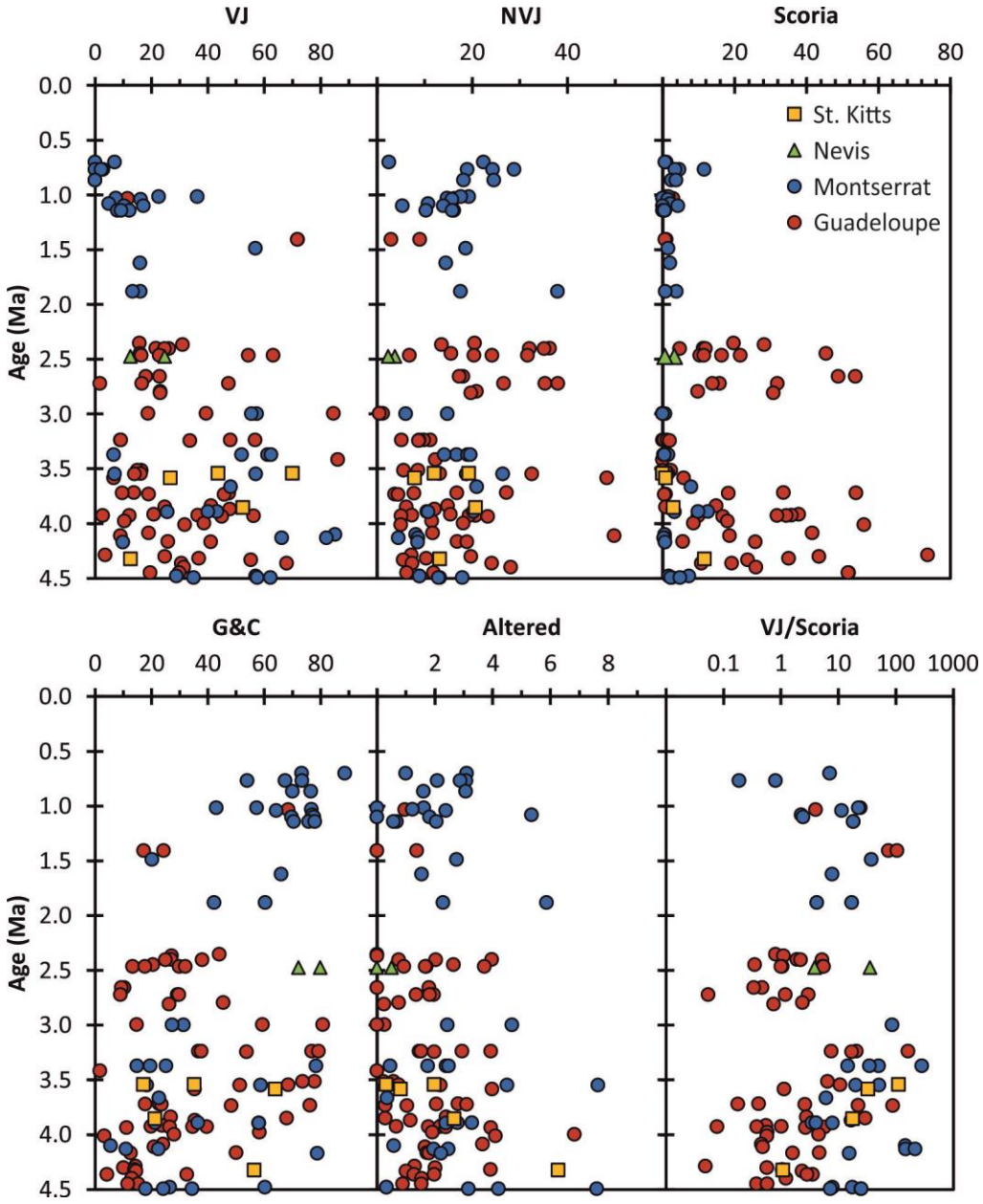

Figure 4.2. Componentry analysis of tephra layers from core U1396C. VJ, vesicular juvenile; NVJ, non-vesicular juvenile; G&C, glass shards and crystal fragments.

content increasing with distance from source, from 10–30% bioclasts proximally, to 40–45% bioclasts distally, formed from either PDC-derived turbidity currents, or volcanic sector collapse. Based on these observed values, any tephra layer in U1396C containing >40% bioclasts are classified as a bioclastic turbidite. Four tephra layers were found to contain >40% bioclasts in core U1396C, and because such deposits are not directly derived from an eruption, they were not analysed for chemistry.

4.4.3 Tephra Layer Provenance

While Montserrat is the closest volcanic island to Site U1396, it has the potential to receive tephra input from multiple nearby islands. Due to the along-arc geochemical gradient of the

Lesser Antilles, the different islands can be separated using a mixture of isotope and trace element ratios. This separation is based on geochemical data from the terrestrial record, and it is inferred that this separation has been present over the past ~4.5 Ma. Pb isotopes can distinguish between Montserrat and all other islands except St. Kitts (Figure 4.3a), and trace elements distinguish between Montserrat and St. Kitts (Figure 4.3b). Of the tephra layers analysed from U1396C, 54 samples (from 44 tephra layers; 44_{TL}) are from Guadeloupe, 27 samples (21_{TL}) plot in the Montserrat-St. Kitts field, and seven samples (from four tephra layers) plot in the Montserrat-Nevis field (Figure 4.3a). Of the samples that fall in the Montserrat-St. Kitts field, 23 (18_{TL}) plot firmly in the Montserrat field on a Th/Nb vs La/Ba plot, while four (3_{TL}) fit in the St. Kitts field (Figure 4.3b), suggesting a St. Kitts provenance. For the seven samples with a Nevis Pb isotope signature, two (2_{TL}) plot within the Nevis-St. Kitts trace element field (thus supporting a Nevis origin), but five (2_{TL}) plot within the Montserrat field (Figure 4.3b). When these five are placed in a temporal context, they appear to be part of a trend of decreasing Pb isotope values (section 4.4.4.1), which coupled with the low Ba/La, are interpreted to mean that they are in fact from Montserrat, not Nevis or St. Kitts.

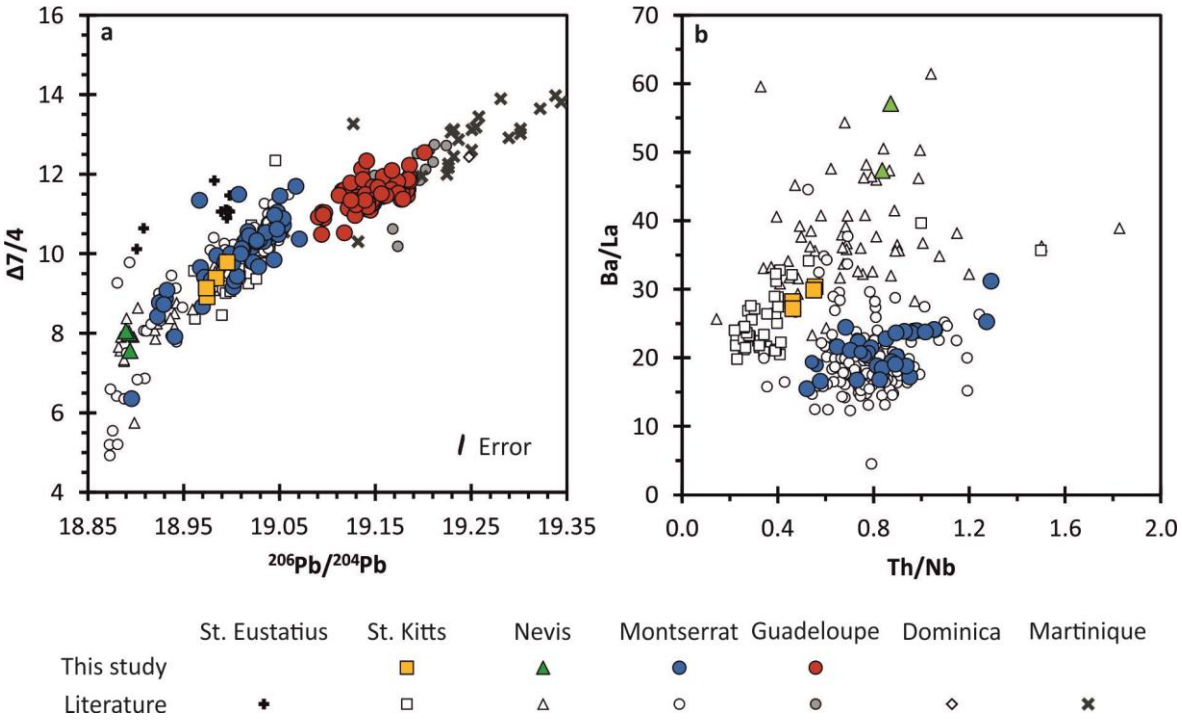

Figure 4.3. (a) $^{206}Pb/^{204}Pb$ vs Δ7/4 for northern islands of the Lesser Antilles, with U1396C core data plotted to determine provenance. (b) Th/Nb vs Ba/La separating Montserrat from St. Kitts and Nevis. Trace element plot showing Montserrat samples can be distinguished from Nevis and St. Kitts. St. Eustatius and Martinique data from Davidson and Wilson, (2011), St. Kitts data from Toothill et al., (2007), Nevis data from R. Taylor (pers. comm.), Montserrat data from Cassidy et al., (2012), Guadeloupe Pb isotope data from M. Palmer (pers. comm.), and Dominica data from (Lindsay et al., 2005).

4.4.4 Temporal Geochemical Variation

For Montserrat, isotope and trace element trends for samples aged 2.2–0 Ma have been described in Chapter 3, so this study focuses on the tephra layers >2.2 Ma. For Guadeloupe, the tephra layers have been split into two age groups 4.5–3.4 Ma, and 3.2–0 Ma. Isotope, trace element, and major element data are presented in Appendix Tables 1–3, respectively.

4.4.4.1 Pb-Nd-Sr isotopes

The separation between Montserrat and Guadeloupe in isotope space has been present throughout the 4.5 Ma record of volcanism contained in core U1396C, with the two islands displaying different temporal trends.

$^{206}Pb/^{204}Pb$, $^{207}Pb/^{204}Pb$ and $^{208}Pb/^{204}Pb$ all display the same temporal trends for Montserrat, increasing over 4.5–3.9 Ma, and then remaining constant from ~3.9–0.45 Ma (Figure 4.4a). The Δ8/4 values are consistently greater than Δ7/4 over the past 4.5 Ma (Figure 4.4a). For $^{143}Nd/^{144}Nd$, samples gradually become slightly less radiogenic over ~4.5–3.0 Ma, after which there is a gap in the record until the time period covered in Chapter 3 (~2.2–0 Ma; Figure 4.4a). There are two possibilities for the temporal trend in $^{143}Nd/^{144}Nd$ over 3.0–1.9 Ma: either there was a decrease in $^{143}Nd/^{144}Nd$ from 3.0–2.2 Ma followed by a stepped increase between 2.2–1.9 Ma, or there was a slight decrease from 3.0–1.9 Ma and the value of 0.512969 at 2.2 Ma is anomalous (Figure 4.4a). For $^{87}Sr/^{86}Sr$, the lowest values are present at 4.5 Ma, after which values maintain a similar range from 4.3–0 Ma (Figure 4.4a).

For Guadeloupe, Pb isotopes remain constant over 4.5–3.4 Ma, followed by a reduction between 3.4–3.2 Ma, then by a gradual increase from ~3.2–2.4 Ma. There is only one Guadeloupe data point <2.4 Ma, showing that Pb isotopes appear to be constant at 2.4 and 1.0 Ma (Figure 4.4b). The literature data shows that Pb isotopes have maintained similar values over 1–0 Ma, although there is a wide spread of values for La Soufrière (Figure 4.4b) (DuFrane et al., 2009; White and Dupré, 1986). A striking feature of the Pb isotope ratios for Guadeloupe is a step change in the relationship between Δ7/4 and Δ8/4 values. For the 4.5–3.4 Ma group, Δ8/4 is greater than Δ7/4 (with the exception of one sample), whereas 3.4–0 Ma samples have Δ7/4 values higher than Δ8/4. $^{143}Nd/^{144}Nd$ appears to increase from 4.5–3.4 Ma, decrease from ~3.2–2.7 Ma, and then remains constant at 2.7 and 1.0 Ma (Figure 4.4b). There are limited data from the literature to support the core data, but $^{143}Nd/^{144}Nd$ values are slightly lower than the core data from 0.55–0 Ma (Figure 4.4b) (DuFrane et al., 2009; White and Dupré, 1986). For $^{87}Sr/^{86}Sr$, there is large scatter in the data from 4.5–3.5 Ma, with a possible increase in values from 4.5–4.0 Ma. There is an increase from 3.2–2.4 Ma, with a further increase to the single sample at 1.0 Ma (Figure 4.4b). This is followed by a

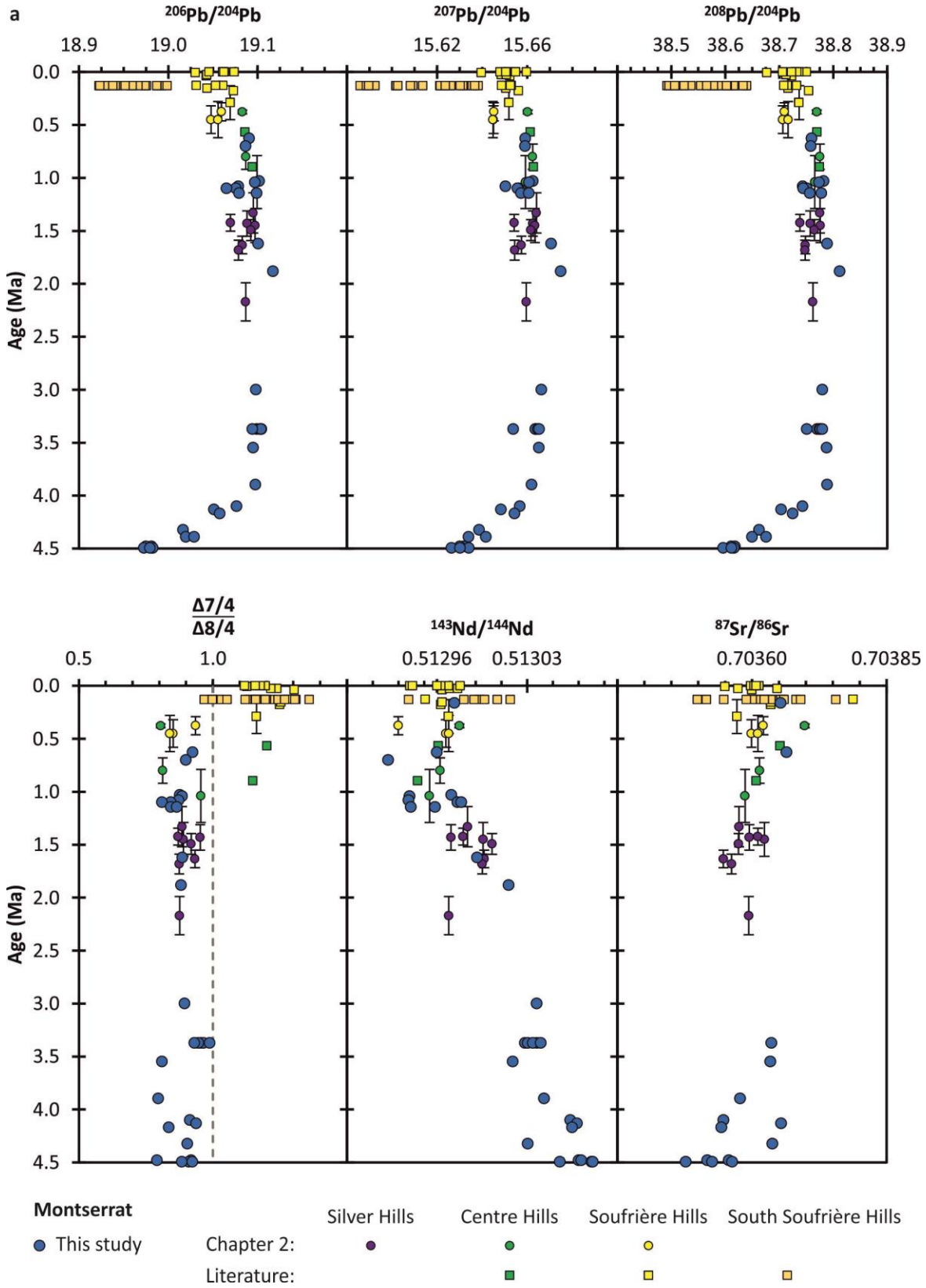

Figure 4.4. Isotope ratios vs age for (a) Montserrat and (b) Guadeloupe. Montserrat literature data from Cassidy et al., (2012), and Guadeloupe literature data from DuFrane et al., (2009), Van Soest et al., (2002) and White and Dupré, (1986). Δ7/4 and Δ8/4 are $^{207}Pb/^{204}Pb$ and $^{208}Pb/^{204}Pb$ calculated to the Northern Hemisphere Reference Line (Hart, 1984). Error bars are smaller than symbols, unless shown.

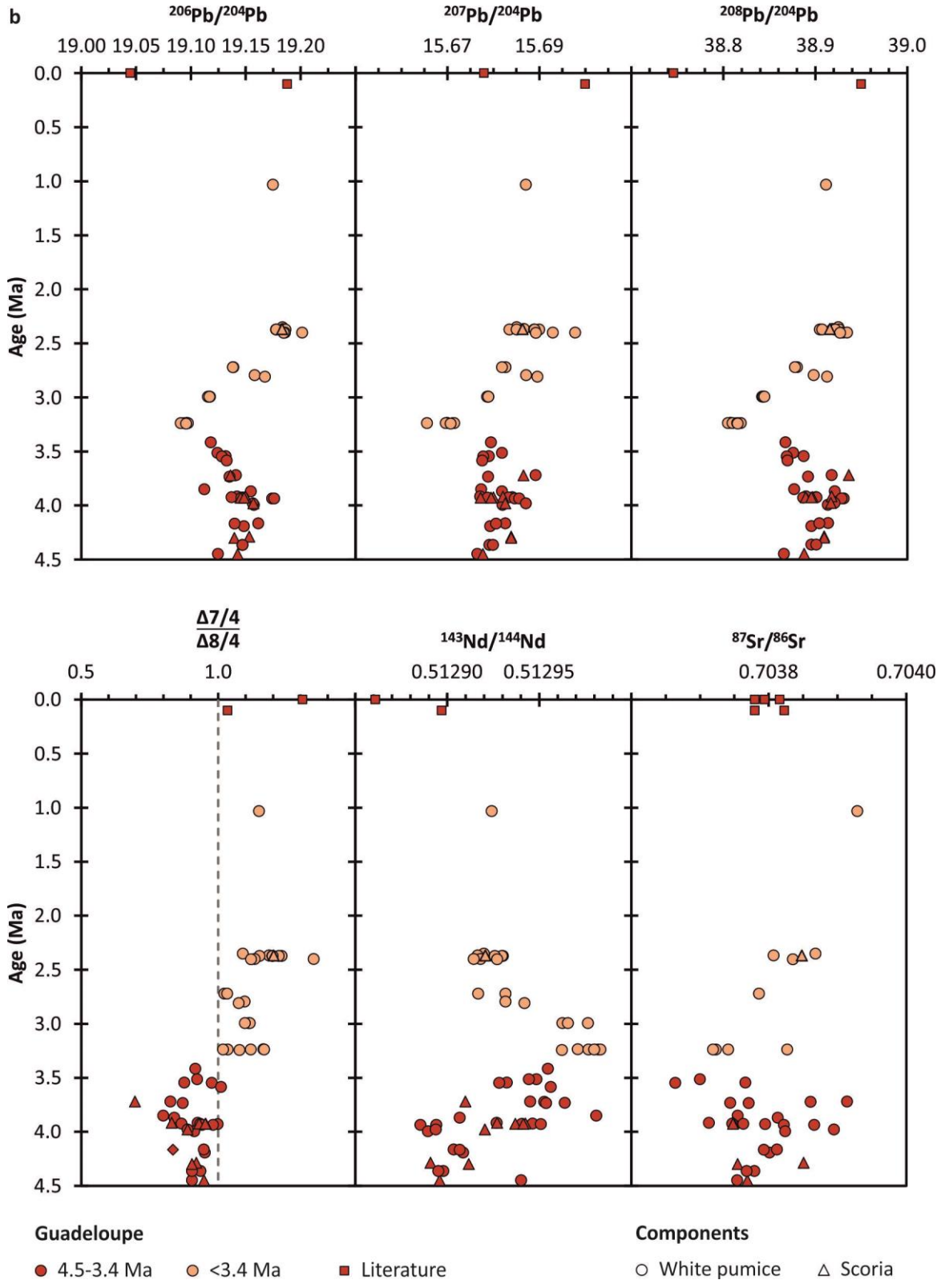

Figure 4.4 continued.

further decrease, as deposits from La Soufrière have $^{87}Sr/^{86}Sr$ values similar to 2.4 Ma tephras.

4.4.4.2 Trace elements

As with isotope data, trace elements also show different temporal trends for Montserrat and Guadeloupe. For Montserrat, the most noticeable trend comes from fluid mobile elements, which display the greatest variation relative to high field strength elements (HFSE), REE, and Th (a key sediment tracer in Lesser Antilles lavas; e.g. DuFrane et al., 2009). They show separation in values between tephra layers from 4.5–3.3 Ma and 2.2–0 Ma, with the 4.5–3.3 Ma tephras being more enriched in all fluid mobile elements (Figure 4.5a). Additionally, within the 4.5–3.3 Ma group, tephras become progressively more enriched in fluid mobile elements over the period of ~4.5–3.9 Ma (Figure 4.5a). There is also variation in REE ratios, as MREE/heavy-REEs (HREE; e.g. Dy/Yb) remain constant over the past 4.5 Ma, while L/HREE (e.g. La/Lu) and L/MREE (e.g. La/Gd; not shown) remain constant over ~4.5–1.5 Ma, after which values are higher with greater scatter (although this may in part be due to the greater number of samples; Figure 4.5a). Nb/Y displays a similar pattern (not shown), but Zr/Y remains constant for the past 4.5 Ma. HFSE/REE ratios vary in behaviour, as Zr/Gd (Figure 4.5a) and Zr/Lu (not shown) remain roughly constant over 4.5–0 Ma, while Zr/La is constant for 4.5–3.3 Ma, with lower values 2.2–0 Ma (Figure 5a).

For Guadeloupe, trace element ratios which vary the most are ones involving REEs; HFSE and fluid-mobile elements over M-HREE ratios (e.g. Cs/Gd, Zr/Yb; Figure 4.5b) all match the Pb isotopic trends, maintaining the same range of values 4.5–3.4 Ma, followed by a step increase over 3.4–3.2 Ma, then decreasing from ~3.2–2.3 Ma. L/MREE and M/HREE (e.g. La/Sm, Dy/Yb) ratios also match this trend (Figure 4.5b). However, fluid-mobile and HFSE over LREEs (e.g. Ba/La, Zr/La) show little change in values over the past 4.5 Ma (Figure 4.5b). The same is true for fluid-mobile to HFSE ratios (e.g. Rb/Nb). Fluid-mobile to Th ratios (e.g. Cs/Th) maintain constant values from 4.5–3.2 Ma, then gradually increase from 3.2–2.3 Ma (Figure 4.5b).

Montserrat and Guadeloupe tephras share similar REE profiles, with LREE enrichment and U-shaped M-HREE pattern (Figure 4.6), indicative of amphibole fractionation (Bottazzi et al., 1999). Most samples also display a negative Eu anomaly (Figure 4.6), resulting from plagioclase fractionation.

4.4.4.3 Major elements

As discussed in Chapter 3, normalising the major element data to volatile-free reduces the uncertainty derived from the unknown LOI values. Even so, there are clearly some inaccuracies in the data. Firstly, SiO_2 ranges in value from 25–79 wt. %, with five samples <45 wt. % (the lower limit for basalt; Figure 4.7). K_2O values also appear erroneously high for many samples, ranging from 0.54–4.17 wt. %, covering the low-K to high-K fields of

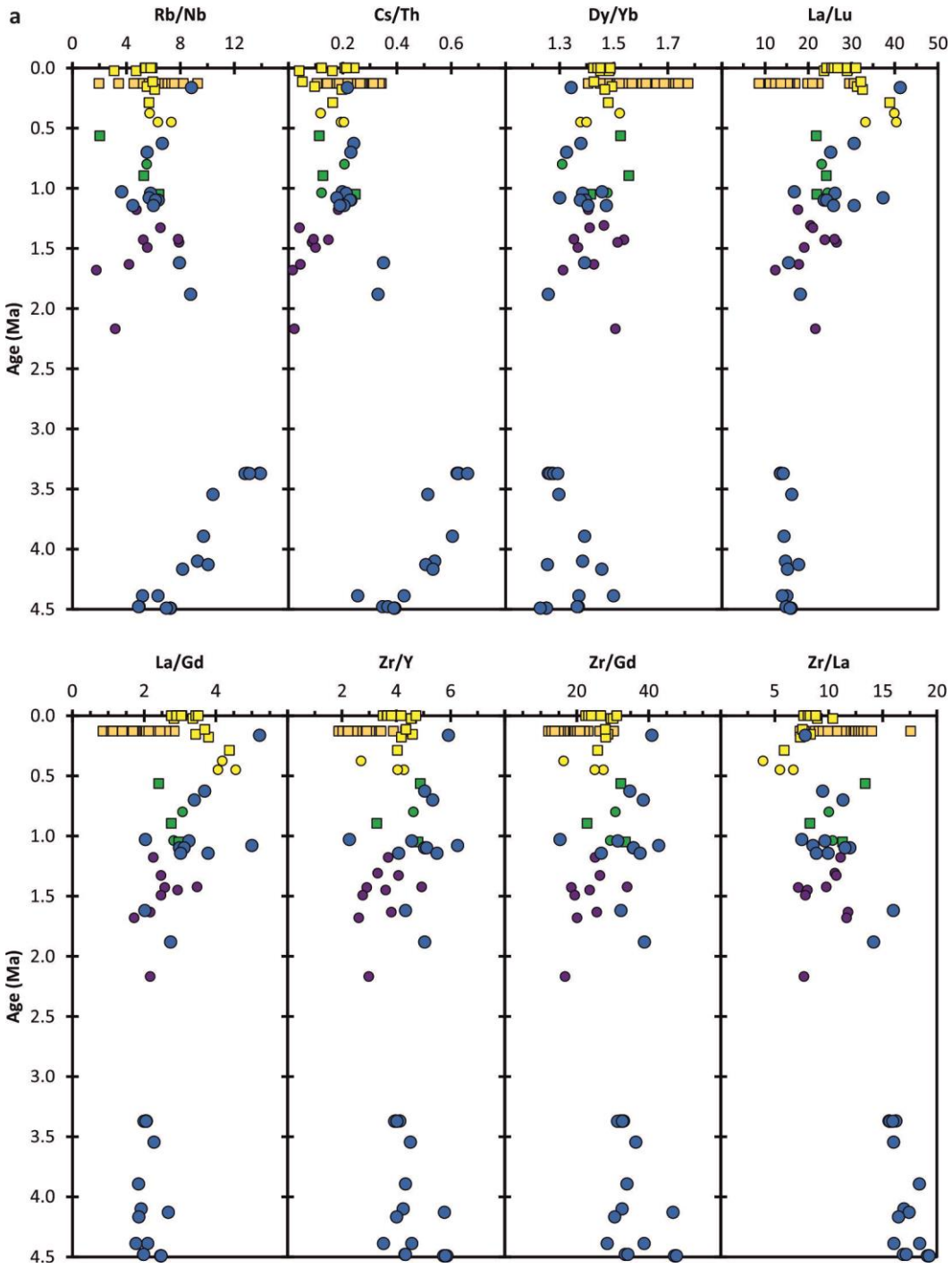

Figure 4.5. Select trace element ratios vs age for (a) Montserrat and (b) Guadeloupe. Montserrat literature data from Cassidy et al., (2012), Coussens et al., (2017) and Zellmer et al., (2003), and Guadeloupe literature data from Boudon et al., (2008), Samper et al., (2009) and Touboul et al., (2007). Symbols same as Figure 4.4.

Le Maitre et al., (2002) (Figure 4.7). For comparison, all analysed lavas in the Lesser Antilles have K_2O content <2.5 wt. % (Macdonald et al., 2000), and for Guadeloupe the highest measured value is 2.31 wt. % (Boudon et al., 2008; DuFrane et al., 2009; Gunn et al., 1980; Samper et al., 2009; Touboul et al., 2007). This is further highlighted on a total alkali-silica (TAS) plot of Le Bas et al., (1986), as many of the samples plot in the alkali suite, from trachy-

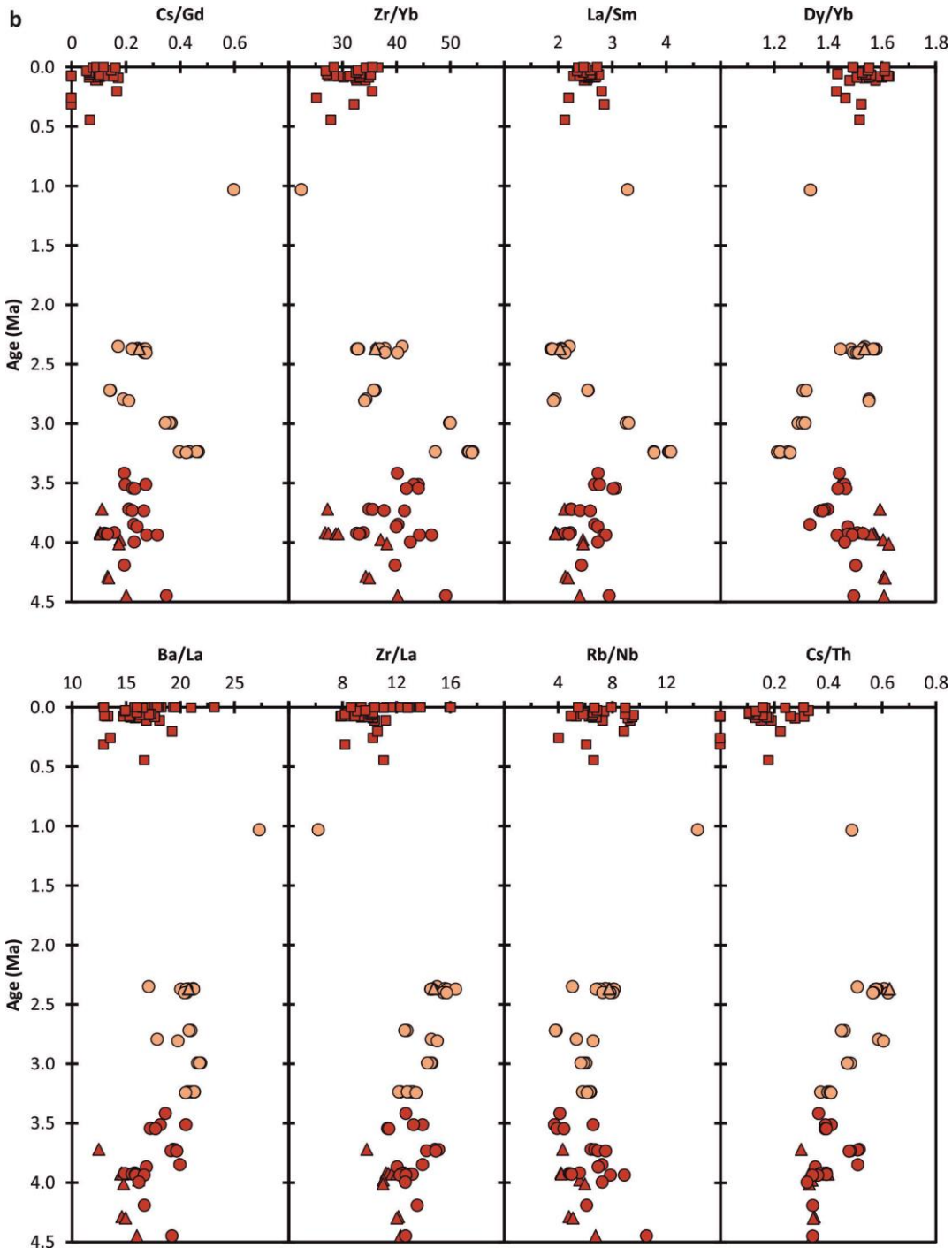

Figure 4.5 continued.

basalt to trachyte, and in extreme cases in basanite and tephra-phonolite (Figure 4.7). Such compositions have not previously been observed either on Montserrat or Guadeloupe, or anywhere else along the arc. Thus, these data are taken to be unreliable. In addition, comparing the SiO_2 versus major element oxide trends of the core samples with literature data (for both Montserrat and Guadeloupe), the MgO values are lower than expected, as well as CaO for some samples. Na_2O data also appears erroneously high for most samples, with only slight overlap between the core and literature data (Figure 4.7). TiO_2, MnO, Al_2O_3, Fe_2O_3 and most CaO values, however, do match the published trends (Figure 4.7). The unusually

high K_2O and Na_2O values are likely the result of low-temperature alteration from seawater, which involves hydrogen exchange of Na^+ and K^+ ions in siliceous volcanic glass, without altering the other major element or trace element compositions (Cerling et al., 1985).

An alternative to the TAS classification comes from Winchester and Floyd, (1977), who classify lavas using Zr/Ti vs Nb/Y. While this method still relies on the major element TiO_2, its low concentration (<2 wt. %) means it is less affected by the uncertainties in LOI, and the fact that the TiO_2 data matches the literature data trends suggests that it is a more reliable of the major element data gathered. Using this classification, the core samples range from the andesite/basalt to rhyolite fields, and importantly do not fall within any alkali compositions (e.g. trachy-andesite; Figure 4.8), as would be expected. The alkali component of this classification is based on Nb/Y, not Zr/Ti (i.e. not by major elements), so further supports the K_2O and Na_2O data being erroneously high, and not representative of the true sample values.

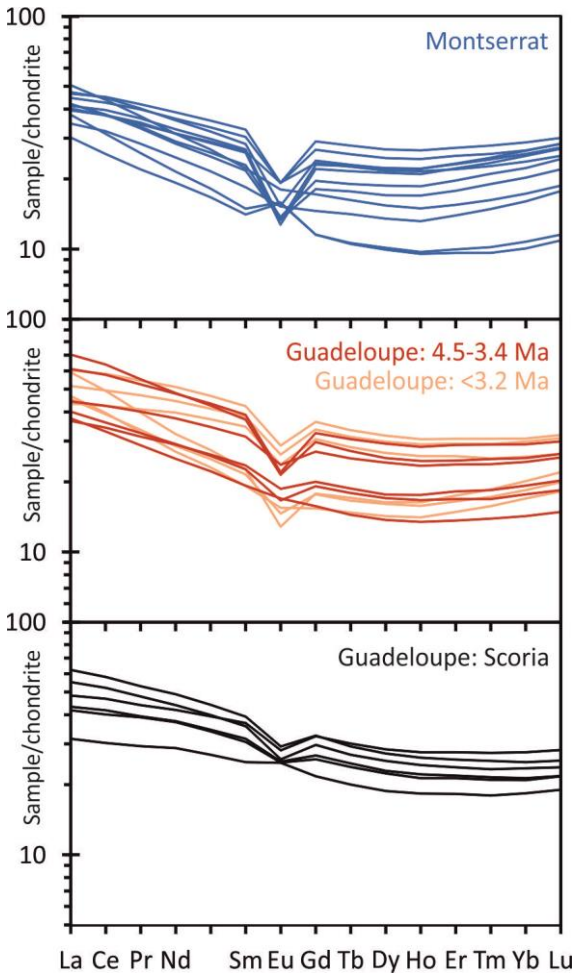

Figure 4.6. Representative REE patterns for tephra layers from Montserrat and Guadeloupe.

Due to the unreliability of the major element data, it will not form part of the discussion.

4.5 Discussion

4.5.1 Crustal assimilation

A common indicator of crustal assimilation is a correlation between isotope ratios and SiO_2, but as discussed the SiO_2 data is unreliable, so trace element data is used as an alternative. As SiO_2 increases with differentiation, so too will the concentration of incompatible trace elements, while isotope ratios remain unchanged. Thus any correlation between incompatible trace elements and isotopes is likely to be the result of crustal assimilation, as would be inferred from a correlation with SiO_2. Using this approach, the trace elements show no correlation between Pb, Nd or Sr and incompatible trace elements for Montserrat,

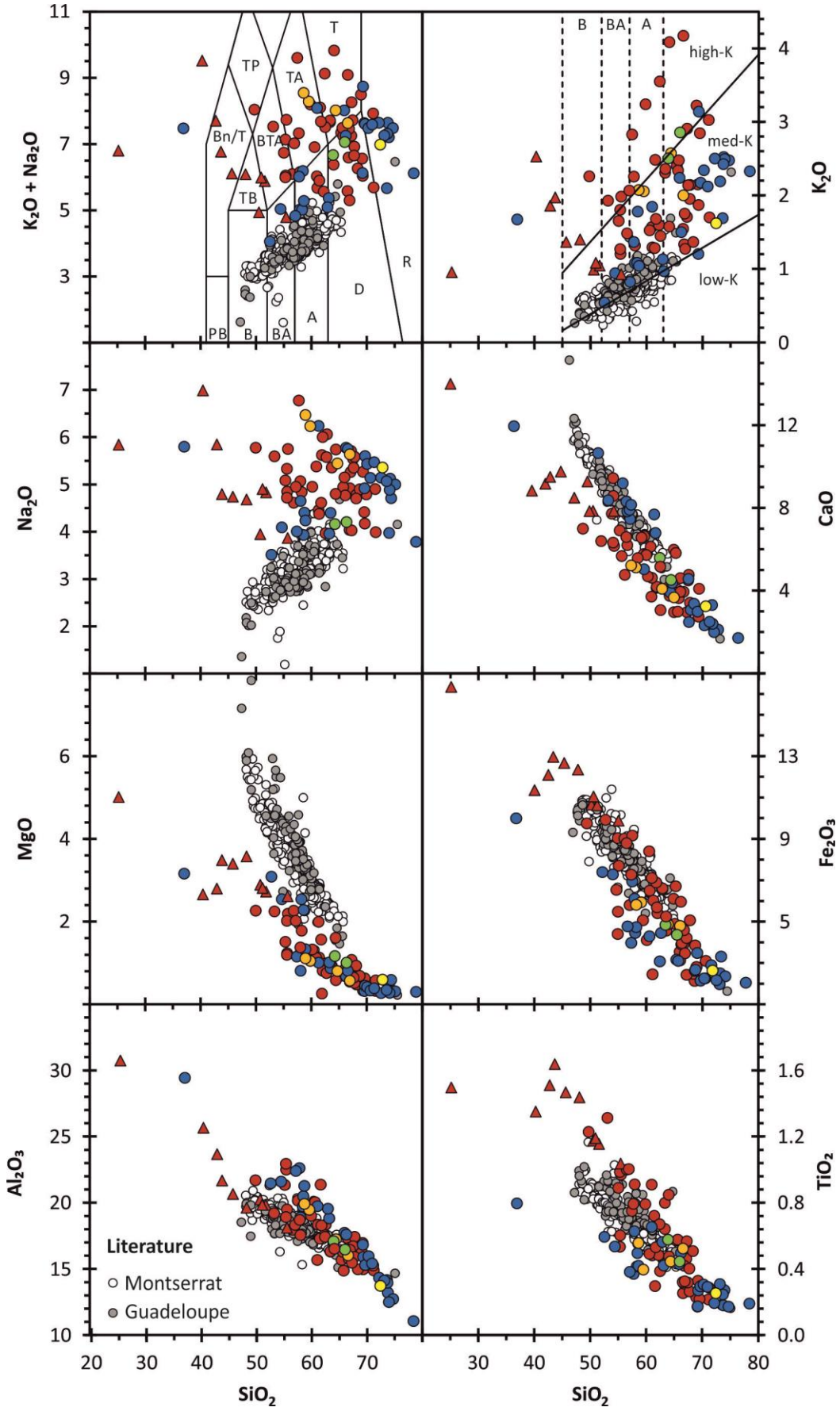
K2O + Na2O
T
TP
TA
Bn/T
BTA
TB
R
D
A
PB
B
BA
B
BA
A
high-K
med-K
low-K
K2O
Na2O
CaO
MgO
Fe2O3
Al2O3
TiO2
Literature
Montserrat
Guadeloupe
SiO2
SiO2

Figure 4.7. Major elements vs SiO_2. The fields in SiO_2 vs $K_2O + Na_2O$ follow the classification of Le Bas et al., (1986): B, basalt; BA, basaltic andesite; A, andesite; D, dacite; R, rhyolite; TB, trachy-basalt; BTA, basaltic trachy-andesite; TA, trachy-andesite; T, trachyte; Bn/T, basanite/tephrite; TP, tephra-phonolite. Low-, med- and high-K fields as defined by (Le Maitre et al., 2002). Montserrat literature data from Cassidy et al., (2012), Coussens et al., (2017) and Zellmer et al., (2003). Guadeloupe data from Boudon et al., (2008), Gunn et al., (1980), Samper et al., (2009) and Touboul et al., (2007). Symbols same as Figure 4.4, in addition to those given.

suggesting they have not been significantly affected by crustal assimilation (Figure 4.9). For Guadeloupe, however, there are positive correlations between Pb and Sr isotopes and M-HREE and Y, and a negative correlation between $^{143}Nd/^{144}Nd$ and all REEs and Y, suggesting crustal assimilation has been a prominent process in the evolution of Guadeloupe magmas (Figure 4.9).

These isotope-REE correlations are also clear in REE ratios, e.g. Dy/Yb, La/Sm (Figure 4.10). Fractionation of amphibole creates a negative correlation between Dy/Yb and SiO_2 (Davidson et al., 2007), with increasing amphibole fractionation reducing Dy/Yb values. As discussed, there is evidence for the involvement of amphibole fractionation in the formation of Guadeloupe tephras, so the correlations between Pb-Nd-Sr isotopes and Dy/Yb (Figure 4.10) indicate that crustal assimilation has affected the chemistry of Guadeloupe tephras, with greatest assimilation occurring at ~3.2 Ma. Furthermore, the increase in $^{143}Nd/^{144}Nd$ and decrease in Pb isotopes with increasing fractionation (i.e. decreasing Dy/Yb) suggests that the assimilant has a MORB-like composition, and is not sedimentary in nature. Alternatively, assimilation of an amphibole-bearing assimilant would increase the Dy/Yb as well as affecting $^{143}Nd/^{144}Nd$. However, this scenario would lead to an enrichment of MREE in the high Dy/Yb samples which would produce a concave-up M-HREE pattern, which is not observed in any of our samples (Figure 4.6). Furthermore, the scoria samples have Pb and Nd isotope ratios in the higher and lower range of values, respectively, indicating that assimilation is driving magma compositions

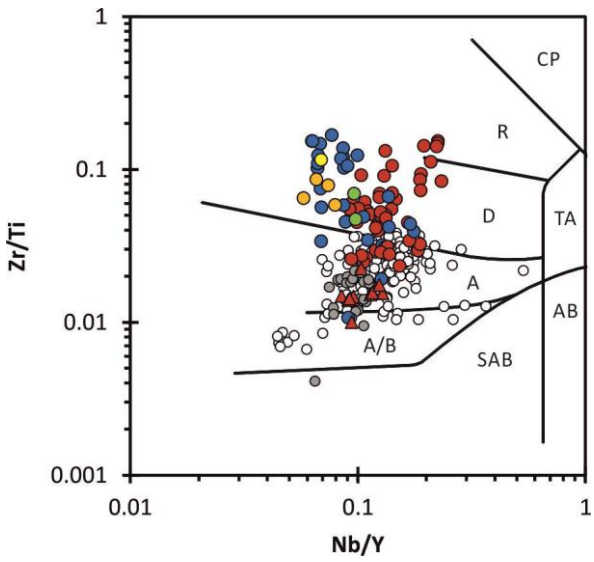

Figure 4.8. Nb/Y vs Zr/Ti. Fields as defined by Winchester and Floyd, (1977): A/B, andesite/basalt; A, andesite; D, dacite; R, rhyolite; CP, comendite pantellerite; SAB, sub-alkaline basalt; AB, alkali basalt; TA, trachy-andesite. Literature data from Cassidy et al., (2012), Coussens et al., (2017) and Zellmer et al., (2003). Symbols same as in Figures 4.4 and 4.7.

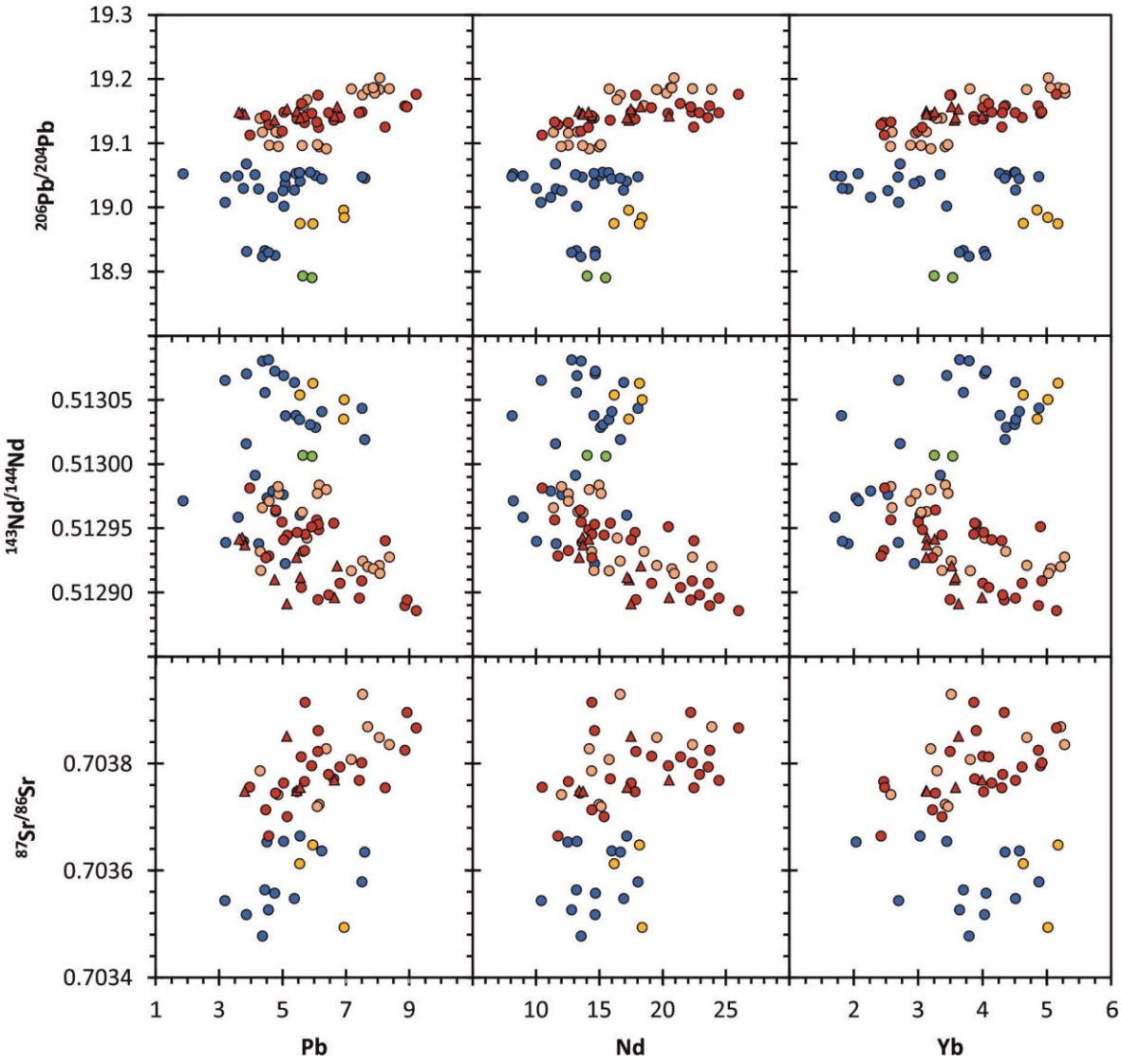

Figure 4.9. Pb, Nd and Yb vs $^{206}Pb/^{204}Pb$, $^{143}Nd/^{144}Nd$ and $^{87}Sr/^{86}Sr$. Symbols same as Figure 4.4.

towards MORB-like values.

There are two possible sources for the MORB assimilant: the subducting altered oceanic crust (AOC), or a MORB component within the overlying crust. Melting of the subducting AOC is only considered possible for relatively young hot slabs (<25 Ma) (Defant and Drummond, 1990), and so the Cretaceous oceanic crust being subducted beneath the Lesser Antilles (Carpentier et al., 2008) is considered too old and cold to melt. Thus the assimilant is likely located within the overlying Caribbean crust. The co-variance of Dy/Yb and $^{143}Nd/^{144}Nd$ indicates that combined assimilation and fractional crystallisation (AFC) is playing a key role in the evolution of magmas beneath Guadeloupe. AFC modelling was performed using the Microsoft Excel spreadsheet program of Ersoy and Helvaci, (2010), which uses the AFC equations of DePaolo, (1981). For trace element concentrations, this is

$$C_l^{AFC} = C_o \left[F^{-z} + \left(\frac{r}{r-1} \right) \frac{C^a}{zC_o} (1 - F^{-z}) \right] \quad (1)$$

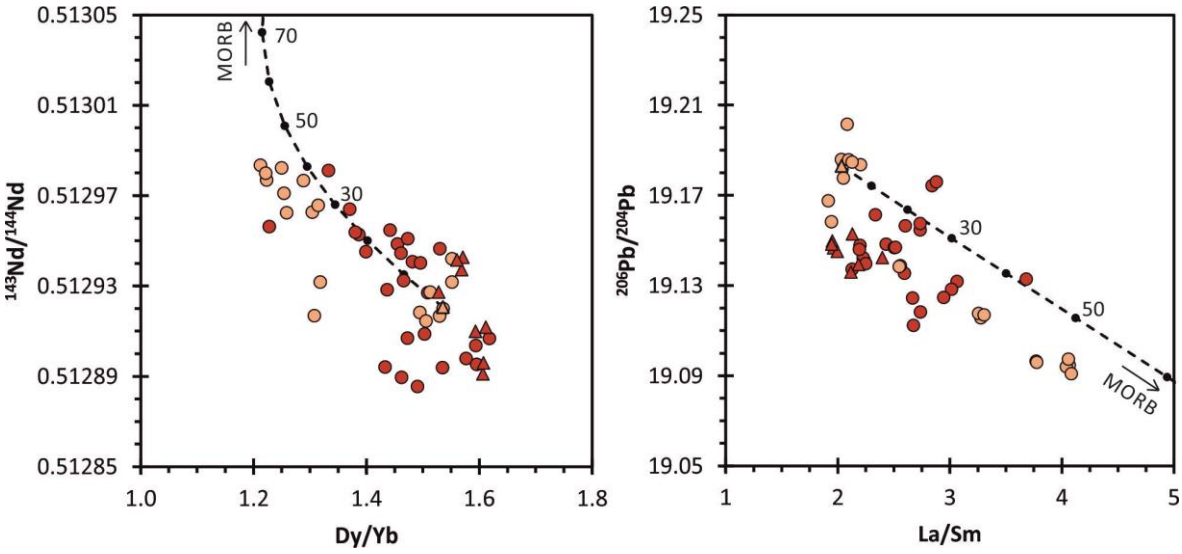

Figure 4.10. Dy/Yb vs $^{143}Nd/^{144}Nd$ and La/Sm vs $^{206}Pb/^{204}Pb$, with modelled AFC mixing lines. Dots on mixing lines denote percent crystallisation, marked every 10%, with 50% labelled. See text for details. Symbols same as Figure 4.4.

Where C_l^{AFC}, C_o, and C_a are the concentration of a given element in the resulting magma, parental magma, and assimilant, respectively, F is the fraction of melt, and r is the relative ratio of assimilant to crystallised material, expressed by

$$r = \frac{m_a}{m_c} \tag{2}$$

Where m_a is the amount of assimilant and m_c is the amount of crystallised material. The z value in equation (1) is expressed by

$$z = \frac{r+D-1}{r-1} \tag{3}$$

Where D is the bulk partition coefficient of the fractionating assemblage. The partition coefficients of Bacon and Druitt, (1988), Brenan et al., (1995b), Dunn and Sen, (1994), Ewart and Griffin, (1994), Nash and Crecraft, (1985) and Philpotts and Schnetzler, (1969) are used, as provided in the spreadsheet. Isotope ratios undergoing AFC are modelled using

$$IC_l^{AFC} = \frac{\left(\frac{r}{r-1}\right)\left(\frac{C_a}{z}\right)(1-F^{-z})IC_a + C_o F^{-z} IC_o}{\left(\frac{r}{r-1}\right)\left(\frac{C_a}{z}\right)(1-F^{-z}) + C_o F^{-z}} \tag{4}$$

Where IC_l^{AFC}, IC_a and IC_o are the isotope ratios in the magma undergoing AFC, in the assimilant, and in the parental magma, respectively. All other values are the same as in equations (1)–(3). 6/2-77S, a 2.37 Ma scoria sample, was used as the starting composition because its high Pb and Sr isotopes, and low $^{143}Nd/^{144}Nd$, indicate it is the least likely to be affected by assimilation of MORB. Using a fractionation assemblage of 45% plagioclase, 35% amphibole, 10% orthopyroxene, 5% clinopyroxene and 5% magnetite, and the average Mid-

Atlantic Ridge (MAR) MORB composition of Debaille et al., (2006) as the assimilant (Table 4.1), the observed variation in REEs can be modelled by up to ~50% crystallisation with an *r* value of 0.55 (Figure 4.10). Changing the mineral proportions by ±10% has little effect on the modelling results; the key feature is the presence of amphibole in the fractionating assemblage, which dominates the REE behaviour. For isotope ratios, the average MORB composition of Debaille et al., (2006) fails to produce a suitable AFC mixing curve. Changing the *r* value by ±0.1 has a minor effect on trace element ratios (particularly Dy/Yb), but a large effect on isotope ratios, so keeping the *r* value fixed at 0.55, the isotope ratios are adjusted to produce a working AFC curve that can produce the observed range of values for up to ~50% crystallisation. This approach yields values of $^{143}Nd/^{144}Nd$=0.513150, $^{206}Pb/^{204}Pb$=17.60, $^{207}Pb/^{204}Pb$=15.37, and $^{208}Pb/^{204}Pb$=36.29 for the assimilant (Table 4.1). These values are within the depleted end of known MORB compositions (Agranier et al., 2005, and references therein), and so are considered plausible, further supporting a MORB component as the

Table 4.1. Variables used in AFC equations (1), (3) and (4)

	C_a	C_o		D
	6/2-77S	MAR*	Calculated	
Rb	37.36	2.32		0.11
Ba	238.00	28.20		0.41
Sr	259.70	118.68		1.39
Pb	8.06	0.29		0.70
Zr	169.20	85.08		0.53
Y	46.45	27.27		1.21
La	11.46	4.00		0.32
Ce	28.65	10.98		0.37
Pr	4.18	1.73		0.06
Nd	19.56	9.09		0.75
Sm	5.64	3.13		0.98
Eu	1.63	1.12		1.23
Gd	6.64	4.39		1.10
Tb	1.13	0.75		1.36
Dy	7.21	5.06		1.32
Ho	1.56	1.07		1.24
Er	4.56	3.22		1.20
Tm	0.70	0.45		0.52
Yb	4.69	2.67		1.03
Lu	0.72	0.44		0.85
$^{206}Pb/^{204}Pb$	19.1831	18.4265	17.6000	
$^{207}Pb/^{204}Pb$	15.6863	15.4846	15.3700	
$^{208}Pb/^{204}Pb$	38.9157	37.9054	36.2900	
$^{143}Nd/^{144}Nd$	0.512921	0.513136	0.513150	
$^{87}Sr/^{86}Sr$	0.703848		0.702190	

* Average MAR MORB value of Debaille et al., (2006).

assimilant. $^{87}Sr/^{86}Sr$ can be successfully modelled using the most depleted depleted-MORB mantle value of Workman and Hart, (2005), which is 0.70219.

The presence of a MORB assimilant is consistent with the Lesser Antilles arc being built upon oceanic crust. Beneath Montserrat, the lower crust extends from ~10–30 km depth, and is interpreted as modified Caribbean crust, similar to that of the Venezuelan Basin, that has been intruded and thickened with differentiated mafic material (Sevilla et al., 2010). Successive intrusion of mafic magma from the mantle into the lower crust leads to the development of a deep crustal hot zone (DCHZ) (Annen et al., 2006). The temperature of DCHZs increases over time as more mafic magma is intruded, and as these magmas crystallise they liberate heat and volatiles which can trigger partial melting of the surrounding crust (Annen and Sparks, 2002). Modelling suggests that temperatures in DCHZs can reach in excess of 1400 K at depths of 30 km (Annen et al., 2006; Solano et al., 2012). Basalt solidus and liquidus temperatures are 993 and 1558 K, respectively, at 1 GPa and 2.5 wt. % water content (Annen et al., 2006), and so the temperatures reached in DCHZ are sufficient to induce partial melting of MORB in the lower crust.

The gradual decrease in MORB assimilation from 3.2–2.4 Ma may be indicative of a gradual decrease in crustal temperatures. The main control on temperature in DCHZs is the magma emplacement rate (Annen et al., 2006), with higher emplacement rates leading to higher temperatures, and vice versa. There is a notable difference in eruption frequency recorded in U1396C between 4.5–3.2 Ma and 3.2–2.4 Ma, with an average emplacement rate of one tephra layer every ~34 ka and ~56 ka for the respective time periods. If this is representative of a true decrease in eruption rate on Basse-Terre, then it could suggest a decrease in magma emplacement rates within the crust. This would reduce the temperature of the DCHZ, thereby reducing the amount of partial melting of the crust and thus the extent of crustal assimilation.

4.5.2 Changes in source component contributions

Crustal assimilation has been ruled out as the driving force for the observed change in Montserrat's chemistry between 4.5–3.9 Ma, and so this change is likely to represent a change in the source components. Using the same source component compositions as Cassidy et al., (2012) and DuFrane et al., (2009), mixing lines are modelled for mixing AOC fluid with a 20% partial melt of slab sediment (collectively called the 'slab component'), and for mixing the slab component with depleted mantle (Figure 4.11). The mixing lines show that Pb isotopes increase towards sedimentary values from 4.5–3.9 Ma, suggesting that this change was driven by an increased sediment contribution from the source region (Figure 4.11). However, if this were driven simply by sediment addition, one would expect a concomitant

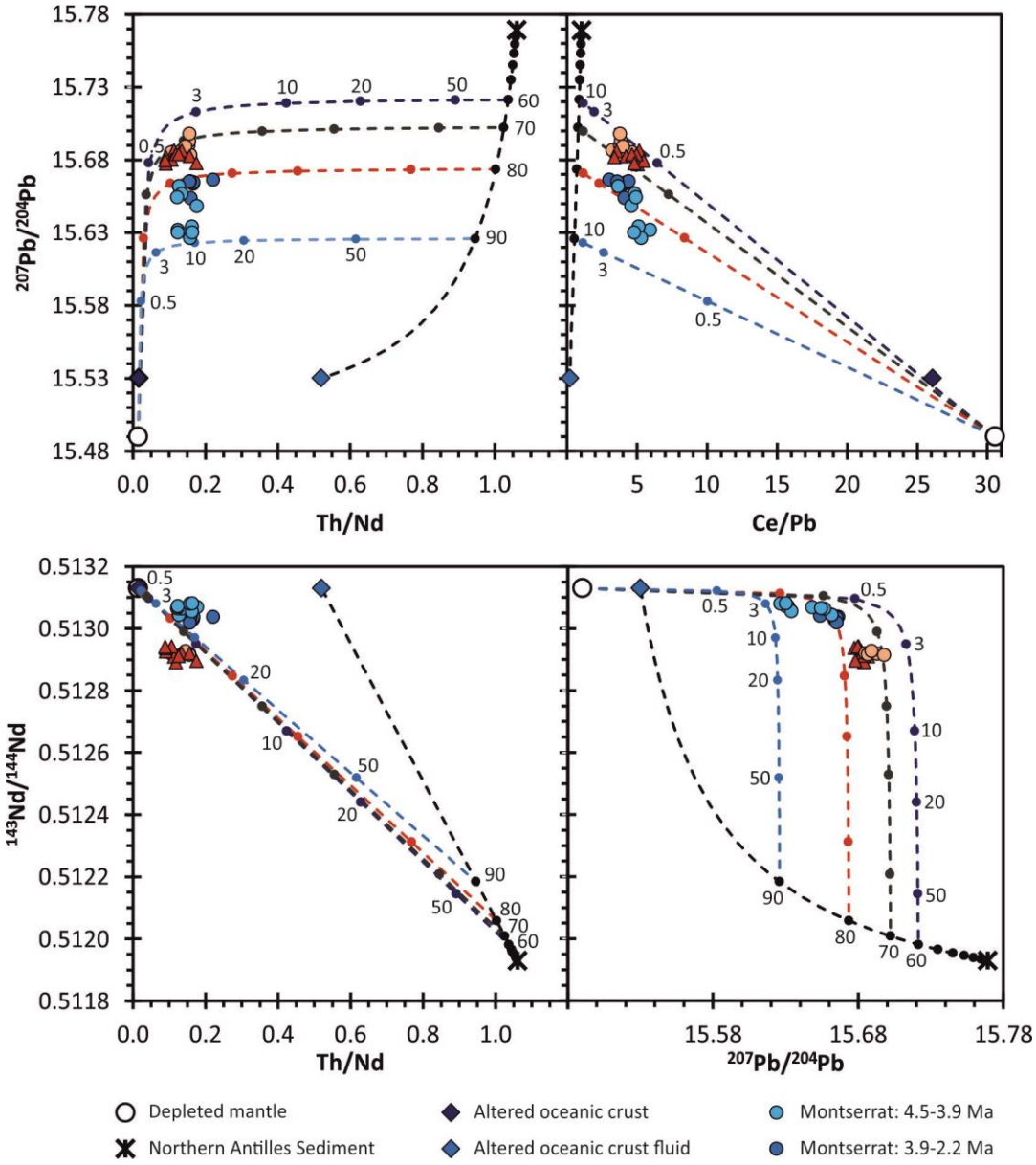

Figure 4.11. Trace element vs isotope mixing models for the different source components producing melts beneath Montserrat and Guadeloupe. Modelled mixing lines are between sediment and AOC (slab component), and between this mixing line and depleted MORB mantle. Numbers indicate percentage of component added. Depleted MORB mantle from DuFrane et al., (2009) and Workman and Hart, (2005). Northern Antilles sediment is a 20% partial melt of the bulk site 543 sediment from Plank and Langmuir, (1998), using the bulk partition coefficients of Johnson and Plank, (1999). A 20% partial sediment melt was used because Cassidy et al., (2012) showed it creates mixing lines which match the Montserrat data, whereas bulk sediment addition does not. AOC from Bach et al., (2003), Hauff et al., (2003) and Kelley et al., (2003). AOC fluid from DuFrane et al., (2009). Symbols same as in Figure 4.4, in addition to those given.

increase in $^{143}Nd/^{144}Nd$, which is not observed. Pb is preferentially partitioned into aqueous fluids, whilst Nd is not (Brenan et al., 1995a), so the increased sediment signature could be sourced from sediment-derived aqueous fluids. This would also explain why the only corresponding change in trace elements with Pb isotopes is an increase in fluid mobile

elements (e.g. increased Rb/Nb; Figure 4.5a). Thus the increase in Pb isotope ratios and fluid-mobile element abundances from 4.5–3.9 Ma was likely driven by an increased sediment-derived fluid into the mantle wedge. The uniformity of Pb and Nd isotopes from 3.9–2.2 Ma suggests that the proportion of source component contributions remained steady during this time period.

By focusing on the samples from Guadeloupe which are most mafic (i.e. scoria) and have been least affected by MORB assimilation (samples at ~2.4 Ma), the contribution of source components to the formation of melts beneath Montserrat can be compared with those formed beneath Guadeloupe. In isotope-isotope space, the modelling shows that a greater amount of slab component is added to the mantle wedge to form the melts beneath Guadeloupe, compared with Montserrat. It also suggests that the slab component has a greater proportion of sediment melt to AOC fluid beneath Guadeloupe (Figure 4.11). The isotope-trace element models produce slightly different results, indicating that there is little difference in the amount of slab component added to the mantle wedge between the two islands. They do however suggest that there is a significant difference in the proportion of sediment melt to AOC fluid in the slab component, with Guadeloupe melts containing a greater sediment contribution (Figure 4.11). Overall, the mixing models suggest than the melts forming beneath Guadeloupe container a greater sediment contribution that those forming beneath Montserrat, which is consistent with the along-arc trend of the Lesser Antilles (e.g. DuFrane et al., 2009; White and Dupré, 1986).

4.6 Conclusions

Trace element and Pb-Nd-Sr isotope data are presented for tephra layers from marine sediment core U1396C, which allow us to reconstruct the geochemical evolution of volcanism on Montserrat and Guadeloupe over the past 4.5 Ma. Montserrat displays a systematic increase in Pb isotope ratios and fluid-mobile trace element ratios (e.g. increasing Cs/Nb, Rb/Gd) over 4.5–3.9 Ma, while $^{143}Nd/^{144}Nd$ remains unchanged. This is interpreted to be the result of an increasing sediment contribution to the mantle wedge, added via an aqueous fluid from the subducting sediment. Over 3.9–2.2 Ma Pb-Nd-Sr isotopes all maintain the same range of values (2.2–0 Ma is covered in Chapter 3), suggesting that the proportion of source component contributions remained steady during this time period.

For Guadeloupe, there is greater variability in trace element and isotope ratios through time, with Pb and Sr isotopes having their lowest values, and $^{143}Nd/^{144}Nd$ its highest values, at 3.2 Ma. Correlations between Pb, Nd and Sr isotopes and incompatible trace elements (REEs in particular) indicate that crustal contamination is responsible for these temporal changes. Furthermore, covariance of Dy/Yb with $^{143}Nd/^{144}Nd$ suggests that AFC is taking place, with

amphibole as a major fractionating phase. AFC modelling identifies a MORB assimilant, with trace element concentrations similar to average MAR MORB (Debaille et al., 2006), and depleted MORB isotope values of $^{143}Nd/^{144}Nd$=0.513150, $^{206}Pb/^{204}Pb$=17.60, $^{207}Pb/^{204}Pb$=15.37, $^{208}Pb/^{204}Pb$=36.29, and $^{87}Sr/^{86}Sr$=0.70219.

Using source component mixing models, comparisons between Montserrat and the Guadeloupe samples least affected by assimilation indicate that melts forming beneath Guadeloupe contain a greater sediment contribution than those forming beneath Montserrat, as is expected based on the along-arc trend of the Lesser Antilles (e.g. DuFrane et al., 2009; White and Dupré, 1986).

4.7 References

Agranier, A., Blichert-Toft, J., Graham, D., Debaille, V., Schiano, P., Albarède, F., 2005. The spectra of isotopic heterogeneities along the mid-Atlantic Ridge. Earth Planet. Sci. Lett. 238, 96–109. doi:10.1016/j.epsl.2005.07.011

Annen, C., Blundy, J.D., Sparks, R.S.J., 2006. The genesis of intermediate and silicic magmas in deep crustal hot zones. J. Petrol. 47, 505–539. doi:10.1093/petrology/egi084

Annen, C., Sparks, R.S.J., 2002. Effects of repetitive emplacement of basaltic intrusions on thermal evolution and melt generation in the crust. Earth Planet. Sci. Lett. 203, 937–955. doi:10.1016/S0012-821X(02)00929-9

Bacon, C.R., Druitt, T.H., 1988. Compositional evolution of the zoned calcalkaline magma chamber of Mount Mazama, Crater Lake, Oregon 98, 224–256.

Bezard, R., Davidson, J.P., Turner, S., Macpherson, C.G., Lindsay, J.M., Boyce, A.J., 2014. Assimilation of sediments embedded in the oceanic arc crust: Myth or reality? Earth Planet. Sci. Lett. 395, 51–60. doi:10.1016/j.epsl.2014.03.038

Bezard, R., Schaefer, B.F., Turner, S., Davidson, J.P., Selby, D., 2015a. Lower crustal assimilation in oceanic arcs: Insights from an osmium isotopic study of the Lesser Antilles. Geochim. Cosmochim. Acta 150, 330–344. doi:10.1016/j.gca.2014.11.009

Bezard, R., Turner, S., Davidson, J.P., Macpherson, C.G., Lindsay, J.M., 2015b. Seeing through the Effects of Crustal Assimilation to Assess the Source Composition beneath the Southern Lesser Antilles Arc. J. Petrol. 56, 815–844. doi:10.1093/petrology/egv018

Bottazzi, P., Tiepolo, M., Vannucci, R., Zanetti, a., Brumm, R., Foley, S.F., Oberti, R., 1999. Distinct site preferences for heavy and light REE in amphibole and the prediction of Amph/L D REE. Contrib. to Mineral. Petrol. 137, 36–45. doi:10.1007/s004100050580

Boudon, G., Komorowski, J.C., Villemant, B., Semet, M.P., 2008. A new scenario for the last magmatic eruption of La Soufrière of Guadeloupe (Lesser Antilles) in 1530 A.D. Evidence from stratigraphy radiocarbon dating and magmatic evolution of erupted products. J. Volcanol. Geotherm. Res. 178, 474–490. doi:10.1016/j.jvolgeores.2008.03.006

Bouysse, P., Westercamp, D., 1990. Subduction of the Atlantic aseismic ridges and late cenozoic evolution of the Lesser Antilles island-arc. Tectonophysics 175, 349–380.

Boynton, C.H., Westbrook, G.K., Bott, M.H.P., Long, R.E., 1979. Seismic Refraction Investigation of Crustal Structure Beneath the Lesser-Antilles Island Arc. Geophys. J. R. Astron. Soc. 58, 371–393. doi:10.1111/j.1365-246X.1979.tb01031.x

Brenan, J.M., Shaw, H.F., Ryerson, F.J., 1995a. Experimental evidence for the origin of lead enrichment in convergent-margin magmas. Nature 378, 54–56. doi:10.1038/378592a0

Brenan, J.M., Shaw, H.F., Ryerson, F.J., Phinney, D.L., 1995b. Mineral-aqueous fluid partitioning of trace elements at 900oC and 2.0 GPa: Constraints on the trace element chemistry of mantle and deep-crustal fluids. Geochim. Cosmochim. Acta 59, 3331–3350.

Briden, J.C., Rex, D.C., Faller, A.M., Tomblin, J.F., 1979. K-Ar geochronology and palaeomagnetism of volcanic rocks in the Lesser Antilles island arc. Philos. Trans. R. Soc. London A Math. Phys. Eng. Sci. 291, 485–528. doi:10.1098/rsta.1948.0007

Brown, G., Holland, J., Sigurdsson, H., Tomblin, J., Arculus, R., 1977. Geochemistry of the lesser Antilles island arc. Geochim. Cosmochim. Acta 41, 785–801.

Brown, K., Davidson, C., 2008. 40Ar/39Ar geochronology of the Silver Hills andesite, Montserrat, West Indies. B. A. Sr. Integr. Exerc. Carlton College, Northfield, Minnesota.

Carlut, J., Quidelleur, X., Courtillot, V., Boudon, G., 2000. Paleomagnetic directions and K/Ar dating of 0 to 1 Ma lava flows from La Guadeloupe Island Implications for time-averaged field models. J. Geophys. Res. 105, 835–849. doi:10.1029/1999JB900238

Carpentier, M., Chauvel, C., Mattielli, N., 2008. Pb-Nd isotopic constraints on sedimentary input into the Lesser Antilles arc system. Earth Planet. Sci. Lett. 272, 199–211. doi:10.1016/j.epsl.2008.04.036

Cassidy, M., Edmonds, M., Watt, S.F.L., Palmer, M.R., Gernon, T.M., 2015. Origin of basalts by hybridization in andesite-dominated arcs. J. Petrol. 56, 325–346. doi:10.1093/petrology/egv002

Cassidy, M., Taylor, R.N., Palmer, M.R., Cooper, R.J., Stenlake, C., Trofimovs, J., 2012. Tracking the magmatic evolution of island arc volcanism: Insights from a high-precision Pb

isotope record of Montserrat, Lesser Antilles. Geochemistry, Geophys. Geosystems 13, 1–19. doi:10.1029/2012GC004064

Cassidy, M., Watt, S.F.L., Palmer, M.R., Trofimovs, J., Symons, W., Maclachlan, S.E., Stinton, A.J., 2014. Construction of volcanic records from marine sediment cores: A review and case study (Montserrat, West Indies). Earth-Science Rev. 138, 137–155. doi:10.1016/j.earscirev.2014.08.008

Cerling, T.E., Brown, F.H., Bowman, J.R., 1985. Low-temperature alteration of volcanic glass: Hydration, Na, K, 18O and Ar mobility. Chem. Geol. Isot. Geosci. Sect. 52, 281–293.

Chabaux, F., Hémond, C., Allègre, C.J., 1999. 238U-230Th-226Ra disequilibria in the Lesser Antilles arc: Implications for mantle metasomatism. Chem. Geol. 153, 171–185. doi:10.1016/S0009-2541(98)00160-0

Christeson, G.L., Mann, P., Escalona, A., Aitken, T.J., 2008. Crustal structure of the Caribbean - Northeastern South America arc-continent collision zone. J. Geophys. Res. Solid Earth 113, 1–19. doi:10.1029/2007JB005373

Christopher, T.E., Humphreys, M.C.S., Barclay, J., Genareau, K., De Angelis, S.M.H., Plail, M., Donovan, A., 2014. Petrological and geochemical variation during the Soufrière Hills eruption, 1995 to 2010. Geol. Soc. London, Mem. 39, 317–342. doi:10.1144/M39.17

Coussens, M., Cassidy, M., Watt, S.F.L., Jutzeler, M., Talling, P.J., Barfod, D., Gernon, T.M., Taylor, R., Hatter, S.J., Palmer, M.R., 2017. Long-term changes in explosive and effusive behaviour at andesitic arc volcanoes: Chronostratigraphy of the Centre Hills Volcano, Montserrat. J. Volcanol. Geotherm. Res. doi:10.1016/j.jvolgeores.2017.01.003

Davidson, J., Turner, S., Handley, H., Macpherson, C., Dosseto, A., 2007. Amphibole “sponge” in arc crust? Geology 35, 787–790. doi:10.1130/G23637A.1

Davidson, J., Wilson, M., 2011. Differentiation and source processes at Mt Pelée and the Quill; Active volcanoes in the Lesser Antilles arc. J. Petrol. 52, 1493–1531. doi:10.1093/petrology/egq095

Davidson, J.P., Harmon, R.S., 1989. Oxygen isotope constraints on the petrogenesis of volcanic arc magmas from Martinique, Lesser Antilles. Earth Planet. Sci. Lett. 95, 255–270.

Debaille, V., Blichert-Toft, J., Agranier, A., Doucelance, R., Schiano, P., Albarede, F., 2006. Geochemical component relationships in MORB from the Mid-Atlantic Ridge, 22-35°N. Earth Planet. Sci. Lett. 241, 844–862. doi:10.1016/j.epsl.2005.11.004

Defant, M.J., Drummond, M.S., 1990. Derivation of some modern arc magmas by melting of

young subducted lithosphere. Nature 374, 662–665. doi:10.1016/0021-9797(80)90501-9

DePaolo, D.J., 1981. Trace element and isotopic effects of combined wallrock assimilation and fractional crystallization 53, 189–202.

Diebold, J., Driscoll, N., Abrams, L., Buhl, P., Donnelly, T., Laine, E., Leroy, S., Toy, A., 1999. New insights on the formation of the caribbean basalt province revealed by multichannel seismic images of volcanic structures in the Venezuelan basin, in: Mann, P. (Ed.), Caribbean Basins.Sedimentary Basins of the World. Elsevier Science B. V., Amsterdam, pp. 561–589. doi:10.1016/S1874-5997(99)80053-7

DuFrane, S.A., Turner, S., Dosseto, A., van Soest, M., 2009. Reappraisal of fluid and sediment contributions to Lesser Antilles magmas. Chem. Geol. 265, 272–278. doi:10.1016/j.chemgeo.2009.03.030

Dunn, T., Sen, C., 1994. Mineral/matrix partition coefficients for orthopyroxene, plagioclase, and olivine in basaltic to andesitic systems: A combined analytical and experimental study. Geochim. Cosmochim. Acta 58, 717–733. doi:10.1016/0016-7037(94)90501-0

Ersoy, Y., Helvaci, C., 2010. FC-AFC-FCA and mixing modeler: A Microsoft Excel spreadsheet program for modeling geochemical differentiation of magma by crystal fractionation, crustal assimilation and mixing. Comput. Geosci. 36, 383–390. doi:10.1016/j.cageo.2009.06.007

Ewart, A., Griffin, W.L., 1994. Application of proton-microprobe data to trace-element partitioning in volcanic rocks. Chem. Geol. 117, 251–284. doi:10.1016/0009-2541(94)90131-7

Expedition 340 scientists, 2013. Site U1396, in: Le Friant, A., Ishizuka, O., Stroncik, N.A., Expedition 340 scientists. (Eds.), Proceedings of the Integrated Ocean Drilling Program, 340. Integrated Ocean Drilling Program Managment Internation, Inc, Tokyo. doi:10.2204/iodp.proc.340.106.2013

Feuillard, M., Allegre, C.J., Brandeis, G., Gaulon, R., Le Mouel, J.L., Mercier, J.C., Pozzi, J.P., Semet, M.P., Mouel, L., Mercier, J.C., Pozzi, J.P., Semet, M.P., 1983. The 1975-1977 crisis of La Soufriere de Guadeloupe (F.W.I): A still-born magmatic eruption. J. Volcanol. Geotherm. Res. 16, 317–334. doi:10.1017/CBO9781107415324.004

Fraass, A.J., Wall-Palmer, D., Leckie, R.M., Hatfield, R.G., Burns, S.J., Le Friant, A., Ishizuka, O., Aljahdali, M., Jutzeler, M., Martinez-Colon, M., Palmer, M.R., Talling, P.J., 2016. A revised Plio-Pleistocene age model and paleoceanography of the northeastern Caribbean Sea:

IODP Site U1396 off Montserrat, Lesser Antilles. Stratigraphy 13, 183–203.

Freymuth, H., Elliott, T., van Soest, M., Skora, S., 2016. Tracing subducted black shales in the Lesser Antilles arc using molybdenum isotope ratios. Geology 44, 987–990. doi:10.1130/G38344.1

Gudmundsdóttir, E.R., Eiríksson, J., Larsen, G., 2011. Identification and definition of primary and reworked tephra in Late Glacial and Holocene marine shelf sediments off North Iceland. J. Quat. Sci. 26, 589–602. doi:10.1002/jqs.1474

Gunn, B.M., Roobol, M.J., Smith, A.L., 1980. Geochemistry of the volcanoes of Basse Terre, Guadeloupe - An example of intra-island variation 43, 403–411.

Harford, C.L., Pringle, M.S., Sparks, R.S.J., Young, S.R., 2002. The volcanic evolution of Montserrat using 40Ar/39Ar geochronology. Geol. Soc. London, Mem. 21, 93–113. doi:10.1144/GSL.MEM.2002.021.01.05

Hatfield, R.G., 2015. Data report: stratigraphic correlation of Site U1396 and creation of a composite depth scale and splice 340, 1–17. doi:10.2204/iodp.proc.340.202.2015

Hatter, S.J., Palmer, M.R., Gernon, T.M., Taylor, R.N., Cole, P.D., Barfod, D.N., Coussens, M., 2018. The Evolution of the Silver Hills Volcanic Center, and Revised 40Ar/39Ar Geochronology of Montserrat, Lesser Antilles, With Implications for Island Arc Volcanism. Geochemistry, Geophys. Geosystems 19. doi:10.1002/2017GC007053

Hawkesworth, C.J., Powell, M., 1980. Magma genesis in the Lesser Antilles Island Arc. Earth Planet. Sci. Lett. 51, 297–308.

Jutzeler, M., Manga, M., White, J.D.L., Talling, P.J., Proussevitch, A.A., Watt, S.F.L., Cassidy, M., Taylor, R.N., Le Friant, A., Ishizuka, O., 2017. Submarine deposits from pumiceous pyroclastic density currents traveling over water: An outstanding example from offshore Montserrat (IODP 340). Bull. Geol. Soc. Am. 129, 392–414. doi:10.1130/B31448.1

Jutzeler, M., Talling, P.J., White, J.D.L., Scientists, E. 340, 2016. Data report: Coring disturbances in IODP 340, a detailed list of intervals with fall-in and flow-in, in: Le Friant, A., Ishizuka, O., Stroncik, N.A., Scientists, the E. 340 (Eds.), Proc. IODP, 340. Integrated Ocean Drilling Program Management International, Inc., Tokyo, Japan.

Kamber, B.S., Gladu, A.H., 2009. Comparison of Pb Purification by Anion-Exchange Resin Methods and Assessment of Long-Term Reproducibility of Th/U/Pb Ratio Measurements by Quadrupole ICP-MS. Geostand. Geoanalytical Res. 33, 169–181. doi:10.1111/j.1751-908X.2009.00911.x

Labanieh, S., Chauvel, C., Germa, A., Quidelleur, X., 2012. Martinique: A clear case for sediment melting and slab dehydration as a function of distance to the trench. J. Petrol. 53, 2441–2464. doi:10.1093/petrology/egs055

Labanieh, S., Chauvel, C., Germa, A., Quidelleur, X., Lewin, E., 2010. Isotopic hyperbolas constrain sources and processes under the Lesser Antilles arc. Earth Planet. Sci. Lett. 298, 35–46. doi:10.1016/j.epsl.2010.07.018

Le Bas, M.J., Le Maitre, R.W., Streckeisen, a., Zanettin, B., 1986. A Chemical Classificatron of Volcanic Rocks Based on the Total Alkali-Silica Diagram. J. Petrol. 27, 745–750. doi:10.1093/petrology/27.3.745

Le Friant, A., Lock, E.J., Hart, M.B., Boudon, G., Sparks, R.S.J., Leng, M., Smart, C.W., Komorowski, J.-C., Deplus, C., Fisher, J.K., 2008. Late Pleistocene tephrochronology of marine sediments adjacent to Montserrat, Lesser Antilles volcanic arc. J. Geol. Soc. London. 165, 279–289. doi:10.1144/0016-76492007-019

Le Maitre, R.W., Streckeisen, A., Zanettin, B., Le Bas, M.J., Bonin, B., Bateman, P., Bellieni, G., Dudek, A., Efremova, S., Keller, J., Lameyre, J., Sabine, P.A., Schmid, R., Sørensen, H., Wooley, A.R., 2002. Igneous rocks: a classification and glossary of terms: Recommendations of the International Union of Geological Sciences subcommision on the systematics of igneous rocks, 2nd Editio. ed. Cambridge University Press, Cambridge.

Macdonald, R., Hawkesworth, C.J., Heath, E., 2000. The Lesser Antilles volcanic chain: A study in arc magmatism. Earth Sci. Rev. 49, 1–76. doi:10.1016/S0012-8252(99)00069-0

Minster, J.B., Jordan, T.H., 1978. Present-day plate motions. J. Geophys. Res. 83, 5331. doi:10.1029/JB083iB11p05331

Nash, W.P., Crecraft, H.R., 1985. Partition coefficents for trace elements in silicic magmas. Geochim. Cosmochim. Acta 49, 2309–2322. doi:http://dx.doi.org/10.1016/0016-7037(85)90231-5

Philpotts, J.A., Schnetzler, C.C., 1969. Phenocryst-matrix partition coeflcients for K, Rb, Sr and Ba, with applications to anorthosite and basalt genesis 54, 307–322.

Ricci, J., Lahitte, P., Quidelleur, X., 2015a. Construction and destruction rates of volcanoes within tropical environment: Examples from the Basse-Terre Island (Guadeloupe, Lesser Antilles). Geomorphology 228, 597–607. doi:10.1016/j.geomorph.2014.10.002

Ricci, J., Quidelleur, X., Lahitte, P., 2015b. Volcanic evolution of central Basse-Terre Island revisited on the basis of new geochronology and geomorphology data. Bull. Volcanol. 77,

84. doi:10.1007/s00445-015-0970-7

Samper, A., Quidelleur, X., Komorowski, J.-C., Lahitte, P., Boudon, G., 2009. Effusive history of the Grande Découverte Volcanic Complex, southern Basse-Terre (Guadeloupe, French West Indies) from new K–Ar Cassignol–Gillot ages. J. Volcanol. Geotherm. Res. 187, 117–130. doi:10.1016/j.jvolgeores.2009.08.016

Samper, A., Quidelleur, X., Lahitte, P., Mollex, D., 2007. Timing of effusive volcanism and collapse events within an oceanic arc island: Basse-Terre, Guadeloupe archipelago (Lesser Antilles Arc). Earth Planet. Sci. Lett. 258, 175–191. doi:10.1016/j.epsl.2007.03.030

Sevilla, W.I., Ammon, C.J., Voight, B., De Angelis, S., 2010. Crustal structure beneath the Montserrat region of the Lesser Antilles island arc. Geochemistry, Geophys. Geosystems 11, 13. doi:10.1029/2010GC003048

Smet, I., De Muynck, D., Vanhaecke, F., Elburg, M., 2010. From volcanic rock powder to Sr and Pb isotope ratios: a fit-for-purpose procedure for multi-collector ICP–mass spectrometric analysis. J. Anal. At. Spectrom. 25, 1025–1032. doi:10.1039/b926335g

Solano, J.M.S., Jackson, M.D., Sparks, R.S.J., Blundy, J.D., Annen, C., 2012. Melt segregation in deep crustal hot zones: A mechanism for chemical differentiation, crustal assimilation and the formation of evolved magmas. J. Petrol. 53, 1999–2026. doi:10.1093/petrology/egs041

Speed, R.C., Smith-Horowitz, P.L., Perch-Nielsen, K. v. S., Saunders, J.B., Sanfilippo, A.B., 1993. Southern Lesser Antilles Arc Platform: Pre-Late Miocene Stratigraphy, Structure, and Tectonic Evolution, in: Speed, R.C., Smith-Horowitz, P.L., Perch-Nielsen J, K.V.S., Saunders, B., Sanfilippo, A.B. (Eds.), Southern Lesser Antilles Arc Platform: Pre-Late Miocene Stratigraphy, Structure, and Tectonic Evolution. Geological Society of America.

Speed, R.C., Walker, J.A., 1991. Oceanic crust of the Grenada Basin in the Southern Lesser Antilles arc platform 96, 3835–3851.

Taylor, R.N., Ishizuka, O., Michalik, A., Milton, J.A., Croudace, I.W., 2015. Evaluating the precision of Pb isotope measurement by mass spectrometry. J. Anal. At. Spectrom. 30, 198–213. doi:10.1039/C4JA00279B

Thirlwall, M.F., Graham, A.M., Arculus, R.J., Harmon, R.S., Macpherson, C.G., 1996. Resolution of the effects of crustal assimilation, sediment subduction, and fluid transport in island arc magmas: Pb-Sr-Nd-O isotope geochemistry of Grenada, Lesser Antilles. Geochim. Cosmochim. Acta 60, 4785–4810. doi:10.1016/S0016-7037(96)00272-4

Touboul, M., Bourdon, B., Villemant, B., Boudon, G., Joron, J.L., 2007. 238U-230Th-226Ra disequilibria in andesitic lavas of the last magmatic eruption of Guadeloupe Soufriere, french Antilles: Processes and timescales of magma differentiation. Chem. Geol. 246, 181–206. doi:10.1016/j.chemgeo.2007.09.009

Trofimovs, J., Fisher, J.K., Macdonald, H.A., Talling, P.J., Sparks, R.S.J., Hart, M.B., Smart, C.W., Boudon, G., Deplus, C., Komorowski, J.C., Le Friant, A., Moreton, S.G., Leng, M.J., 2010. Evidence for carbonate platform failure during rapid sea-level rise; ca 14 000 year old bioclastic flow deposits in the Lesser Antilles. Sedimentology 57, 735–759. doi:10.1111/j.1365-3091.2009.01117.x

Trofimovs, J., Foster, C., Sparks, R.S.J., Loughlin, S., Le Friant, A., Deplus, C., Porritt, L., Christopher, T., Luckett, R., Talling, P.J., Palmer, M.R., Le Bas, T., 2012. Submarine pyroclastic deposits formed during the 20th May 2006 dome collapse of the Soufrière Hills Volcano, Montserrat. Bull. Volcanol. 74, 391–405. doi:10.1007/s00445-011-0533-5

Trofimovs, J., Sparks, R.S.J., Talling, P.J., 2008. Anatomy of a submarine pyroclastic flow and associated turbidity current: July 2003 dome collapse, Soufrière Hills volcano, Montserrat, West Indies. Sedimentology 55, 617–634. doi:10.1111/j.1365-3091.2007.00914.x

Trofimovs, J., Talling, P.J., Fisher, J.K., Sparks, R.S.J., Watt, S.F.L., Hart, M.B., Smart, C.W., Le Friant, A., Cassidy, M., Moreton, S.G., Leng, M.J., 2013. Timing, origin and emplacement dynamics of mass flows offshore of SE Montserrat in the last 110 ka: Implications for landslide and tsunami hazards, eruption history, and volcanic island evolution. Geochemistry, Geophys. Geosystems 14, 385–406. doi:10.1002/ggge.20052

Turner, S., Hawkesworth, C., Van Calsteren, P., Heath, E., Macdonald, R., Black, S., 1996. U-series isotopes and destructive plate margin magma genesis in the Lesser Antilles. Earth Planet. Sci. Lett. 142, 191–207. doi:10.1016/0012-821X(96)00078-7

Van Soest, M.C., Hilton, D.R., Macpherson, C.G., Mattey, D.P., 2002. Resolving Sediment Subduction and Crustal Contamination in the Lesser Antilles Island Arc: a Combined He-O-Sr Isotope Approach. J. Petrol. 43, 143–170. doi:10.1093/petrology/43.1.143

Wadge, G., Shepherd, J.B., 1984. Segmentation of the Lesser Antilles subduction zone. Earth Planet. Sci. Lett. 71, 297–304. doi:10.1016/0012-821X(84)90094-3

Wall-Palmer, D., Coussens, M., Talling, P.J., Jutzeler, M., Cassidy, M., Marchant, I., Palmer, M.R., Watt, S.F.L., Smart, C.W., Fisher, J.K., Hart, M.B., Fraass, A., Trofimovs, J., Le Friant, A., Ishizuka, O., Adachi, T., Aljahdali, M., Boudon, G., Breitkreuz, C., Endo, D., Fujinawa, A.,

Hatfield, R., Hornbach, M.J., Kataoka, K., Lafuerza, S., Maeno, F., Manga, M., Martinez-Colon, M., McCanta, M., Morgan, S., Saito, T., Slagle, A.L., Stinton, A.J., Subramanyam, K.S. V., Tamura, Y., Villemant, B., Wang, F., 2014. Late Pleistocene stratigraphy of IODP Site U1396 and compiled chronology offshore of south and south west Montserrat, Lesser Antilles. Geochemistry, Geophys. Geosystems 15, 3000–3020. doi:10.1002/2014GC005402

White, W.M., Dupré, B., 1986. Sediment subduction and magma genesis in the Lesser Antilles: Isotopic and trace element constraints. J. Geophys. Res. 91, 5927. doi:10.1029/JB091iB06p05927

Whitmarsh, R.B., Keen, C.E., Steinmetz, L., Tomblin, J., Whitmarsh, R.B., Donegan, M., Lilwall, R.C., Loncarevic, B.D., Nichols, B., Shepherd, J., 1983. A lithospheric seismic refraction profile in the western North Atlantic Ocean. Geophys. J. Int. 75, 23–69. doi:10.1111/j.1365-246X.1983.tb01912.x

Winchester, J.A., Floyd, P.A., 1977. Geochemical discrimination of different magma series and their differenatiation products using immobile elements. Chem. Geol. 20, 325–343.

Workman, R.K., Hart, S.R., 2005. Major and trace element composition of the depleted MORB mantle (DMM). Earth Planet. Sci. Lett. 231, 53–72. doi:10.1016/j.epsl.2004.12.005

Zellmer, G.F., Hawkesworth, C.J., Sparks, R.S.J., Thomas, L.E., Harford, C.L., Brewer, T.S., Loughlin, S.C., 2003. Geochemical Evolution of the Soufrière Hills Volcano, Montserrat, Lesser Antilles Volcanic Arc. J. Petrol. 44, 1349–1374. doi:10.1093/petrology/44.8.1349

Chapter 5: Discovery of a large 2.4 Ma Plinian eruption on Basse-Terre, Guadeloupe, from the marine sediment record

This chapter is an expanded version of a paper that has been published in *Geology*:

Palmer, M. R., S. J. Hatter, T. M. Gernon, R. N. Taylor, M. Cassidy, P. Johnson, A. Le Friant, and O. Ishizuka (2016), Discovery of a large 2.4 Ma Plinian eruption of Basse-Terre, Guadeloupe, from the marine sediment record, *Geol.* , *44*(2), 123–126, doi:10.1130/G37193.1.

It has been expanded to include work which was performed as part of this study, but was omitted from publication due to the short format nature of *Geology*. In particular, this expansion presents the componentry data, and provides more detail about determining the mode of deposition of the tephra layer studied. The paper was written by M. R. Palmer and S. J. Hatter, with most laboratory work carried out by S. J. Hatter; Pb isotope and trace element data were collected by P. Johnson as part of a Masters Thesis. Data interpretation was a joint effort between M. R. Palmer and S. J. Hatter, with additional input from T. M. Gernon and R. N. Taylor. M. Cassidy, A. Le Friant and O. Ishizuka provide feedback on the manuscript.

Abstract

Large volcanic eruptions are major geohazards, so identifying their frequency in the geologic record is critical for making predictions and hazard assessments. Following the discovery of a thick (18 cm), tephra layer in marine sediments from IODP Site U1396 between Montserrat and Guadeloupe in the Caribbean Sea, we document here how high precision Pb isotopes, trace elements, and grain morphological analyses of the tephra can be used, together with volcanological models, to identify a large (Volcanic Explosivity Index ~6) Plinian eruption from Basse-Terre, Guadeloupe, ~2.36 Ma. This previously unrecognized eruption is believed to be the largest documented volcanic event in this region since this time. We hypothesize that this large eruption was associated with the final stage in the evolution of an individual volcanic centre, which has implications for prediction of geohazards in this setting.

5.1 Introduction

Reconstructing the history of island arc volcanoes is critical for determining their petrological evolution and potential geohazards, but such studies are difficult because erosion and later

eruptions destroy and obscure the subaerial record of volcanoes, with much of the erupted material rapidly transported to the oceans (Le Friant et al., 2015). While marine sediment cores can provide more complete histories of arc volcanism, this approach requires identification of the depositional mode of marine tephra layers and their precise origin from closely-spaced and compositionally similar volcanoes.

This problem is exemplified in the Lesser Antilles, where volcanism has been active since ~40 Ma. To the north of Martinique, the arc is divided into two chains. The eastern, inactive, chain is older, with carbonate platforms covering volcanic basement. Tectonic adjustments during the Miocene modified the orientation of the subducting slab, causing westward migration of the volcanic front and initiation of a new arc that includes all the active volcanoes (Pindell and Barrett, 1990). In order to reconstruct a long term record of volcanism in the northern Lesser Antilles, International Ocean Discovery Program (IODP) Expedition 340 occupied four sites in 2012 offshore the currently active island of Montserrat. Site U1396 is located on a topographic high (water depth ~780 m), ~35 km southwest of Montserrat and ~75 km west of Guadeloupe (Figure 5.1). Of the three holes cored at the site with the advanced piston corer, two were continuous (U1396A, 140.5 m; U1396C, 145.9 m) records that extend back ~4.5 Ma (Hatfield, 2015). The sediments comprise hemipelagic (largely carbonate) sediment and volcaniclastic mud, with >150 visible (>0.5 cm thick) tephra layers intercalated in hemipelagic background sediments (Le Friant et al., 2015). The present study uses geochemical, grain morphology and volcanological techniques to identify the origin and magnitude of the eruption that generated the second thickest tephra layer from U1396.

5.2 Methods

5.2.1 Geochemistry

15–25 mg of volcanic grains were handpicked from the >63 μm fraction of sieved tephra samples and powdered in an agate mortar. Trace element concentrations were measured by a Thermo Fisher Scientific X-Series 2 ICP-MS, with precision better than 3.5%. Pb isotope analyses were carried out on ~30–190 mg of handpicked grains (depending on Pb concentration), using the method described by Cassidy et al. (2012). Pb isotope ratios were measured on a MC-ICP-MS (Neptune), using the double spike technique to correct for instrumental bias (Taylor et al., 2015). NBS 981 standard gave the following results: 16.9422 ± 0.0012 (2SD) for $^{206}Pb/^{204}Pb$, 15.4985 ± 0.0013 for $^{207}Pb/^{204}Pb$ and 36.7219 ± 0.0034 for $^{208}Pb/^{204}Pb$ during the course of the analyses reported here. The small sample sizes available preclude the use of XRF analysis, so the major elements were also determined by ICP-MS

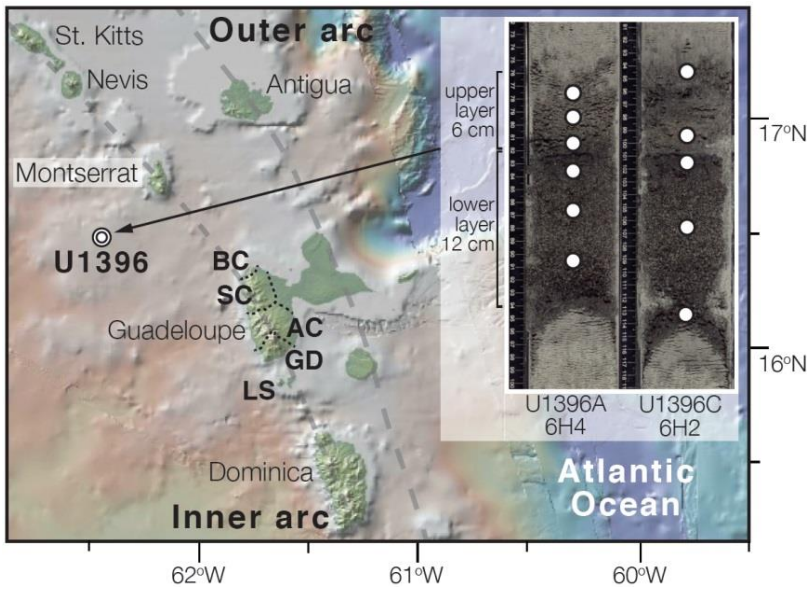

Figure 5.1. Northern Lesser Antilles (Caribbean Sea) map with IODP Expedition 340 Site U1396 location. Inset shows image of tephra layer T2.36. Also shown are Guadeloupe volcanic centres: Basal Complex (BC), Septentrional Chain (SC), Axial Chain (AC), Grande Découverte (GD), and Les Saintes (LS) (Samper et al. 2007, 2009). White circles indicate sampling locations for grain-size analyses (Hole U1396A) and geochemistry and grain morphology (Hole U1396C). The base of the tephra layer is at a depth of 48.97 m below sea floor.

using the same mother solutions as for traces. SiO_2 wt% concentrations were determined by subtracting the sum of the other major elements from 100%. While this method is less accurate than traditional techniques, the inter-element relationships are consistent with trends observed for subaerial exposures on Guadeloupe (Samper *et al.* 2007, 2009). All geochemical data is presented in Appendix Tables 5.1–5.2.

5.2.2 Age Assignment

The sediments recovered from Holes U1396A and U1396C were primarily correlated using shipboard magnetic susceptibility (MS) which was acquired at 2.5 cm intervals prior to the core being split on the Whole Round Multi Sensor Logger (WRMSL). To independently corroborate MS correlations, and assist decisions if MS correlation became ambiguous, density data - measured through Gamma Ray Attenuation on the WRMSL at 2.5cm intervals - and Natural Gamma Ray (NGR) radiation data - measured at 10cm intervals on the NGR system - were also used for correlation.

5.2.3 Grain Characteristics Analysis

Grain size analyses were carried out on ~1 cm^3 of bulk samples that were added to 30 ml of Calgon solution (as a dispersant), and run through a Malvern Mastersizer 2000 particle size analyser to measure grain sizes in the 0.02-2000 μm size interval. The data were entered into

the Gradistat program (Blott and Pye, 2001) to determine the sorting value (Folk & Ward, 1957). The samples were then wet sieved into a >100 μm fraction and dried. This fraction was photographed under a stereo microscope using an integrated digital camera (Leica EZ4D). Images were processed and analyzed using ImageJ software, and the area, perimeter and aspect ratio of 320–450 grains were measured according to the procedure outlined by Cassidy et al. (2014).

5.2.4 Componentry analysis

After being run through the Malvern Mastersizer 2000 samples were passed through a 100 μm sieve and dried in an oven. For componentry analysis ~300–400 grains of the >100 μm fraction were counted and placed into the following categories based on the classifications of Le Friant et al. (2008), Cassidy et al. (2014) and Wall-Palmer et al. (2014): (1) vesicular juvenile, which are unaltered pumice grains; (2) scoria, which are glassy black and brown vesicular to poorly-vesicular grains; (3) non-vesicular juvenile, which are light to dark grey crystalline lava fragments commonly containing phenocrysts; (4) glass shards and crystal fragments; (5) altered grains, which are lava or pumice grains which display orange-red discolouration, thought to be the result of hydrothermal alteration; (6) bioclasts, typically foraminifera tests.

5.3 Sediment Core Observations

5.3.1 Tephra Provenance

Tephra was likely delivered to U1396 from different sources, but prevailing wind directions and seafloor topography suggest, however, these were predominantly from volcanoes on Montserrat and Guadeloupe. The erupted material on both islands consists mainly of andesites, with lesser amounts of basalts and basaltic andesites (Harford et al., 2002; Samper et al., 2007), but there is a clear north-south gradation in the Pb isotope ratio of volcanic rocks in the Lesser Antilles that has been present for ~5 Myr (Lindsay et al., 2005; Labanieh et al., 2010) and Pb isotope analyses of Montserrat (Cassidy et al., 2012) and Guadeloupe lavas (White and Dupré, 1986) show that the two centres are distinguishable (Figure 5.2). The one Dominican Pb isotope datum that lies in the Guadeloupe field is from the <40 ka Morne Anglais centre (Lindsay et al., 2005). Of 29 samples of visible tephras analysed from U1396 and shown in Figure 5.1, 17 fall in the Montserrat Pb isotope field and 12 in the Guadeloupe field. Of the latter, 5 come from an ~18 cm thick tephra layer (sub cores 6H4-U1396A and 6H2-U1396C). The other samples with a Guadeloupe origin come from tephra layers <5 cm thick.

5.3.2 Tephra Age

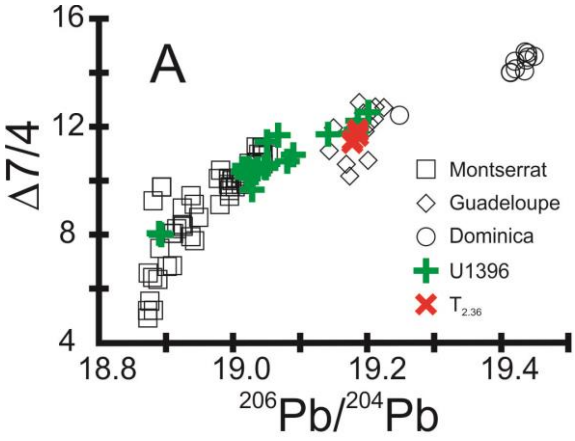

Figure 5.2. Δ7/4 ($^{207}/^{204}$Pb relative to northern hemisphere reference line; Hart, 1984) versus ^{206}Pb/^{204}Pb. Pb isotope data for islands from Dominica, (Lindsay et al., 2005), Montserrat (Cassidy et al., 2012), Guadeloupe (White & Dupré, 1986; C. Chauvel Pers. Commun.). Green symbols are for IODP Site U1396C, and red symbols are for tephra $T_{2.36}$.

The 82 cm mark in U1396A 6H4 (6H4-82) and 101 cm mark in U1396C 6H2 (6H2-101) both lie at a composite core depth (CCSF-A) of 53.35 m below seafloor. This CCSF-A depth is bracketed by the C2r.1n (B) Reunion polarity zone (2.148 Ma) at a mid-point CCSF-A of 45.11 m and the C2r.2r (B) Gauss/Matuyama polarity zone (2.581 Ma) at a mid-point CCSF-A of 61.59 m (Hatfield, 2015). If sedimentation rates are assumed to be linear, this depth corresponds to a depositional age of 2.36 Ma. The uncertainties in this age arise from the presence of any hiatuses in sedimentation, variations in the background hemipelagic sedimentation rate, and the number and thickness of tephra layers above and below $T_{2.36}$. There was no evidence during shipboard core logging of any hiatuses in this interval (Le Friant et al., 2015). Biostratigraphic and $\delta^{18}O$ stratigraphical analysis of the upper 7 m (past 250 kyr) of sediments from U1396C showed that background sedimentation rates varied from 2.8 to 9.4 cm ka^{-1} (Wall-Palmer et al., 2014). The period of rapid sedimentation was confined to an interval of ~0.5 m (~50 kyr) in the uppermost part of the core, and the Hemipelagic sedimentation rates were relatively constant (~2.8±0.5 cm ka^{-1}) through the rest of the upper 7 m. Overall, however, there is no clear evidence to suggest the putative age for 2.36 Ma is biased towards younger or older ages by variations in the hemipelagic sedimentation rate. Visual shipboard core logging and magnetic susceptibility data (Le Friant et al., 2015) (as a proxy for volcanogenic component of the sediments; Cassidy et al. 2014) shows there were similar levels of tephra deposition in both the lower and upper portions of the section bound by the two polarity zones. Hence the true depositional age of 2.36 Ma is unlikely to be significantly biased to older or younger ages than 2.36 Ma based on the assumption of linear sedimentation rates, thus this tephra layer is referred to hereafter as $T_{2.36}$.

5.3.3 Number of Eruptions

It is difficult to unequivocally determine whether more than one eruption was responsible for deposition of $T_{2.36}$. Hemipelagic sedimentation rates of ~2.8 cm kyr^{-1} make sub-centennial gaps between eruptions difficult to identify. Heterogeneous grain-size distribution,

morphology and geochemistry are also observed in single large deposits (Wiesner et al., 2004), so cannot easily be used to address this problem, but visual inspection of $T_{2.36}$ indicates that it is composed of an upper layer of ~6 cm and a lower layer of ~12 cm thickness (Figure 5.1).

5.4 Mode of Deposition

5.4.1 Primary fallout versus flow deposit

Tephra layers from the top 7 m of core U1396C were analysed by Wall-Palmer et al., (2014), who defined primary fallout tephra layers as being relatively well sorted, containing <5% bioclasts, lacking basal erosion and internal traction structures, and typically have a sharp base. The upper and lower layers of $T_{2.36}$ both meet these criteria, as they are relatively well sorted compared with the deposits from Cassidy et al. (2014) (Figure 5.3) and Wall-Palmer et al. (2014), contain <5% bioclasts (with the exception of the top of the upper layer; Figure 5.4), do not exhibit cross-bedding or erosional bases and have sharp bases (although the base of the lower layer exhibits minor up-arching, likely as a result of coring; Figure 5.1), suggesting that $T_{2.36}$ is a primary fallout tephra layer. However, a pyroclastic density current-derived turbidite from the 2003 dome collapse of Soufrière Hills contained only 0.8-5.1% bioclasts (Trofimovs et al., 2008), showing that even flow deposits can have low bioclast abundances.

A more thorough approach for determining the mode of deposition comes from analysing grain morphology. A detailed study of tephra deposits from the current phase of Montserrat activity provides clear objective grain size and morphology parameters for distinguishing fallout and flow deposits (Cassidy et al., 2014). Five samples taken from different horizons within $T_{2.36}$ (Figure 5.1) were measured for sorting index, angularity and elongation. The samples show a range in these parameters, but except for the uppermost sample (6H2 94/95), they all fall within the primary tephra fallout field (Figure 5.3).

Further support for a primary tephra fallout origin of $T_{2.36}$ comes from grain-size distribution data. The grain-size distribution of pyroclastic deposits from the recent eruption of Soufrière Hills (1995–2010) have been analysed for fallout (Bonadonna et al., 2002) and flow (Cole et al., 2002) deposits. Cole et al. (2002) analysed deposits of block-and-ash flow, pumice-and-ash flow and pyroclastic surge deposits, which had a mixture of unimodal and bimodal grain-size distributions. The unimodal deposits typically have modes between 0 and 3 φ, while the bimodal deposits typically have a finer and coarser mode between 0 and 3 φ, and -4 and -5 φ, respectively. This differs notably from the grain size distribution of fallout tephras from Vulcanian explosions, which are mostly bimodal with finer and coarser modes

between 4 and 6 φ, and 0 and 1 φ, respectively (Bonadonna et al., 2002). Figure 5.5 shows that the grain-size distribution data for $T_{2.36}$ matches closely that of fallout tephra from Montserrat, with both the upper and lower layers having a bimodal grain-size distribution with finer and coarser modes between ~5.5 and 6.5 φ, and -0.5 and 0.5 φ, respectively.

5.4.2 Depositional processes

Tephra fallout onto the ocean surface is transported to the sea floor by vertical density currents, which have a plume-like structure. This process leads to settling velocities of individual particles 2–3 orders of magnitude faster than settling by Stokes Law. However, the largest and/or densest grains may have Stokes Law settling velocities greater than plume velocities of the vertical density currents, and so can outrun the plume to fall individually through the water column (Manville and Wilson, 2004). This process can explain the higher proportion of denser material (lithics and crystals) found at the base of both lower and upper $T_{2.36}$ (Figure 5.4).

The finer, more dilute upper part of a vertical density current may be removed by the formation of dilute density currents when deposited on a slope, meaning material could be removed from a site before it has been deposited. This syn-depositional lateral transport can thus reduce the 'true' thickness of a deposit, which has important implications when determining eruption sizes (Manville

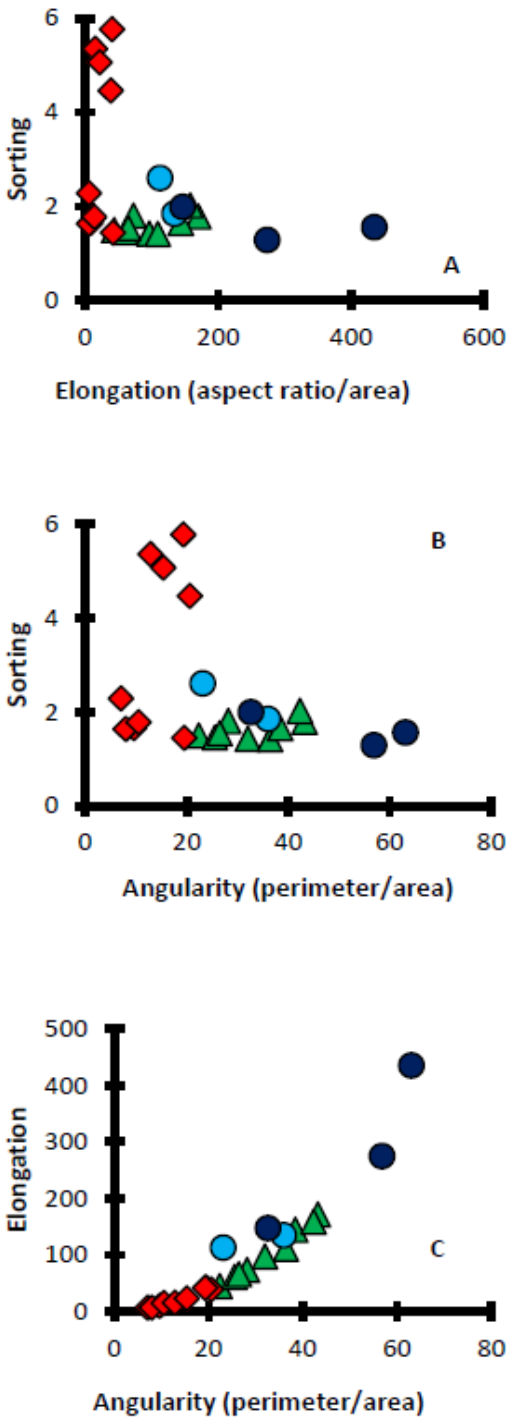

Figure 5.3. Grain size characteristics of tephra samples from Site U1396C. Green and red symbols are data from Cassidy et al. (2014) defining characteristics of primary fallout tephra and reworked tephra, respectively. Upper $T_{2.36}$ (light blue) refers to samples 94/95 and 99/100 from U1396C, and lower $T_{2.36}$ (dark blue) refers to samples 101/102, 106/107 and 113/114 from U1396C.

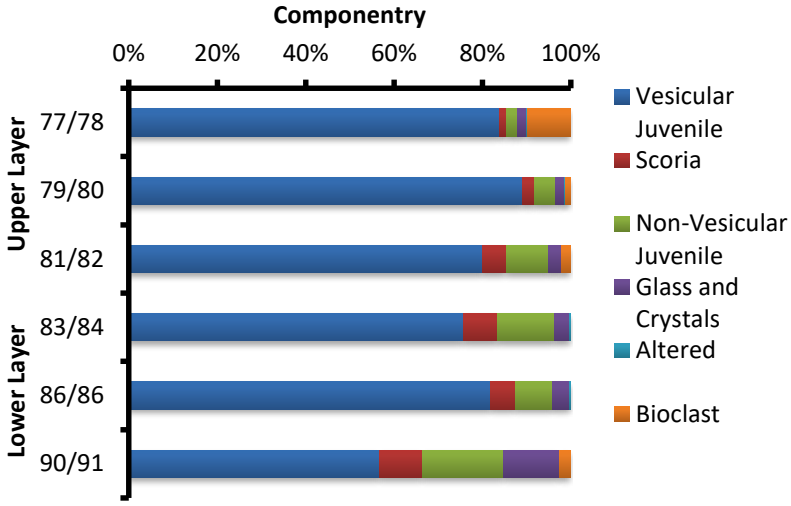

Figure 5.4. Componentry data of tephra samples from U1396A. (77/78, etc. refer to depth intervals in Figure 5.1).

and Wilson, 2004). Allan et al. (2008) invoke this process to account for three sediment cores within 100's of metres of each other often showing discrepancies, with a given tephra layer only occurring in 1 or 2 of the cores, and of varying thickness. The slight difference in thickness of $T_{2.36}$ between cores U1396A and U1396C, just ~30 m apart, may also be a result of this process.

5.4.3 Eruption column

Grain-size analyses of the upper and lower layers of U1396A show the lower layer is coarser-grained, while the upper layer contains a higher percentage of fine-grained particles (Figure 5.5). This pattern is similar to that observed in andesitic fallout deposits (coarser-grained) overlain by finer-grained co-pyroclastic/co-ignimbrite flow cloud deposits from the 2004–2006 eruptions of Colima, Mexico (Evans et al., 2009), and in both subaerial and marine tephra deposits of the Campanian ignimbrite (Engwell et al., 2014), and suggest that $T_{2.36}$ comprises the products of a Plinian eruption (lower layer) and associated lofted co-pyroclastic/co-ignimbrite flow deposits (upper layer).

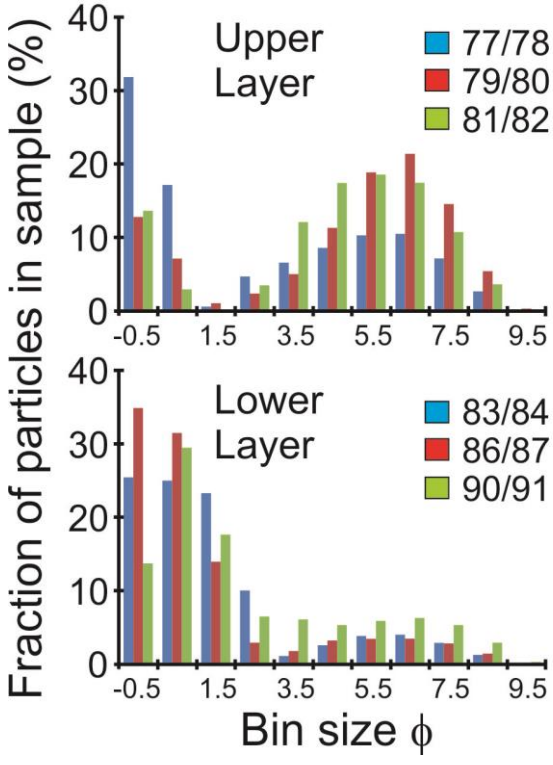

Figure 5.5. Grain size analyses of tephra samples from U1396A (77/78, etc. refer to depth intervals in Figure 5.1).

5.5 Comparison with the Subaerial Record

Basse-Terre forms the western half of Guadeloupe, and comprises four major volcanic massifs; the Basal Complex (2.79–2.68 Ma), the Septentrional Chain (1.81–1.15 Ma), the Axial Chain (1.02–0.44 Ma) and the Grande Découverte volcanic complex (314 ka to present) (Samper et al. 2007, 2009) (Figure 5.1). K-Ar ages show a north-south migration of volcanic activity, with a relatively large age gap between the youngest dates for the Basal Complex (2.68 ± 0.04 Ma) and the oldest age for the Septentrional Chain (1.81 ± 0.03 Ma). In addition, there are K-Ar dates for the two volcanic islands – Les Saintes (Terre-de-Bas; 0.92–0.88 Ma, and Terre-de-Haut; 2.98–2.00 Ma) – that lie ~10 km south of Basse-Terre (Zami et al., 2014).

The latitude of the source of $T_{2.36}$ is uncertain, but is likely south of the older Basal Complex (~16°19'N). The depositional age of $T_{2.36}$ lies within the age range of activity on Terre-de-Haut, but the La/Sm ratio of samples from $T_{2.36}$ fall on the Basse-Terre trend that is distinct from Terre-de-Haut lavas (Figure 5.6). Hence geochemical and age data suggest $T_{2.36}$ likely derived from Basse-Terre, with equivalent deposits of this source now buried beneath the Septentrional and Axial Chain centres.

The 5 sampled layers from $T_{2.36}$ have MgO and SiO_2 concentrations that range from 1.12 to 2.75 wt% and 59.4–64.6 wt%, respectively, which are typical of andesites from Basse-Terre (Samper et al., 2007, 2009).

5.6 Eruption Reconstruction

Today, the wind direction over Guadeloupe is exclusively east to west at altitudes >17.5 km and <5 km, and exclusively west to east between ~9–15 km. Just beneath the tropopause (~16.5 km) and between ~5–8.5 km the wind direction reverses from east to west in the wet season, to west to east in the dry season. Furthermore, large mesoscale systems, such as tropical storms, periodically reverse winds in the lower troposphere to west to east (Komorowski et al., 2008). Stratospheric circulation at this latitude is controlled by Brewer-Dobson circulation (Andrews et al., 1987), so there is no a priori reason to expect stratospheric wind directions would have been different 2.36 Ma.

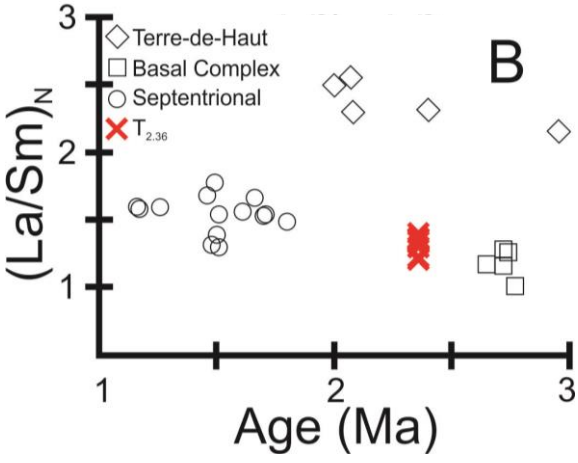

Figure 5.6. Chondrite normalized La/Sm versus age for T2.36 and lavas from Guadeloupe (Samper et al., 2007; Zami et al., 2014).

It would be preferable to have multiple sites to produce an isopach map to constrain the eruption parameters, but this is not possible in this instance. Nevertheless, González-Mellado & De la Cruz-Reyna (2010) used tephra distributions from 14 eruptions to propose and calibrate a model relating the tephra thickness (T, cm) at a single site to the eruption column height (H, km), wind speed (U, km hr^{-1}), eruption duration (τ, hr), distance from the eruption site (r, km), angle to the main axis of deposition (θ, degrees), and tephra density (ρ, kg m^{-3}):

$$T(r,\theta) = 14.28\frac{H^4\,\tau^{\frac{\alpha}{2}}}{(2D)^{\left(1-\frac{\alpha}{2}\right)}\rho}\,e^{-\left[\frac{U}{2D}r(1-cos\theta)\right]}r^{-\alpha} \quad (1)$$

Where, D and α are empirical constants given by:

D = 52.822H - 770.17 (for H >15 km); or D = -4.189H + 114.407 (for H <15 km) (2)

$$\alpha = 2.535 - 0.051H \quad (3)$$

The thicknesses of the $T_{2.36}$ layers are 12 cm and 6 cm, r is ~80 km (Figure 5.1), and the average ρ is measured as 1100 kg m^{-3}. We first consider the case of the lower $T_{2.36}$ layer being derived from a Plinian (stratospheric) eruption. Present day stratospheric U values range from 32 to 48 km hr^{-1} – dry and wet season, respectively (Komorowski et al., 2008). The stratospheric wind direction is from 90° and Site U1396 lies on a bearing of ~290° from the Septentrional Chain (Figure 5.1) (θ = 20°). If these parameters are fixed, it is possible to calculate values of H (eruption column height) and for a given value of τ (eruption duration). The results of this calculation are illustrated in Figure 5.7 for the 12 cm thick tephra layer at Site U1396, together with observed values and VEI of 27 andesitic and silicic eruptions (Mastin et al., 2009). While there is only one site for reconstructing the $T_{2.36}$ eruption parameters, marine tephra deposits from the Campanian ignimbrite deposit have been shown to yield a more regular pattern of exponential thinning from the source than their subaerial counterparts (Engwell et al., 2014). The main uncertainties in the model concern values of U and θ. For example, if θ = 0° (i.e., U1396 lay directly under the main axis of deposition) the calculated values of τ are ~25% lower for a given value of H, whereas τ increases by a factor of ~2–3 if θ is increased to 40° (an eruption from the southern tip of Les Saintes). Similarly, if U is reduced to 12.5 km hr^{-1} (half the minimum present day stratospheric wind velocity; Komorowski et al., 2008) the calculated values of τ fall by ~15% for any given value of H and if U is increased to 144 km hr^{-1} (double the maximum present day stratospheric wind velocity; Komorowski et al., 2008) calculated values of τ increase by a factor ~2.

Calculations for the $T_{2.36}$ upper layer could be taken to indicate that it was deposited from a smaller Plinian eruption than the lower layer (Figure 5.7), but the lack of hemipelagic sediment between the two layers and the grain size distributions (Figure 5.5) indicates that the upper layer likely represents the co-pyroclastic/co-ignimbrite phase of the same eruption. By comparison, the Plinian phase of the 1815 Tambora eruption lasted for 3–4 h and reached a height of 40–43 km, whereas the co-ignimbrite phase lasted for ~2 days and reached 25 km elevation (Kandlbauer and Sparks, 2014) (Figure 5.7). Thus, while there are uncertainties in the model, we believe comparison of these calculation results with data from modern volcanoes (Mastin et al., 2009) suggests that $T_{2.36}$ was deposited from a ~VEI 6 Plinian eruption.

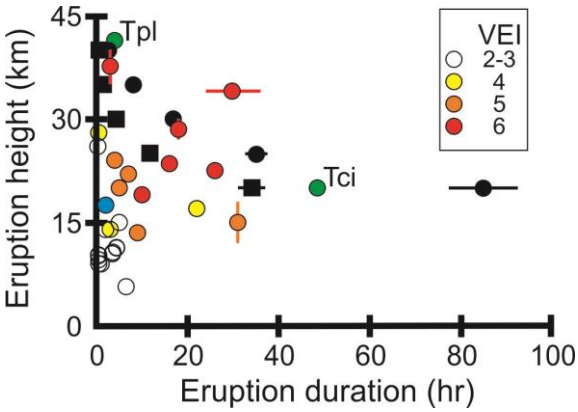

Figure 5.7. Relationship between volcanic eruption height and duration. Black circles and squares are calculated values (equation (2)) for lower and upper portions of $T_{2.36}$, respectively. Green circles are Tambora Plinian (Tpl) and co-ignimbrite (Tci) eruptions (Kandlbauer and Sparks, 2014). Blue circle is Montserrat 20th May 2006 (Wadge et al., 2014). All other data points are colour-coded for the explosivity index (VEI) and are from various volcanoes with height, duration and VEI as reported by Mastin et al. (2009; Table 1).

By comparison, one of the largest eruptions from the 1995–2012 Montserrat activity was the VEI 3, 20th May 2006 dome collapse (Wadge et al., 2014). There are no reported Holocene eruptions in the Lesser Antilles with a VEI greater than 4 (Global Volcanism Program, 2013), and the LaMEVE database (Crosweller et al., 2012) lists only two Quaternary Lesser Antilles eruptions with VEI of 6 or greater – the ~27 ka Grande Savanne Ignimbrite and the ~36 ka Roseau Tuff. Recent studies suggest, however, that both these deposits are made up of a series of smaller eruptions (Howe et al., 2014). Thus, the model calculations presented here (Figure 5.7) suggest that the eruption that generated $T_{2.36}$ was of far greater magnitude than any known eruption in the Lesser Antilles.

It has been suggested that larger eruptions occur during the later stages of the life of a volcanic centre (Caricchi et al., 2014). Thus one hypothesis for the large size of the $T_{2.36}$ event (compared to typical eruptions in the region) is that it represents the last phase of activity of the Basal Complex, during which development of a thick crust allowed the volcanic system to enter a period of magma storage (cf. Caricchi *et al.* 2014) that ended with the large $T_{2.36}$ eruption. Hence, the largest and potentially most hazardous eruptions in this setting may be

associated with mature volcanic centres that become reactivated following a lengthy period of dormancy.

5.7 References

Allan, A.S.R., Baker, J. a., Carter, L., and Wysoczanksi, R.J., 2008, Reconstructing the Quaternary evolution of the world's most active silicic volcanic system: insights from an ~1.65 Ma deep ocean tephra record sourced from Taupo Volcanic Zone, New Zealand: Quaternary Science Reviews, v. 27, no. 25–26, p. 2341–2360, doi: 10.1016/j.quascirev.2008.09.003.

Andrews, D.G., Holton, J.R., and Leovy, C.B., 1987, Middle Atmosphere Dynamics: Academic Press, Orlando, Florida.

Blott, S.J., and Pye, K., 2001, GRADISTAT: a Grain Size Distribution and Statistics Package for the Analysis of Unconsolidated Sediments: Earth Surface Processes and Landforms, v. 26, p. 1237–1248, doi: 10.1002/ESP.261.

Bonadonna, C., Mayberry, G.C., Calder, E.S., Sparks, R.S.J., Choux, C., Jackson, P., Lejeune, a. M., Loughlin, S.C., Norton, G.E., Rose, W.I., Ryan, G., and Young, S.R., 2002, Tephra fallout in the eruption of Soufrière Hills Volcano, Montserrat: Geological Society, London, Memoirs, v. 21, no. 1, p. 483–516, doi: 10.1144/GSL.MEM.2002.021.01.22.

Carey, S.N., and Sigurdsson, H., 1978, Deep-sea evidence for distribution of tephra from the mixed magma eruption of the Soufrière on St. Vincent, 1902: Ash turbidites and air fall: Geology, v. 6, no. 5, p. 271–274, doi: 10.1130/0091-7613(1978)6<271:DEFDOT>2.0.CO;2.

Caricchi, L., Annen, C., Blundy, J., Simpson, G., and Pinel, V., 2014, Frequency and magnitude of volcanic eruptions controlled by magma injection and buoyancy: Nature Geoscience, v. 7, no. 2, p. 126–130, doi: 10.1038/ngeo2041.

Cassidy, M., Taylor, R.N., Palmer, M.R., Cooper, R.J., Stenlake, C., and Trofimovs, J., 2012, Tracking the magmatic evolution of island arc volcanism: Insights from a high-precision Pb isotope record of Montserrat, Lesser Antilles: Geochemistry, Geophysics, Geosystems, v. 13, no. 5, p. 1–19, doi: 10.1029/2012GC004064.

Cassidy, M., Watt, S.F.L., Palmer, M.R., Trofimovs, J., Symons, W., Maclachlan, S.E., and Stinton, A.J., 2014, Construction of volcanic records from marine sediment cores: A review and case study (Montserrat, West Indies): Earth-Science Reviews, v. 138, p. 137–155, doi: 10.1016/j.earscirev.2014.08.008.

Cole, P.D., Calder, E.S., Sparks, R.S.J., Clarke, A.B., Druitt, T.H., Young, S.R., Herd, R.A., Harford,

C.L., and Norton, G.E., 2002, Deposits from dome-collapse and fountain-collapse pyroclastic flows at Soufrière Hills Volcano, Montserrat: Geological Society, London, Memoirs, v. 21, p. 231–262, doi: 10.1144/GSL.MEM.2002.021.01.11.

Crosweller, H.S., Arora, B., Brown, S.K., Cottrell, E., Deligne, N.I., Guerrero, N.O., Hobbs, L., Kiyosugi, K., Loughlin, S.C., Lowndes, J., Nayembil, M., Siebert, L., Sparks, R.S.J., Takarada, S., et al., 2012, Global database on large magnitude explosive volcanic eruptions (LaMEVE): Journal of Applied Volcanology, v. 1, no. 1, p. 1–13, doi: 10.1186/2191-5040-1-4.

Engwell, S.L., Sparks, R.S.J., and Carey, S., 2014, Physical characteristics of tephra layers in the deep sea realm: the Campanian Ignimbrite eruption, *in* Austin, W.E.N., Abbott, P.M., Davies, S.M., Pearce, N.J.G., and Wastegård, S. eds., Marine Tephrochronology, Geological Society, London, Special Publications, p. 47–64.

Evans, J.R., Huntoon, J.E., Rose, W.I., Varley, N.R., and Stevenson, J.A., 2009, Particle sizes of andesitic ash fallout from vertical eruptions and co-pyroclastic flow clouds, Volcán de Colima, Mexico: Geology, v. 37, no. 10, p. 935–938, doi: 10.1130/G30208A.1.

Le Friant, A., Ishizuka, O., Boudon, G., Palmer, M.R., Talling, Basset, D., Watts, A., Bahr, A., Jimenez-Espejo, F.J., Kolasinac, N., Grunert, P., Hernández-Molina, F.J., Rohl, U., Voelker, A.H.L., Escutia, C., et al., 2015, Submarine record of volcanic island construction and collapse in the Lesser Antilles arc: First scientific drilling of submarine volcanic island landslides by IODP Expedition 340: Geochemistry Geophysics Geosystems, v. 18, no. 1–2, p. 1541–1576, doi: 10.1002/2014GC005684.Key.

Le Friant, A., Lock, E.J., Hart, M.B., Boudon, G., Sparks, R.S.J., Leng, M., Smart, C.W., Komorowski, J.-C., Deplus, C., and Fisher, J.K., 2008, Late Pleistocene tephrochronology of marine sediments adjacent to Montserrat, Lesser Antilles volcanic arc: Journal of the Geological Society, v. 165, p. 279–289, doi: 10.1144/0016-76492007-019.

Global Volcanism Program, 2013, Volcanoes of the World, v. 4.4.1 (E. Venzke, Ed.): Smithsonian Institution. Downloaded 01 Dec 2015.

González-Mellado, A.O., and De la Cruz-Reyna, S., 2010, A simple semi-empirical approach to model thickness of ash-deposits for different eruption scenarios: Natural Hazards and Earth System Science, v. 10, no. 11, p. 2241–2257, doi: 10.5194/nhess-10-2241-2010.

Harford, C.L., Pringle, M.S., Sparks, R.S.J., and Young, S.R., 2002, The volcanic evolution of Montserrat using 40Ar/39Ar geochronology: Geological Society, London, Memoirs, v. 21, no. 1, p. 93–113, doi: 10.1144/GSL.MEM.2002.021.01.05.

Hatfield, R.G., 2015, Data report: stratigraphic correlation of Site U1396 and creation of a composite depth scale and splice: v. 340, p. 1–17, doi: 10.2204/iodp.proc.340.202.2015.

Howe, T.M., Lindsay, J.M., Shane, P., Schmitt, A.K., and Stockli, D.F., 2014, Re-evaluation of the Roseau Tuff eruptive sequence and other ignimbrites in Dominica, Lesser Antilles: Journal of Quaternary Science, v. 29, no. 6, p. 531–546, doi: 10.1002/jqs.2723.

Kandlbauer, J., and Sparks, R.S.J., 2014, New estimates of the 1815 Tambora eruption volume: Journal of Volcanology and Geothermal Research, v. 286, p. 93–100, doi: 10.1016/j.jvolgeores.2014.08.020.

Komorowski, J.-C., Legendre, Y., Caron, B., and Boudon, G., 2008, Reconstruction and analysis of sub-plinian tephra dispersal during the 1530 A.D. Soufrière (Guadeloupe) eruption: Implications for scenario definition and hazards assessment: Journal of Volcanology and Geothermal Research, v. 178, no. 3, p. 491–515, doi: 10.1016/j.jvolgeores.2007.11.022.

Labanieh, S., Chauvel, C., Germa, A., Quidelleur, X., and Lewin, E., 2010, Isotopic hyperbolas constrain sources and processes under the Lesser Antilles arc: Earth and Planetary Science Letters, v. 298, no. 1–2, p. 35–46, doi: 10.1016/j.epsl.2010.07.018.

Lindsay, J.M., Trumbull, R.B., and Siebel, W., 2005, Geochemistry and petrogenesis of late Pleistocene to Recent volcanism in Southern Dominica, Lesser Antilles: Journal of Volcanology and Geothermal Research, v. 148, no. 3–4, p. 253–294, doi: 10.1016/j.jvolgeores.2005.04.018.

Manville, V., and Wilson, C.J.N., 2004, Vertical density currents: a review of their potential role in the deposition and interpretation of deep-sea ash layers: Journal of the Geological Society, v. 161, no. Kennett 1981, p. 947–958, doi: 10.1144/0016-764903-067.

Mastin, L.G., Guffanti, M., Servranckx, R., Webley, P., Barsotti, S., Dean, K., Durant, A., Ewert, J.W., Neri, A., Rose, W.I., Schneider, D., Siebert, L., Stunder, B., Swanson, G., et al., 2009, A multidisciplinary effort to assign realistic source parameters to models of volcanic ash-cloud transport and dispersion during eruptions: Journal of Volcanology and Geothermal Research, v. 186, no. 1, p. 10–21, doi: 10.1016/j.jvolgeores.2009.01.008.

Pindell, J., and Barrett, S., 1990, Geological evolution of the Caribbean region: A plate tectonic perspective, *in* The Geology of North America, vol. H, Geological Society of America, Boulder, Colorado, p. 405–432.

Samper, A., Quidelleur, X., Komorowski, J.-C., Lahitte, P., and Boudon, G., 2009, Effusive history of the Grande Découverte Volcanic Complex, southern Basse-Terre (Guadeloupe, French West Indies) from new K–Ar Cassignol–Gillot ages: Journal of Volcanology and

Geothermal Research, v. 187, no. 1, p. 117–130, doi: 10.1016/j.jvolgeores.2009.08.016.

Samper, A., Quidelleur, X., Lahitte, P., and Mollex, D., 2007, Timing of effusive volcanism and collapse events within an oceanic arc island: Basse-Terre, Guadeloupe archipelago (Lesser Antilles Arc): Earth and Planetary Science Letters, v. 258, no. 1–2, p. 175–191, doi: 10.1016/j.epsl.2007.03.030.

Taylor, R.N., Ishizuka, O., Michalik, A., Milton, J.A., and Croudace, I.W., 2015, Evaluating the precision of Pb isotope measurement by mass spectrometry: Journal of Analytical Atomic Spectrometry, v. 30, p. 198–213, doi: 10.1039/C4JA00279B.

Trofimovs, J., Sparks, R.S.J., and Talling, P.J., 2008, Anatomy of a submarine pyroclastic flow and associated turbidity current: July 2003 dome collapse, Soufrière Hills volcano, Montserrat, West Indies: Sedimentology, v. 55, no. 3, p. 617–634, doi: 10.1111/j.1365-3091.2007.00914.x.

Wadge, G., Voight, B., Sparks, R.S.J., Cole, P.D., Loughlin, S.C., and Robertson, R.E.A., 2014, An overview of the eruption of Soufrière Hills Volcano, Montserrat from 2000 to 2010: Geological Society, London, Memoirs, v. 39, no. 1, p. 1–40, doi: 10.1144/M39.1.

Wall-Palmer, D., Coussens, M., Talling, P.J., Jutzeler, M., Cassidy, M., Marchant, I., Palmer, M.R., Watt, S.F.L., Smart, C.W., Fisher, J.K., Hart, M.B., Fraass, A., Trofimovs, J., Le Friant, A., et al., 2014, Late Pleistocene stratigraphy of IODP Site U1396 and compiled chronology offshore of south and south west Montserrat, Lesser Antilles: Geochemistry, Geophysics, Geosystems, v. 15, no. 7, p. 3000–3020, doi: 10.1002/2014GC005402.

White, W.M., and Dupré, B., 1986, Sediment subduction and magma genesis in the Lesser Antilles: Isotopic and trace element constraints: Journal of Geophysical Research, v. 91, no. B6, p. 5927, doi: 10.1029/JB091iB06p05927.

Wiesner, M.G., Wetzel, A., Catane, S.G., Listanco, E.L., and Mirabueno, H.T., 2004, Grain size, areal thickness distribution and controls on sedimentation of the 1991 Mount Pinatubo tephra layer in the South China Sea: Bulletin of Volcanology, v. 66, no. 3, p. 226–242, doi: 10.1007/s00445-003-0306-x.

Zami, F., Quidelleur, X., Ricci, J., Lebrun, J.-F., and Samper, A., 2014, Initial sub-aerial volcanic activity along the central Lesser Antilles inner arc: New K-Ar ages from Les Saintes volcanoes: Journal of Volcanology and Geothermal Research, v. 287, p. 12–21, doi: 10.1016/j.jvolgeores.2014.09.011.

Andrews, D.G., Holton, J.R., and Leovy, C.B., 1987, Middle Atmosphere Dynamics: Orlando, Florida, Academic Press, 489 p.

Blott, S.J., and Pye, K., 2001. GRADISTAT: a grain size distribution and statistics package for the analysis of unconsolidated sediments: Earth Surface Processes and Landforms, v. 26, p. 1237-1248, doi: 10.1002/esp.261.

Carey, S.N., and Sigurdsson, H., 1978, Deep-sea evidence for distribution of tephra from the mixed magma eruption of the Soufrière on St. Vincent, 1902: Ash turbidites and air fall: Geology, v. 6, p. 271-274.

Caricchi, L., Annen, C., Blundy, J., Simpson, G., and Pinel, P., 2014, Frequency and magnitude of volcanic eruptions controlled by magma injection and buoyancy: Nature Geoscience, v. 7, p. 126–130, doi:10.1038/ngeo2041.

Cassidy, M., Taylor, R.N., Palmer, M.R., Cooper, R.J., Stenlake, C., and Trofimovs, J., 2012, Tracking the magmatic evolution of island arc volcanism: Insights from a high precision Pb isotope record of Montserrat, Lesser Antilles: Geochemistry Geophysics Geosystems, v. 13, p. Q05003, doi:10.1029/2012GC004064.

Cassidy, M., Watt, S.F.L., Palmer, M.R., Trofimovs, J., Symons, W., Maclachlan, S.E., and Stinton, A.J., 2014, Construction of volcanic records from marine sediment cores: A review and case study (Montserrat, West Indies): Earth-Science Reviews, v. 138, p. 137–155, doi:org/10.1016/j.earscirev.2014.08.008.

Crosweller, H.S., and 14 others, 2012, Global database of large magnitude explosive volcanic eruptions (LaMEVE): Journal of Applied Volcanology, v.1:4, doi:10.1186/2191-5040-1-4

Engwell, S.L., Sparks, R.S.J., and Carey, S., 2014, Physical characteristics of tephra layers in the deep sea realm: The Campanian Ignimbrite eruption: Geological Society, London, Special Publication 398, p. 47–64, doi:org/10.1144/SP398.7.

Evans, J.R., Huntoon, J.E., Rose, W.I., Varley, N.R., and Stevenson, J.A., 2009, Particle sizes of andesitic ash fallout from vertical eruptions and co-pyroclastic flow clouds, Volcán de Colima, Mexico: Geology, v. 37, p. 935–938, doi:10.1130/G30208A.1.å

Folk, R.L., and Ward, W.C., 1957. Brazos River bar: studying the significance of grain-size parameters: Journal of Sedimentary Petrology, v. 27, p. 3-26.

Global Volcanism Program, 2013. Volcanoes of the World, v. 4.4.1. Venzke, E (ed.). Smithsonian Institution. 01 Dec 2015. dx.doi.org/10.5479/si.GVP.VOTW4-2013

González-Mellado, A.O., and De la Cruz-Reyna, S., 2010, A simple-empirical approach to model thickness of ash-deposits for different eruption scenarios: Natural Hazards and Earth System Sciences, v. 10, p. 2241–2257, doi:10.5194/nhess-10-2241-2010.

Harford, C.L., Pringle, M.S., Sparks, R.S.J., and Young, S.R., 2002, The volcanic evolution of Montserrat using 40Ar/39Ar geochronology: Memoirs of the Geological Society of London, v. 21, p. 93–113, doi:0435–4052/02/$15.

Hart, S.R., 1984, A large-scale isotope anomaly in the southern-hemisphere mantle: Nature, v. 309, p. 753–757, doi:10.1038/309753a0.

Hatfield, R.G., 2015, Data Report: Stratigraphic correlation of Site U1396 and creation of a composite depth scale and splice: IODP 340: Data Report, (in press).

Howe, T.M., Lindsay, J.M., Shane, P., Schmitt, A.K., Stockli, D.F., 2014, Re-evaluation of the Roseau Tuff eruptive sequence and other ignimbrites in Dominica, Lesser Antilles: Journal of Quaternary Science, v. 29, p. 531-546, doi: 10.1002/jqs.2723.

Kandlbauer, J. and Sparks, R.S.J., 2014, New estimates of the 1815 Tambora eruption volume: Journal of Volcanology and Geothermal Research, v. 286, p. 93–100, doi:org/10.1016/j.jvolgeores.2014.08.020.

Komorowski, J.C., Legendre, Y., Caron, B., and Boudon, G., 2008, Reconstruction and analysis of sub-Plinian tephra dispersal during the 1530 A.D. Soufrière (Guadeloupe) eruption: Implications for scenario definition and hazards assessment: Journal of Volcanology and Geothermal Research, v. 178, p. 491–515, doi:10.1016/j.jvolgeores.2007.11.022.

Labanieh, S., Chauvel, C., Germa, A., Quidelleur, X., and Lewin, E., 2010, Isotopic hyperbolas constrain sources and processes under the Lesser Antilles arc: Earth and Planetary Science Letters, v. 298, p. 35–46, doi:10.1016/j.epsl.2010.07.018.

Le Friant, A., et al., 2008, Late Pleistocene tephrochronology of marine sediments adjacent to Montserrat, Lesser Antilles volcanic arc: Journal of the Geological Society, v. 165, p. 279-289, doi: 10.1144/0016-76492007-019

Le Friant, A., et al., 2015, Submarine record of volcanic island construction and collapse in the Lesser Antilles arc: First scientific drilling of submarine volcanic island landslides by IODP Expedition 340: Geochemistry Geophysics Geosystems, v. 16, p. 420–442, doi:10.1002/2014GC005652.

Lindsay, J.M., Trumbull, R.B., and Siebel, W., 2005, Geochemistry and petrogenesis of late Pleistocene to Recent volcanism in Southern Dominica, Lesser Antilles: Journal of Volcanology and Geothermal Research, v. 148, p. 253–294, doi:10.1016/j.jvolgeores.2005.04.018.

Manville, V., and Wilson, C. J. N., 2004, Vertical density currents: a review of their potential role in the deposition and interpretation of deep-sea ash layers: Journal of the Geological Society, London, v. 161, p. 947-958.

Mastin, L.G., et al., 2009, A multidisciplinary effort to assign realistic source parameters to models of volcanic ash-cloud transport and dispersion during eruptions: Journal of Volcanology and Geothermal Research, v. 186, p. 10–21, doi:10.1016/j.jvolgeores.2009.01.008.

Mulder, T., and Alexander, J., 2001. The physical character of subaqueous sedimentary density flows and their deposits: Sedimentology, v. 48, p. 269-299, doi: 10.1046/j.1365-3091.2001.00360.x.

Newhall, C. G., and Self, S. S., 1982, The Volcanic Explosivity Index (VEI): An estimate of explosive magnitude for historical volcanism: Journal of Geophysical Research, v. 87, p. 1231-1238.

Pindell, J., and Barrett, S., 1990, Geological evolution of the Caribbean region: A plate tectonic perspective, in The Geology of North America, vol. H, The Caribbean Region: Boulder, Colorado, Geological Society of America, p. 405–432.

Pyle, D. M., 1999, Widely dispersed Quaternary tephra in Africa: Global and Planetary Change, vol. 21, p. 95-112.

Samper, A., Quidelleur, X., Lahitte, P., and Mollex, D., 2007, Timing of effusive volcanism and collapse events within an oceanic arc island: Basse-Terre, Guadeloupe archipelago (Lesser Antilles Arc): Earth and Planetary Science Letters, v. 258, p. 175–191, doi:10.1016/j.epsl.2007.03.030.

Samper, A., Quidelleur, X., Komorowski, J.C., Lahitte, P., and Boudon, G., 2009, Effusive history of the Grande Découverte Volcanic Complex, southern Basse-Terre (Guadeloupe, French West Indies) from new K-Ar Cassignol-Gillot ages: Journal of Volcanology and Geothermal Research, v. 187, p. 117–130, doi:10.1016/j.jvolgeores.2009.08.016.

Sparks, R.S.J., et al., 1998. Magma production and growth of the lava dome of the Soufrière Hills Volcano, Montserrat, West Indies: November 1995 to December 1997: Geophysics Research Letters, v. 25, p. 3421-3424, doi: 10.1029/98GL00639.

Taylor, R.N., Ishizuka, O., Michalik, A., Milton, J.A., and Croudace, I.W., 2015. Evaluating the precision of Pb isotope measurement by mass spectrometry. Journal of Analytical Atomic Spectroscopy, 30, 198-213, doi:10.1039/c4ja00279b.

Wadge, G., Voight, B., Sparks, R.S.J., Cole, P.D., Loughlin, S.C., and Robertson, R.E.A., 2014, An overview of the eruption of Soufrière Hills Volcano, Montserrat from 2000–2010: Geological Society of London Memoirs, v. 39, p. 1–39, doi:10.1144/M39.1

Wall-Palmer, D., et al., 2014, Late Pleistocene stratigraphy of IODP Site U1396 and compiled chronology offshore of south and southwest Montserrat, Lesser Antilles: Geochemistry, Geophysics, Geosystems, v. 15, p. 3000-3020, doi: 10.1002/2014GC005402.

White, W.M., and Dupré, B., 1986, Sediment subduction and magma genesis in the Lesser Antilles: Isotopic and trace element constraints: Journal of Geophysical Research, v. 91, p. 5927–5941, doi:10.1029/JB091iB06p05927.

Wiesner, M.G., Wetzel, A., Catane, S.G., Listanco, E.L., and Mirabueno, H.T., 2004, Grain size, areal thickness distribution and controls on sedimentation of the 1991 Mount Pinatubo tephra layer in the South China Sea: Bulletin of Volcanology, v. 66, p. 226–242, doi:10.1007/s00445-003-0306-x.

Zami, F., Quidelleur, X., Ricci, J., Lebrun, J.F., and Samper, A., 2014, Initial sub-aerial volcanic activity along the central Lesser Antilles inner arc: New K–Ar ages from Les Saintes volcanoes: Journal of Volcanology and Geothermal Research, v. 287, p. 12–21, doi:10.1016/j.jvolgeores.2014.09.011.1.

Chapter 6: Conclusions and future work

6.1 Conclusions

This thesis provides the first detailed record of the volcanic activity and geochemical evolution of the Silver Hills volcanic centre, Montserrat, with new $^{40}Ar/^{39}Ar$ and marine tephra layer (from marine sediment core U1396C) ages providing a geochronological framework. Furthermore, this thesis has constructed the most detailed record of the geochemical evolution of both Montserrat and Guadeloupe spanning ~4.5 Ma, by studying tephra layer layers from core U1396C, which for Montserrat is combined with new data from the terrestrial record. The key findings of this study are summarised below, answering the original thesis questions.

Chapter 2: The evolution of the Silver Hills volcanic centre, and revised $^{40}Ar/^{39}Ar$ geochronology of Montserrat, Lesser Antilles, with implications for island arc volcanism

Q2.1: Did the style of volcanic activity change over the lifetime of the Silver Hills, and how does it compare to the Centre Hills and Soufrière Hills?

The Silver Hills volcanic centre exhibited the same eruption styles throughout its period of activity, which was dominated by effusive eruptions of andesitic lava domes and dome collapses. There is also evidence for accompanying Vulcanian style eruptions, and the identification of debris avalanche deposits indicates that the Silver Hills experienced periodic sector collapse. This indicates that the Silver Hills was characterised by the same style of eruptions as have been observed for the Centre Hills and Soufrière Hills. A notable difference between the centres is the absence of evidence of any large sustained explosive eruptions at the Silver Hills, which have been recorded throughout the lifetime of the Centre Hills, and in the middle stages of Soufrière Hills. However, this may be the result of a preservation bias.

Q2.2: Did the petrology of the volcanic deposits of the Silver Hills change over the course of Silver hills activity?

The petrology of the Silver Hills volcanic deposits remained constant throughout its ~2.2–1.03 Ma period of activity, comprising dominantly plagioclase, clinopyroxene, orthopyroxene, and Fe-Ti oxides. However, a new period of volcanic activity of the Soufrière Hills has been discovered, which erupted hornblende-orthopyroxene andesites, similar to those erupted from the Soufrière Hills from ~112–0 ka. This indicates that the petrology of the Soufrière

Hills has changed at least twice over the past ~450 ka, because it erupted two-pyroxene andesites during ~290–130 ka.

Q2.3: Has volcanic activity on Montserrat always been focused at one volcanic centre at any given time, or has there been overlap in activity between two volcanic centres?

The new ages for the Silver, Centre and Soufrière Hills reveal that there was overlap in volcanic activity between the Silver and Centre Hills during at least ~1.14–1.03 Ma, and between the Centre and Soufrière Hills during at least ~0.45–0.38 Ma. This shows that overlap between successive volcanic centres has been a common process on Montserrat, and has also been documented on Guadeloupe, Dominica and Martinique.

Chapter 3: Geochemical evolution of the Silver Hills volcanic centre

Q3.1: Does the chemistry of the Silver Hills volcanic centre systematically change during its lifetime?

There is no systematic change in the major and trace element geochemistry of the Silver Hills volcanic centre throughout its period of activity. The only observed difference between the multiple lava domes of the Silver Hills is lower U/Th values for North Marguerita and Yellow Hole domes. Pb and Sr isotopes also display no systematic variation throughout the Silver Hills. However, $^{143}Nd/^{144}Nd$ displays a systematic shift towards less radiogenic values over time, which is most likely caused by mantle heterogeneity.

Q3.2: Can the lavas of the Silver Hills be produced from fractionation of magmas with similar chemical compositions as the mafic enclaves hosted within the lavas?

The mafic enclaves are isotopically distinct from their host lavas, indicating that these lavas could not have formed from fractionation of the enclave parent magmas. Furthermore, the mafic enclaves (basalts to basaltic andesites) have incompatible trace element concentrations greater than the host lavas (andesites to dacites), indicating that the Silver Hills lavas could not have formed from differentiation of parent magmas with similar compositions as the mafic enclaves.

Chapter 4: Geochemical evolution of volcanism on Montserrat and Guadeloupe (Lesser Antilles arc), revealed from marine sediment core U1396C

Q4.1: How does the geochemistry of arc islands evolve through time, and what is the dominant process driving any change (i.e. variations in mantle source components versus crustal assimilation)?

For Montserrat, variations in the mantle source components appear to have been the main driver of geochemical evolution of volcanism over the past ~4.5 Ma, with the most pronounced change in geochemistry occurring at ~4.5–3.9 Ma. This was most likely caused by an increase in the sediment contribution to the mantle wedge via an aqueous fluid. For Guadeloupe, however, geochemical evolution appears to have been controlled by changes in the extent of crustal assimilation of a MORB component, with the greatest assimilation occurring ~3.2 Ma. Together, Montserrat and Guadeloupe show that both changes to the subduction zone source components, and to the extent of crustal assimilation, play key roles in the geochemical evolution of island arc magmas.

Q4.2: What is the cause of the difference in isotope geochemistry between Montserrat and Guadeloupe?

By comparing the tephra from Montserrat (which shows no evidence for crustal assimilation) with the tephra from Guadeloupe that has been least affected by crustal assimilation, comparisons can be made of the relative contributions of the source components which formed the melts beneath the islands. Source component mixing models indicate that the difference in isotope geochemistry between Montserrat and Guadeloupe is caused by a greater sediment contribution to the source region beneath Guadeloupe, compared to Montserrat. This is consistent with the along-arc trend documented for the Lesser Antilles.

Chapter 5: Discovery of a large 2.4 Ma Plinian eruption of Basse-Terre, Guadeloupe, form the marine sediment record

Q5.1: What is the mode of deposition of tephra layer $T_{2.36}$?

Tephra layer $T_{2.36}$ can be split into two layers: an upper 6 cm layer, and lower 12 cm layer. The lower layer was deposited from tephra fallout of an eruption column, while the upper layer was most likely deposited from a co-ignimbrite cloud from the same eruption.

Q5.2: What sized eruption produced tephra layer $T_{2.36}$?

The eruption reconstruction equations of González-Mellado and De la Cruz-Reyna, (2010) indicate that $T_{2.36}$ was produced from a VEI 6 eruption.

6.2 Future Work

This thesis has substantially increased our understanding of volcanism on Montserrat and Guadeloupe, but it has raised a number of new questions, with scope for future work.

In Chapter 2, a new period of activity of the Soufrière Hills was discovered, raising the following questions:

What caused the petrology of the Soufrière Hills lavas to change twice during its period of activity? Was the change sudden or transitional? Why was the petrology of the Silver Hills constant throughout its lifetime, when the Centre Hills and Soufrière Hills both displayed a change at least once?

The cause of the change in petrology of the Centre Hills towards the end of its life (Coussens et al., 2017), and in the Soufrière Hills between ~300 and 290 ka (Chapter 2), and ~130 and 112 ka (Harford et al., 2002), is unknown, but a means of answering these questions may come from the pyroclastic sequence contained in Garibaldi Hill, which contains both two-pyroxene andesites and hornblende-hypersthene andesites (Rea, 1974); the stratigraphic relationship between the two andesite types here is not documented. A detailed stratigraphy of Garibaldi Hill may provide constraints on the timing of the change in petrology, while electron microprobe analyses of samples from both andesite types may provide insight into the process(es) controlling the change in petrology. Amphibole stability is controlled by magma H_2O content, and the pressure and temperature of the magma chamber in which it is growing, so the appearance or disappearance of amphibole as a major phenocryst phase may be related to changes in one or more of these conditions. Electron microprobe analyses have been used to estimate the pressure, temperature, and H_2O content of lavas erupted during the recent eruption (1995–2010) of the Soufrière Hills (e.g. Barclay et al., 1998; Edmonds et al., 2016). If similar studies were conducted on two-pyroxene andesites, comparisons between the two andesite types may reveal any differences in magma chamber conditions between them, thus helping determine the reason for the change in petrology. Answering these questions may enhance our understanding of how magma storage regions develop over the lifetime of a volcano.

Detailed mapping of the Silver Hills in Chapter 2 has revealed the characteristic eruption styles exhibited by this volcanic centre, but raises the following questions:

Is the absence of sustained explosive eruption deposits of the Silver Hills the result of a preservation bias? Or is it due to a genuine lack of such eruptions?

The absence of deposits of sustained explosive eruptions of the Silver Hills is potentially the result of a preservation bias, because the present day exposure of the Silver Hills is of its central dome complex, comparable to that of the present day Soufrière Hills. There are pumiceous deposits from the Silver Hills present in core U1396C, but they are limited in number, which may be due to site U1396 being tangential to the dominant wind direction, thus limited the ability for eruption columns to reach site U1396C. Coring off-shore to the west of the Silver Hills volcanic centre may contain a more complete record of Silver Hills volcanism, and provide a record of explosive activity for this centre. This would determine if

the Silver Hills truly did not experience any sustained explosive eruptions, which both the Centre Hills and Soufrière Hills did. Answering these questions has implications for the behaviour of island arc volcanoes, and periodicity studies of large eruptions, which feeds into hazard assessment and prediction.

In Chapter 3, modelling indicates that the low Al_2O_3-high Fe_2O_3 lavas of the Silver Hills are mostly likely formed from a parent magma which experienced up to 25% more plagioclase fractionation than the parent magma of the normal lavas, and raises the question:

Is the difference in fractionation histories between the normal and low Al_2O_3-high Fe_2O_3 lavas the result of a difference in magmatic H_2O content?

This hypothesis could be tested by measuring the H_2O content of melt inclusions for both normal and low Al_2O_3-high Fe_2O_3 lavas, to determine if there is any significant difference. If there is a difference in H_2O content, then the observation that the enclaves appear to follow the major element compositional trends of the normal lavas, raises follow-on questions:

Did the enclave magmas have low H_2O contents but not stall within the crust long enough for plagioclase fractionation to occur? Or did the enclave magmas have a higher H_2O content than their host magmas, similar to the normal composition lavas?

These questions could also be answered by obtaining measurements of the water content of melt inclusions in the Silver Hills enclaves, and may have implications for variable timescales of magma transport through the crust.

In core U1396C there is only one tephra layer from Guadeloupe covering 2.3–0 Ma, providing a significant gap within our record. This time period is, however, covered by the terrestrial record, which has been subject to extensive radiometric dating of all volcanic centres (Carlut et al., 2000; Ricci et al., 2015a, 2015b, Samper et al., 2007, 2009,). Producing isotope, and major and trace element data for these dated samples would complement the record constructed in this thesis, producing a longer and more detailed record of the geochemical evolution of Guadeloupe.

While this thesis has focussed on the geochemical record stored in core U1396C, there is also scope to study the size of the eruptions which produced the tephra layers, to answer questions such as:

What size eruptions were typical for Montserrat and Guadeloupe over the past ~4.5 Ma? And how frequent were Plinian sized eruptions?

Combined componentry, grain size and grain morphology analyses of each tephra layer could be performed to determine their mode of deposition. Then, eruption reconstructions could

be applied to any identified fallout deposits to determine eruption sizes, following the method of Palmer et al., (2016). Constructing a record of past eruption sizes, and identifying any Plinian sized eruptions, will provide further insight into how volcanic activity has evolved on Montserrat and Guadeloupe, and aid with hazard assessments and predictions.

6.3 References

Barclay, J., M. J. Rutherford, M. R. Carroll, M. D. Murphy, J. D. Devine, J. Gardner, and R. S. J. Sparks (1998), Experimental phase equilibria constraints on pre-eruptive storage conditions of the Soufrière Hills magma, *Geophys. Res. Lett.*, *25*(18), 3437, doi:10.1029/98GL00856.

Carlut, J., X. Quidelleur, V. Courtillot, and G. Boudon (2000), Paleomagnetic directions and K/Ar dating of 0 to 1 Ma lava flows from La Guadeloupe Island Implications for time-averaged field models, *J. Geophys. Res.*, *105*, 835–849.

Coussens, M., M. Cassidy, S. F. L. Watt, M. Jutzeler, P. J. Talling, D. Barfod, T. M. Gernon, R. Taylor, S. J. Hatter, and M. R. Palmer (2017), Long-term changes in explosive and effusive behaviour at andesitic arc volcanoes: Chronostratigraphy of the Centre Hills Volcano, Montserrat, *J. Volcanol. Geotherm. Res.*, doi:10.1016/j.jvolgeores.2017.01.003.

Edmonds, M., S. C. Kohn, E. H. Hauri, M. C. S. Humphreys, and M. Cassidy (2016), Extensive, water-rich magma reservoir beneath southern Montserrat, *Lithos*, *252–253*, 216–233, doi:10.1016/j.lithos.2016.02.026.

González-Mellado, A. O., and S. De la Cruz-Reyna (2010), A simple semi-empirical approach to model thickness of ash-deposits for different eruption scenarios, *Nat. Hazards Earth Syst. Sci.*, *10*(11), 2241–2257, doi:10.5194/nhess-10-2241-2010.

Harford, C. L., M. S. Pringle, R. S. J. Sparks, and S. R. Young (2002), The volcanic evolution of Montserrat using 40Ar/39Ar geochronology, *Geol. Soc. London, Mem.*, *21*(1), 93–113, doi:10.1144/GSL.MEM.2002.021.01.05.

Palmer, M. R., S. J. Hatter, T. M. Gernon, R. N. Taylor, M. Cassidy, P. Johnson, A. Le Friant, and O. Ishizuka (2016), Discovery of a large 2.4 Ma Plinian eruption of Basse-Terre, Guadeloupe, from the marine sediment record, *Geol.* , *44*(2), 123–126, doi:10.1130/G37193.1.

Rea, W. J. (1974), The volcanic geology and petrology of Montserrat, West Indies, *J. Geol. Soc. London.*, *130*(1), 341–366, doi:10.1144/gsjgs.130.4.0341.

Ricci, J., P. Lahitte, and X. Quidelleur (2015a), Construction and destruction rates of volcanoes

within tropical environment: Examples from the Basse-Terre Island (Guadeloupe, Lesser Antilles), *Geomorphology*, *228*, 597–607, doi:10.1016/j.geomorph.2014.10.002.

Ricci, J., X. Quidelleur, and P. Lahitte (2015b), Volcanic evolution of central Basse-Terre Island revisited on the basis of new geochronology and geomorphology data, *Bull. Volcanol.*, *77*(10), 84, doi:10.1007/s00445-015-0970-7.

Samper, A., X. Quidelleur, P. Lahitte, and D. Mollex (2007), Timing of effusive volcanism and collapse events within an oceanic arc island: Basse-Terre, Guadeloupe archipelago (Lesser Antilles Arc), *Earth Planet. Sci. Lett.*, *258*(1–2), 175–191, doi:10.1016/j.epsl.2007.03.030.

Samper, A., X. Quidelleur, J.-C. Komorowski, P. Lahitte, and G. Boudon (2009), Effusive history of the Grande Découverte Volcanic Complex, southern Basse-Terre (Guadeloupe, French West Indies) from new K–Ar Cassignol–Gillot ages, *J. Volcanol. Geotherm. Res.*, *187*(1), 117–130, doi:10.1016/j.jvolgeores.2009.08.016.

Appendices

Appendix A

Inductively-Coupled Plasma Mass Spectrometer (ICP-MS) analysis

Samples were dissolved in a HNO_3-HF mix on a hotplate at 130^{o}C for 24 hrs, evaporated to dryness, re-dissolved in 6M HCl, evaporated to dryness, then re-dissolved in 10 ml 6M HCl to produce mother solutions. 2.5 ml of the mother solution was evaporated to dryness, then re-dissolved in 10 ml of 3% HNO_3 spiked with 5 ppb In, 5 ppb Re and 20 ppb Be to form daughter solutions with a dilution factor of ~4,000 for trace element analysis. 1 ml of the daughter solution was sub-sampled, evaporated to dryness, then re-dissolved in 10 ml of 3% HNO_3 spiked with 5 ppb In, 5 ppb Re and 20 ppb Be to form a daughter solution with a dilution factor of ~40,000 for major element analysis. Elemental abundances were measured using a Thermo Fisher Scientific X-Series 2 ICP-MS (Bremen, Germany). Data was acquired in peak-jumping mode with an analysis time of 4x25 seconds per sample. After each sample analysis, a wash solution containing 3% HNO_3 was run until background levels were achieved (3 minutes). The raw data was blanked and internally corrected, and then calibrated against rock standards. Standards BHV02, BIR2, JB1a, JB3, JGb1 and a calibration blank were used to construct a calibration curve, and to access the precision of analyses (along with standards JA2, BAS206 and BRR1).

External reproducibility (relative standard deviation) was calculated from standards JA-2 (Jun 2011 to Sep 2017), BRR-1 (Mar 2012 to Sep 2017) and BAS206 (Jan 2012 to Sep 2017). For trace elements the reproducibility of JA-2 is <5% for all except Ta, which is <10%, and Zn, which is 15% (n=53–87).). For BRR-1, reproducibility is <5% for Li, Sc, V, Cr, Co, Ni, Sr, Y, REEs, U, <8% for Cu, Zr, Nb, Ba, Hf, <11% for Zn, Rb, <21% for Cs, <32% for Pb, <42% for Th, 50% for Ta (n=40–69). For BAS206, reproducibility is <5% for all trace elements except Cr, Sr, Cs, Gd which are <8%, Zn, Rb, Ba, U which are <12%, Pb which is <15% and Ta which is <18% (n=48–79).

For major elements the external reproducibility of JA-2 is <5% for all except Fe, which is <7% (n=24–44). For BRR-1, reproducibility is <4% for all except K, which is <29% (n=21–35). For BAS206, reproducibility is <4% for all except K, which is 7% (BAS206; n=21–35).

The following data tables of analysed standards are on the accompanying CD:

Appendix Table 1.1. Trace element standards

Appendix Table 1.2. Major element standards

Appendix Table 1.3. Pb isotope standards

Appendix Table 1.4. Nd isotope standards

Appendix Table 1.5. Sr isotope standards

Appendix B

The following data tables for Chapter 2 are on the accompanying CD:

Appendix Table 2.1. Original and recalculated literature $^{40}Ar/^{39}Ar$ dates

Appendix Table 2.2. $^{40}Ar/^{39}Ar$ results for lava samples

Appendix Table 2.3. $^{40}Ar/^{39}Ar$ results for pumice samples

Appendix Table 2.4. Whole-rock geochemistry data

Appendix C

The following data tables for Chapter 3 are on the accompanying CD:

Appendix Table 3.1. XRF and ICP-MS major element data

Appendix Table 3.2. XRF and ICP-MS trace element data

Appendix Table 3.3. Isotope data

Appendix D

The following data tables for Chapter 4 are on the accompanying CD:

Appendix Table 3.1. Componentry data

Appendix Table 3.2. Isotope data

Appendix Table 3.3. Trace element data

Appendix Table 3.4. Major element data

Appendix E

The following tables present data for Chapter 5.

Appendix Table 5.1. Trace element and isotope data

Sample U1396C 6H2	La (ppm)	Sm (ppm)	$^{206}Pb/^{204}Pb$	$^{207}Pb/^{204}Pb$	$^{208}Pb/^{204}Pb$	Δ7/4
94/95WP	11.50	5.58	19.1858 ± 8	15.6900 ± 8	38.9262 ± 24	11.9
99/100 WP	16.80	8.00	19.1776 ± 9	15.6835 ± 8	38.9050 ± 26	11.4
101/102 WP	12.30	5.70				
101/102 VJ	9.15	4.90	19.1779 ± 22	15.6851 ± 20	38.9074 ± 64	11.5
106/107 WP	12.30	5.89				
106/107 VJ	8.02	4.26	19.1856 ± 8	15.6889 ± 7	38.9210 ± 23	11.8
113/114 NVJ	8.35	4.13				
113/114 VJ	7.56	3.98	19.1863 ± 26	15.6890 ± 24	38.9218 ± 75	11.8

WP, white pumice; VJ, vesicular juvenile; NVJ, non-vesicular juvenile.

Appendix Table 5.2. Major element data

Sample U1396C 6H2	SiO_2 wt%	TiO_2 wt%	Al_2O_3 wt%	Fe_2O_3 wt%	MnO wt%	MgO wt%	CaO wt%	Na_2O wt%	K_2O wt%
94/95	62.6	0.95	17.0	7.06	0.23	1.96	5.46	3.29	1.51
99/100	64.6	0.58	17.0	6.10	0.23	1.12	5.06	3.75	1.56
101/102	59.4	0.90	17.8	7.83	0.25	2.75	6.78	3.08	1.24
106/107	63.6	0.71	17.7	5.50	0.16	1.62	5.69	3.64	1.37
113/114	59.5	1.06	16.6	8.72	0.27	2.73	6.72	3.20	1.14